Implementation of the New Dutch Guidelines on the Macrostability Assessment of Dikes using Different Constitutive Models

Case study: KIJK Dike in the Netherlands

TU DELFT / CRUX ENGINEERING
CHRISTAKIS IEREIDIS
4622618

Implementation of the New Dutch Guidelines on the Macrostability Assessment of Dikes using Different Constitutive Models

Case study: KIJK Dike in the Netherlands

By

Christakis Iereidis
Student number: 4622618

In partial fulfilment of the requirements for the degree of

Master of Science
In Geo-Engineering

At the Delft University of Technology,
to be defended on May 21st, 2019.

Thesis Committee

Prof. Dr. C. Jommi	Geo-Engineering	TU Delft (chair)
Dr.Ir. R.B.J. Brinkgreve	Geo-Engineering	TU Delft
Ir. H.J. Lengkeek	Hydraulic Engineering	TU Delft
Ir. Ing. M. de Koning	Geotechnical Engineer	CRUX Engineering
Ir. Ing. E. Kaspers	Geotechnical Engineer	CRUX Engineering

Delft University of Technology

Table of Contents

Table of Figures

Table of Tables

Acknowledgements

Around the 7th month doing my research I fall into a phrase that changed entirely the way I was handling my thesis process. The phrase was rather simple but very intriguing for me; "Too much analysis brings paralysis". Indeed, the overthinking can lead to delays, doubts of choices and eventually add an unnecessary non-deserving stress in your daily life neglecting your continuous efforts. Do not get me wrong. It is always correct to analyse your choices, but in a productive way. Do not let the imperfection stop you. Move forward, accept your vulnerabilities, stay motivated, give your all and through humbleness you will succeed. Realise that the Master Thesis is the final chapter of your long-lasting academic journey and no matter the outcome, upon completion you took a major step in becoming the strongest version of yourself. This is what matters. To become a stronger version of yourself not only scientifically but also character wise. TU Delft challenges you at both.

I was very lucky and proud to form a committee with one of the most established experts in the field. Thus, in my acknowledgements I want to express my deep gratitude and appreciation to Professor Cristina Jommi. Her remarks and advices along with our fruitful discussions and the constant willingness of guidance were extremely important and valuable to me.

Same applies and for Mr. Ronald Brinkgreve which was always there; giving me his valuable feedback and remarks. Our discussions served as a paramount cornerstone for the Thesis process.

I additionally want to express my deep appreciation and gratitude to Mr. Arny Lengkeek which was my external supervisor - mentor. His feedback and remarks along with his willingness to help and our valuable discussions were critical for the accomplishment of the Thesis.

Following my academic supervisors, I have to express my profound gratitude to my CRUX ENGINEERING supervisors, namely Mr. Michel, Mr. Ekke and Mr. Yos. Their willingness to help from day one until completion were helpful - valuable for me.

At this point I would like also to thank my friends and colleagues for their inspiration and useful ideas.

The author is grateful to Het Hoogheemraadschap van Schieland en de Krimpenerwaard for providing the data.

Last but not least, I want to express my sincere gratitude to my family and girlfriend namely, Michalakis Iereidis, Androulla Iereidi, Marina Iereidi and Katerina Vagena - Antonopoulou. Their support and continuous encouragement were the number one reason I eventually reached the point of finalising my academic journey.

I want to finish my acknowledgements with the great words of Kavafis
"When you set out for Ithaca
Hope your journey will be long
Filled with adventure, filled with knowledge".

The author
Christakis Iereidis

Abstract

The National Flood Protection Program (HWBP) periodically calls for safety assessments to ensure that the primary flood defenses in the Netherlands meet the safety standards. During the 3rd National Testing Round (LRT3) it was established that a large portion of the KIJK dike which serves as a primary flood protection of the adjacent Hollandsche IJssel failed to comply a macrostability inspection of its inner slope. The macrostability of the dike is of critical importance in the safety analysis since this can lead to severe outcomes (e.g. fatalities and economical losses). Nowadays in the Netherlands there is an explicit cluster, namely POV-M which deals with this assessment. The efficiency is achieved through the development of concrete and unequivocal guidelines. These guidelines are applied in successive phases which are implemented in the stage construction mode of PLAXIS finite element code with the final aim to determine the FoS (factor of safety) of the dike at critical loading under undrained conditions using the CSSM (Critical State Soil Mechanics) framework. The FoS is determined with the use of the strength reduction method. Moreover, the CSSM framework is coupled with the SHANSEP (Stress History and Normalized Soil Engineering Properties) concept enabling the incorporation of the effect of stress history and the stress path characterizing the undrained shear strength in the design. The CSSM framework is applied in the design by determining the strength parameters of clays from an axial strain level equal to 25% under triaxial compression whereas for peats at 40% shear strain level under direct simple shearing conditions. In this study the strength parameters were additionally determined from the service conditions strain levels which are the 2% and 5% strain levels for clays and peats, respectively.

In this study, the assessment of the KIJK dike follows the new guidelines given by POV-M 2018 using PLAXIS. The macrostability assessment and design of the dike is examined for two cases. In the first case the dike is assessed based on the in-situ conditions (Green dike) whereas in the second case a cantilever sheet pile wall is used in the design (Blue dike) to strengthen the dike. Prior to the analysis the interpretation of the available laboratory data that were executed according to the new protocol (WBI 2017) and the parameter determination of the necessary input parameters of the considered constitutive models (SHANSEP NGI-ADP, Hardening Soil, Soft Soil models) is established. The models presented herein are also used in the calculation schemes proposed by POV-M for finite element modelling purposes. On top of that, in this study the response of the recently introduced advanced constitutive model SHANSEP NGI-ADP is compared with the advanced constitutive models Hardening Soil (HS) and Soft Soil (SS) which are commonly used in engineering practice. The undrained shear strength (s_u) of the SHANSEP NGI-ADP model is based on the SHANSEP concept and the normalised s_u ($S_{(NC, OC)}$) and the strength increase exponent (m) parameters are needed. For the HS and the SS models the effective strength parameters φ and c are required. To properly achieve the comparison of the models at critical loading the Undrained A option is applied for the HS and SS models and the s_u is derived based on the effective strength parameters considering an effective stress path.

The necessary strength parameters for the constitutive models are determined in the considered strain levels exposing their influence for both clays and peats. Moreover, the study includes the examination of the constitutive models at a single element level conducted in the Soil Test facility available in PLAXIS. The aim is the optimization of the stiffness parameters along with the examination of the influence of the K_0 value used in the consolidation phase of a triaxial test on the resulting undrained shear strength. The evaluation of the models in terms of stress strain response showed that the response of the SHANSEP NGI-ADP is exemplary in the sense that the model was able to reproduce accurately the strain hardening of both peats and clays. The HS model captured properly the elastoplastic behaviour of the materials where the SS model

produced the poorest results. As it concerns the development of the pore pressures with strain and the stress path it was found that the HS and SS models were able to capture properly the behaviour of a normally or a nearly normally consolidated soil. Conversely, the models were unable to capture the response of an over consolidated soil (e.g. generation of dilative pore pressures) and the q_{max} was underestimated. Concerning the applied K_0 value, the investigation points out that when the OCR is considered in the K_0 value there are considerable gains in terms of strength.

When it comes to the design analysis, it was found that the SHANSEP NGI-ADP model fits properly the s_u determined from a cone penetration test. The combination of the $S_{(NC)}$ and the m along with the proper incorporation of the OCR are beneficial for predicting appropriately the s_u. The HS and SS models based on the effective strength parameters in combination with the limitation of the models to reproduce adequately the behaviour of an OC soil may result in an undrained shear strength profile which deviates from the s_u that the soils exhibits in the field. In addition, this study suggests the importance of considering the strain level dependency of the N_{kt} value for the resulting s_u based on a CPT. In other words, the derived value of the N_{kt} will be different if the $s_{u(OC)}$ is determined from the service conditions strain levels, the peak or the critical state and in turn this affects the s_u determined from a CPT due the $s_{u(CPT)} = q_{net} / N_{kt}$.

The study points out that both the strain level dependency of the strength parameters and the selection of the constitutive model at critical loading influence the results in terms of the developed failure plane and the FoS, especially in the case of Green dikes.

The study also elaborates the response of the models in regard to the design requirements for the calculation of displacements and the structural forces. Finally, this study answers the knowledge gap regarding how the strain level influences the strength of the examined soils and how this should be translated in the design along with the explanation on the effects of the selected constitutive model on the results.

List of symbols / Acronyms

Acronyms

A = Active
ADP = framework for describing the active, passive and direct simple shear model of loading below a dike body.
$C_{KO}UC$ = anisotropically consolidated undrained triaxial compression tests
$C_{K0}UE$ = anisotropically consolidated undrained triaxial extension tests
CRS = constant rate of strain test
CPT= cone penetration test
CPTu = cone penetration test which measures the generated pore pressures
CSSM= Critical State Soil Mechanics
DSS = direct simple shear
FEM = Finite Element Method
FoS= Factor of Safety
HS = Hardening Soil Model
KIJK = Krachtige IJsseldijken Krimpenerwaard
LI = Liquidity Index
LRT3 = 3rd National Testing Round
MC = Mohr Coulomb
NAP = measurement in meters from sea level in the Netherlands
NC = Normally Consolidated
NGI = Norwegian Geotechnical Institute
SS = Soft Soil Model
SFmin = Minimum Safety Factor
ΣMsf = factor of safety (PLAXIS)
SHANSEP = Stress History and Normalized Soil Engineering Properties
St = sensitivity
TXC =triaxial compression tests
TXE = triaxial extension tests
P = Passive
PI = Plasticity Index
POV = Project Overstijgende Verkenningen
POV-M = Project Overstijgende Verkenningen Macro-stability
Pw = Excess Pore Pressures
OC = Over Consolidated
WBI = Legal Assessment Instruments

Notations - Latin letters

c' = effective cohesion
e = void ratio
e_o = initial void ratio
E_{50} = secant modulus obtained from the 50% of the maximum deviatoric stress
E_{oed} = tangent oedometric modulus
E_i = is the initial secant stiffness
E_{50}^{ref} = Secant stiffness in standard drained triaxial test

E_{oed}^{ref} = Tangent stiffness for primary oedometer loading
E_{ur} = unloading reloafing young modulus
E_{ur}^{ref} = Unloading/reloading stiffness
F_{kt} min = minimum values of residues
G_{50} = shear modulus obtained from 50% of the maximum shear strength
G_{ur} = unloading reloading shear modulus
K_0 = coefficient of lateral earth pressure in over consolidation
K_0^{NC} = coefficient of lateral earth pressure in normal consolidation
m = strength increase exponent
n = number of tests
N_{kt} = empirical correlation factor
OCR_{min} = Minimum over consolidation ratio
p^0 = the initial value of the mean effective stress
p_c = preconsolidation pressure
p_{ref} = refferense pressure
POP_{min} = Minimum pre-overburden pressure
q_t = the corrected tip resistance
q_c = the CPT tip resistance
R^2 = Reliability index
R_f = Failure ratio qf/qa
s_u = undrained shear strength
s_u^A = active undrained shear strength
$s_u^A{}_{inc}$ = Increase of shear strength with depth
$s_u^A{}_{ref}$ = Reference plane strain active shear strength
$s_{u\ min}$ = Minimum undrained shear strength
$s_{u,I}$ = the undrained shear strength from laboratory tests consolidated with in situ stresses at the depth i
s_u^{DSS} = undrained shear strength in direct simple shear
s_u^P = passive undrained shear strength
$S_{(NC)}$ = normalized undrained shear strength ratio under NC conditions
$S_{(OC)}$ = normalized undrained shear strength under OC conditions
$S_{(NC)\ or\ (OC)\ 25,\ 40\%}$ = normalised strength obtained from the critical state strain levels
$S_{(NC)\ or\ (OC)\ 2,\ 5\%}$ = normalised strength obtained from the service conditions strain levels
$t_{0.1;\ n-1}$ = the 10% value of the Student-t distribution
u_2 = the pore pressure measured behind the cone shoulder (u_2) position
v' = poisons ratio
y_{ref} = reference depth
v_{ur} = the unloading reloading poison ratio
VC_{Nkt} = standard deviation of the Nkt value
W = water content
Xaverage = the average value of parameter x
xkar = the characteristic 5% lower limit value of parameter x

Notations - Greek Letters

$α$ = the data distribution parameter
$β_{eis;dsn;Geo}$ = required reliability index at a cross section level
$γ_b$ = schematization factor

γ_d = model factor

γ_f^c = shear strain at failure in compression

γ_f^E = shear strain at failure in extension

γ_f^{Dss} = shear strain at failure in direct simple shear

γ_{sat} = saturated unit weight of the soil

γ_n = material factor

γ^{PS} = the plastic strain hardening parameter

Δu = Excess Pore Pressures

ε_1 = axial strain

ε_v = volumetric strain

ε_v^0 = the initial volumetric strain

κ^* = Modified swelling index

κ_1 = hardening parameter NGI-ADP

λ^* = Modified compression index

σ'_{vc} = effective vertical consolidation stress (kPa)

σ'_p = preconsolidation pressure

σ_{vm} = consolidation stress applied for the determination of $S_{(NC)}$

σ'_3 = principal horizontal effective stress

σ'_v = vertical effective stress

σ_{yy} = vertical consolidation stress symbolism in the DSS in the STF (PLAXIS)

σ_{xx} = horizontal consolidation stress symbolism in the DSS in the STF (PLAXIS)

σ_f = vertical stress at failure

σ_t = Tension cut-off and tensile strength

$\sigma_{tension}$ = Tensile strength

σ'_h = horizontal effective stress

σ_{v0} = the total vertical stress

ΣMsf = factor of safety

τ = shear stress

τ_f = shear stress at failure

τ_0 = initial mobilization

φ = (Effective) angle of internal friction

φ_{cv} = critical friction angle

$\varphi_{cv\ 25,\ 40\%\ kar}$ = Friction angle determined from the critical state strain levels

$\varphi_{cv2,5\%}$ = Friction angle determined from the service conditions strain levels

ψ = Angle of dilatancy

Chapter 1 - Introduction

1.1 Background

The protection against flooding is vitally important in the Netherlands since a large proportion of the land lies below sea level and major rivers among which Rhine and Meuse flow through the country on their way to reach the sea. This makes about 60% of the country susceptible to flooding (Vergouwe, 2016). Earth structures such as dikes compose the primary protection of the country and therefore there is a constant attempt for enhancing the knowledge on the complex phenomena governing their behaviour. To this end, necessary innovations are taking place regularly and the safety standards are continuously updated.

In order to obtain the necessary support for these innovations, the National Flood Protection program (Hoogwaterbeschermingsprogramma or HWBP) along with the water boards and several research institutes initiated the cross-project explorations (in Dutch: Project Overstijgende Verkenningen - POV). The purpose of the POV is to reduce knowledge gaps in dike reinforcement projects and to provide uniformity over the projects with the final goal to establish safety standards, which enable better, faster and cheaper designs. From the dike safety program VNK (Veiligheid Nederland in Kaart) it was pointed out that macrostability of dikes is of critical importance in the safety analysis. Correspondingly, a recent study from the Rijkswaterstaat (Ministry of Transportation, 2013) revealed that several dike sections throughout the Netherlands are prone to macro-instability (Figure 1). Considering that the macro-instability of dikes can lead to severe outcomes (e.g. fatalities and economical losses) a separate cluster originated explicitly dealing with this phenomenon. The goal of the POV-M (POV-Macrostability) is to tackle this failure mechanism in a more efficient manner and to optimize the design guidelines for its examination.
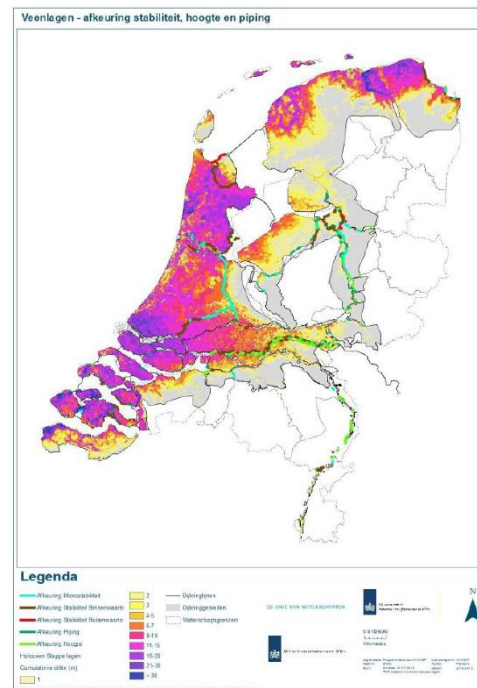
Figure 1: Rejected section on macro-instability (inward shaded in brown, outward shaded in red). (Rijkswaterstaat, 2013)

The efficiency in the design is achieved through the development of concrete and unequivocal guidelines with the ultimate goal of obtaining reliable, non-overconservative results. The coupling between the efficiency and the reliability is accomplished through a semi–

probabilistic analysis. In this way model uncertainties (e.g. loads, strength and stiffness of the materials) are counteracted by the use of partial factors. Therefore, the developed guidelines established from the POV-M are meant for assessing the dike stability through a series of consecutive steps which incorporate the use of partial factors when it is necessary.

According to the POV-M (2018) there is a distinct difference in assessing the macrostability of dikes with structural elements "Blue dikes" and the dikes without structural elements "Green dikes" since the safety assessment and design of Blue dikes incorporates the use of structural components. A brief overview regarding the strength characteristics of the Green and Blue dikes used in the safety assessment along with a synopsis of the current design methods proposed by the WBI 2017 which are relevant for this study are provided in Subchapter 1.2. The motivation and the objectives of this study will be described in Subchapter 1.3. The methodology and the contents of the thesis are given in Subchapter 1.4. Finally, the Chapter 1 concludes with the research contents and the research boundaries which are given in subchapters 1.5 and 1.6 respectively.

1.2 Current Practice

According to the WBI 2017 the assessment of the Green dike stability is performed under undrained conditions. This implies that the response of clays and peats which exhibit low values of permeability and are located below the phreatic line, should be assumed undrained. For the Green dikes the strength characteristics of the soils are derived from the critical state of the soil since it provides a more realistic approach to the soil strength behaviour (Zwanenburg, 2015). In addition, the undrained shear strength profile of the dike is assessed based on the SHANSEP (Stress History and Normalized Soil Engineering Properties) framework (Ladd and Foott, 1974). This concept benefits from a theoretical framework to relate the over consolidation ratio (OCR), and the normalised shear strength (s_u/σ'_{vc}) of the soil (Seah and Lai, 2003) (Eq. 1). In this way, a good replication of the field conditions that the soil experiences in its current and future stress state can be achieved.

$$s_u = \sigma'_{vc} \, S_{(NC)} OCR^m \qquad\qquad\qquad (1)$$

where:
- s_u : undrained shear strength (kPa)
- $S_{(NC)}$: normalized undrained shear strength ratio under NC conditions (-)
- σ'_{vc} : effective vertical consolidation stress (kPa)
- OCR : over consolidation ratio (-)
- m : strength increase exponent (-)

The approach described above is directly linked with the updated procedure of determining the soil properties from laboratory tests. The current guideline (WBI 2017) suggests that for clays single stage anisotropically consolidated triaxial tests should be executed ($C_{K0}UC$). The applied K_0 (the ratio between σ_h'/σ_v') consolidation is equal to 0.45 for clays with a volumetric weight of the soil higher than 14 kN/m^3 while the K_0 is equal to 0.35 for clays with a volumetric weight lower than 14 kN/m^3 (van Duinen, 2014). Some of the soil samples are consolidated beyond the maximum preconsolidation pressure that the soil experienced in the field to achieve a normally consolidated (NC) state. The other samples are consolidated with in-situ stresses, thus maintaining their over-consolidated (OC) state.

In the case of peats, single stage constant volume direct simple shear tests are applied for both NC and OC conditions. The soil samples that are consolidated beyond p_c are used for the determination of $S_{(NC)}$. The $S_{(OC)}$ is estimated based on the soil samples consolidated with in-situ stresses which is later combined with the OCR (σ'_p / σ'_{vc}) of the same soil sample which is obtained from one dimensional compression tests (oedometer or CRS tests). The estimation of σ'_p is achieved by applying the empirical methods, such as Casagrande.

Upon derivation of $S_{(NC)}$, $S_{(OC)}$ and the OCR the SHANSEP curve can be established (Figure 2). The resulting m parameter is calculated based on the produced power regression line. More information regarding the CSSM (critical state soil mechanics) and the SHANSEP concept is given in subchapters 2.3 and 2.4 respectively. The detailed derivation of the normalized S parameter and the strength increase exponent m parameter are given in subchapters 3.2.1 and 3.2.2.
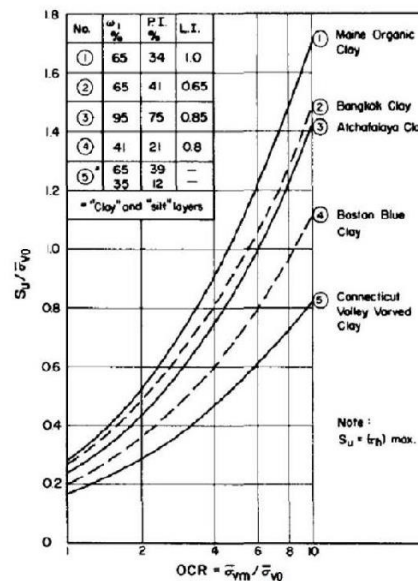
Figure 2: SHANSEP curve for five different clays. (Ladd and Foott, 1974)

According to the WBI 2017, the strength parameters in the critical state are determined from 25% strain level for clays under triaxial conditions while for peats at 40% strain level under DSS conditions. Similarly, with the Green dikes the global safety of the Blue dike is assessed under undrained conditions (POVM, 2018) with the use of CSSM.

In addition, the current calculation methods incorporate the use of the Finite Element Method (FEM) through the PLAXIS software. The use of the FEM enables the improved examination of the displacements as well as the calculation of structural forces under normative and limit state conditions. This is further accomplished with the use of the recently developed user defined soil model (UDSM) based on hardening plasticity, namely the SHANSEP NGI-ADP model. In this model, the SHANSEP concept (Ladd and Foott, 1974) is applied in the standard NGI-ADP model. Therefore, the effect of stress history and stress path characterizing the undrained shear strength can be considered. Furthermore, the NGI-ADP model is intended for anisotropic undrained soil strength conditions (Panagoulias and Brinkgreve, 2017). The anisotropy in the NGI-ADP model is captured through the different undrained shear strength profiles for active (A), direct simple shear (DSS) and passive (P) loadings. These undrained shear strength profiles are given as input parameters along with their corresponding shear strains at failure (γ_f^c, γ_f^E, and γ_f^{Dss}). More information regarding the NGI-ADP model is given in subchapter 3.1.3.

1.3 Motivation and research objectives

The National Flood Protection program (HWBP) periodically applies safety assessments to ensure that the primary flood defences in the Netherlands meet the safety standards. During the 3rd National Testing Round (LRT3), held by the Hoogheemraadschap van Schieland and Krimpenerwaard it was established that **a large portion of the Hollandsche IJsseldijk on the Krimpenerwaard side failed a macrostability assessment of its inner lope.** The dike is located in relatively densely populated areas and has a length of approximately 10 km. It lays upon soft soils, such as organic clays and peats. Strengthening the KIJK (Krachtige IJsseldijken Krimpenerwaard) dike is a challenging process since numerous structures and monumental buildings are constructed along its length. Additionally, the dike forms an important connection for cars, bikes and cargo transport.

Given the described conditions of the dike (i.e. lack of space) it can be concluded that the most versatile and appropriate reinforcement technique is the use of (un)anchored sheet pile walls. Thereby, the lack of space is becoming a less of an issue for the design. In addition, with the use of specific design methods (e.g. front face of sheet pile wall covered with bricks) the preservation of the high aesthetics describing the area can also be achieved.

At the start of year 2015 a detailed site investigation along the total length of the KIJK dike was initiated. The soil investigation consisted of CPTs, CPTu´s and borings. Samples were retrieved from various depths from the crest and the toe areas of the dike. Thereafter, the soil samples were subjected to one dimensional compression testing as well as to shear tests following the protocol given from the WBI 2017. Additionally, in some of the clayey samples Atterberg limits are determined.

It is worth mentioning that the KIJK project is identified as one of the pilot projects that implements the new guidelines (Visschedijk, 2018), The first aspect lies on the fact that all the executed laboratory tests fall into the framework of the most updated protocol for determining the strength-stiffness parameters of the soil. Secondly, the assessment of the global safety of the dike without structural elements is based on the new guidelines (WBI 2017). Thirdly, the project also offers the opportunity for the utilization of the advanced constitutive model SHANSEP NGI-ADP in the analysis of the dike which is strengthen with the use of structural elements.

When using the finite element method, the KIJK dike safety assessment and design need to follow the recently introduced POV-M 2018 guidelines. This guideline includes a series of steps that need to be followed for the examination of the KIJK dike with and without structural elements. These steps are applied successive phases which are implemented in the stage construction mode in PLAXIS with the final aim to examine the FoS (factor of safety) at critical loading under undrained conditions. On top of that, this project offers a great opportunity for the comparison of the SHANSEP NGI-ADP constitutive model with other fundamental isotropic constitutive models such as Hardening Soil (HS) and Soft Soil (SS) which are commonly used in engineering practice. Moreover, the HS and SS models are used in the calculation schemes proposed by POVM 2018 for assessing the dike stability with the use of finite element method. In this study, the undrained shear strength conditions for the HS and SS models are captured through the Undrained A option. More information regarding the Undrained A option will be given in Chapter 3.1.4.

By taking into consideration the addressed information in the current and previous subchapters the following research objectives arise.

Main Objective 1

> *To determine the required input parameters (strength – stiffness) for the SHANSEP NGI-ADP, Hardening Soil (HS) and Soft Soil (SS) constitutive models from laboratory tests executed under the updated protocol (WBI 2017).*

Based on the main objective 1, the following questions should be addressed:

> *Determine the strength parameters from the service conditions strain levels and the "critical" state strain levels. How does the strain level influence the strength of the examined clays and peats and how should this be translated in the design?*
> *After the application of the two proposed methods given by the WBI 2017, what are the differences in the resulting value of the strength increase exponent m and which method is recommended for use in the design?*
> *Which soil input parameters of the constitutive models incorporate the highest uncertainties and difficulties for their determination considering the WBI 2017 protocol?*
> *What is the influence of applying the same K_0 value on the resulting undrained shear strength and the stiffness, in both the normally consolidated (NC) and over consolidated (OC) soil samples? How does this affect the results?*

Main Objective 2

> *Examine the macrostability of the Green dike with the proposed guidelines from POV-M, 2018 based on the strength parameters derived from the critical state of the soil.*
> *Examine the macrostability of the Blue dike with the proposed guidelines from POV-M, 2018 based on the strength parameters determined from the service conditions strain levels of the soil.*

Sub question of main objective 2

> *What are the response of the considered constitutive models regarding the safety factor, the developed failure mechanisms, the resulting displacements as well the forces acting on the sheet pile wall (in the case of Blue Dike)?*
> *What is the influense of the strain level dependency of the strength parameters in the desing analysis of the "Green" and the "Blue" dike?*

1.4 Methodology

The initial step for the realization of this study is the interpretation of the available laboratory executed under the new protocol given in the WBI 2017. The analysis of these data served as a basis for the estimation of the required strength and stiffness parameters for the considered constitutive models.

The strength parameters of the soil are determined from the service conditions and the critical state strain levels. In this way, a direct comparison between the two can be established for both peat and clayey type of soils. Factors such as versatility of estimating the input parameters for the considered models along with the issues encountered upon derivation and recommendations are addressed. Special attention is attributed to the S and m parameters obtained from small strain levels since this proposed examination is one of the research objectives

of the study. In addition, the estimated parameters are subjected to further examination through the SoilTest facility in PLAXIS with the goal to optimize and verify the estimated stiffness parameters. Furthermore, the influence of the K_0 value in the resulting parameter determination is assessed through the SS and HS constitutive model with the use of the SoilTest facility and the available literature. Afterwards, based on the available site investigation data a two-dimensional configuration of a cross-section across the KIJK dike is created. Subsequently, the cross-section is examined under the frameworks and guidelines proposed from POV-M for both Green and Blue dikes. The results based on the considered constitutive models in terms of the obtained safety factor, developed failure mechanisms and generated displacements are presented. In addition, the modelling issues encountered upon the application of the recently introduced guidelines are addressed. Moreover, the investigation of the strength level dependency of the strength parameters in the design for both the Green and the Blue dike is discussed. Lastly, the flowchart as presented below (Figure 3) provides an overview of the methodology applied for this study.
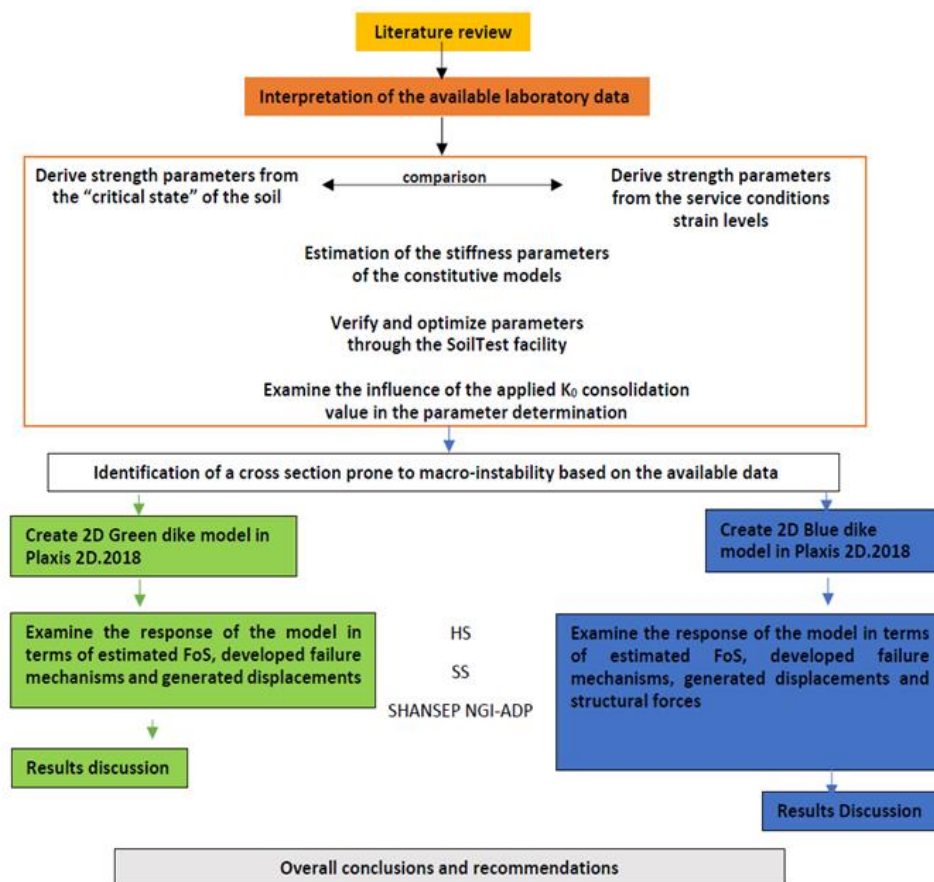
Figure 3 Flow-chart illustrating the methodology steps for the realisation of this study.

1.5 Thesis outline

The thesis outline is structured as follows:

> ➢ *In Chapter 1 the study background is presented along with the formulated research objectives and the methodology applied for this study.*

➢ *In Chapter 2 the literature review is given. Initially the motivation behind the switch to the undrained analysis is addressed. Afterwards, emphasis is given to the factors which influence the undrained shear strength and are relevant for this study (e.g. normalized behaviour, strength anisotropy). Then, the critical state concept and the SHANSEP framework are introduced followed by a brief elaboration on the macrostability failure mechanism together with the benefits using the sheet pile wall as a dike reinforcement technique. This chapter concludes with the geotechnical conditions of the KIJK dike.*

➢ *In Chapter 3 the full derivation of the strength and stiffness parameters for the considered constitutive models is presented along with further calibration of the soil stiffness parameters through the SoilTest Facility in PLAXIS. Prior to the parameter determination, the applied constitutive models are briefly described.*

➢ *In Chapter 4 the Green dike analysis is presented. This chapter is divided into three sections. The first section elaborates the design guidelines along with the information regarding the selected cross-section (i.e. geometry, water levels, mesh). In addition, the partial factors used for the analyses are explained. The second section focusses on the results obtained in terms of the factor of safety, developed failure mechanisms and generated displacements. Lastly, in the third section the conclusion of Chapter 4 are given.*

➢ *In Chapter 5 the Blue dike analysis is presented maintaining a similar format of analyses as that of Chapter 4.*

➢ *In Chapter 6 the overall conclusions of the study along with future research recommendations are addressed.*

1.6 Boundaries and Limitations

To achieve the research objectives of the presented study some boundaries are set as follows:

➢ *For this study, the analyses in terms of the safety factor and generated displacements are established explicitly with PLAXIS finite element code. The decision is considered reasonable since all the instructions and examples described in the POV-M 2018 are based on PLAXIS. Another compelling argument for this decision lies on the fact that PLAXIS is capable for assessing both the Green and Blue type of dikes.*

➢ *Being mostly interested in the critical event of the system the response of the dike and the comparison of the considered models is investigated only under critical loading conditions.*

➢ *Only the NGI-ADP model is capable of modelling the anisotropic strength conditions of the soils. The rest of the models presented herein cannot account for soil strength anisotropy. In addition, none of the considered models accounts anisotropy in terms of soil structure and physical properties.*

➢ *Time dependent deformation is not considered. The decision is considered reasonable mainly for two reasons: a) according to POVM 2018 the examination of the influence of time dependent deformation is necessary for horizontally placed longitutinal structures (e.g. geosynthetics), b) as a result of creep the apparent OCR increases which influences the resulting s_u based on the SHANSEP formulation. Thus, research is needed which will explicitly deal with this phenomenon.*

Chapter 2 – Literature review

In this chapter, the motivation behind the switch to the undrained analysis is presented. Factors governing the undrained shear strength of the soil relevant for this study are discussed. Afterwards, the CSSM and the SHANSEP framework are introduced, followed by the information regarding the macrostability of the dikes along with the benefits of using sheet pile walls as a dike reinforcing technique. The chapter concludes with the presentation of the geotechnical characteristics of the KIJK dike in combination with the reasons behind the selection of the dike cross section used for the analysis.

2.1 Switching to undrained analysis

In the Netherlands, a major contribution for updating the existing knowledge of dike behaviour along with the advancement of the design guidelines and calculation methods originates from the regular imposed full-scale trial tests applied in several dikes across the country. The purpose of these tests is to reduce the knowledge gaps related to the instability of the dikes as well as to enlighten the interaction behaviour of the dike with various types of structural elements.

As it concerns the stability of the dikes, one notable conclusion derived from these trial tests is that the dikes may become unstable upon shearing in relatively fast periods of time. In the macrostability test at the IJkdijk the instability occurred within few minutes after the first noticeable deformation. Similarly, in the Bergambachtproef the largest deformation developed within an hour, while in the Streefkerk test in 1984, the largest deformation took place within one day period (van Duinen, 2014).

The described durations are very short in time in relation with the permeability of the soils located at these areas. The soils consist of clays, organic clays and peats. Given the low permeability of these soils in comparison with the duration of the imposed shear, the response is classified as undrained. In short, the undrained behaviour occurs in soils which exhibit very low values of permeability (i.e. clays) and are subjected to relatively fast rate of shearing. This results in the generation of excess pore pressures which can dissipate over time. Thus, for the soils located at these areas no pore pressure dissipation occurred at the time of interest. In addition, the back analysis of the collapsed dikes displayed an overestimation of the shear strength of the soil using the existing working methods based on the drained shear strength. The degree to which the shear strength overestimated was in a factor ranging from 1.4 to 2 times the available shear strength. In contrary, when the undrained shear strength applied for the examined clays, organic clays and peats, the analysis provided a realistic response of the available strength and the actual shear displacements generated in the field (van Duinen, 2014).

Despite the overall benefits of the undrained analysis, many studies done throughout the years e.g. (Bjerrum, 1973; Jamiolkowski, 1985; Ladd and DeGroot, 2003) revealed that the determination of undrained shear strength (s_u) is rather a challenging process. Besides the dependency of s_u in numerous properties of the soil (e.g. water content) the s_u is further affected by several physical factors, among which, the preconsolidation pressure (normalized behaviour and stress history of the soil), the direction of loading, the rate of strain, and the creep-aging effects.

2.2 Strain compatibility and strength anisotropy

Ladd and DeGroot (2003) emphasized the importance of considering the effect of strain compatibility since, the maximum mobilized strength in triaxial compression, direct simple shear and triaxial extension tests occurs at different strain levels (Figure 4). Typically, the maximum mobilized shear strength in normally or nearly normally consolidated clays in triaxial compression occurs at small strain levels followed by strain softening. Figure 4 also suggests that in the other modes of shearing, the peak strength is reached at larger strains. In general, the direct simple shear strength lies in the middle of triaxial compression and triaxial extension with the triaxial extension being the lowest. The described behaviour is attributed to the strength anisotropy of the soil. It should be noted the data illustrated in Figure 4a concern an AGS plastic marine clay (Ladd, 1991) and 4b concern a soft Norwegian clay (Karlsrud and Hernandez-Martinez, 2013)
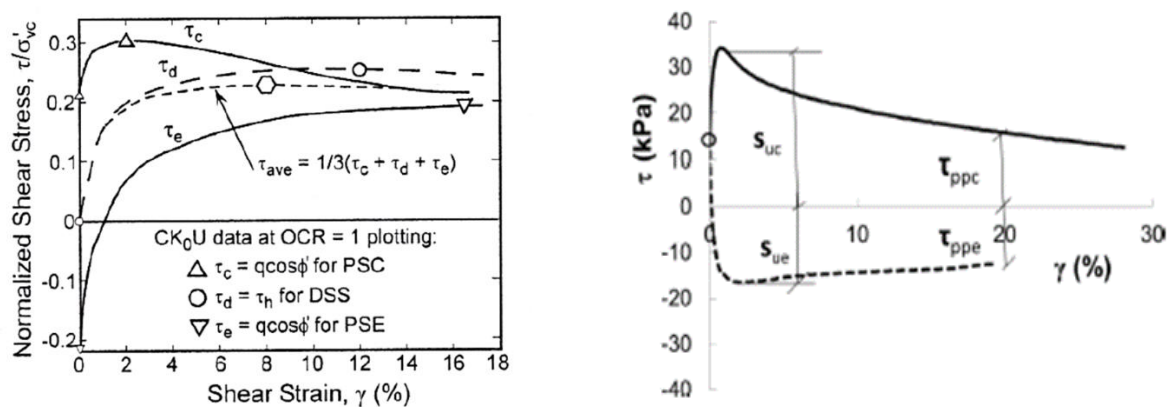
Figure 4: (a)Stress strain response under different modes of shearing (Ladd and DeGroot, 2003), (b) stress strain response in triaxial compression and extension (Karlsrud and Hernandez-Martinez, 2013).

The undrained shear strength anisotropy is a widely known factor which has been reported from various researchers, for example Bjerrum (1973) and Ladd and DeGroot (2003). According to Bjerrum (1973) the anisotropy can be divided in two components. One component is the inherent anisotropy, which is the outcome of extensive differences in the soil structure that arise during the geological formation of the soil. Oblong and flaky particles tend to become oriented in a horizontal direction during one-dimensional deposition and subsequent loading. Clays that have alternate layers of silt and clay have a high degree of inherent anisotropy (Lofroth, 2008). Fissured clays are also governed from inherent anisotropy because fissures are planes of weakness (Duncan et al., 2014). The other component is the stress induced anisotropy, which occurs from the fact that effective consolidation stresses are not equal in all directions since the coefficient of earth pressure at rest for normally consolidated soils (K_0^{NC}) is not equal to 1.

The combined result of inherent and stress induced anisotropy is that the undrained shear strength of clay varies with the orientation of the principal stress at failure and with the orientation of the failure plane (Duncan et al., 2014).

Bjerrum (1973) proposed a simple approach to model the varying anisotropic undrained shear strength along a slip surface (Figure 5). The approach suggests measuring the undrained shear strength from test types, which are relevant in different locations of the potential failure surface. This approach is called "ADP", where "A" stands for active, "D" for direct shear and "P" for passive. Near the top of the shear surface (active zone), the major principal stress at failure is vertical, and the shear surface is oriented about 60 degrees from horizontal. In the middle part

of the shear surface, where the shear surface is horizontal (direct simple shear), the major principal stress at failure is oriented about 30 degrees from horizontal. At the toe of the slope (passive zone) the major principal stress at failure is horizontal, and the shear surface is inclined about 30 degrees past horizontal.
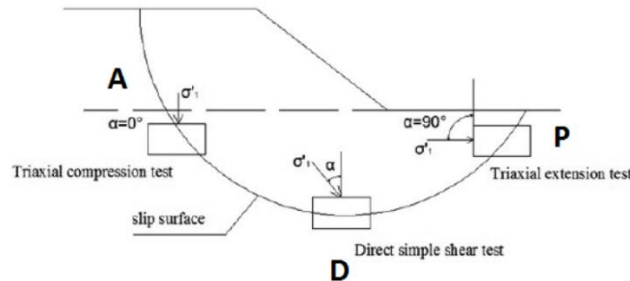
Figure 5: Simplified elaboration of the different modes of shearing below and next to the dike. (Ukritchon and Boonyatee, 2015)

Anisotropy can be reliably measured in the laboratory through triaxial (or plane strain) compression and extension tests together with direct simple shear tests, provided that the soil specimens are anisotropically consolidated, before shearing, at stress level representative of the in-situ conditions (Bjerrum, 1973). The anisotropic consolidation of the soil samples ensures that the stress conditions applied to the samples are replicating the in-situ regimes in a more realistic manner.

In Table 1 the values of undrained shear strength ratios s_u^{DSS} / s_u^A and s_u^P/s_u^A for several clays from different studies are summarized. There is a fairly high variability of the anisotropic undrained shear strength ratios with the values ranging from 0.30 to 0.81 for s_u^P/s_u^A and from 0.53 to 0.89 for s_u^{DSS} / s_u^A. In Table 1 the w denotes the water content whereas the PI the plasticity index of the clays.

Table 1: Values of anisotropic undrained shear strength ratios for clays. (D'Ignazio, 2016)

Authors	Soil Type	s_u^{DSS} / s_u^A	s_u^P/s_u^A
Jamiolkowski et al. (1985)		0.53 − 0.79	0.51 − 061
Ladd (1991)		0.72 − 0.89	0.50 − 0.81
Karlstud et al. (2005) (Norwegian clays) w = 25 to 70%, IP = 10 to 50%		0.60 − 0.80	0.30 − 0.55
Lunne and Andersen (2007) w = 28 to 67%, IP = 6 to 43%	Clays	0.78 − 0.82	0.59 - 0.65
Karlsrud and Hernandez Martinez (2013), Norwegian low sensitive clays (St < 15) w = 25 to 75%		0.57 − 0.82	0.30 − 0.52
Karlsrud and Hernandez – Martinez (2013), Norwegian sensitive clays (St > 15) w = 25 to 56%		0.56 − 0.66	0.22 − 0.32
Thakur et al. (2014b) Norwegian clays PI < 10%		0.63	0.35
Thakur et al. (2014b) Norwegian clays PI > 10%		0.63 − 0.80	0.35- 0.50

Table 2: Values of undrained shear strength ratios based on literature for peats.

Authors	Soil Type	s_u^A / σ'_{vc}	s_u^{DSS}/ σ'_{vc}	s_u^P/ σ'_{vc}
Yamaguchi et al., 1985		0.53 − 0.55		0.8
Zwanenburg and Jardine 2015	Peats	0.44 − 0.70	0.47	
Hanzawa et al. 1994		0.45		
Edil and Wang (2001)		0.40-0.77		

Moreover, from Table 1 it can be observed that the clays exhibit strength anisotropy and typically the direct simple shear strength of clays lies in the middle of the active and passive strength with the passive being the lowest.

It has to be mentioned that many studies have been conducted regarding the strength anisotropy of soft cohesive soils concerning clays. For peats, the studies regarding the material anisotropy are still limited.

Peat is mainly composed of fibrous organic matters i.e. partially decomposed plants such as leaves and stems and shows unique mechanical properties in comparison with clays and silts (Yamaguchi et al., 1985). The stiffness and strength characteristics of peats are governed by the presence of fibers and their properties. The quantity, the properties and the orientation of fibers act as a reinforcement providing additional strength to the soil inducing anisotropy. Yamaguchi et al. (1985) reported that the undrained deformation and the strength properties of the examined peats with a contained organic matter ranging from 10% to 80% experience a distinct difference upon shearing in extension and compression. It was found that the dominance of the anisotropic fibers remained after the end of consolidation causing a considerable difference in the shear phase under compression and extension loadings. Lastly, it was indicated that the undrained shear strength properties of peat can be normalized with consolidation stress for both extension and compression mode and the values are given in Table 2.

Edil and Wang (2001) found out that the normalized undrained shear strength of anisotropically consolidated peats and isotopically consolidated peats show no apparent differences and give an average value of 0.59 (Figure 6a). Furthermore, it was reported that fibrous peats are governed with higher values of normalized undrained shear strength in comparison with amorphous peats and organic soils (Figure 6b). Another outcome of their research is that the K_0^{NC} of peats varies with organic content where the fibrous peats exhibit a typical value of 0.3 while the amorphous peats have a higher value equal to 0.5 (Figure 7a and 7b).
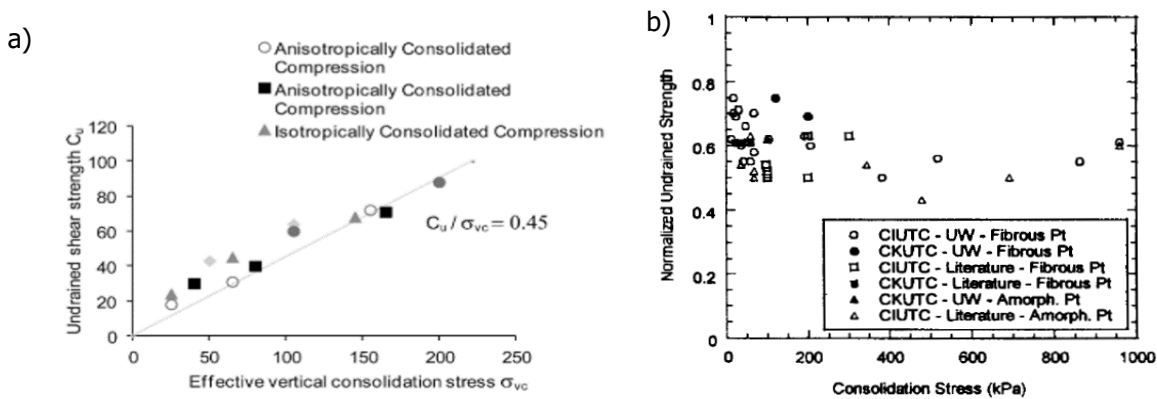
Figure 6: (a) Illustration of the uniform values obtained from $C_{KO}UC$ CIUC tests on peats (after Edil and Wang, 2001), (b) The graph shows the typical international su/σ'vc gathered values obtained for fibrous and amorphous peats.
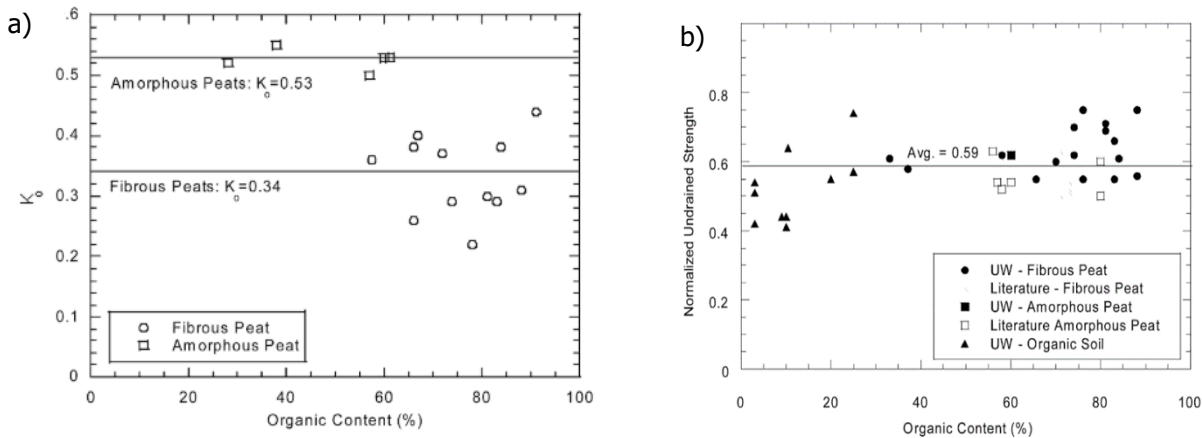
Figure 7: (a) Illustration of the K_0^{NC} value of fibrous and amorphous peats, (b) Demonstration of the variation of the peats and organic soils with organic content (after Edil and Wang, 2000).

After conducting a full-scale test on peat layers Zwanenburg and Jardine (2015) reported that the normalized undrained shear strength obtained from isotropic compression tests in peats showed an average value of 0.60 while the mean value obtained from DSS was around 0.47 reflecting also the shear strength anisotropy of Dutch peat soils as presented in Table 2.

Coming back to the strain compatibility, another important characteristic is that at large strains, where the ultimate shear strength (or critical state strength) of the soil is reached, the various modes of shearing exhibit comparable values as illustrated in Figure 4. With the presupposition that the shear strength is mobilized along the entire slip circle (van Duinen, 2014) in the WBI 2017 the undrained shear strength is better described from a normalized undrained shear strength ratio (S), obtained from the critical state of the soil. For clays the S value is obtained from 25% strain level with triaxial compression whereas for peat from 40% strain level with direct simple shearing. At these strain levels, the clayey material experienced the softening behaviour while the peat reached the maximum shear strength. Therefore, the effects of strength anisotropy are becoming less significant.

In the case of an existing dike design according to Zdravković and Jardine (2001) and POV-M (2018) the effect of pre-shearing has to be taken into consideration. The effect of pre-shearing is a result of the rotated principal stresses under and the crest and the slope of the dike. This results in a higher mobilized strength in the soil below the dike than the unloaded soil next to the dike. The pre-shearing influences the ADP framework proposed by Bjerrum (1973) since the ground in triaxial compression and DSS modes share approximately the same mobilized shear strength while the soil in passive mode does not experience any imposed shear. Moreover, according to van Duinen (2014) the effect of pre-shearing increases the peak strength potential of the soil but in case of surpassing it the soil experiences a rapid decrease of the strength. In other words, the effect of pre-shearing makes the soil behaviour more brittle. In its formulation the NGI-ADP model deals with the preshearing through the input parameter τ_0/s_u^A (initial mobilization). More information regarding the τ_0/s_u^A is given in subchapter 3.2.5. The effects of pre-shearing, the strength in the critical state and the ADP framework can be visualized in Figure 8 where the S (normalized s_u) vs the length of a sliding surface (L) is illustrated.
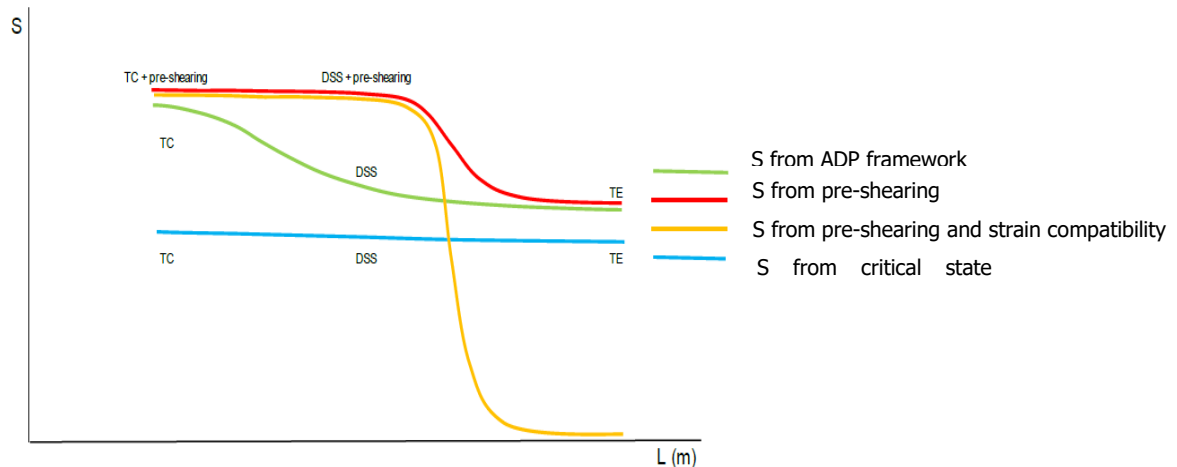
Figure 8: Simplified approach illustrating the different modes of shearing below the dike with taking into consideration the critical state (blue line), the strength anisotropy proposed from Bjerrum)green line, the effect of preshearing red line and the effect of preshearing with strain compatibility yellow line. Modified in English (after Visschedijk, 2018).

2.3 Critical State Soil Mechanics (CSSM)

The Critical State Soil Mechanics (CSSM) (Schofield and Wroth, 1968) is an effective stress framework describing the mechanical response of soils. It merely ties together the relationships between the shear stress, the normal stress and the void ratio of the soils. In other words, through critical state soil mechanics the interdependence of the soil behaviour in oedometer and shear loading is described. According to the WBI 2017 the macrostability of dikes has to be analyzed based on the critical state soil mechanics concept.

In its essence, the presupposition of the CSSM is that all soils irrespective of their initial state or drainage type strive towards and eventually end up in the critical state line. When reaching the critical state line, the soil does not exhibit any change in volume upon shearing.

Current practice in the Netherlands suggests that the determination of the φ_{cv} is accomplished after combining the data of NC samples obtained from several single stage $C_{K0}UC$ for clays and constant volume DSS for peats.

In Figure 9 the blue line represents the direct simple shear test failure envelope line through the measured value of the shear stress τ in the σ´ graph (tan φ = τ / σ´). For triaxial tests the failure envelope is given from the average of the principal stresses s´ and the half of deviatoric stress t. The values of s´ and t represent the peak of the Mohr circles (red line). Therefore, for determining the failure envelope a conversion is performed with t/s' = sin φ', as shown in Figure 9. Similarly, the conversion is applied and to the DSS assuming that the failure envelope is given from the peaks of the Mohr-circles (Potts et al., 1987; Farrell et al., 1999). Thus, the shear strength in critical state for both clays and peats is given based on the equation 2

$$t = s'sin\varphi_{cv} \tag{2}$$

More information regarding the derivation of φ_{cv} for the examined soils is given in subchapter 3.2.3.
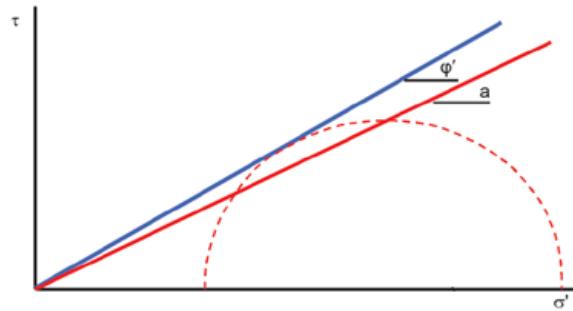
Figure 9: Conversion established from WBI 2017. (van Duinen, 2014)

Figure 10 shows a simplified example showing the behaviour of Normally Consolidated (NC) and Over Consolidated (OC) soils upon drained and undrained loading in the one-dimensional compression tests (σ'_v vs e) and stress path plots (σ'_v vs τ). The typical stress paths of the soils are denoted with the numbers 1,2,3,4 for the normally consolidated drained, normally consolidated undrained, over consolidated drained and over consolidated undrained behaviour of the soil respectively. It has to be noted that this simplified elaboration accounts only for the fully drained and undrained behaviour of the soil. No information is given for any other drainage conditions of the soils (semi undrained - drained).

Initially, the behaviour of a normally consolidated soil is illustrated in drained conditions (1). The soil experiences a contractive volume change where the initial void ratio e_o reduces to final void ratio e_f. In the τ, σ'_{vc} plot the soil follows a drained path (Δu=0) until it reaches the critical state line. In the case of an undrained loading of the same NC soil (2) there is no change in volume and the soil experiences the development of positive excess pore water pressures resulting in a lower $τ_{max}$ which equals to the undrained shear strength (s_u) of the soil. In the case of an over consolidated soil, the OC line is introduced (swelling line). In the drained behaviour (3) the soil experiences a dilative behaviour (increase in volume) while a drained path (Δu=0) response is followed in the τ, σ'_{vc} plot. Finally, in the case of an undrained loading of the same OC soil (4), no change in volume is experienced by the soil and negative excess pore pressures are generated leading to an undrained shear strength higher than the drained shear strength of the same OC soil.
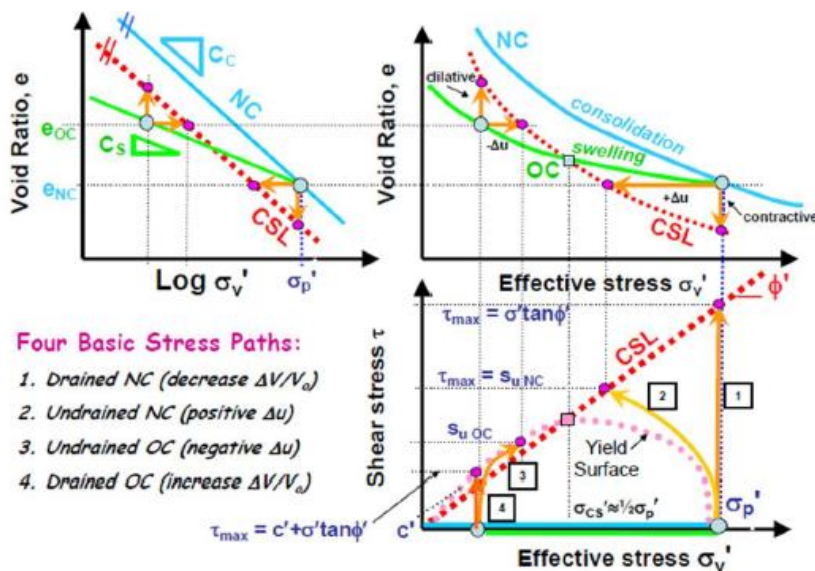
Figure 10: Common stress path in CSSM. (Tan et al., 2006)

The apparent conclusion from the illustrations presented in Figure 10 is that the undrained shear strength of a soil in normally consolidated conditions is lower than the drained strength. As stated in the subchapter 2.1, most of the dikes in the Netherlands are constructed with clayey materials and rest upon soft soils (organic clays and peats). The response of these soils is classified as undrained since they possess very low values of permeability preventing the pore pressure dissipation at the time of interest. Based on this and on factors such as strain compatibility the current guidelines require the macrostability of the dikes to be assessed under the undrained conditions with the strength obtained from the critical state of the soil.

2.4 SHANSEP framework

The complexity of the undrained shear behaviour of soft clays originated the motivation for developing a new design procedure for the stability of soft clays. The SHANSEP (Stress History and Normalized Soil Engineering Properties) framework was initially introduced by Ladd and Foott (1974) and later verified by several researches for instance Seah and Lai (2003) and Abdulhadi et al (2012).

Work done from the 1960´s to the present have proved the proposition of Ladd and Foott (1974) that most cohesive soils with identical over consolidation ratios (OCR) display normalized behaviour. Therefore, when the stress strain response of the clay material is normalized over the vertical consolidation stress, the resulting stress strains responses behave similarly (Figure 11).
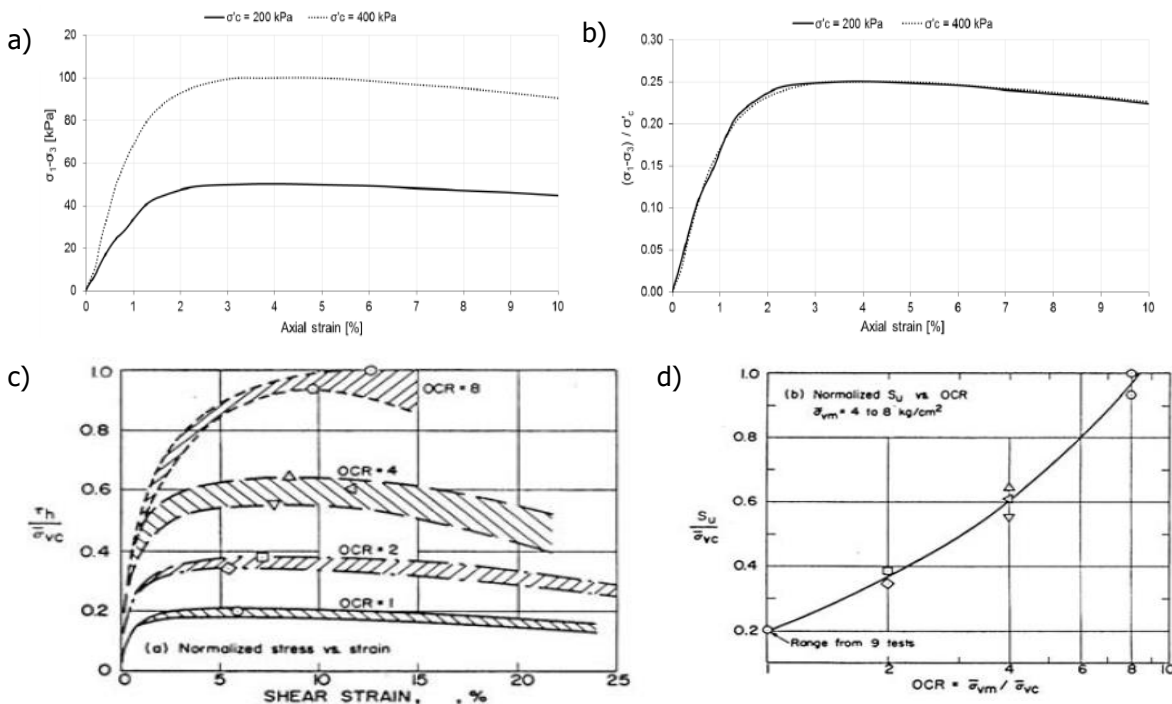
Figure 11: (a) Homogenous clay consolidated with σ'_c equals to 200 kPa and 400 kPa, (b) Illustration of the normalized behaviour of the homogenous clay (Ladd and Foott, 1974), (c) Illustration of the normalized behaviour of a homogenous clay under different over consolidated levels, (d) Normalized undrained shear strength against OCR (Ladd and Foott, 1974).

The undrained shear strength (s_u) for undrained soil layers based on the SHANSEP framework is calculated through:

$$s_u = \sigma'_{vc}\, S_{(NC)} OCR^m \tag{3}$$

where:
- s_u : undrained shear strength (kPa)
- $S_{(NC)}$: normalized undrained shear strength ratio under NC conditions (-)
- σ'_{vc} : effective vertical consolidation stress (kPa)
- OCR : over consolidation ratio (-)
- m : strength increase exponent (-)

Ladd and Foott (1974) proposed a list of necessary steps that needs to be followed to establish a valid examination of the SHANSEP parameters, as given below:

1. Select samples and use one-dimensional consolidation testing, to calculate properly the preconsolidation pressure (σ´p).
2. Using specimens from the same sample and anisotropically consolidate them with consolidation pressures 1.5, 2.5 and 4.0 times higher than the established σ´p.
3. These tests should show a constant relationship between shear strength and consolidation pressure (su/σ´vc). This should at least be true for the higher two pressures in the above steps. If not, the SHANSEP procedure does not apply and consequently, the Eq. (3) can no longer be used to describe the su in the field.
4. The pressure that shows a constant su/σ´vc relationship is selected as the laboratory consolidation pressure σvm.
5. The specimens are consolidated to the pressure equal to (σvm) and then allowed to swell to the known over consolidation ratio (OCR). After shearing these specimens, the S(OC) will be obtained, which is a necessary parameter for the derivation of the m parameter through the S (NC, OC) versus OCR plot as demonstrated in Figure 2.

The second step is crucial for the proper normalization of the examined soils. In Chapter 3 it will be explained that the selection of the correct consolidation stress can be proved critical for the correct estimation of the S and m parameters. Steps 4 and 5 were not applied in the series of the applied laboratory shear tests and the limitations of not following these steps will be described in Chapter 3.

According to Ladd and Foott (1974) the main advantage of the SHANSEP framework is the cost effectiveness due to the decrease in number and complexity of testing. Furthermore, once the S and m parameters are derived for a particular soil, the undrained shear strength can be calculated from the stress history that the soil exhibits in the field. The application of additional shear tests can redefine or optimize the normalized parameters S and m leading to a more accurate value of the undrained shear strength. Moreover, the SHANSEP procedure provides an understanding of the relationship between the gain in strength from the overconsolidation which will allow an accurate back calculation of the in-situ strength based on in-situ OCR's (Bay et al., 2005). The latter will be a point of interest in Chapter 4.

Despite the overall benefits, the normalized behaviour exhibits some limitations. Firstly, the normalized behaviour is not as perfect as illustrated in Figure 11. Quick clays and naturally cemented clays do not display normalized behaviour since the inherent soil structure is destroyed during consolidation. Moreover, the SHANSEP method can only be applied in high quality samples without any prior disturbance.

The relation between the CSSM and the SHANSEP framework is accomplished through the determination of the normalized S and m parameters from 25% or 40% strain levels for clays

and peats respectively. Lastly, in the case of the stability analysis of dikes with structural elements, the strength parameters need to be determined based on engineering strain levels, which are 2% or 5% for clays and peats, respectively. The determination of the S and m parameters according to this guideline will be elaborated in subchapters 3.2.1 and 3.22 respectively.

2.5 Macrostability of dikes towards hinterland

A dike slope can fail either towards the protected area (sliding of the inner slope) or outwards (sliding of the outer slope). However, this study is focused only on the macrostability assessment towards the protected area as illustrated in Figure 12. As already mentioned in the Introduction, the KIJK dike failed to comply the macrostability when assessed according to the new safety standards after a detail investigation from HWSP. The purpose of this subchapter is to present the macro-instability phenomenon and to briefly show the benefits of a stability measure by means of the sheet pile walls.

Macro-instability involves a large-scale stability problem. This implies that the generated failure concerns both the dike body and the soil layers underneath the dike. The macro-instability occurs when the maximum shear resistance of the soil in the developed sliding plane is lower than the driving load. The loss of balance occurs due to the high-water level events, periods of extensive rainfalls in combination with factors such as height of the dike, steepness of the slopes, strength of the subsoil etc. The rise of river water level causes a subsequent increase in the head of the aquiferous sand layer as well as the phreatic level inside the dike body. Consequently, the soil experiences a reduction in the effective stress resulting in a lower shearing resistance of the soil.
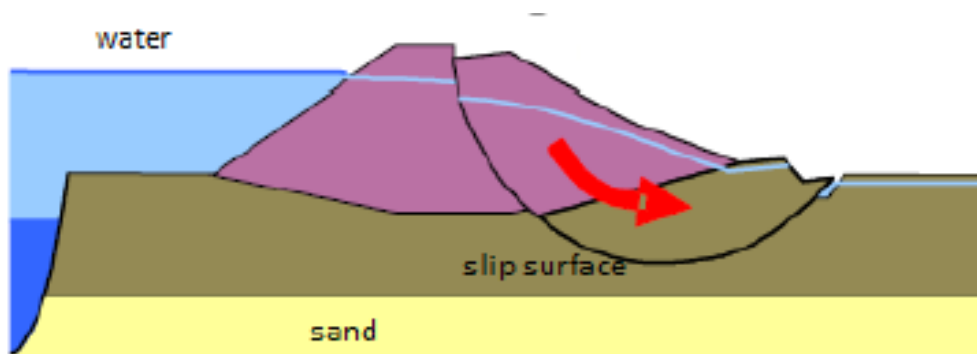
Figure 12: illustration of inwards macro-instability (WBI 2017)

According to the WBI 2017 the default model to assess slope stability of a river dike is the Uplift-Van model developed by Van (2001). The model allows for a non-circular slip circle and can accommodate uplift conditions, which typically occur due to high water pressures in the sand layer below the softer top layers in the polder side of the dike. The failure mechanism based on the Uplift-Van model is described by two circular slip circles: one on the active zone and another on the passive zone bound by a horizontal slip plane. This horizontal line, which is part of the passive zone usually lies along the bottom of a weak soil layer as illustrated in Figure 13.
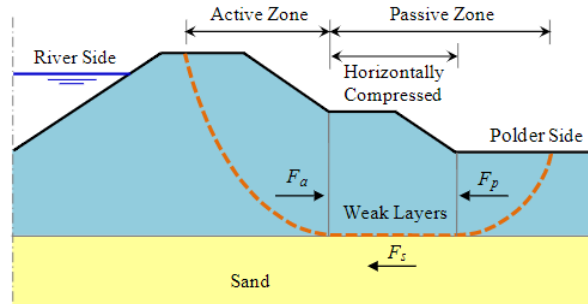
Figure 13: The uplift-Van Model. (Rijkswaterstraat, 2017)

As presented in Figure 14, there are several ways to reinforce a dike, among others the construction of a berm, and by the use of retaining structures such as, diaphragm wall and sheet pile wall.
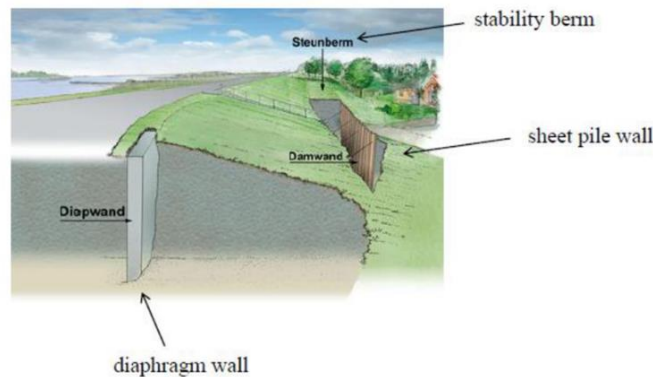
Figure 14: Reinforcement techniques for a dike (Rippi, 2015).

Besides using a berm, the use of (un)anchored sheet pile walls is also common to strengthen a dike. Figure 15 gives an insight regarding the locations where reinforcement techniques have been used in the Netherlands, with the red dots indicating the locations of the sheet pile walls.
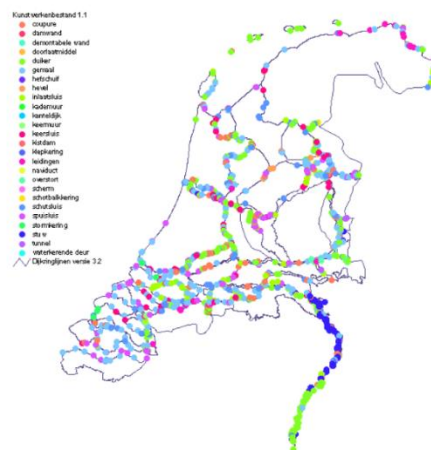
Figure 15: Locations of applied sheet pile walls in the Netherlands, denoted with red dots (Rijkswaterstaat, 2009)

In the recent years, steel sheet piles are widely used in river control structures and flood defences. They are traditionally used for strengthening the dikes and protecting the river banks. Some of the advantages of using the sheet piles are the ease of use, speed of execution, long service life and the ability to be driven in the water. For the case of strengthening a dike (i.e. river dikes) the sheet pile walls can serve as a cut-off. The required water tightness of sheet pile wall cut-offs is often obtained through natural deposition of soil in the interlocks. If necessary, seepage through a sheet pile cut-off can be reduced by introducing a highly effective sealing system into the interlocks. A sheet pile cut-off not only reduces leakage but also improves the overall stability of a dike. Sheet pile walls are particularly beneficial in the case of lack of space in the existing dikes to strengthen them. In addition, other benefits of using steel sheet pile walls are environmentally friendliness and the possibility to maintain the aesthetics of the area.
More information on the design of a sheet pile wall is given in Chapter 5, where the detailed analysis of the Blue dike is presented.

2.6 Study area

The KIJK dike is located between the Krimpen aan de IJssel and Gouderak cities (Figure 16). It serves as a primary flood protection of the adjacent Hollandse IJsssel river.
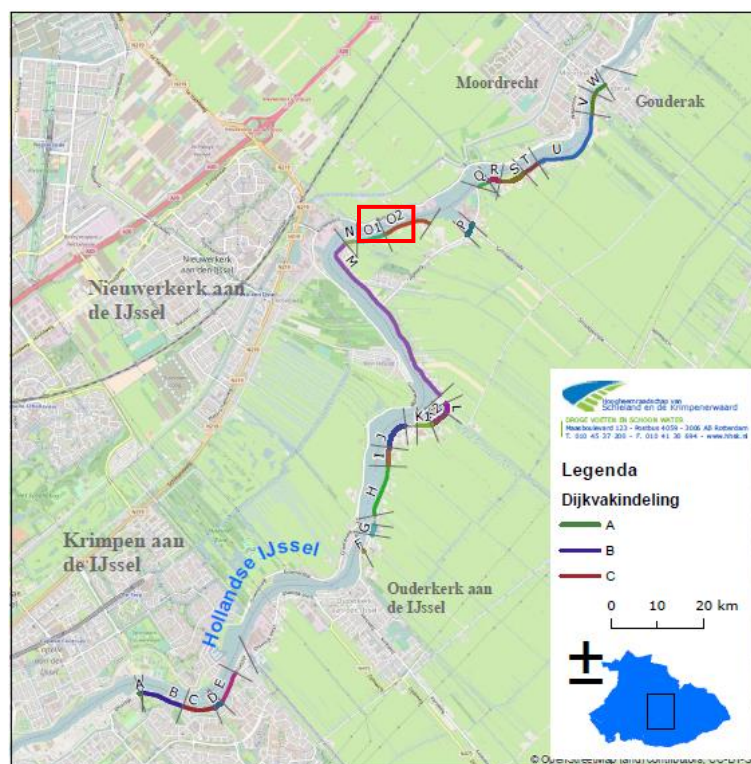
Figure 16: KIJK dike location.

The level of the dike crest is ranging from NAP +3.5 to +3.8 m, while the polder side is at the elevation of approximately NAP -2 m. The dike body mainly consists of a clay dike material possessing very low values of permeability ($k_v \approx 10^{-9}$ m/s). The soil stratigraphy below the dike material consists of an upper organic clay material (in Dutch: klei met plantenresten or klei humeus) which rests upon a peat soil (in Dutch: Hollandveen). Below the peat, a deep organic clay layer is found which in some areas of the dike lies over deeper cohesive soil layers, namely

clay Kreftenheye and peat Bassisveen. These latter two are thin layers which are found at large depths. For simplicity, the Organic Clay 1 is noted as the upper clay layer while the Organic Clay 2 as the lower. Below the lower cohesive soil layers rests a Pleistocene sand layer. Table 3 and 4 summarize the properties of the soil layers, specifically the saturated volumetric weight (γ_{sat}), the void ratio (e) and the plasticity index (PI) for the clay layers, and the volumetric weight, the void ratio and the water content (w) for the peat layer. Additionally, these tables contain the average values of the OCR for the examined soils as measured from p_c / σ'_{vc} with the p_c calculated from one dimensional compression tests. Distinction has been made between the crest and the toe area of the dike since the material properties among which the volumetric weight is higher in the crest area of the dike where the soils are more compressed. In contrary, the void ratio and the OCR are higher in the toe area of the dike since the soils in these locations do not experience the overburden pressure of the dike body. The strength and stiffness characteristics of the soil layers are elaborated in chapter 3.

Table 3: Examined soil properties crest.

Soil	γ_{sat} (kN/m^3)	e (-)	w (%)	PI (%)	OCR (-)
Clay dike	17.5 – 18.5	0.80		14 - 55	1.6 – 2.5
Organic clay 1	15 - 17	1.60		22 - 88	1.4 – 1.7
Peat	9 - 12	1.7 – 5.2	121 - 427		1.25 – 1.8
Organic clay 2	15 - 17	2.30		22 - 88	1.1 – 1.5

Table 4: Examined soil properties toe.

Soil	γ_{sat} (kN/m^3)	e (-)	w (%)	PI (%)	OCR (-)
Anthropogenic clay	17.5 – 18. 5	0.80		14 - 55	2 - 4
Organic clay 1	12 - 15	1.93		22 - 88	1.5 - 4
Peat	8 - 12	3 – 6.5	221 - 440		1.4 - 3
Organic clay 2	12 - 15	2.70		22 - 88	1.25 – 2.75

In Figure 17 several dike profiles are given across a dike section of the KIJK dike. However, the most critical profile is represented by the thick black line and is applied in this study. It can be seen that the selected profile has a relatively high crest and a steep inward slope of V:H equal to 1:2. Based on the CPTs, the soil stratigraphy for the examined cross-section indicates that there is a thick peat layer with the thickness of 3 m in the crest area (Table 5) which is enlarged to 4.6 m in the toe area (Table 6) of the dike. Therefore, the selected cross section is considered to be critical in view of the dike geometry, which rests upon relatively unfavourable subsoil combinations. The critical cross section is located in the dike section O as indicated by the red box in Figure 16. The relevant CPTs are 33.9+10Kr and 33.9+10T for the crest and toe area of the dike respectively (Figure 18). The thickness of each soil layers according to these CPTs for the soil profile in the dike body as well as in the hinterland is summarized in Table 5 and 6, respectively. It should be mentioned that the peat Bassisveen layer of approximately 30 cm has been excluded from the analysis in this study due to the neglectable thickness at very large depths.

Therefore, the created dike profile (i.e. geometry[1], soil stratigraphy, and water levels) used in the macrostability analyses is based on the information obtained from the borings and CPTs data associated to the location of the dike cross-section under consideration.

---

[1] In the Appendix A the soil stratigraphy of the dike section O is given, including all the relevant CPTs
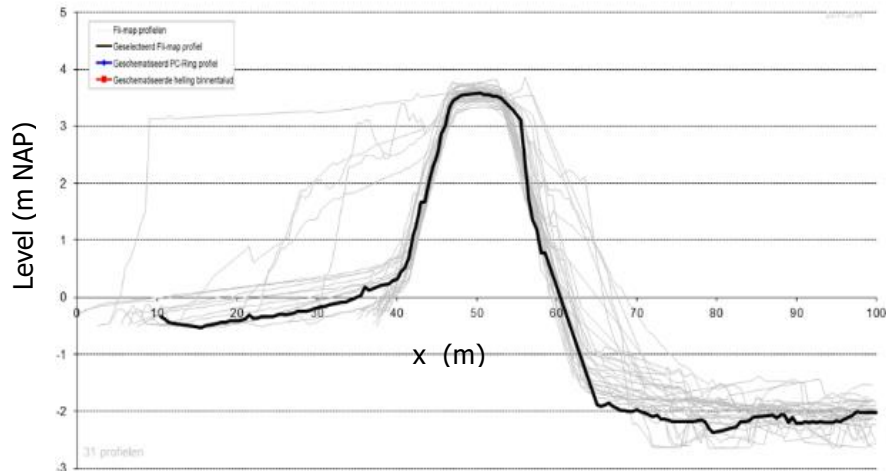
Figure 17: Selected cross section.

Table 5: Soil layers thickness in the crest area of the dike.

Crest			
Soil Stratigraphy			
Thickness (m NAP)	Level (m NAP)		Soil Type
	Top	Bottom	
6.13	3.63	-2.5	Clay dike
5	-2.5	-7.5	Organic clay 1
3	-7.5	-10.5	Peat
2.1	-10.5	-12.6	Organic clay 2
9.9	-12.6	-23	Sand

Table 6: Soil layers thickness in the toe area of the dike.

Toe			
Soil Stratigraphy			
Thickness (m NAP)	Level (m NAP)		Soil Type
	Top	Bottom	
2	-2.05	-4.05	Clay anthropogenic
1.35	-4.05	-5.4	Organic clay 1
4.6	-5.4	-10	Peat
3	-10	-13	Organic clay 2
10	-13	-23	Sand

In this study, distinction has been made between the implemented geometries for the examination of Green and Blue type of dikes. In the case of the Green dike, the calculations will be made based on the existing dike conditions, while for the Blue dike the geometry implemented refers to the year 2075. For the Blue dike an adjustment to the slopes needs to be made, which is V:H equal to 1:3 for the inward slope, and 1:2.5 for the outer slope. Moreover, factors such as the settlement in the soils due to creep and the increase of water level due to climate change are considered when determining the required height of the dike by the year 2075. These are based on the KIJK project recommendations. The daily normal river water level, the high river water level, and the piezometric head under the daily and high-water level conditions are schematized

in Figure 19. To determine the phreatic level in the dike under high water level conditions factors such as climate changes, storm intensity and duration are taken into consideration according to the design high water level recommendations given in the POV-M (2017). Finally, the exact dike profile implemented in PLAXIS for the Green and Blue dike analyses are given in Chapters 4 and 5, respectively.
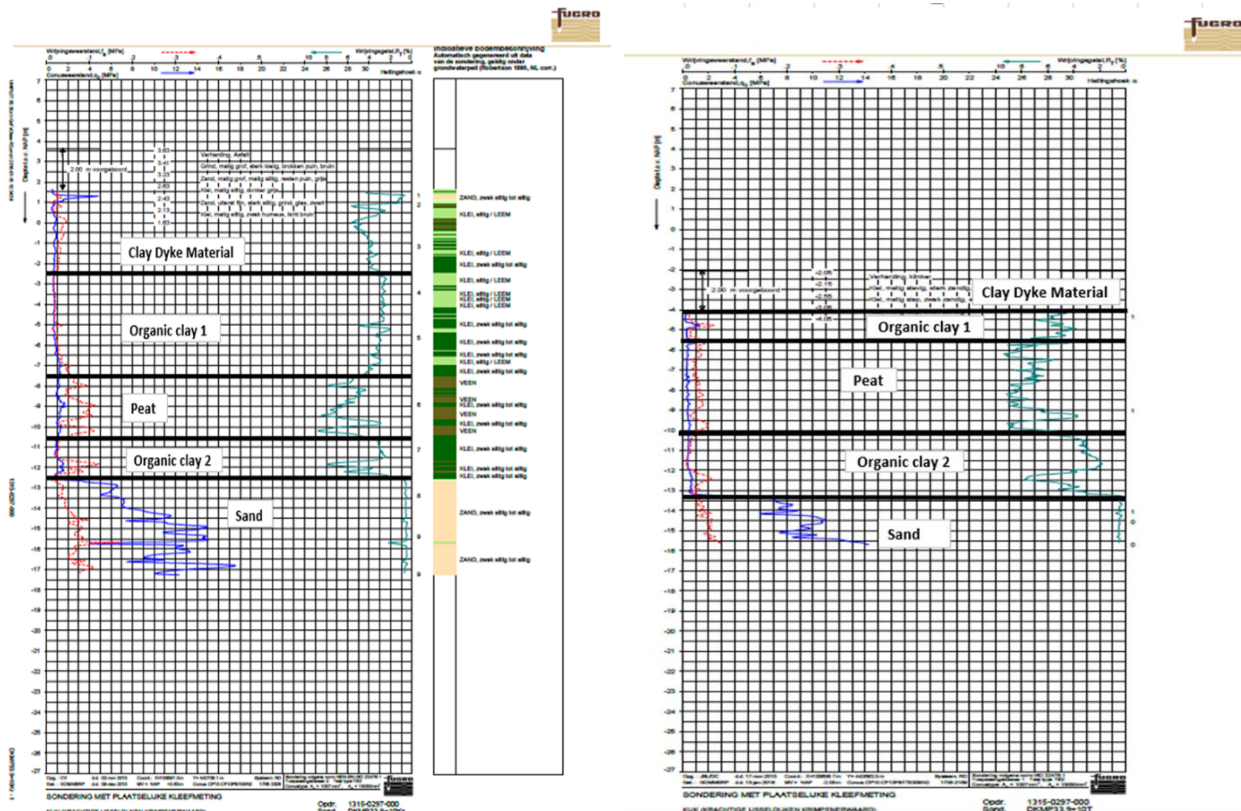
Figure 18: Soil Stratigraphy.
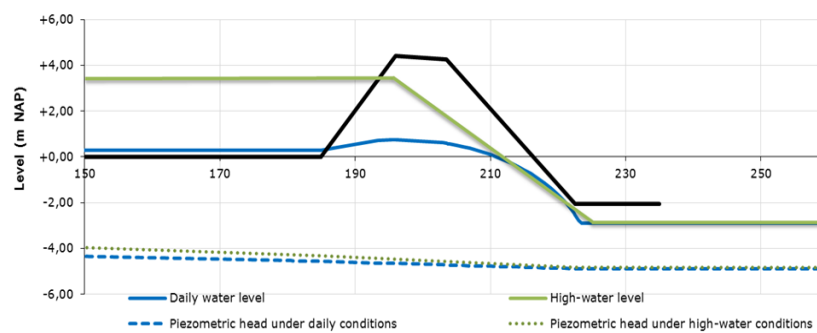
Figure 19: Schematization of water levels.

Chapter 3 –Constitutive Models and Parameter determination

The chapter 3 comprises from five sections. The first section deals with the brief presentation of the considered constitutive models followed by the concise description of the undrained A option which is used for assessing the overall safety of the dike under undrained conditions for the Hardening soil (HS) and the Soft soil (SS) constitutive models. The second section presents the full derivation of the strength and stiffness parameters of the examined constitutive models. The third section demonstrates the influence of the K_0 value in the resulting undrained shear strength and exposes its influence in the parameter determination of the examined soils. The fourth part deals with the calibration of the stiffness parameters for the considered constitutive models with the Soil TestFacility offered from PLAXIS. The last section presents the overall conclusions of the Chapter.

3.1 Constitutive models and undrained A option

3.1.1 Hardening Soil

The Hardening Soil constitutive model (HS) was proposed by Schanz (1998); Schanz et al. (1999) in order to reproduce basic behaviour of soils such as:

➢ *stress dependent stiffness, i.e. observed increasing stiffness moduli with increasing stress level*
➢ *soil stress history, i.e. accounting for preconsolidation effects*
➢ *plastic yielding, i.e. development of irreversible strains when reaching a yield criterion*

The HS model describes failure with the use of the Mohr-Coulomb (MC) failure criterion, and the plastic yielding occurs using two yield surfaces. The one yield surface accounts for the development of plastic strains due to shearing (shear hardening yield surface) while the second accounts for the development of plastic strains due to primary compression (cap yield surface).

The magnitude of soil deformations can be modelled more accurately by incorporating three input stiffness parameters corresponding to the triaxial loading stiffness (E_{50}), the triaxial unloading-reloading stiffness (E_{ur}), and the oedometer loading modulus (E_{oed}).

The hardening yield function for shear mechanism f^s, is described using the concept of hyperbolic approximation of the relation between the vertical strain ε_1 and deviatoric stress q for a standard drained triaxial compression test (Figure 20). The yield condition is therefore expressed as follows:

$$f^s = \frac{2}{E_i} \frac{q}{1 - q/q_\alpha} - \frac{2q}{E_{ur}} - \gamma^{PS} \qquad (4)$$

Where: γ^{PS} is the plastic strain hardening parameter, E_i is the initial secant stiffness, q_a is the asymptotic deviatoric stress which is defined by the ultimate deviatoric stress q_f and the failure ratio R_f through $q_{a = q_f} / R_f$. A suitable value of $R_f = 0.9$ is set by default. For most soils, the value of R_f falls between 0.75 and 1 (Obrzud, 2010).
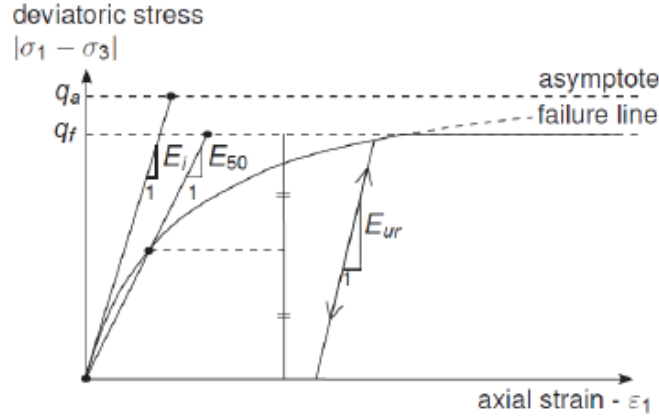
Figure 20: Hyperbolic stress strain relationship and the definition of different moduli in the triaxial drained test condition. (Obrzud, 2010)

The hyperbolic relation is restrained by the ultimate deviatoric stress q_f. The q_f is described by the MC failure criterion which is given in the following equation:

$$q_f = \frac{2\,sin(\varphi)}{1-sin(\varphi)}\,(\sigma'_3 + c\,cot\varphi) \tag{5}$$

The secant modulus E_{50} which corresponds to 50% of the value of q_f is stress dependent through the adopted power law:

$$E_{50} = E_{50}^{ref}\left(\frac{c\,cos_\varphi - \sigma'_3 sin_\varphi}{c\,cos_\varphi + p_{ref} sin_\varphi}\right)^m \tag{6}$$

Where E_{50}^{ref} is a reference stiffness modulus corresponding to the reference stress p_{ref} (default value 100 kPa). The actual stiffness depends on the minor principal stress σ'_3 which is the effective horizontal confining pressure in a triaxial test. The amount of stress dependency is given by the power m. In natural soil, the exponent m varies between 0.3 and 1.0. Janbu (1963) reported values of 0.5 for Norwegian sands and silts, whereas Kempfert (2006) provided values between 0.38 and 0.84 for soft lacustrine clays and Seah and Lai (2003) showed that soft Bangkok clays are better described with an m value equal to 1. The E_{50} largely controls the magnitude of the plastic strains which are related to the shear yield mechanism.

For unloading and reloading stress path the unloading reloading stiffness modulus is used through:

$$E_{ur} = E_{ur}^{ref}\left(\frac{c\,cos_\varphi - \sigma'_3 sin_\varphi}{c\,cos_\varphi + p_{ref} sin_\varphi}\right)^m \tag{7}$$

The cap yield surface (Figure 21) is expressed as follows:

$$f^c = \frac{q^2}{M^2} - p'^2 - p_p^2 \tag{8}$$

Where: p_p is a state parameter that remembers the position of the cap and M controls the steepness of the cap. The value of parameters M is determined automatically by PLAXIS, based

on K_0^{NC}. The M is an auxiliary parameter that related to the K_0^{NC}. The value of coefficient of earth pressure for normal consolidation is calculated by default as $K_0^{NC} = 1 - \sin(\varphi)$ (Jaky, 1944).

For primary loading the tangent stiffness modulus from an oedometer test is used and is defined through the equation:

$$E_{oed} = E_{oed}^{ref}(\frac{ccos_\varphi - \frac{\sigma'_3}{K_0^{NC}}sin_\varphi}{ccos_\varphi + p_{ref}sin_\varphi})^m \tag{9}$$
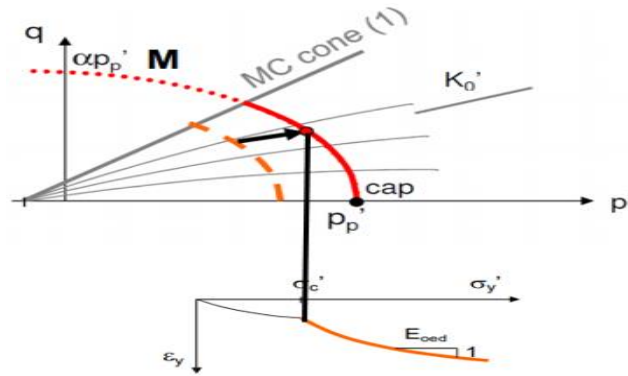
Figure 21: Yield cap of the HS model. (Obrzud, 2010)

The initial conditions in the HS model are set through the input parameters of OCR or POP and the preconsolidation pressure in the model is converted to p_p. The OCR and POP are given from: $\sigma_p = OCR \, \sigma'_{yy}{}^0$ and $\sigma_p = \sigma_{yy}{}^0 + POP$ as shown in Figure 22.
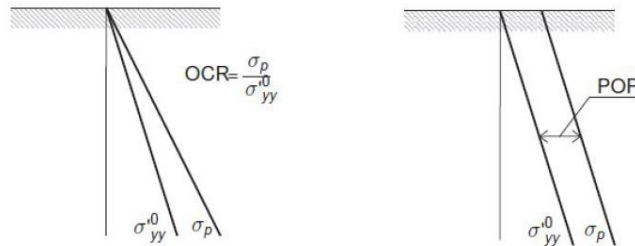
Figure 22: Definition of preconsolidation pressure (Plaxis, 2018)

The initial horizontal effective stress is calculated based on: $\sigma_{xx}{}^0 = K_0\sigma_{yy}{}^0$ with K_0 calculated through:

$$K_0 = OCR \, K_0^{NC} - (\frac{v_{ur}}{1 - v_{ur}})(OCR - 1) \tag{10}$$

Where v_{ur} is the unloading reloading poison ratio (default v_{ur}=0.2)

Despite the overall benefits, the model incorporates and some limitations. The HS model is not able to reproduce softening effects associated with soil dilatancy and soil destructuration. Moreover, the model formulation does not account for large amplitudes of soil stiffness related to transition from very small strain to engineering strain levels ($\varepsilon \approx 10^{-3} - 10^{-2}$). Moreover, the HS model is not capable to reproduce hysteretic soil behaviour observed during cycling loading.

The model does not account does not account anisotropy and secondary compression. Lastly, in the Table 7 the overall input parameters of the model are shown.

Table 7: Input parameters for the HS model. (Plaxis, 2018a)

Failure parameters as in Mohr-Coulomb model:		
c	(Effective) cohesion	(kN/m^2)
φ	(Effective) angle of internal friction	(o)
ψ	Angle of dilatancy	(o)
σ_t	Tension cut-off and tensile strength	(kN/m^2)
Basic parameters for soil stiffness:		
E_{50}^{ref}	Secant stiffness in standard drained triaxial test	(kN/m^2)
E_{oed}^{ref}	Tangent stiffness for primary oedometer loading	(kN/m^2)
E_{ur}^{ref}	Unloading/reloading stiffness (default $E_{ur}^{ref} = 3E_{50}^{ref}$)	(kN/m^2)
m	Power for stress-level dependency of stiffness	(-)
Advanced parameters:		
v_{ur}	Poisson's ratio for unloading-reloading (default v_{ur}=0.2)	(-)
p^{ref}	Reference stress for stiffnesses (default p^{ref}=100kN/m²)	(kN/m^2)
K_0^{nc}	K0 value for normal consolidation (default K_0^{nc}=1-sinφ)	(-)
R_f	Failure ratio q_f/q_a (default R_f=0.9)	(-)
$\sigma_{tension}$	Tensile strength (default $\sigma_{tension}$=0)	(kN/m^2)

3.1.2 Soft Soil

The Soft Soil (SS) model is an advanced constitutive model in PLAXIS that can simulate the behaviour of normally consolidated soft soils. The special features of these soils are the high degree of compressibility as well the linear stress dependency of their oedometer stiffness. The SS model has been developed within the Critical State Soil Mechanics frameworks and assumes a logarithmic relation between the volumetric strain ε_v and the mean effective stress p'. During isotropic virgin compression, along the normal consolidation line, this relation is formulated as:

$$\varepsilon_v - \varepsilon_v^0 = -\lambda^* ln(\frac{p' + ccot\varphi}{p^0 + ccot\varphi}) \tag{11}$$

Where λ^* is the modified compression index determining the elasto-plastic behaviour of the material during primary loading, p^0 is the initial value of the mean effective stress and ε_v^0 is the initial volumetric strain.
In the case the soil is subjected to unloading or reloading the stress path is different and is formulated as:

$$\varepsilon_v^e - \varepsilon_v^{e0} = -\kappa^* ln(\frac{p' + ccot\varphi}{p^0 + ccot\varphi}) \tag{12}$$

Where κ^* is the modified swelling index, ε_v^e is the volumetric elastic strain and ε_v^{e0} is the initial elastic volumetric strain. The elastic behaviour is described by Hooke's law. The illustration of the parameters λ^* and κ^* is shown in Figure 23:
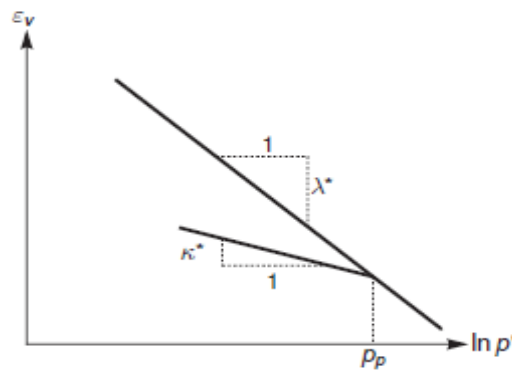
Figure 23: Illustration of the logarithmic relation between volumetric strain and mean stress. (Plaxis, 2018)

To distinguish between recompression and the primary loading, a stress history parameter is introduced namely pre-consolidation pressure p_p. The p_p can be specified by the value of the Overconsolidation Ratio (OCR) or by the Pre-Overburden Pressure (POP) (refer to figure 22).

The cap yield surface of the Soft Soil Model is formulated as:

$$f_c = \frac{q^2}{M^2\,(p' + ccot\varphi)} + p' \tag{13}$$

Where, q is the similar deviatoric stress quantity as illustrated for the cap yield surface in the HS model.

Figure 24 illustrates the ellipse shape yield surfaces of the SSM. The Mohr-Coulomb failure criterion is adopted in the Soft soil model, which governs failure. Therefore, the drained strength parameters φ' and c', are required. The Parameter M determines the shape and steepness of the yield surface. Moreover, the parameter M is not a direct input parameter in the model. Particularly, it is calculated internally from the input parameters (K_0^{NC}, v_{ur} and λ^*/κ^*). This implies that M can exist only as an approximation and the dominant parameter is K_0^{NC}.
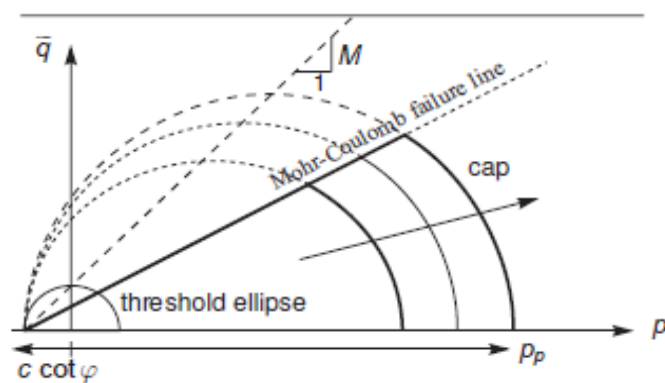
Figure 24: Threshold cap yield surface of the SS model.

The ellipses that can exist are infinite and all depend on the value of the mean effective pre-consolidation pressure. In other words, it determines the extent of the ellipse along the p' axis. In addition, the Figure 24 illustrates that during loading and after surpassing the pre-consolidation pressure, the cap expands, and plastic volumetric strains are accumulated. The Soft-Soil model limitations are the incapability of reproducing softening behaviour. Moreover, the

model does not account for anisotropy and secondary compression. Lastly, in the Table 8 the overall input parameters of the model are shown.

Table 8: SS model input parameter

Basic parameters:		
λ^*	Modified compression index	[-]
κ^*	Modified swelling index	[-]
c	Effective cohesion	[kN/m^2]
φ	Friction angle	[^{o}]
ψ	Dilatancy angle	[^{o}]
σ_t	Tensile strength	[kN/m^2]
Advanced parameters:		
v_{ur}	Poisson's ratio for unloading-reloading	[-]
K_0^{nc}	Coefficient of lateral stress in normal consolidation	[-]
M	K_0^{nc}-parameter	[-]

3.1.3 SHANSEP NGI-ADP

It should be mentioned that the following elaboration concerns the NGI-ADP model formulation. The reader can refer to the SHANSEP framework in subchapter 2.4. In addition, at the end of the subchapter the elaboration on how the SHANSEP concept is facilitated in the NGI-ADP model is explained.

The NGI-ADP is an advanced elastoplastic constitutive model (Grimstad et al. 2012) which accounts for the stress path dependency of the s_u. The stress path dependency is related to the ADP framework proposed by Bjerrum (1973), in the sense that there is a distinction in the undrained shear strength profiles for active (A) or triaxial compression (TXC), direct simple shear (DSS) and passive (P) or triaxial extension (TXE) loadings. For simplicity, the plane strain "A (active)" strength is assumed almost equal to the triaxial compression strength (s_u^{TXC} / s_u^A = 0.99), and correspondingly, the plane strain "P (passive)" strength is assumed equal to the triaxial extension strength. According to Ladd and Foott (1977) for plane strain problems the use of triaxial testing can be used safely, although there is a possibility of predicting slightly conservative results. Thus, the model requires as input parameters the undrained shear strengths (s_u^A, s_u^P, s_u^{DSS}) ratios along with the associated shear strains (γ_f^A, γ_f^P, γ_f^{DSS}) in the three directions of shearing. The non-linear strain hardening anisotropic behaviour is illustrated in Figure 25. By interpolation between the three input curves, the model can predict the anisotropic behaviour of saturated clays for a general 3D stress state.

Furthermore, according to (Bjerrum, 1973; Ladd and Foott, 1974) the undrained triaxial tests which are used to determine the input parameters should be anisotropically consolidated based on the in-situ stress ($C_{K0}UC$ and $C_{K0}UE$ tests). Thus, the curves shown in Figure 25 start from an initially mobilized shear stress τ_0. The elastic stiffness is given from the unloading reloading shear modulus (G_{ur}). The s_u in the model varies linearly with depth across the soil layers. The TXC compression su is given with the s_u^A $_{ref}$ at a reference depth y_{ref}. The potential increase of the s_u with depth is given from s_u^A $_{inc}$. The s_u dependency on the stress path is defined as fractions of the s_u^A through the s_u^{DSS}/s_u^A and s_u^P /s_u^A respectively.

.
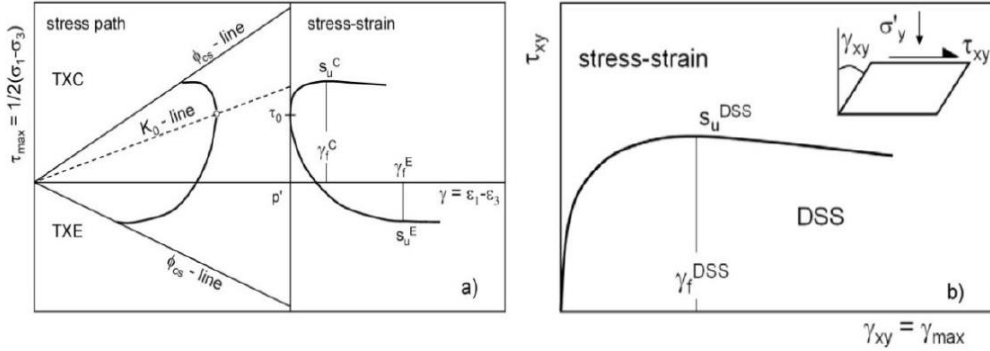
Figure 25: Typical stress paths and stress strain-curves for triaxial compression and triaxial extension tests (left). direct simple shear test with definition of stress strain quantities (Ukritchon and Boonyatee, 2015).

The formulation of NGI-ADP model for a general 3D stress space is based on an anisotropic approximated Tresca yield criterion (Grimstad et al. 2012). The yield function F for NGI-ADP model is defined as:

$$F = \sqrt{(H(\omega) \cdot \hat{J}_2} - \kappa_1 \cdot \frac{s_u^A + s_u^P}{2} = 0 \qquad (14)$$

The $\hat{J}_2$ is the modified second deviatoric invariant. The function H (ω) approximates the Tresca criterion. The κ_1 is the hardening parameter and it is computed from:

$$\kappa_1 = 2 \cdot \frac{\sqrt{\gamma^P/\gamma_P^P}}{1+\gamma^P/\gamma_P^P}, \text{for } \gamma^P < \gamma_P^P \qquad (15)$$

Where the γ^P and $\gamma_P{}^P$ are the plastic shear strain and plastic "peak" shear strain, respectively. Figure 26 shows the hardening response in compression and extension for $\gamma^P{}_{fC}$ = 0.01, $s_u{}^E/s_u{}^C$ = 0.4 and $\gamma^P{}_{fE}$ =0.05.

The function H (ω) is defined as:

$$H(\omega) = cos^2 \left[\frac{1}{6} arccos(1 - 2 \cdot \alpha_1 \cdot \omega)\right] \qquad (16)$$

Where:

$$\omega = \frac{27}{4} \frac{\hat{J}_3^2}{\hat{J}_2^3}$$

Where: $\hat{J}_3$ is the third deviatoric invariant and a_1 the rounding ratio, defined as the ratio between $s_u{}^{TXC}$ and $s_u{}^{PS}$. a_1 = 0.97-0.99 is always chosen as default value.

Figure 27 shows the NGI-ADP yield criterion for plane strain conditions. Contours of plastic shear strain and the elliptical failure curve (κ_1 = 1) in the plane strain deviatoric stress plot are shown. In Figure 28, the failure criterion of the NGI-ADP model in the π plane (for Cartesian stresses) with default rounding ratio is shown. The criterion is continuous, differentiable and described by a single function (Grimstad et al. 2012).
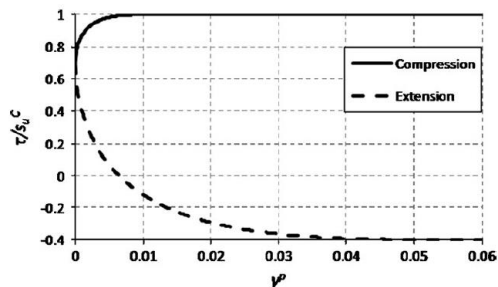
Figure 26: Typical difference in hardening response in compression and extension.
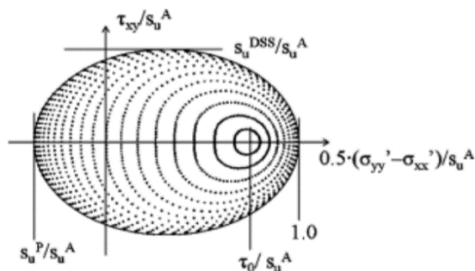
Figure 27: "Typical" deviatoric plane strain plot of equal shear strain contours for the NGI-ADP model (Grimstad et al. 2012).
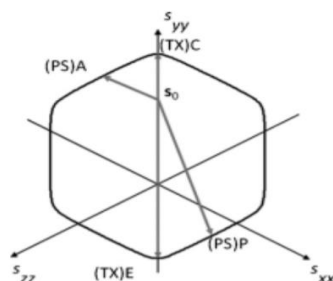
Figure 28: Failure criterion used in the NGI-ADP model in the π-plane (Grimstad et al. 2012).

The NGI-ADP constitutive model does not incorporate cyclic behaviour, rate effects strain softening and generation of shear-induced pore pressures. The Table 9 contains the required input parameters for the model.

Finally, the subchapter concludes with a brief elaboration on how the SHANSEP concept is applied in the NGI-ADP model and on how the model is utilised in the design guidelines. The material model for the SHANSEP NGI-ADP is facilitated through a user-defined soil model by means of DLL files. For the activation of the SHANSEP NGI-ADP model the soil clusters are switched to the SHANSEP approach by the user in the phase where an undrained analysis is considered. For doing so, a specific file is stored from the user within the project folder, namely data.ngiadprs.rs# at the phase of interest. Thus, the soil layers which will exhibit undrained behaviour are set to the SHANSEP NGI-ADP model and based on the $S_{(NC)}$, m the OCR and the vertical effective principal stress the s_u^A is calculated for each soil layer. The OCR is transferred from the preceding steps where the soil clusters were described by advance constitutive models (i.e. HS, SS models). For these models an OCR or POP value is specified from the user. The s_u^A is then determined based on equation 17.

Table 9: SHANSEP NGI-ADP parameters

Parameter	Symbol	Description	Unit
NGI-ADP MODEL	G_{ur}/s_u^A	Ratio unloading reloading shear modulus over plane strain active shear strength	[-]
	γ_f^C	Shear strain at failure in triaxial compression	%
	γ_f^E	Shear strain at failure in triaxial extension	%
	γ_f^{DSS}	Shear strain at failure in direct simple shear	%
	$s_u^A.ref$	Reference plane strain active shear strength	kN/m²
	y_{ref}	Reference depth	m
	$s_u^A.inc$	Increase of shear strength with depth	(kN/m²)/m
	s_u^P/ s_u^A	Ratio of plane strain passive shear strength over (plain strain) active shear strength	[-]
	τ_0/ s_u^A	Initial mobilisation	[-]
	s_u^{DSS}/ s_u^A	Ratio of direct simple shear strength over (plane strain) active shear strength	[-]
	v	Poisson's ratio	[-]
	v_u	Poisson's ratio undrained	[-]
SHANSEP	alpha a	Normalised undrained shear strength in NC conditions	[-]
	Power (m)	Strength increase exponent	[-]
	$s_{u\ min}$	Minimum undrained shear strength	kN/m²
	OCR_{min}	Minimum over consolidation ratio	[-]
	POP_{min}	Minimum pre-overburden pressure	kN/m²

Remarks on the constitutive models

Firstly, the HS and the SS constitutive models allow the option of applying a dilatancy angle ψ. For the purposes of this study the values of ψ were set equal to zero in all the examined soil layers for both the Hardening soil and the Soft soil. Particularly, dilatancy should never be used in combination with an undrained behaviour since it leads to an infinite shear strength.

Regarding the SHANSEP NGI-ADP it has to be mentioned that the parameter S is denoted as alpha α (refer to Table 9). Moreover, the stress used to compute the OCR and the undrained shear strength in PLAXIS is the major effective principal stress (σ'_1) and thus the s_u based on the SHANSEP NGI-ADP model is given from:

$$s_u = \sigma'_1 \, S_{(NC)} OCR^m \qquad\qquad (17)$$

This is assumed to be more objective parameter than effective vertical stress σ'_{vc} because it is the most compressive value, independent of the Cartesian system of axis. When soil layering is horizontal both parameters would result in the same value of OCR. In contrast, when the soil layers are inclined a rotation of the principal axis can be expected. Consequently, the use of σ'_{vc} would result in slightly lower values of OCR and s_u for soil elements adjacent to the slope.

3.1.4 Undrained A

The Undrained (A) is a special option offered from PLAXIS that enables the modelling of undrained behaviour using effective strength and stiffness parameters. The effective strength parameters are the φ', c' and ψ' while the effective stiffness parameters are the E_{50} (HS only) and v'. PLAXIS automatically adds the stiffness of water to the stiffness matrix in order to distinguish between effective stresses and excess pore pressures (Plaxis, 2018a). Thereby, the resulting effective stress path and therefore the maximum shear strength is governed by the development of the excess pore pressures.

The Figure 29 demonstrates the various stress paths that can be obtained from the HS and SS models when the undrained A option is adopted. However, most soil models are not capable of providing the right effective stress path in undrained loading. This is because the effective stress path followed in an undrained analysis may deviate from reality, due to limitations of the applied soil model. As a result, wrong output of undrained shear strength is produced if the material's strength is specified based on effective strength parameters. It is therefore important to carefully calibrate the model outcome against the actual in-situ undrained shear strength profile. The latter will be shown in subchapters 3.3 and 3.4.
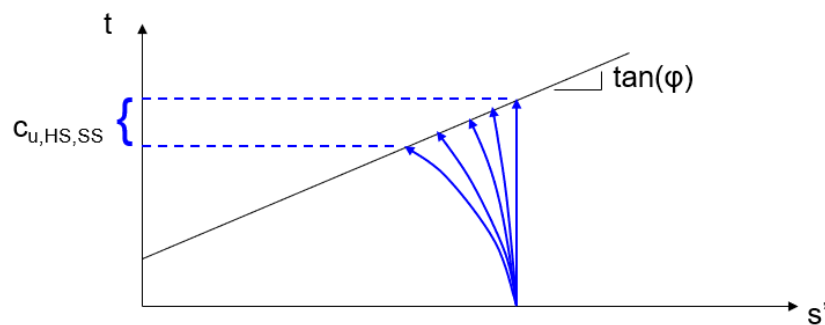
Figure 29: Illustration of various generated stress paths with the use of the SS and HS soil model.

Speaking in terms of a safety analysis from Figure 30 it can be seen that although, the material strength is governed by the undrained shear strength, the Factor of Safety is defined as initial drained strength parameters over limit drained strength parameters. Upon a safety analysis the effective strength parameters are reduced until the limit s_u is reached through the equation:

$$\Sigma Msf = \frac{tan_{\varphi input} + c_{input}}{tan_{\varphi reduced} + c_{reduced}} \tag{18}$$
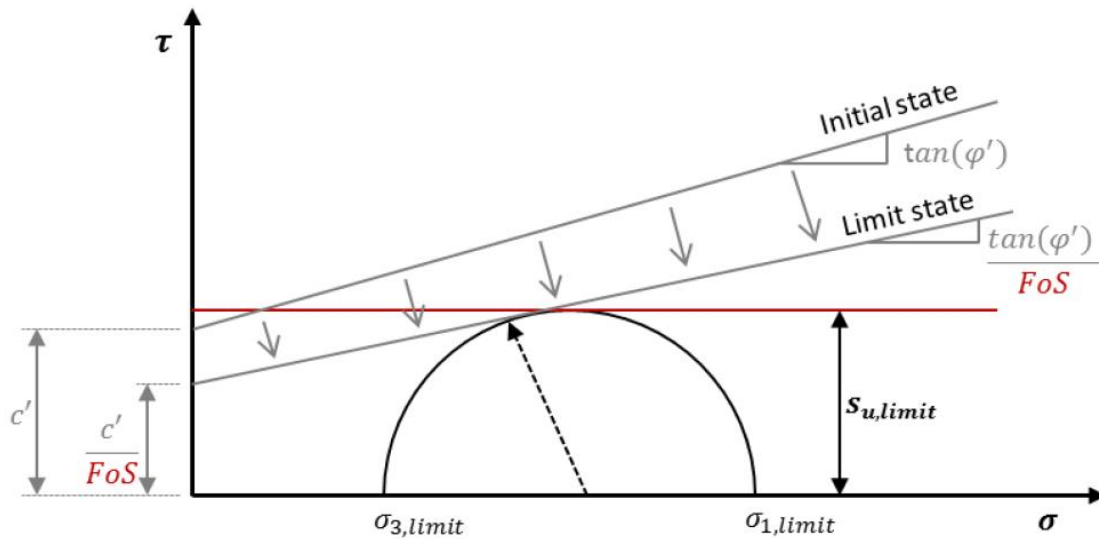
Figure 30: Undrained A analysis in terms of safety analysis. (Raissakis, 2012)

It is noteworthy to mention that in the case in the case of the SHANSEP NGI-ADP model the FoS is calculated based on the undrained shear strength and the equation is as follows:

$$\Sigma Msf = \frac{s_u^{input}}{s_u^{equilibrium}} \qquad (19)$$

In summary, the characteristic features of the Undrained (A) method relevant for this study are:

➢ *The undrained shear strength is calculated based on the effective strength parameters considering an effective stress path.*
➢ *The pore pressures generated from the models may deviate from the reality. This is more relevant for the stress path of an OC soil when using the HS and SS models due the incapability of generating dilative pore pressures.*
➢ *The resulting s_u is a product of the constitutive models and thus, is not given through an input parameter.*

3.2 Parameter Determination

In this section of the chapter the detailed determination of the strength and stiffness parameters of the considered constitutive models is established. The laboratory tests were executed under the protocol of the WBI (2017).
The section is structured in two parts. The first part deals with the strength parameters of the constitutive models; specifically, the S and m parameters for the SHANSEP NGI-ADP model and the effective strength parameters φ', c' for the HS and SS models. The S and m parameters are necessary for the correct estimation of the s_u based on the SHANSEP framework (refer to eq.1). The φ' and c' parameters are necessary for describing the drained strength of the soil and the undrained shear strength s_u (refer to subchapter 3.1.4). The second part demonstrates the estimation of the stiffness parameters of the constitutive models.

3.2.1 Normalised S parameter

The normally consolidated undrained shear strength ratio $S_{(NC)}$ is a friction parameter for characterizing the undrained shear strength of soil under normally consolidated conditions. The normally consolidated state of the sample is achieved by applying a vertical consolidation stress beyond the preconsolidation pressure (σ'_p) (Ladd and Foott, 1974).

For the determination of the $S_{(NC)}$ parameter the undrained shear strength was plotted against the applied vertical consolidation stress. The normalized behaviour is illustrated in Figure 31. Distinction has been made between S parameter obtained from 2%, 25% strain levels for clays and 5%, 40% strain levels for peats.
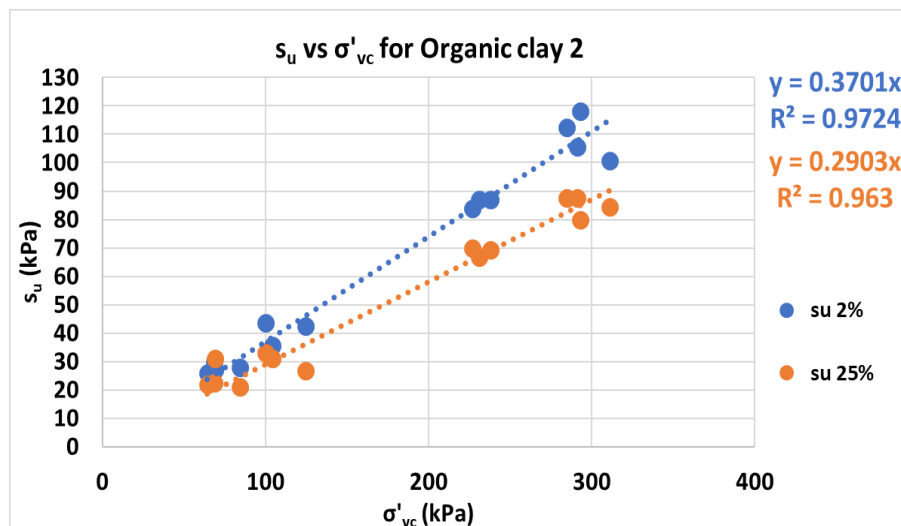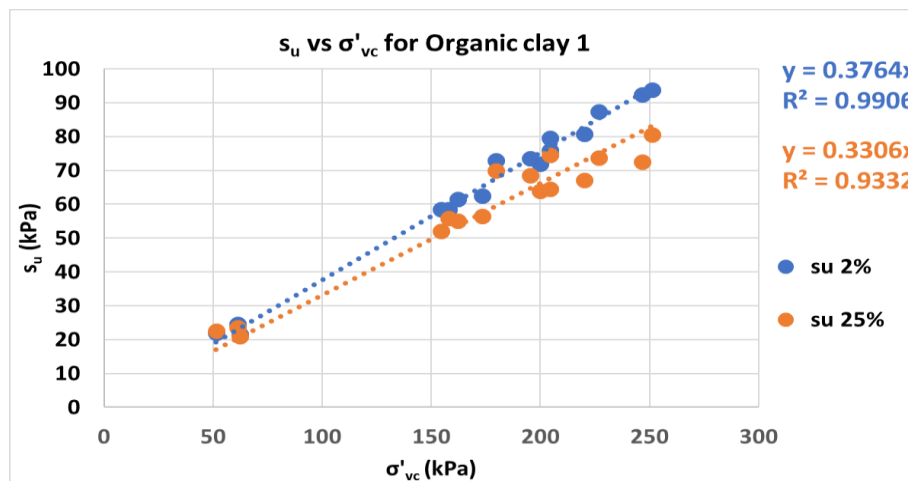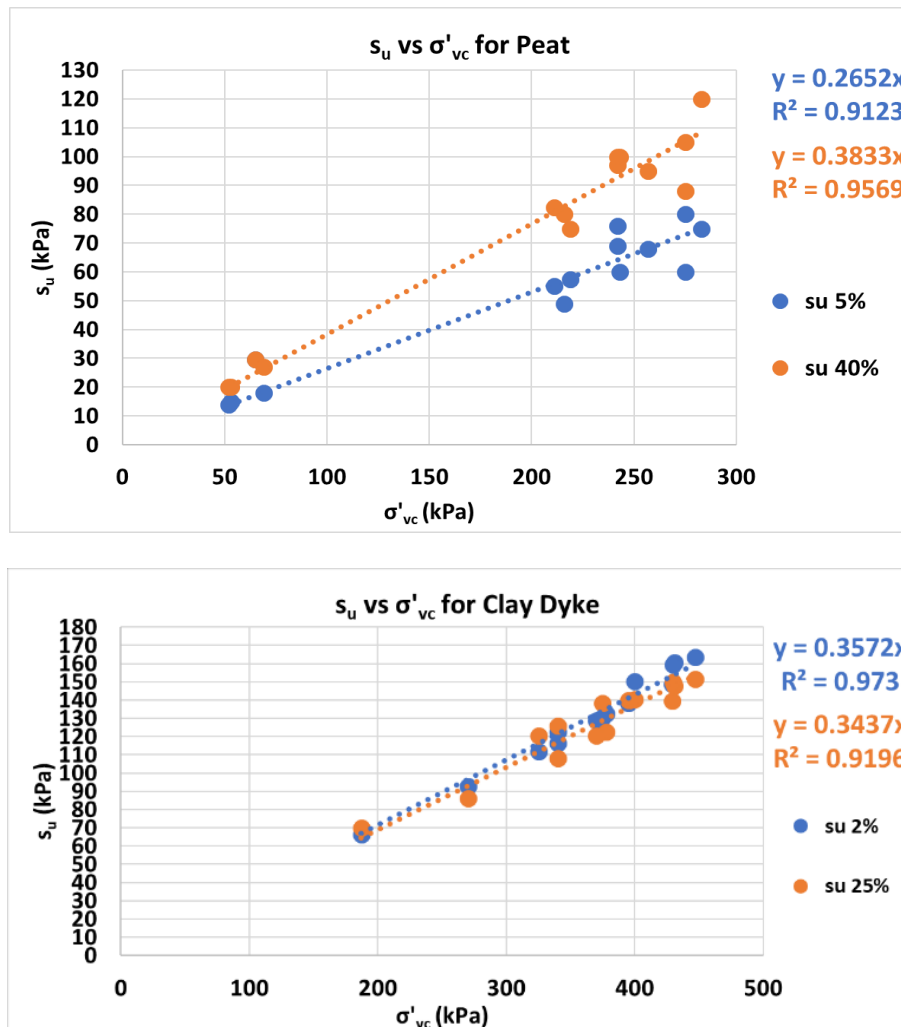
Figure 31: $S_{(NC)}$ for the examined soil layers.

The examined soils display reasonably well the normalised behaviour (undrained shear strength proportional to the confining pressure). The $S_{(NC)}$ is the result of the s_u divided by σ'_{vc}. In addition, it is evident that the value of S parameter in service conditions strain levels (2,5%) is notably higher for clays than peats. In contrary, within the larger strains (25,40%) it is the peat which shows considerably higher values than clays. This is explained by the fact that in service conditions strain levels the clays are almost experiencing their peak strength in contrast with peats that their maximum shear strength lies well beyond 5% strain level. On the other hand, in 25% and 40% strain levels, the peats reached their maximum strength where clays after the peak strength exhibited strain softening and their resulting S value in 25% strain level is lower. The behaviour of the clays which are reaching their maximum strength at approximately 2% strain level (when consolidated beyond σ'_p) will become an important aspect considering the parameter determination of the m parameter and it is elaborated in the next subchapter.

In chapter 2 it was demonstrated that the resulting undrained shear strength under different modes of shearing exhibits considerable deviations. On top of that, the resulting undrained shear strength in triaxial extension and DSS seems to be material dependent. For instance, Ladd and DeGroot (2003) reported that the S $_{(NC)}$ is dependent on the PI (plasticity

index) for DSS and Triaxial Extension modes of loading. No dependency was recorded for Triaxial Compression.

a)

b)
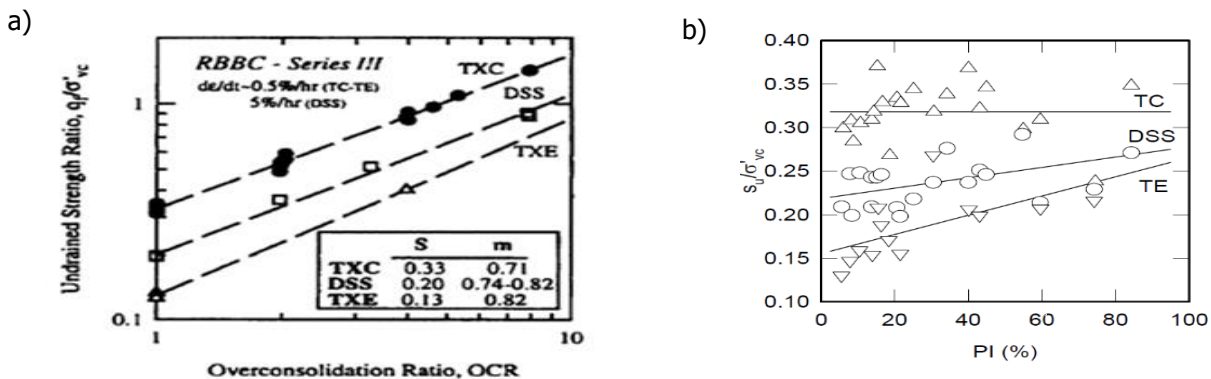
Figure 32: (a) Illustration of the resulting normalised strength vs OCR with different modes of shearing (Ladd and DeGroot, 2003), (b) normalised undrained shear strength dependency on PI for TXC, TE, DSS models of loading (on the right) (Ladd and DeGroot, 2003).

Figure 33 shows the PI vs the $S_{(NC)}$ obtained from $C_{K0}UC$ for the examined clayey soils. The PI seems to have no influence on the $S_{(NC)}$ obtained from triaxial compressions tests which agrees with the findings of the previous researchers.
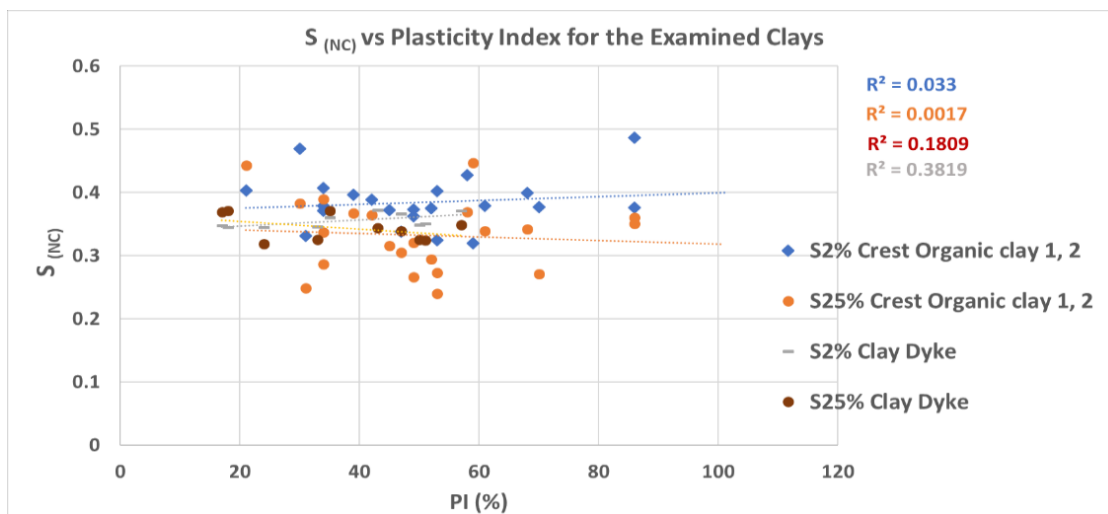
Figure 33: S (NC) dependency on Plasticity Index for the examined clayey soils

Similarly, Larrson (2007) verified the findings of the previous researchers conducting a study in homogenous and saturated Scandinavian clay deposit. Moreover, though his experimental observations it was concluded the S value is nearly material independent for Triaxial Compression while it is strongly material dependent for DSS and Triaxial Extension. In his study he delivered equations where he links directly the S value in DSS, Passive mode with the liquidity index (LL). Based on his study, the resulted $S_{(NC)}$ in triaxial compression, DSS and extension are 0.36, 0.25, 0.2 respectively.
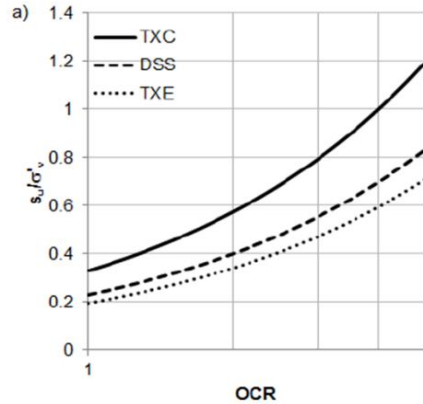
Figure 34: Normalised behaviour of homogenous and saturated Scandinavian clay deposit. (Larrson, 2007)

The derived equations from Larrson (2007) are given below:

$$\frac{su^A}{\sigma'_{vc}} = 0.33\, OCR^{0.8} \tag{20}$$

$$\frac{su^{DSS}}{\sigma'_{vc}} = \left(0.125 + 0.205 * \frac{LL}{1.17}\right) * OCR^{0.8} \tag{21}$$

$$\frac{su^P}{\sigma'_{vc}} = \left(0.055 + 0.275 * \frac{LL}{1.17}\right) * OCR^{0.8} \tag{22}$$

Thakur et.al (2014) collected data on anisotropic undrained shear strength of Norwegian clays measured from triaxial compression, direct simple shear and triaxial extension tests. The anisotropic strength ratio for both extension and DSS conditions was found to be bi-linearly depending on the plasticity index (Figure 35). In smaller values of PI there is no apparent dependency while with increasing PI a linear dependency is noted. Karlsrud and Hernandez-Martinez (2013) observed, for Norwegian clays, that S (NC) = 0.08 - 0.35 dependent on water content/plasticity and sample quality.
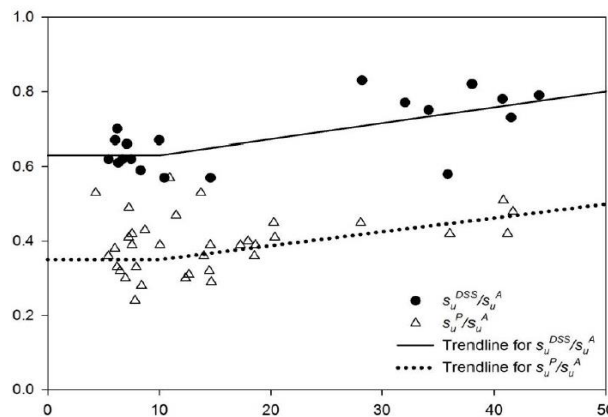
Figure 35: Anisotropy ratio vs plasticity index for Norwegian clays (Thakur et.al, 2014).

As it concerns peat, Carlsten (2000) reported values of 0.4 to 0.65 for direct shear tests on Swedish Peats (Figure 36). Moreover, he expressed that S $_{(NC)}$ ratio displays an increasing trend with increasing void ratio.

The void ratio against the $S_{(NC)}$ for small and large strains was analysed for the examined peat. As it can be seen from Figure 37 there is an apparent increasing trend of the $S_{(NC)}$ with increasing void ratio. The reliability becomes the higher in the large strains where the maximum strength of the peat is mobilized. The obtained reliability though does not display a clear dependency of these factors with the $S_{(NC)}$ of peat and direct conclusions cannot be drawn and further examination is required.
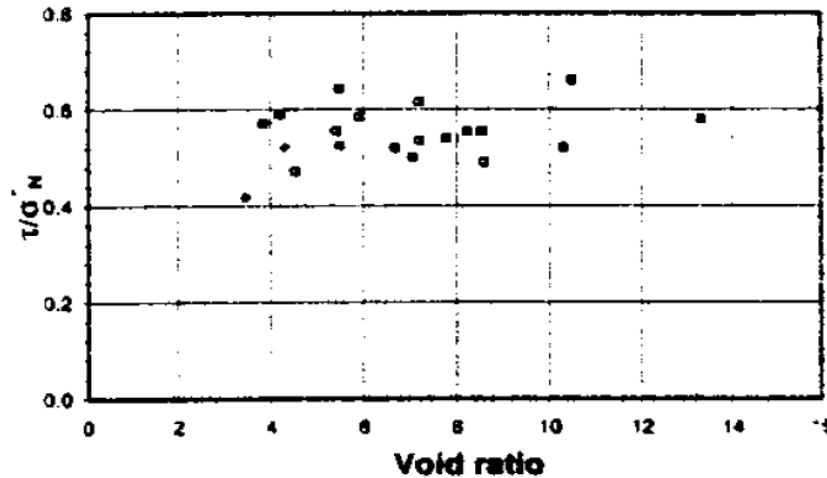
Figure 36: S$_{(NC)}$ vs void ratio (Carlsten, 2000).
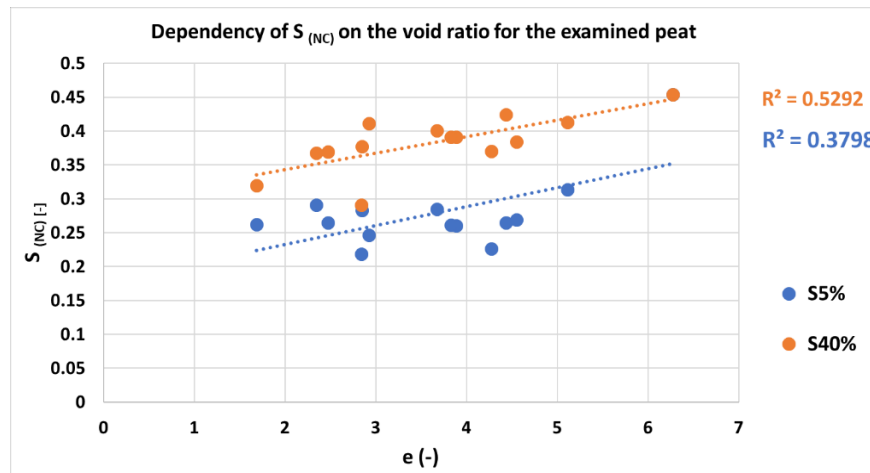
Figure 37: Dependency of S(NC) in the void ratio for the examined peat.

Before concluding the determination of the S parameter, it is noteworthy to address that upon the initial stages of determining the $S_{(NC)}$ parameter, it was noticed that several values displayed considerable discrepancy between their mean as well from what was expected from literature. To examine this inconsistency, the ratio of the applied vertical consolidation stress over the preconsolidation stress σ'_{vc} / σ_p versus the $S_{(NC)}$ value was plotted (Figure 38). A distinction was made between the samples obtained from the crest and the toe area of the dike to examine any sample location dependency.
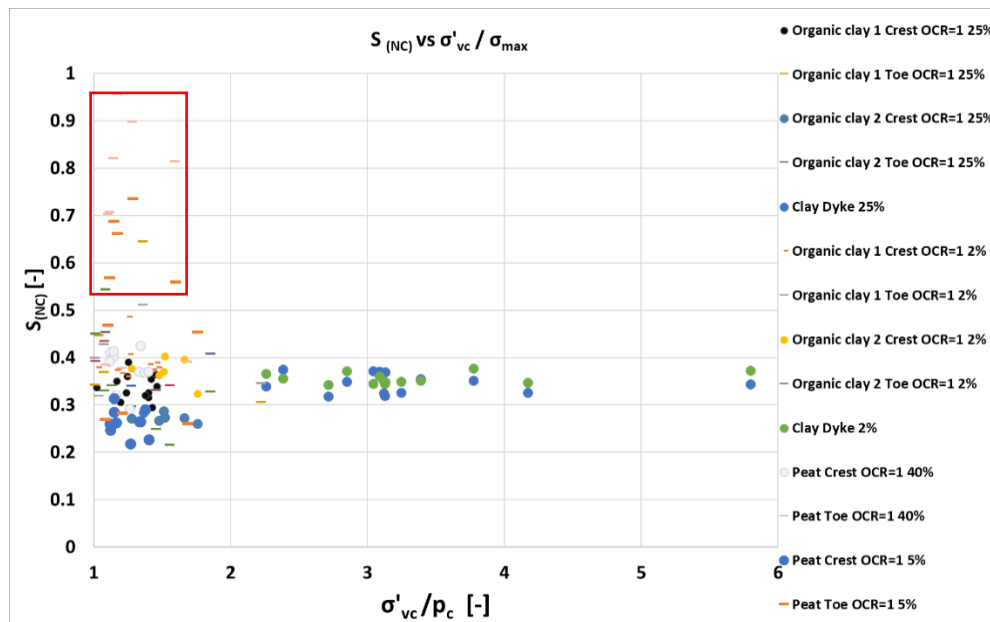
Figure 38: Influence of the applied consolidation stress in the resulting values of the $S_{(NC)}$ parameter for the examined soils in all considered strains. For simplicity, the samples obtained from the toe area of the dike are given in dash while the samples obtained from the crest with bullets.

A closer examination of Figure 38 reveals that the inconsistent values belongs to samples obtained from the toe area of the dike. A possible explanation of this dissimilarity is attributed in the selected value of the applied consolidation stress. In the case of the clay dike material the applied vertical consolidation stress was always two times higher than the preconsolidation pressure in contrary with the organic clay 1 and 2 and peat samples. The vast majority of these soil samples were consolidated with consolidation stress lower than 1.5 times the preconsolidation pressure. As indicated in Chapter 2 where the stepwise SHANSEP procedure is given by Ladd and Foott (1974), in step 2 it is clearly suggested that the applied consolidation stress needs always to be higher than 1.5 times the preconsolidation pressure. Only then the normalised behaviour will yield in a more constant value of S parameter. Therefore, it is concluded, that for the correct application of the SHANSEP technique the soil samples should consolidate with values preferably >1.5 times higher the σ_p. This will consequence all the soil samples to behave truly normally consolidated.

From Figure 38 it is evident that this is even more necessary to the samples that were subjected to higher over consolidation ratio in the field. Lastly, other factors that might cause the diversity are the soil sample quality and improper laboratory test execution. The average values along with the characteristic design values of the S parameter for all the examined layers are given in Table 10. The characteristic values were based in the equations given in POVM, 2017 and are shown below. The equations 23 and 24 concerns the mean and the standard deviation respectively while the equation 25 derives the characteristic values. For the calculation of the characteristic values a regional data distribution parameter $\alpha = 0.75$ is considered since the data used in the calculations are derived from different cross sections and boring locations (POVM, 2017).

$$x_{average} = \frac{\sum_{x=1}^{x=n}(x_i \ldots x_n)}{n} \tag{23}$$

$$\sigma_x = \sqrt{\left(\frac{\sum_{x=i}^{x=n}(x_i - x_{average})^2}{n-1}\right)} \tag{24}$$

$$x_{kar} = x_{average} - \sigma_x \times t_{0.1;n-1} \times \sqrt{\frac{1}{n} + (1-a)} \tag{25}$$

Where:

- $X_{average}$ = the average value of parameter x;
- x_{kar} = the characteristic 5% lower limit value of parameter x;
- n = number of tests
- σ_x = is the standard variation of parameter x;
- $t_{0.1; n-1}$ = the 10% value of the Student-t distribution
- a = the data distribution parameter

Table 10: Derived and mean values of S for the examined soil layers.

Soil	$S_{mean\ 2,5\%}$	$S_{kar\ 2,5\%}$	$S_{mean25,40\%}$	$S_{kar25,40\%}$
Clay dike	0.36	0.34	0.34	0.33
Peat	0.27	0.25	0.38	0.36
Organic clay 1	0.38	0.35	0.33	0.31
Organic clay 2	0.37	0.35	0.29	0.27

3.2.2 Strength Increase Exponent m

The strength increase exponent m determines the extent of the impact of the OCR in the resulting undrained shear strength. The derivation of the parameter is accomplished from two methods (van Duinen, 2014). The first method is done by performing several singe stage Triaxial or DSS tests for the same soil at in-situ stresses. In this way, the determination of $S_{(OC)}$ is established. Since, the soil samples are taken from dissimilar locations and depths for a particular soil the OCR varies. The combination of the $S_{(OC)}$ and the OCR establishes the SHANSEP curve (refer to Figure 2) and the m is derived from the power regression line of the $S_{(NC, OC)}$ vs OCR plot. The second recommended method is done by performing a series of one-dimensional compression tests (oedometer, CRS tests). Van Duinen (2014) reported that m can be determined from the isotach parameters m ≈ (b - a) / b. Alternatively, the CR and RR may be used via the equation m ≈ (CR - RR) / CR (Zwanenburg and Jardine, 2015).

Typical values of the m parameter are in the range of m ≈ 0.7 − 0.9 with the most dominant being m ≈ 0.8 (D'Ignazio, 2016). Similarly, with the $S_{(NC)}$ parameter the m parameter was determined at service conditions (2%,5%) and critical state strain (25%,40%) levels. At first, as shown in Figure 39 the calculated m parameter at service conditions strain levels in organic clays deviates from the m parameter obtained from critical strain levels. This was an expected outcome since in the previous subchapter it was shown that the S value is strain level dependent. The value of m in the critical strain level displayed values which replicate better the expected value of the parameter while the estimated value of m in service conditions strain levels for clays displayed lower values than the expected. The described inconsistency was attributed to the different stress strain responses of the samples that were consolidated with in-situ stresses and with a consolidation stress higher than the preconsolidation pressure. Figure 41 shows clearly that the NC samples, in a strain level of 2% are already experiencing the maximum strength they

can mobilize in contrary with the OC samples where the s_u obtained from 2% strain level lies below the maximum undrained shear strength (s_u peak). Therefore, in the case of the NC state samples the $S_{(NC)}$ is obtained from the peak strength of the soil, where in the case of over consolidated state samples the $S_{(OC)}$ is derived at a strain level which is lower than the peak strength. The outcome of this can be visualized further by observing the downward movement of the power regression line with increasing OCR in the case of the $S_{(OC)}$ obtained from 2% strain level. To avoid this inconsistency, the $S_{(OC)}$ was derived from 5% strain and the determined values are also given in Figure 39. The 5% strain level was thought to be a reasonable decision since, the values of $s_{u5\%}$ are much closer to the peak strength of the soil and additionally the strain level of 5% is as close as possible to the proposed 2% strain level which is required for the analysis of a Blue dike. The aforementioned behaviour is addressed also from Bay et al. (2005). Purpose of their research was a detailed study of the SHANSEP parameters for soft Bonneville clays. They reported that the samples that were consolidated beyond the maximum preconsolidation pressure reached their maximum strength (q_{max}) at considerably lower strains than the samples where the overconsolidation was maintained (Figure 42). However, for determining the $S_{(OC)}$ in their study the SHANSEP stepwise procedure given from Ladd and Foott (1974) was followed as given in the subchapter 2.4. The derived value of m from their study was equal to 0.82 with a reliability almost equal to 1 (Figure 43). Likewise, Abdulhadi (2009) performed a study on resedimented Boston Blue clays following the stepwise SHANSEP procedure allowing the samples to swell to known OCR levels and the derived values of the m parameter displayed very high values of reliabilities (Figure 43). This implies that when the m parameter is derived based on the stepwise SHANSEP procedure the reliability of the derived value of the m parameter drastically increases.

The second method (Figure 40) resulted in m values dominantly ranging from 0.88 – 0.99 for all the examined soil layers. These values are in the upper edge of the expected range of the m parameter. Lastly, the Table 11 contains the derived values of the m parameter.
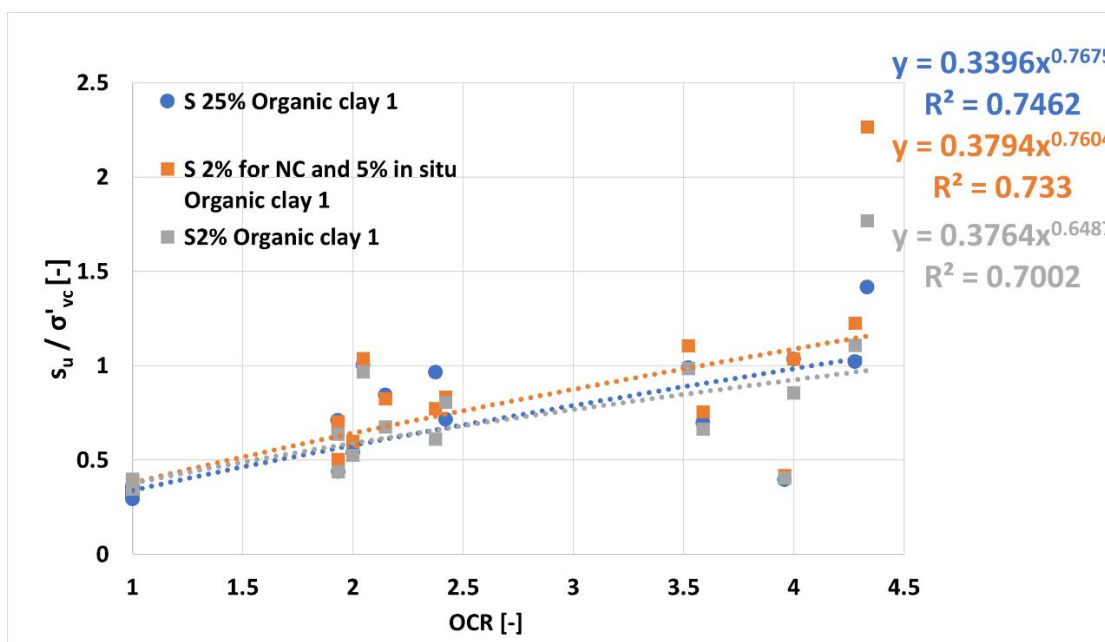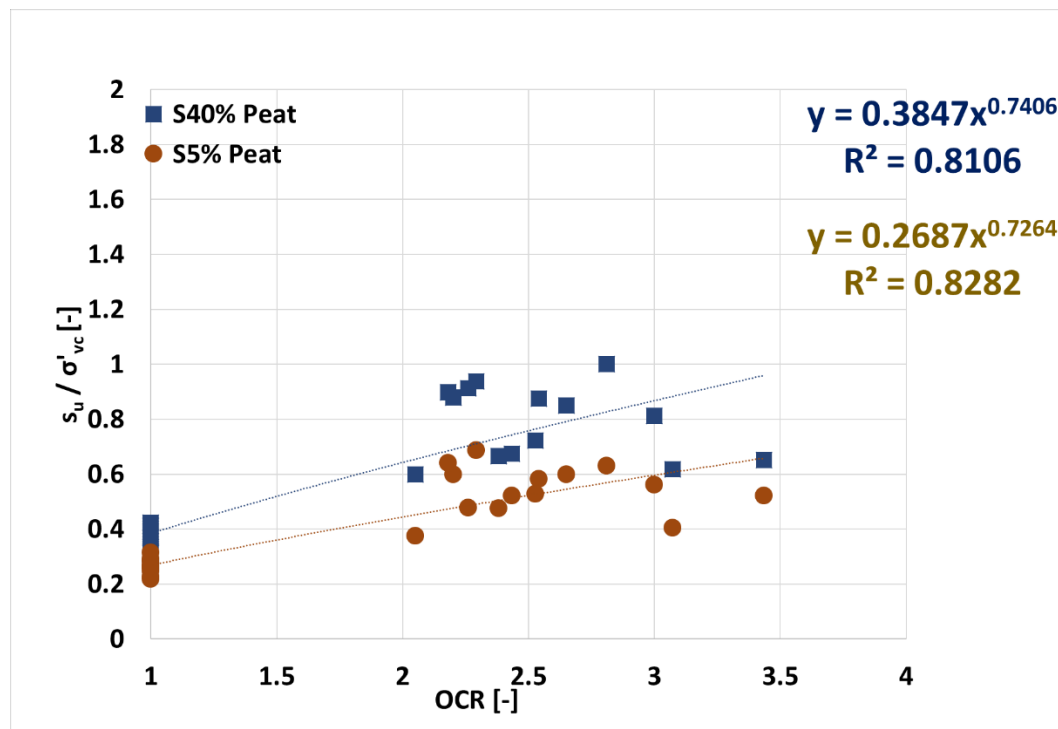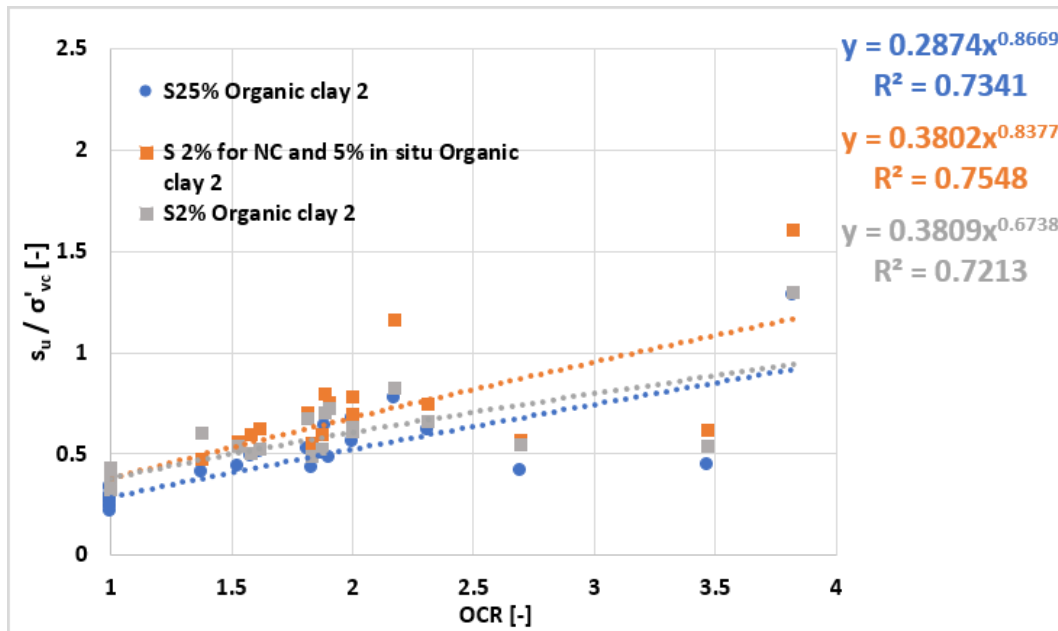
Figure 39: m determination for the examined soil layers with method 1. It has to be noted that for the clay dike material limited number of samples consolidated with OCR ≠ 1 were available and the SHANSEP curve for this material could not established.
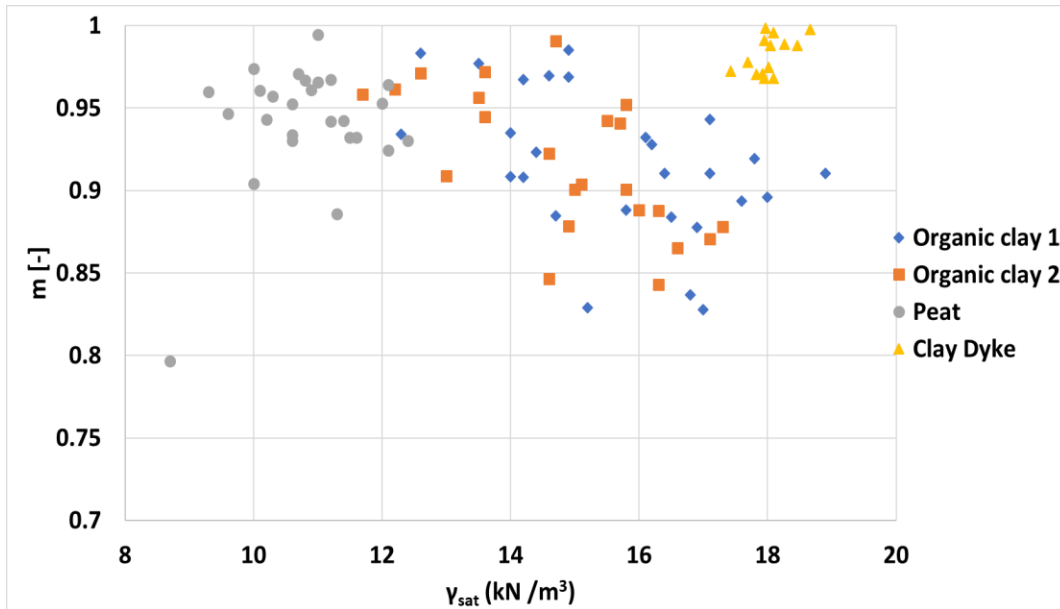
Figure 40: m vs γ_sat for the examined soil layers (second method).
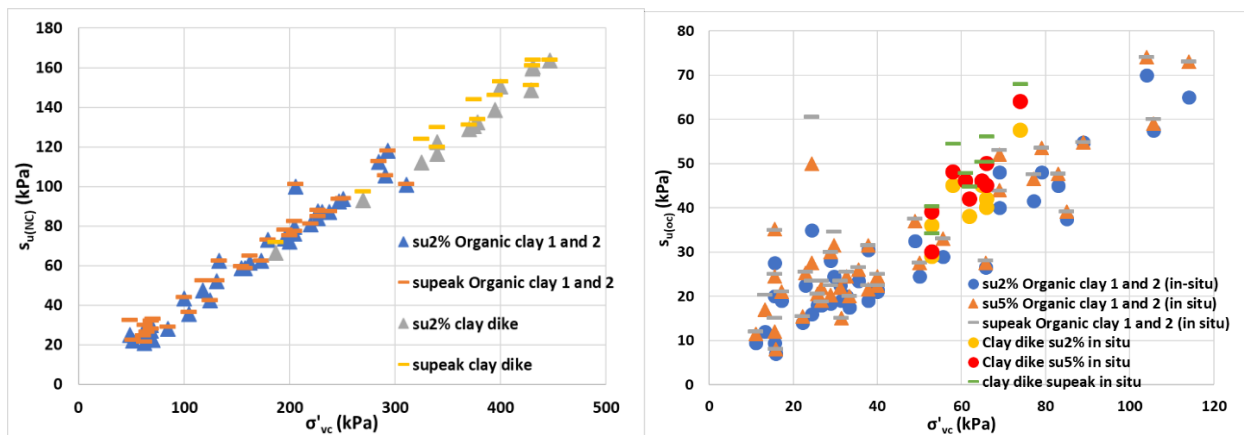
Figure 41: Illustration of the similarity of the s_u obtained from 2% strain level and the peak strength for the NC soil samples (left). On the right it is demonstrated that in the case of the OC samples the s_u at 5% strain level is closer to the peak strength of the soil.
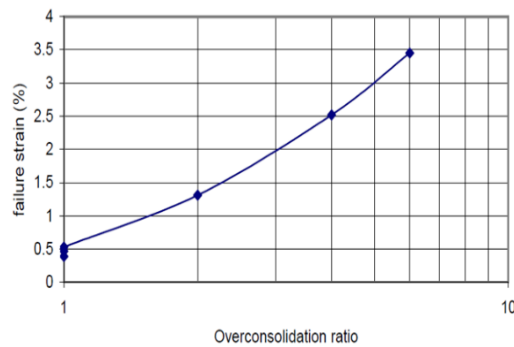
Figure 42: Axial strain at failure against increasing OCR (Bay et al., 2005).
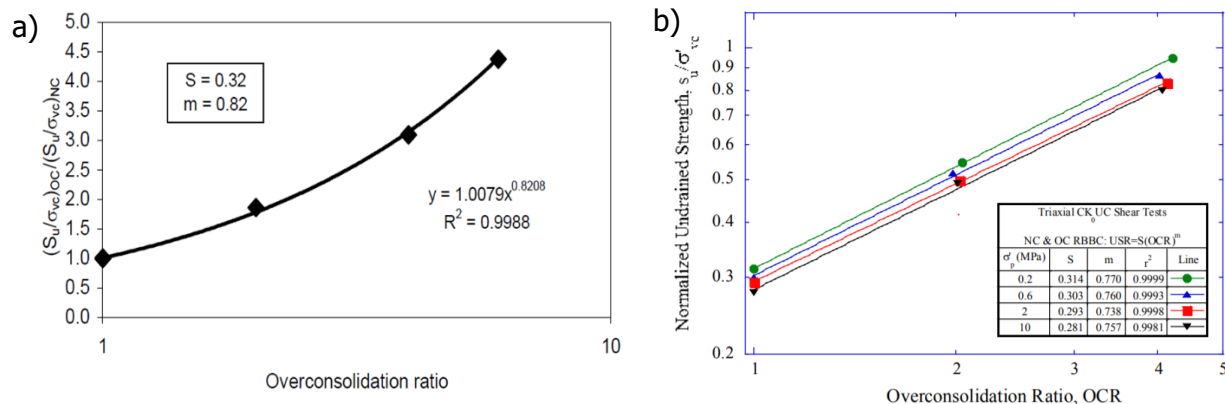
Figure 43: Determination of the m parameter with samples that were allowed to swell to known OCR levels. a) Soft Bonneville clays (Bay et al., 2005) b) RBBC clays (Abdulhadi, 2009).

Table 11: Derived m from the 1st and 2nd method.

Soil	1st method		2nd method	
	$m_{mean2,5\%}$	$m_{mean25,40\%}$	m_{mean}	m_{kar}
Clay dike	-	-	0.98	0.97
Peat	0.73	0.74	0.94	0.91
Organic clay 1	0.76	0.77	0.92	0.89
Organic clay 2	0.84	0.87	0.93	0.9

3.2.3 Determination of Friction angle and cohesion of the soils

The Friction angle and the cohesion describe the effective strength of the soil in drained conditions. These effective strength parameters are required input parameters for the Hardening and Soft Soil constitutive models. The determination of the friction angle was made for service conditions strain levels (2,5%) and critical state strain levels (25,40%). The value of cohesion is assessed only in the case of engineering strains since, in critical state, the c'= 0.

In the case of clays, the effective strength parameters were derived based on the least square method using as input the values of effective average of the principal stresses $s' = (\sigma_1 + \sigma_3) / 2$ (x axis), against the half deviatoric stress $t = (\sigma_1 - \sigma_3) / 2$ (y axis). For peats, the effective strength parameters were assessed from the vertical effective stress σ'_{vc} (x axis) against the shear stress τ (y axis). From the slope $\tan_\alpha = t/s'$ (for clays) and $\tan_\alpha = \tau/\sigma'_{vc}$ (for peats). The friction angle is calculated from $\tan_\alpha = \sin_\varphi$ (van Duinen, 2014). Figure 44 shows the obtained friction angle and cohesion of the examined soils. It has to be noted that the lower bound values of 2%, 5% strain levels produced a cohesion equal to 0 kPa and therefore are not included in Figure 44.
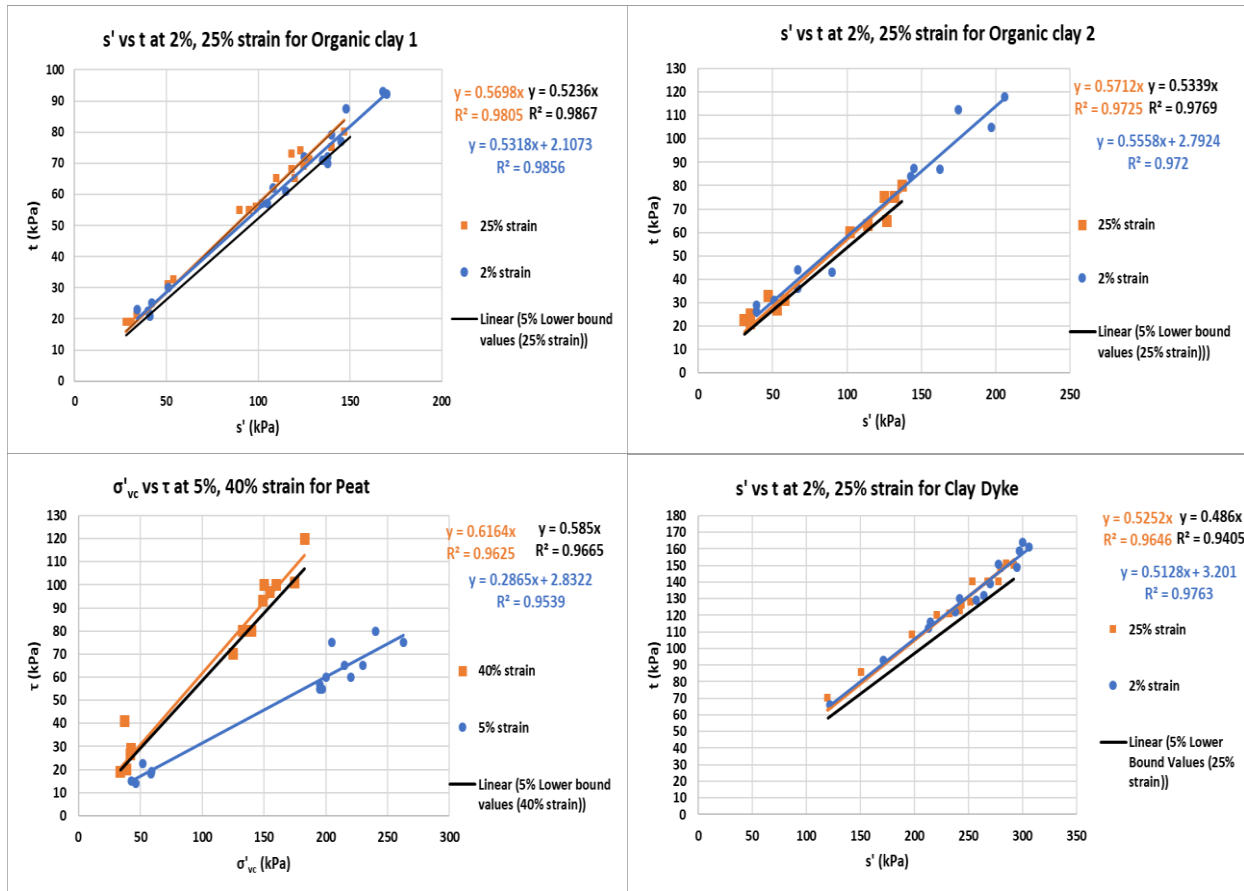
Figure 44: Determination of cohesion and friction angle for the examined soils.

The way of determining the frictional resistance and cohesion of the soil incorporates and some limitations. The parameters are derived from data obtained from single stage anisotropic consolidated undrained triaxial tests for clays and single stage constant volume direct simple shear tests for peats. The data might contain errors arising from the heterogeneity between the different soil samples along with the probable varying sample disturbance prior to the execution of each laboratory test. Finally, the Table 12 includes the derived values of friction angle along with the derived values of the K_0^{NC} based on $K_0^{NC} = 1 - \sin(\varphi_{25,40\%})$.

Table 12: Derived mean and kar values for the friction angle and cohesion of the examined soils

Soil	$\varphi_{mean2,5\%}$ (degrees)	$\varphi_{mean25,40\%}$ (degrees)	$\varphi_{25\%\ lower\ bound}$ (degrees)	$c_{2,\ 5\%}$ (kPa)	K_0^{NC}
Clay dike	30.85	31.68	29.10	3.2	0.47
Peat	16.65	38.05	35.73	2.8	0.38
Organic clay 1	32.14	34.7	31.6	2.1	0.43
Organic clay 2	33.92	34.84	32.68	2.8	0.43

3.2.4 G_{ur} / s_u^A, E_{50}^{ref}, E_{ur}^{ref} and E_{oed}^{ref}

The SHANSEP NGI-ADP constitutive model requires the normalised unloading and reloading shear modulus (G_{ur}) over the undrained shear strength. The parameter can be obtained from the slope of unloading reloading path of stress strain curves of triaxial compression,

extension and direct simple shear tests. The DSS test gives direct determination of G_{ur}, but the TXC, TXE tests provide unloading reloading Young's modulus (E_{ur}) where G_{ur} can be calculated as $G_{ur} = E_{ur} / (2 (1+v'))$. Unfortunately, the described procedure of obtaining unloading reloading paths from triaxial compression, extension and direct simple shear tests is very unlikely in engineering practise. Consequently, the G_{ur} is not available in the triaxial and direct simple shear stress strain curves used for this research. The parameter derivation was done for G_{50} / s_u^A. It has to be noted that the use of G_{ur} is given as an input parameter for the model since this stiffness is valid for all the different stress paths as shown in Figure 45. In addition, the derived G_{50} / s_u^A for the examined soil layers will be further investigated in subchapter 3.4 through the Soil TestFacility offered from PLAXIS.
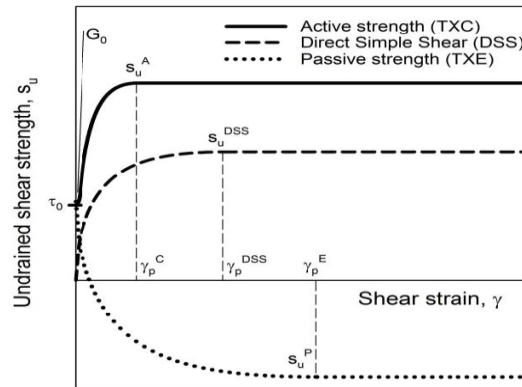
Figure 45: Determination of Gur for the different stress paths.(Visschedijk, 2018)

Ladd and Foott (1974) mentioned that besides the normalised behaviour of the undrained shear strength, soft soils usually display normalised behaviour in the stiffness E_u / σ'_{vc}. In other words, the undrained Young's modulus is dependent on the applied consolidation stress. The E_{u50} obtained from the $C_{K0}UC$ tests in clays translated to E_{50} and in turn to G_{50} based on the transformation formulas recommended from POVM, 2017.

The drained modulus E'_{50} have been calculated based on:

$$E'_{50} = \frac{E_{u50\,(1+v')}}{(1 + v_u)} \qquad\qquad (26)$$

Where:
- E_{u50} is the undrained Young's modulus at 50% of the peak shear strength
- E'_{50} is the drained Youngs Modulus at 50% of the peak shear strength
- v_u is the Poisson's ratio for undrained conditions
- v' is the Poisson's ratio for drained conditions

The drained values of Poisson's ratio are typically on the range of $0.1 < v' < 0.3$. For this research an average value of 0.2 is used. The undrained Poisson ratio was set equal to 0.495. The G_{50} is calculated based on the equation, $G_{50} = E_{50} / 3$ (Constantinou, 2017).

Figure 46 and Figure 47 illustrate the dependency of the stiffness with consolidation stress. The increase in consolidation stress results in higher values of stiffness. Moreover, the plot demonstrates that the larger values of stiffness belongs to the soil samples that were consolidated beyond σ'_p (OCR=1). This was an expected outcome since, the values of σ'_3 applied for achieving the normally consolidated state of the samples are substantially higher than the σ'_3 applied for the samples consolidated with in situ stresses. Moreover, in the previous chapters it was explained that the samples that were consolidated beyond the σ'_p reached their maximum mobilized shear

strength at low strains, thus stiffer responses than the soil samples consolidated with in situ stresses.
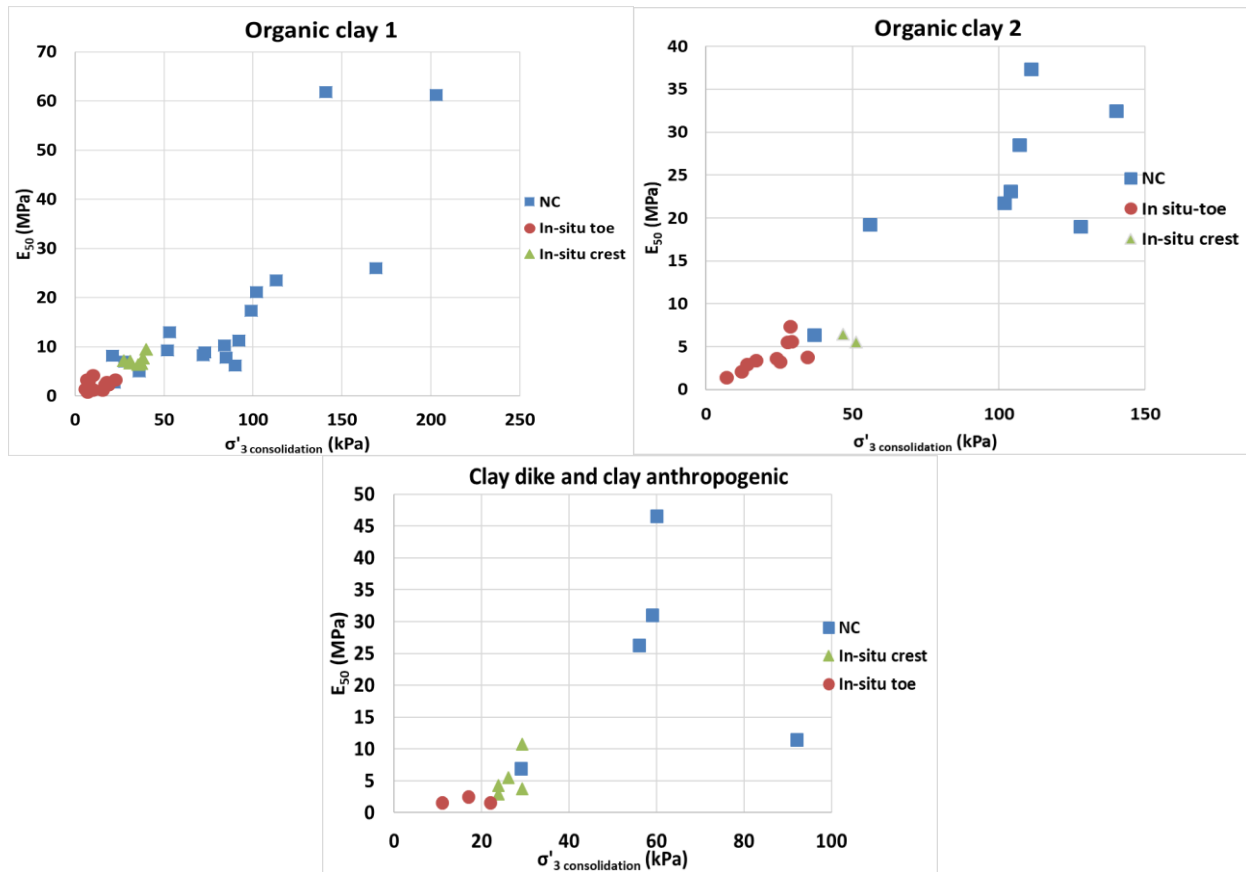
Figure 46: Illustration of the stress dependency of stiffness on the examined clay layers.
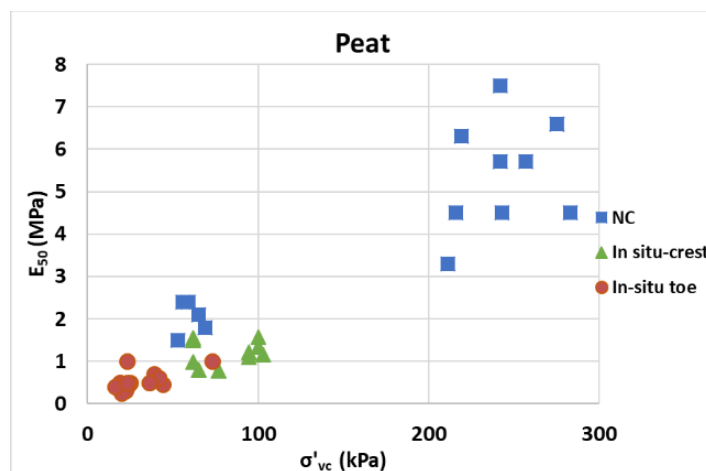
Figure 47: Illustration of the stress dependency of stiffness on the examined peat.

To account for the observed stress level dependency of the Young's modulus the data is normalized with respect to a reference stress of 100 kPa (p^{ref} = 100 kPa) and plotted in a $Ln(E_{50})$ versus $Ln(\sigma'_3/p_{ref})$ graph (where σ'_3 is the minor principal consolidation stress) for samples tested at in situ stress conditions and for samples tested at normally consolidated conditions. In the case

of peats, the σ'_3 equals to the σ'_{vc} applied in the DSS shear test. The stress dependent stiffness modulus can be given by the following equation:

$$E'_{50} = E_{50}^{ref}(\frac{\sigma'_3}{p^{ref}})^m \tag{27}$$

The resulting m of the clays for NC samples and the samples consolidated with in situ stresses for clays is 0.99 and 0.91 respectively and it is shown in Figure 48. In the case of peats, the resulting m equals to 0.98 for the NC samples and 0.78 for the samples consolidated with in-situ stresses (Figure 49).
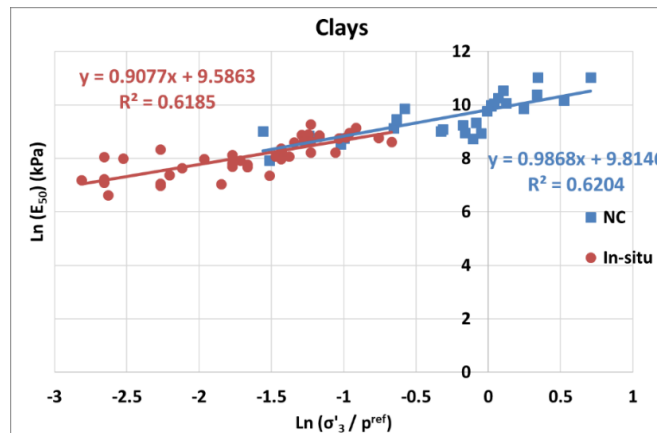
Figure 48: m derivation for NC and in-situ stresses for clays.
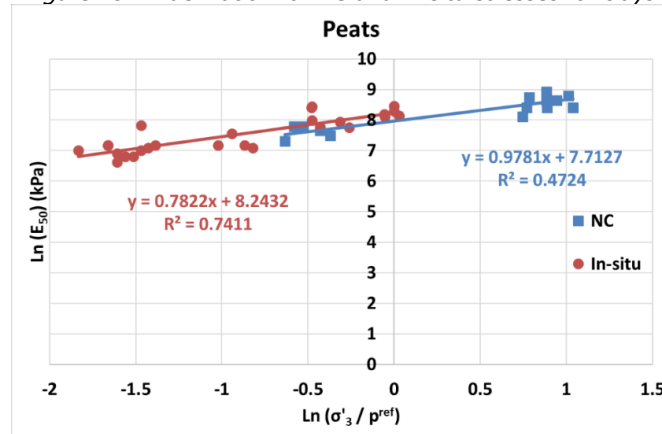
Figure 49: m derivation for NC and in-situ stresses for peats

The Figure 50 display the normalised G_{50} / s_u^A for the Organic clay 1, 2 clay dike and the peat. The values of G_{50} / s_u^A of the samples consolidated with in-situ stresses lie between 20 - 80 with an average of 38, 31 and 32 for Organic clay 1, 2 and clay dike respectively. Additionally, the NC samples displayed considerable deviation from their average. A possible reason was attributed to the dependency of $G_{50} / s_u^A{}_{NC}$ with the plasticity index (Figure 51). Previous research made from Vermeer et al. (1985) and a recent study from Constantinou, (2017) reported that the $G_{50} / s_u^A{}_{NC}$ is decreasing with increasing plasticity which is an agreement with the finding of this investigation. Another possible mechanism for this inconsistency can be attributed to the different increasing rates between E_{50} and s_u with increasing consolidation stress. The latter is possibly causing the difference of the different G_{50} / s_u^A for the samples obtained from the crest and the

toe area of the dike. In the case of the organic clay 1 and the clay dike the values of the samples consolidated with in situ stresses in the crest are marginally higher than the ones in the toe area of the dike. Nevertheless, direct conclusions for the latter cannot be drawn since the observed behaviour is not consistent to all the examined soil layers and further investigation is required. For Peat the derived values in NC and OC state are in greater agreement with an average value of G_{50} / s_u^A = 23 (Figure 50). Therefore, for clays it is concluded that only the G_{50}/s_u^A $_{(OC)}$ is recommended for use.

As it concerns the determination of the G_{ur} / s_u^A the first step was the determination of the G_{50} / s_u^A as shown previously. Afterwards, the average value of the G_{50} / s_u^A $_{(OC)}$ was correlated with the average value of G_{ur} / s_u^A which was determined from the best fit simulated stress strain curves with the use of the STF (Figure 52 and 53). Thus, the analysis was achieved by obtaining several experimental stress strain curves from each soil layer with the aim to reproduce the best fit simulated curve with the experimental. The decision of applying this analysis is considered reasonable and useful for Dutch practise since the G_{50} parameter is given for all the available DSS tests of peats while for clays the G_{50} is straightforwardly derived based on the equations given from POVM (refer to equation 26). In addition, the empirical equations given from WBI and POVM for determining the G_{ur} incorporate large uncertainties (i.e. $G_{ur} = 2E_{oed}$, $G_{ur} = 2 - 5\ G_{50}$) which may result in a determined value of G_{ur} / s_u^A which deviates notably from the reality. The investigation revealed that for the Organic clay 1, 2 and the clay dike material the G_{ur} / s_u^A lies in a factor of 1.55, 1.65 and 1.85 respectively larger than the G_{50}/s_u^A $_{(OC)}$. On the other hand, for peats it was found that the determined value of G_{50}/s_u^A $_{(NC,\ OC)}$ can be safely used as G_{ur} / s_u^A. The ranges of the best fit G_{ur} / s_u^A for all the examined soil layers are also given in the Table 13.
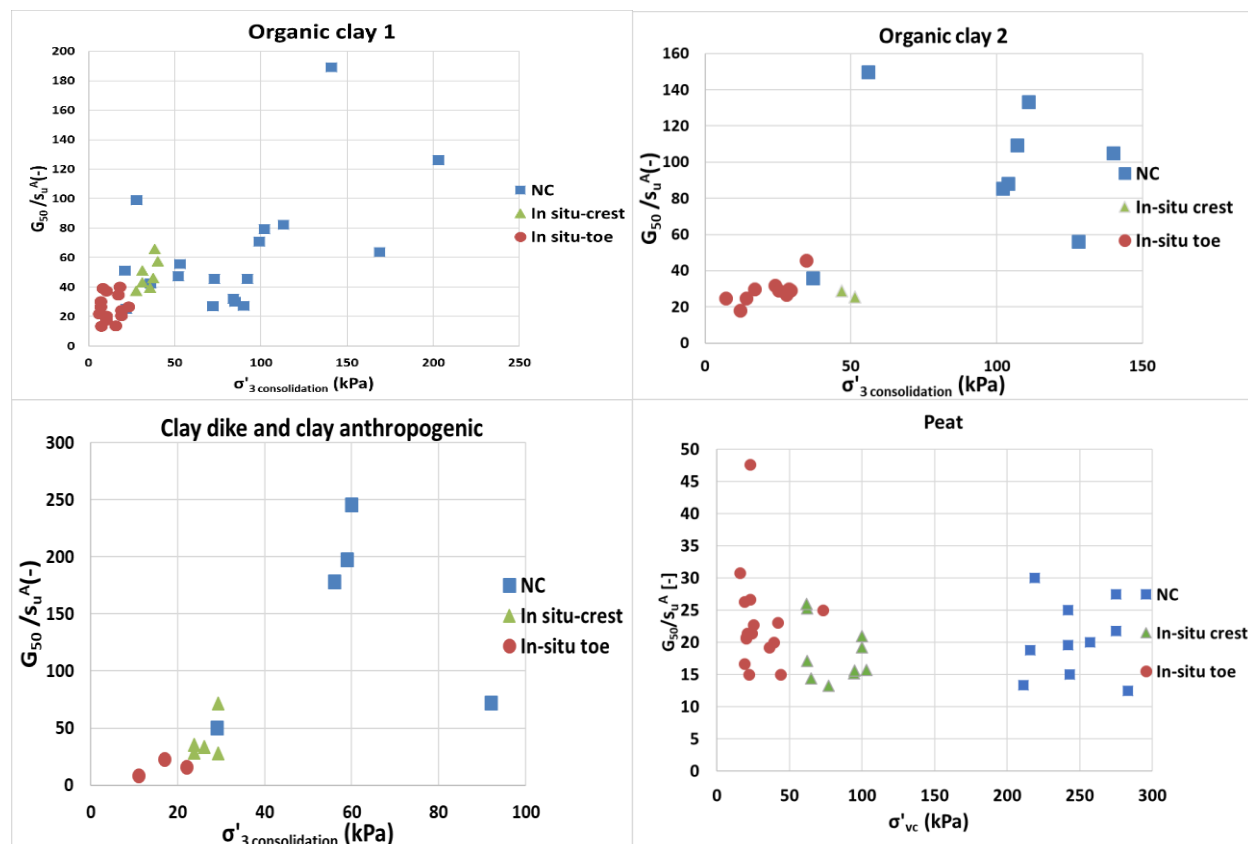
Figure 50: Illustration of the G_{50} / s_u^A for the examined soil layers.
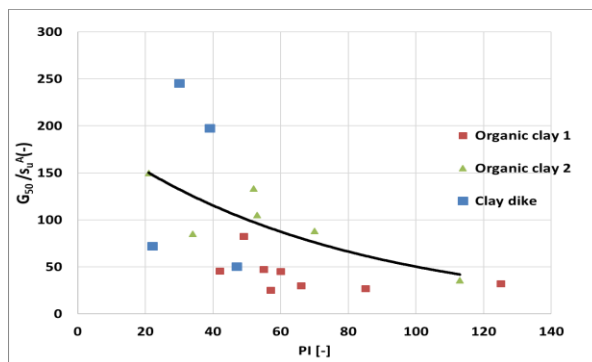
Figure 51: Relation of G_{50} / s_u^A (NC) with plasticity index.
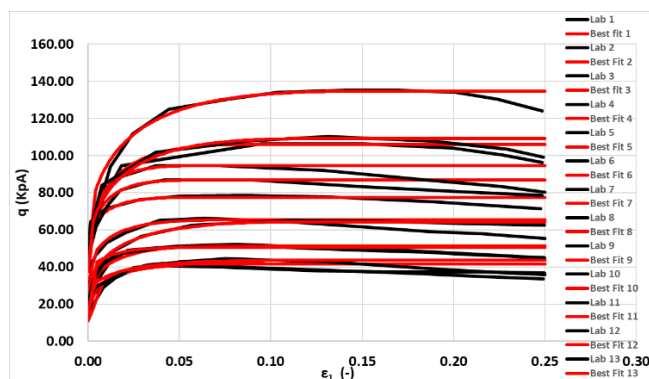
Figure 52: Best fit curves obtained from the SHANSEP NGI-ADP for the examined clays.
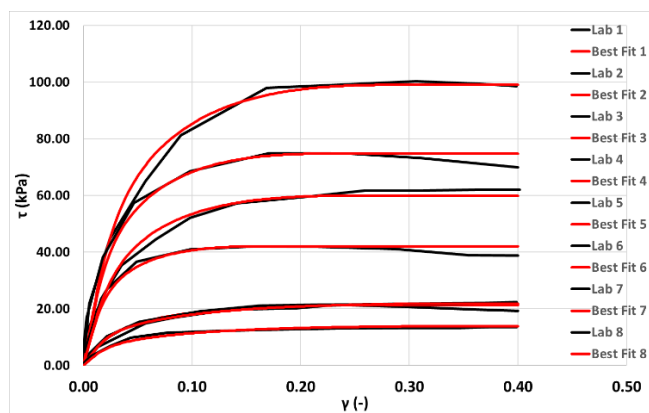
Figure 53: Best fit curves obtained from the SHANSEP NGI-ADP for the examined peat.

Table 13: Correlation of G_{ur} / s_u^A with the G_{50} / s_u^A.

Soil Type	Number of samples used in the analysis	Range G_{ur} / s_u^A	Average G_{ur} / s_u^A	Range G_{50} / s_u^A	Average G_{50} / s_u^A	Factor
Clay dike and clay anthropogenic	5	55 - 80	65	15 - 70	35	1.85
Organic clay 1	7	50 - 80	58	15 - 65	38	1.55
Organic clay 2	7	45 - 80	53	20 - 45	32	1.65
Peat (NC)	3	25 - 35	27	13 - 30	23	1.15
Peat (OC)	7	25 - 35	28	14 - 31	25	1.1

The E_{oed}^{ref} was estimated based on the equation 25 (Obrzud, 2010).

$$E_{oed}^{ref} = E_{50}^{ref} (K_0^{NC})^m \tag{28}$$

Von Soos 1991 suggested ranges for the stiffness exponent m for oedometric modulus and are given in Table 14.

Table 14: Typical values of m obtained from oedometer tests.

Soil type	m_{oed} [-]
Silt: low plasticity	0.6 - 0.8
Silt: medium and high plasticity	0.7 - 0.9
Clay: low plasticity	0.9 - 1.0
Clay: medium plasticity	0.95 - 1.0
Clay: high plasticity	1.0
Silt or Clay: organic	0.85 - 1.0
Peat	1.0
Mud	0.9 - 1.0

For the E_{ur}^{ref} the default value given from Plaxis remained unchanged. The value can be considered as an average since for soft soils the $E_{ur}^{ref}/E_{50}^{ref} = 2 - 6$ and the $E_{ur} = 3E_{50}$ can be considered as an average.

Table 15: Derived values of the m, the E_{50}^{ref}, the E_{oed}^{ref} and the E_{ur}^{ref} for the examined soil layers

Soil	m derived for E_{50}^{ref} (NC)	m derived for E_{50}^{ref} (in situ)	m used for E_{oed}^{ref}	E_{50}^{ref} (kPa)	E_{oed}^{ref} (kPa)	E_{ur}^{ref} (kPa)
Clay dike	0.99	0.91	0.95	16653	6973	49959
Peat	0.98	0.78	1	3594	1505	10782
Organic clay 1	0.99	0.91	0.95	18145	77113	55245
Organic clay 2	0.99	0.91	0.95	16600	6951	49800

Table 16: Estimated values of the G_{50} / s_u^A for the examined soil layers

Soil	G_{50}/s_u^A NC	G_{50}/s_u^A In-situ
Clay dike	185	35
Peat	23	22
Organic clay 1	77	38
Organic clay 2	100	31

3.2.5 τ_0 / s_u^A Initial mobilization

The initial mobilization describes the extent in which the undrained shear strength has been mobilized along with the associated shear strain. In other words, the initial mobilization describes the amount of pre-shearing the soil exhibited in the field. The default value given from PLAXIS is equal to 0.7. A great way to illustrate the influence of the τ_0 / s_u^A in the behaviour of the soil is done through the Soil Test Facility Option offered from PLAXIS. Figure 54 shows than when the τ_0 / s_u^A is set equal to 0.95 the soil response is stiff and almost completely elastic until failure because of the excessive pre-shearing imposed in the soil. On the other hand, when the τ_0 / s_u^A is set equal to 0.4 the soil experience strain hardening from the start of the shearing. For

this illustration all the parameters of the model were constant and the value of τ_0 / s_u^A varied according to the values shown in the Figure 54.
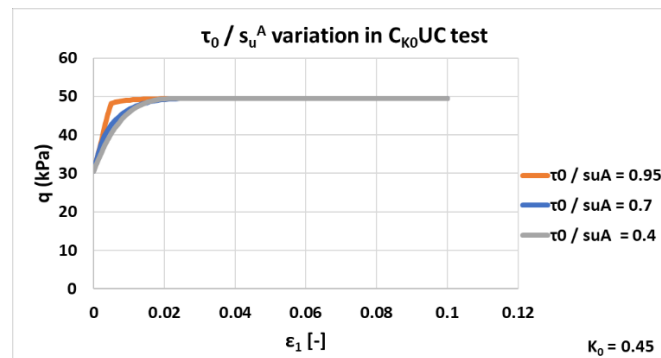
Figure 54: τ_0 / s_u^A variation.

3.2.6 Shear Strains at Failure.

The shear strains independently describe the failure strains for the Triaxial Compression, Triaxial Extension and DSS tests. Each shear strain at failure is dependent on the associate undrained shear strength in the different modes of loading. Therefore, the γ_f^c, γ_f^E, and γ_f^{Dss} are pairs of the s_u^A, s_u^P and s_u^{DSS} respectively. The determination of these parameters is an extremely difficult task mainly because it is rather unlikely to apply more than one shear test in a soil sample. Moreover, according to the new laboratory protocols (WBI 2017) the shear strain at failure for clays is described explicitly from triaxial compression tests while for peats from DSS tests.

Ladd and DeGroot (2003), reported that the shear strains at failure are considerably different under different modes of shearing. From the Figure 4 it is obvious that the shear strain at failure in triaxial compression is reached at low strains (approximately 2%) while in triaxial extension at considerably higher strains at approximately 16%. The strength for a direct simple shear is generally mobilized to a shear strain level between the compression and extension.

Similar study was made from Karlsrud and Hernandez-Martinez (2013) where he verified the findings of Ladd and DeGroot (2003). In his study he additionally reported that the highest deviation belongs to the shear strain at failure in triaxial compression with values ranging from 0.2% up until 5%. Moreover, another finding of his study was that the shear strains at failures were dependent in the sensitivity of the clays. A higher sensitivity produced lower values of shear strains at failure especially for the loading paths in extension and direct simple shear.

The values of shear strains at failure from several studies are given in Table 17 . It is evident that the shear strain level needed to mobilize the compression, or active, strength (inclination of major principal stress is 0° from the vertical), is lower than the shear strain that would mobilize the extension, or passive, strength (inclination of major principal stress is 90° from the vertical). In addition, the strength for direct simple shear (DSS) conditions is normally mobilized to a strain level between compression and extension. Table 17 illustrates than the difference of the γ_f^C with the γ_f^E for the induced NC samples it is considerably higher than the difference of these strain levels for the samples where the OCR was maintained (replicates in situ stresses).
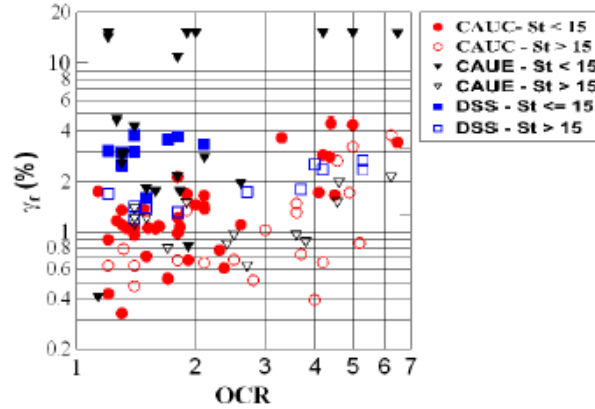
Figure 55: Shear strains at failure under different modes of loading and their dependency in the sensitivity (St) value.

Table 17: Values of shear strains at failure from various studies

Authors	Soil type	γ_f^C (%)	γ_f^{DSS} (%)	γ_f^E (%)	Ratio $\gamma_f^{DSS}/\gamma_f^C$	Ratio γ_f^E/γ_f^C
Ladd and DeGroot (2003)	Various clays (OC)	3-9	10-12	20-26	1.85	3.75
Ladd and Foott (2003)	Various clays (NC)	2	11	26	5	13
Karlsrud and Hernandez (2013)	Norwegian soft marine (OC)	0.3 - 5	1.5 - 5	0.4 - 19	1.25	3.7
Van Duinen (2014)	Clay shale (NC)	1-2	5-8	30	4	20
D Ignazio (2016)	Pernio clay (NC)	2	4	7.5	2	3.25

D'Ignazio (2016) after conducting research in the undrained shear strength of Finish clays it was concluded that upon limited data the calculation of the shear strains at failure are better described from the equations 29 and 30.

$$\gamma_f^E = (2.5 \ to \ 4) \, \gamma_f^c \tag{29}$$

$$\gamma_f^{DSS} = (1.5 \ to \ 2) \, \gamma_f^c \tag{30}$$

The shear strains at failure for the triaxial compression were calculated based on the equation:

$$\gamma_f^c = \frac{3}{2} \varepsilon_1^C \tag{31}$$

Where: ε_1^C denotes that axial strain at failure in triaxial compression tests. Similarly, in Triaxial Extension tests the γ_f^E is given from:

$$\gamma_f^E = \frac{3}{2} \varepsilon_1^E \tag{32}$$

Where: ε_1^E the axial strain at failure in extension.

The derived γ_f^c and γ_f^{DSS} for the examined clays and peat are shown in the Figure 56. All clays displayed a fairly high variability of the γ_f^c with an average value of 11% and 9% and 12% for Organic clay 1, 2 and clay dike respectively. Regarding peat an average value of 31% γ_f^{DSS} is reported. This was expected since the maximum strength in peat is mobilized at high strains. Lastly, no dependency of the shear strains at failure $\gamma_f^{C,\ DSS}$ with OCR was found (Figure 57) which agrees with the findings of Karlsrud and Hernandez-Martinez (2013). It is also evident that the shear strains at failure of the NC samples are remarkably lower than the shear strains at failure of the samples consolidated with in situ stresses for the Organic clays whereas for peats the samples consolidated with in situ stresses in some cases did not mobilise the maximum shear strength even after reaching the 40% strain level. Lastly, in parallel with the identification of a representative value of $G_{ur}\ /\ s_u^A$ as illustrated in subchapter the verification of the equation for determining the γ_f^C was conducted. The investigation showed that the determined value based on the equation describes properly the γ_f^C which produced the best fit value. For peats the γ_f^{DSS} which is determined from the stress strain curve obtained from a peat sample matches entirely the identified best fit γ_f^{DSS}.
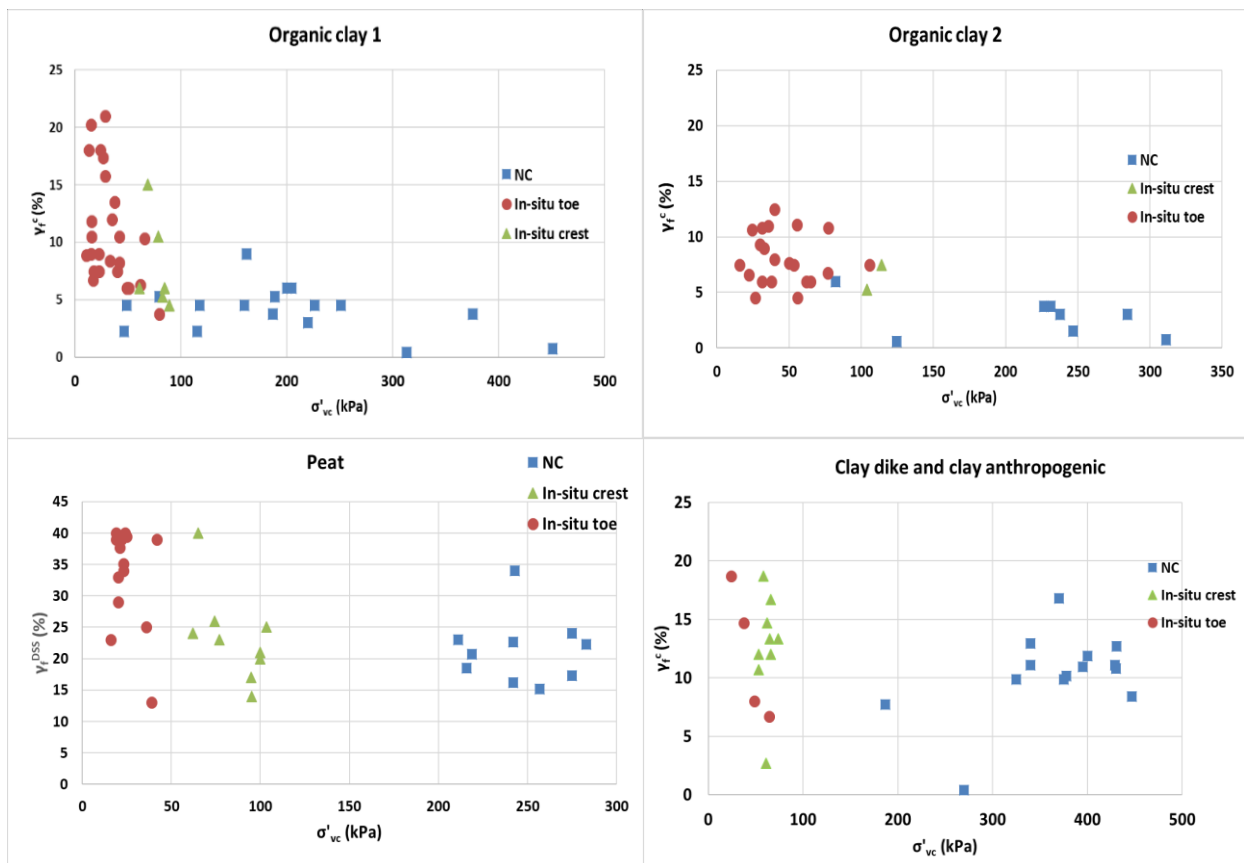
Figure 56: Shear strains at failure for the examined soils.

Table 18: Determined and best fit value of the shear strains at failure for clays and peats.

Soil Type	$\gamma_f^C = 3/2\ \varepsilon_{1f}^C$ (for clays) γ_f^{DSS} (%)	Best fit γ_f^C γ_f^{DSS} (%)	Average Deviation of γ_f^C determined and best fit in %
Clay dike Clay anthropogenic	16	18	10
	10.5	12	
	15	16	
	11.5	9	
	11.5	13	
Organic clay 1	9	8	9
	6	7	
	6.5	7	
	7.5	9	
	9	9	
	7.5	7	
	11	10	
Organic clay 2	10.5	12	11
	7.5	10	
	9	10	
	12	13	
	9	9	
	10	11	
	10	10.5	
Peat	18.5	19	1
	40	40	
	23	28	
	40	40	
	20	22	
	22	22	
	40	40	
	40	40	
	25	25	
	40	40	

Figure 57: OCR vs $\gamma_f^{C,\ DSS}$ for the examined soils.

Table 19: Derived values of the shear strains at failure for the examined soils.

Soil	γ_f^C , γ_f^{DSS} % (NC)	γ_f^C , γ_f^{DSS} % (in situ)
Clay dike	11.5	16
Peat	21	31
Organic clay 1	4	11
Organic clay 2	2.5	9

3.2.8 λ*, κ* Modified Compression and Swelling Index

The modified compression and swelling indexes are required stiffness parameters for the Soft Soil constitutive model. These parameters can be obtained from an isotropic compression test including unloading step. The WBI 2017 suggests that λ* equals the isotach parameter b (λ* = b) while the k* equals two times the isotach a parameter (κ* = 2a).

The isotachen model parameters a, b was derived from plots of the logarithm of the effective vertical stress, p', as a function of the vertical strain, ε_v^H. The slope of the primary loading line gives the value of the modified compression index, b, while the slope of the unloading gives the modified index a. The Figure 58, 59, 60 and 61 shows the determined values of the modified compression and swelling indexes for all the examined soils. In addition, these Figures display the dependency of λ* with the volumetric weight of the soil. The decreasing unit weight leads to an increase of the modified compression index since, a lower density implies higher compressibility. This signifies that the soils located in the toe of the dike should probably modelled with higher values of λ*. Lastly, the higher value of λ* belongs to the Peat which is a highly compressible material.
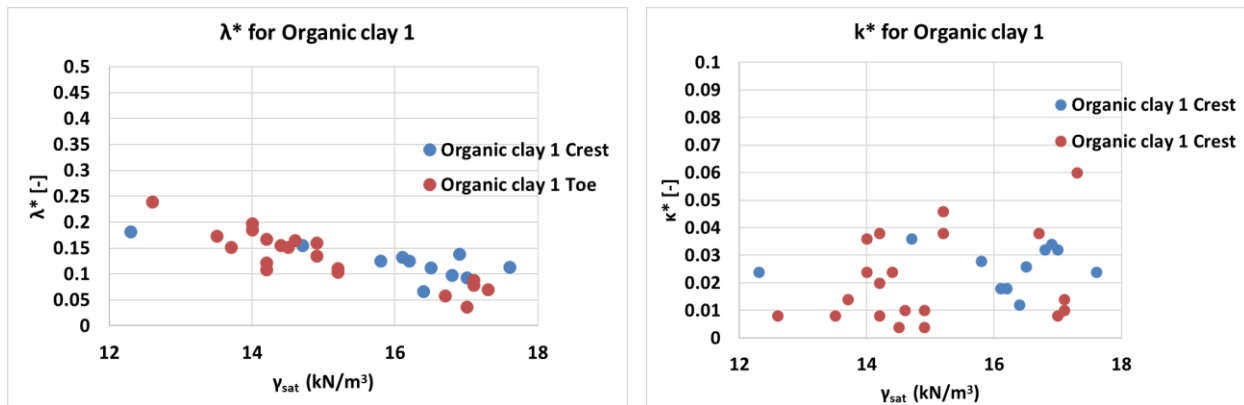
Figure 58:λ* and k* for Organic clay 1.
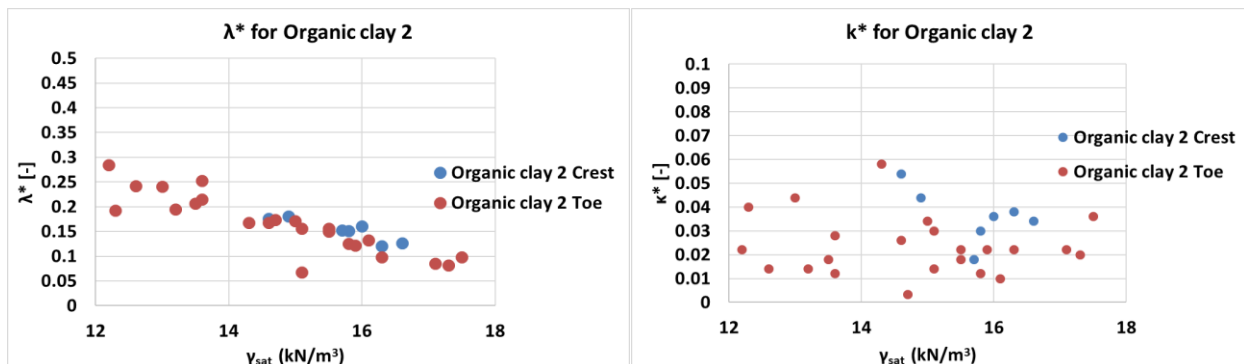
Figure 59. λ* and κ* for Organic clay 2.

Figure 60: λ* and κ* for Peat.
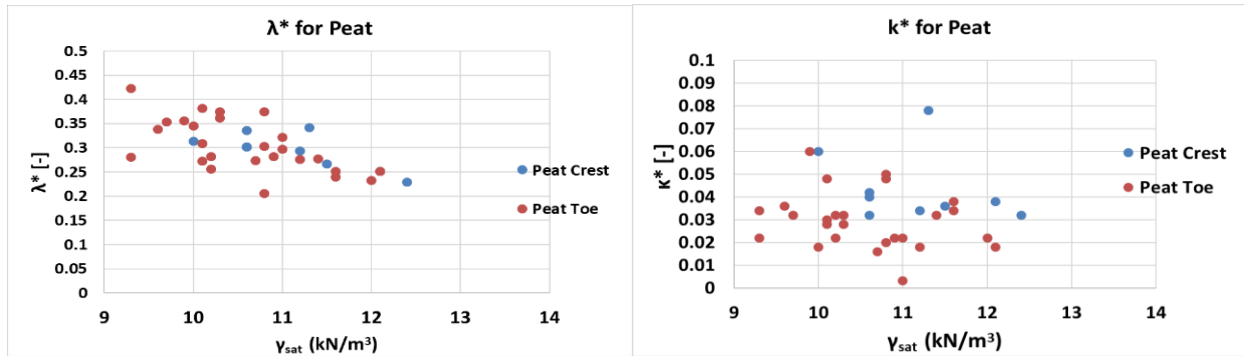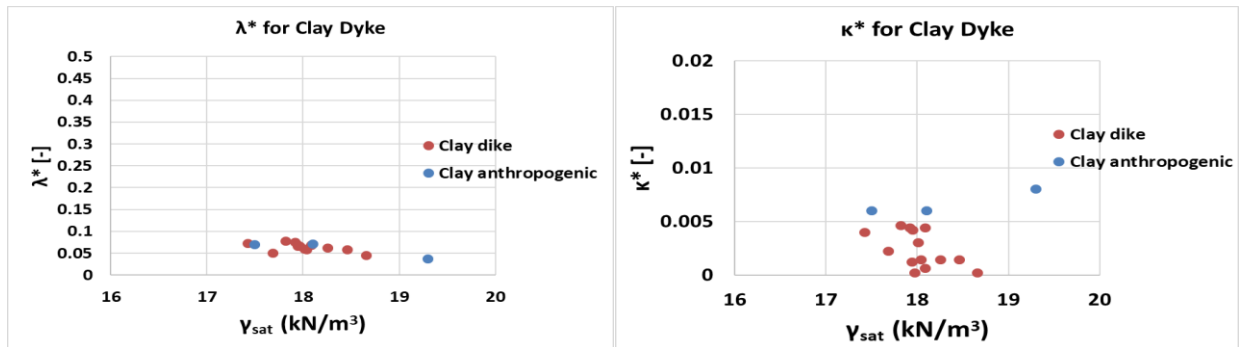
Figure 61: λ* and κ* for Clay Dike.

3.3 Influence of the K_0 value in the parameter determination.

As indicated in Chapter 1 the current laboratory protocol suggests that for evaluating the strength parameters of clays a series of anisotropically consolidated undrained triaxial tests should be conducted. The anisotropic consolidation of the soil samples ensures that the stress conditions applied to the samples are replicating the in-situ regimes in a more realistic manner. The applied K_0 used for the anisotropically consolidated triaxial tests is in all the cases equal to 0.44 - 0.45 for both NC and OC soil samples, with $\gamma_{sat} > 14$. A small number of clayey samples that were identified with $\gamma_{sat} < 14$ consolidated with a $K_0 = 0.35$. The purpose of this subchapter is to evaluate the influence of the applied K_0 value in the parameter determination. In order to accomplish that, the SS and HS constitutive models were used, and the analysis was made through the Soil Test Facility offered from PLAXIS 2D. Through the SS the response of the models in a p' - q space is shown whereas with the HS soil the response in terms of q vs ε_1. In this way, the potential influence of the increasing K_0 value and thus the σ'_3 in the resulting stiffness parameter E_{50} can be assessed due the advance feature of the model to account for stress level dependency of the stiffness.

For achieving the investigation some boundaries need to be set. The soil sample exhibits an in situ vertical consolidation stress equal to 50 kPa (remains constant) with a friction angle of 30 degrees and a cohesion equal to 1 kPa. The K_0^{NC} is given from the Jaky equation $K_0^{NC} = 1 - \sin\varphi_{cv}$. In the case of an OC soil the calculation of the K_0^{OC} is made through $K_0^{OC} = K_0^{NC}OCR^{1/2}$. The horizontal stress is derived from $\sigma'_h = K_{0(NC, OC)}\sigma'_{vc}$ and the σ_p is calculated from $\sigma_p = OCR \, \sigma'_{vc}$. The examination was done for three different OCR levels, specifically, OCR=1 (NC state), OCR= 1.5 (Lightly OC state) and OCR= 2.5 (OC state). The σ'_h varies with the increasing values of the estimated K_0 value. The Table 20 indicates the cases considered along with the associated parameters required for the investigation.

Table 20: Input values in STF for the three different levels in OCR. Please note that for simplicity, in the case of OCR=1 the K_{0lab} was set equal to K_{0Field} due the minor difference between the two. In other words, instead of $K_0=0.5$ the value of $K_0=0.45$ used.

OCR=1	K_0	σ'_h (kPa)	p_c (kPa)
$K_{0Lab, Field}$	0.45 (lab value)	22.5	50
$K_{0Isotropic}$	1	50	50
OCR=1.5	K_0	σ'_h	p_c
K_{0Lab}	0.45 (lab value)	22.5	75
K_{0Field}	0.6	30	75
$K_{0Isotropic}$	1	50	75
OCR=2.5	K_0	σ'_h	p_c
K_{0Lab}	0.45 (lab value)	22.5	125
K_{0Field}	0.8	40	125
$K_{0Isotropic}$	1	50	125

In Figure 62 the input parameters that were set in the Soil Test Facility for the OCR=1.5 are shown. In the case of OCR=1 and OCR = 2.5 the changes made concerns the input values of $p_c=\sigma'_p$ and $\sigma_3=\sigma'_{xx}$. The σ'_{vc} always kept equal to 50 kPa.
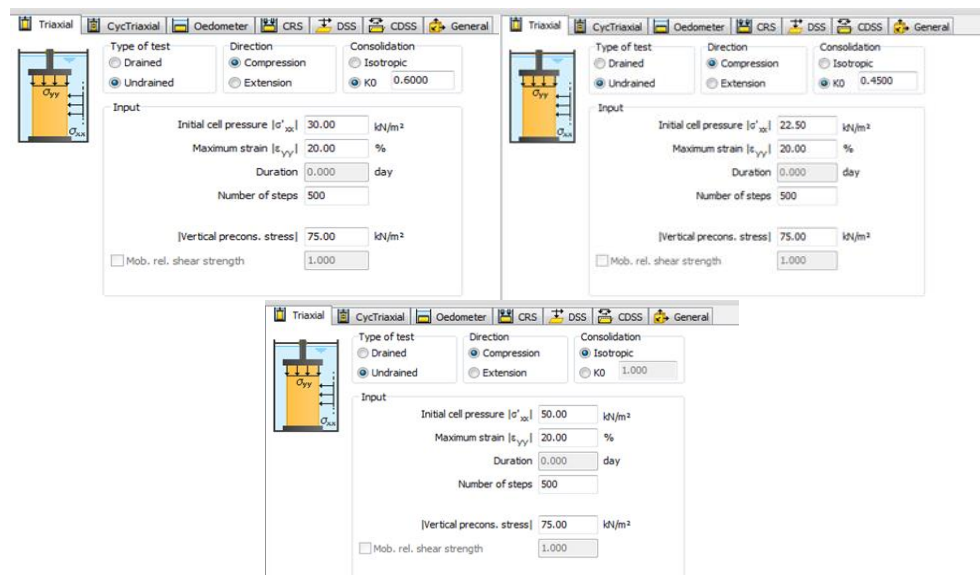
Figure 62: In the top left the input parameter for the illustrates K_{0Lab} are shown. In the top right the K_{0Field} and in the bottom the $K_{0Isotropic}$.

The Figure 63 shows clearly that when the OCR is considered in the applied K_0 value(K_0 field) the resulting q_{max} yields in a higher value and therefore larger values of undrained shear strength ($s_u = q_{max} / 2$). In contrary, the figure also demonstrates that when the K_{0lab} is applied in the OC samples the resulting q_{max} is identical; underestimating the s_u. Lastly, it is obvious that the isotropic consolidation conditions result in the larger q_{max} values.

The investigation with the HS model revealed that increasing K_0 led to an increase in the measured E_{50}. From Figure 64 and 65 it is illustrated that with increasing K_0 value and in turn an increase in σ'_3 the resulting E_{50} is higher. For clarity, in Figure 64 the results obtained from the case of the lightly over consolidated soil are explicitly shown. Therefore, by applying the same K_0

for both the NC and the OC samples an underestimation for both the stiffness and the strength of the materials is expected. Additionally, both the HS and SS displayed identical s_u values which are shown in the Table 21 below.

Table 21: Derived values of s_u and $S_{(OC)}$ based on the SS examination.

OCR=1 [-]	$K_{0\,[-]}$	$\sigma'_{h\,(kPa)}$	$S_{u\,(kPa)}$	$S_{(NC)\,peak\,[-]}$
$K_{0Lab,\,Field}$	0.45 (lab value)	22.5	17.5	0.35
$K_{0Isotropic}$	1	50	22.5	0.45
OCR=1.5 [-]	$K_{0\,[-]}$	$\sigma'_{h\,(kPa)}$	$S_{u\,(kPa)}$	$S_{(OC)\,peak\,[-]}$
K_{0Lab}	0.45 (lab value)	22.5	20	0.4
K_{0Field}	0.6	30	23	0.46
$K_{0Isotropic}$	1	50	26.5	0.53
OCR=2.5 [-]	$K_{0\,[-]}$	$\sigma'_{h\,(kPa)}$	$S_{u\,(kPa)}$	$S_{(OC)\,peak\,[-]}$
K_{0Lab}	0.45 (lab value)	22.5	20	0.4
K_{0Field}	0.8	40	27.2	0.55
$K_{0Isotropic}$	1	50	31.5	0.63

Moreover, it has to be noted that the applied K_{0Lab} = 0.45 for the case of OC samples is a conservative approach. On the other hand, in the case of NC samples it seems that the applied K_0 lab is not always in the conservative side since the organic clays in some cases displayed a K_0^{NC} lower than the applied 0.45. For the clay dike material, the applied K_{0lab} describes the K_0^{NC} adequately. The φ_{cv} given in the Figure 66 is the measured φ_{cv} at 25% strain level for the NC examined clays.

The applied investigation reveals the limitation of the examined constitutive models with the option of the Undrained A analysis. In NC state the resulting behaviour shows a realistic path (not necessarily fully correct), but in the case of OC state the expected dilative behaviour is not captured. Therefore, the resulting q_{max} obtained from real soil samples (especially for the OC state) would probably yield to an even higher q_{max} than what is illustrated in Figure 63. Moreover, in reality the resulting stress path and therefore the undrained shear strength might not be fully identical for the cases of K_{0lab} for the 1.5 and 2.5 cases of OCR.

Another limitation of this examination is the presupposition that the K_0 values in the field are indeed fully described from the Jaky equations. Moreover, this examination also assumes that the angle of frictional resistance remains the same with varying K_0 value. Research done in previous years showed that the friction angle of the soil exhibits neglectable influence by the K_0 values (Kulhawy and Mayne, 1990).

The explained behaviour has a strong interconnection with the parameter determination of the m parameter. By replicating the "correct" K_0 value for the OC soils the resulting $S_{(OC)}$ in both 2% and 25% strain levels will possibly yield in a different value. Therefore, the SHANSEP curves established in subchapter would result in a different power regression line due the updated $S_{(OC)}$ and therefore an updated value of m.
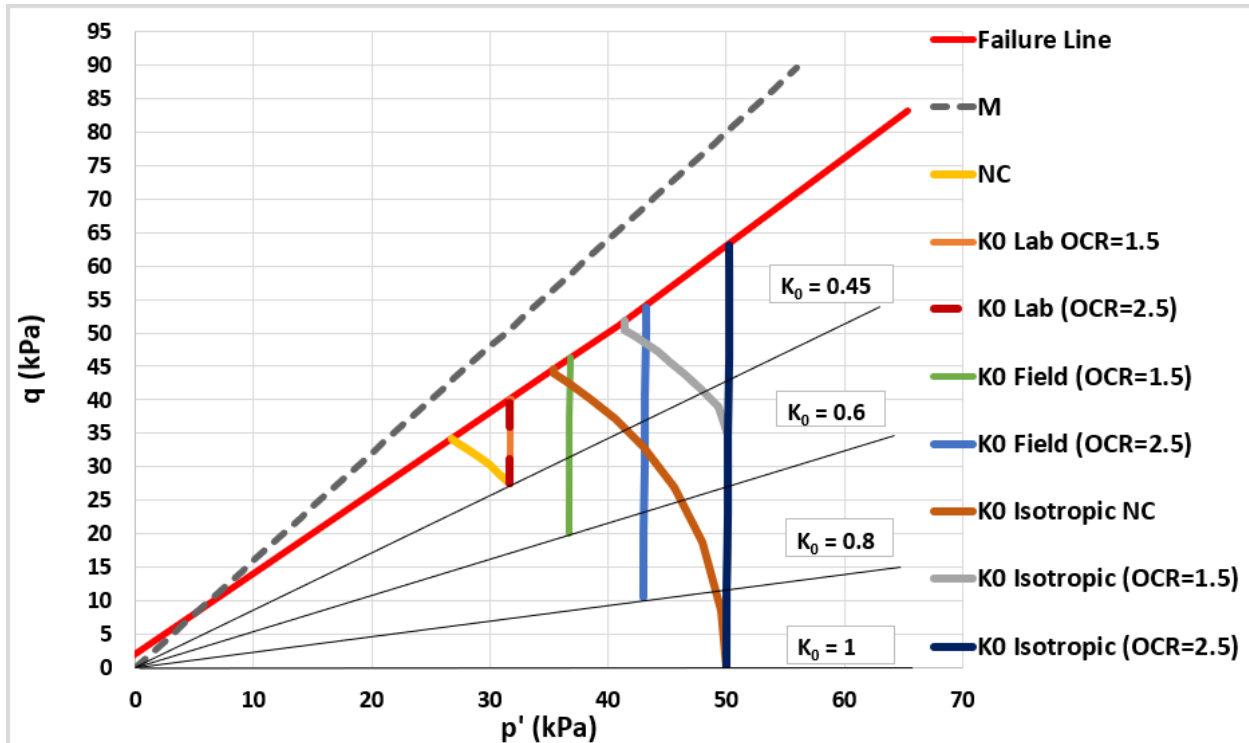
Figure 63: Stress path under different K_0 values with the use of the SS constitutive model.
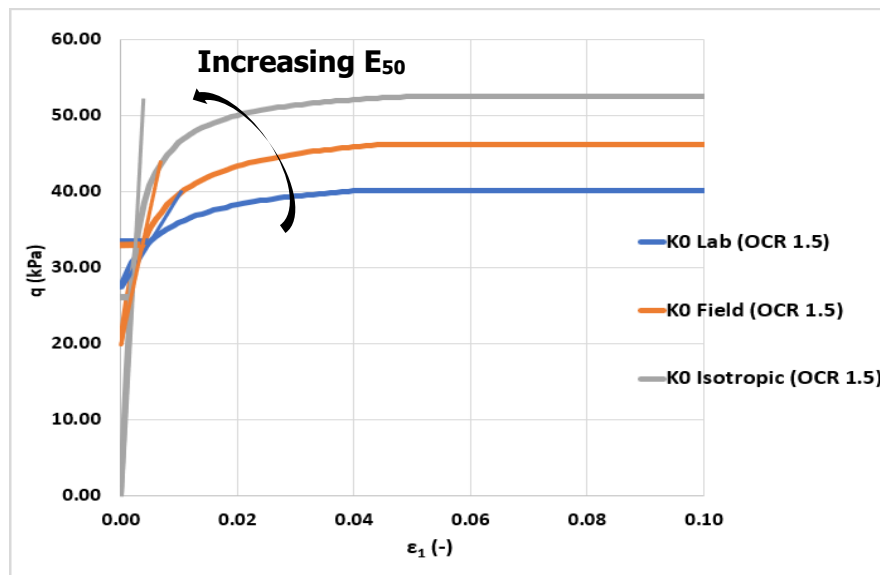
Figure 64: Increasing E_{50} with increasing K_0 value.
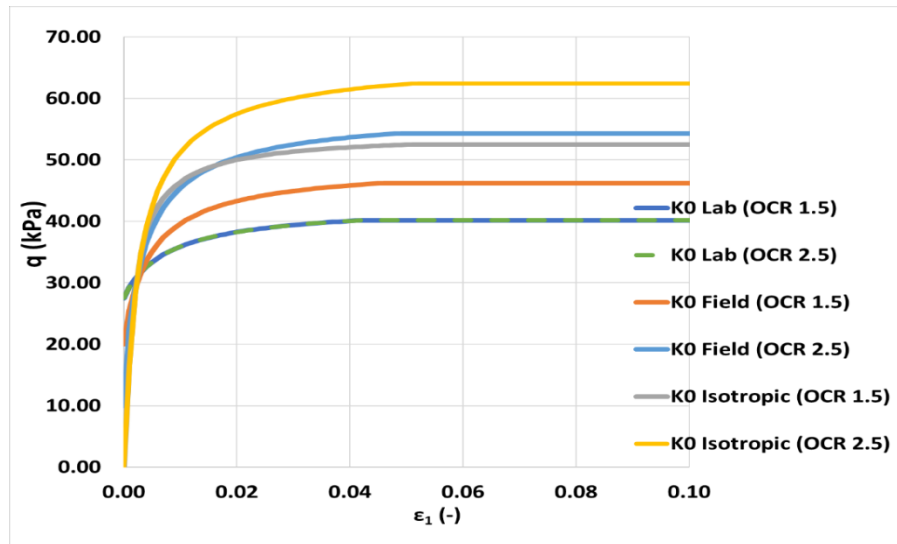
Figure 65: Resulting stress strain plots with the use of the Hardening soil for increasing K_0 values.
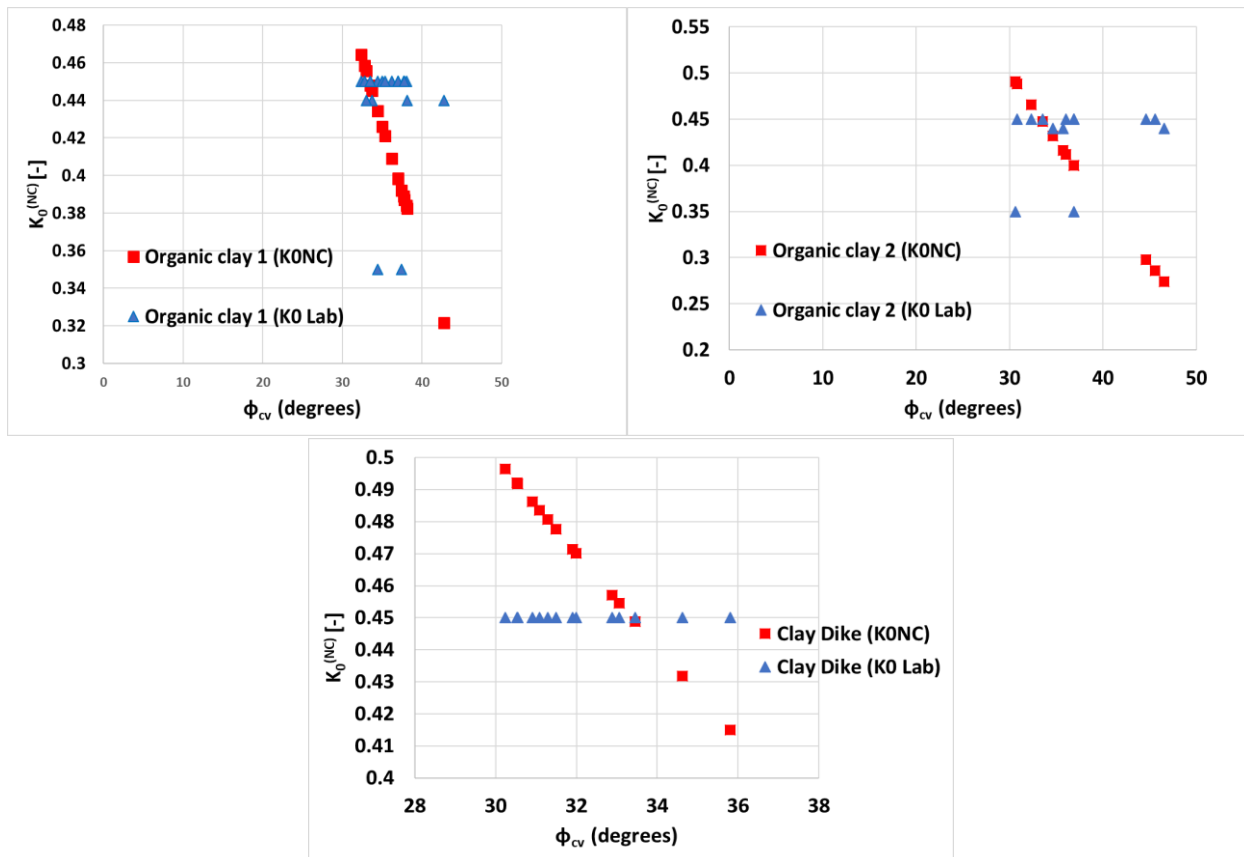
Figure 66. Comparisson of the K_0 value between the one applied in the lab and the calculated.

The results shown are in agreement with a study made from Kamei (1996) where he examined the undrained shear strength and its interrelationship among the application of CIUC, C_{K0}UC, CIUE and C_{K0}UE triaxial tests for an undisturbed Yokohama clay. The comparison from the four different types of triaxial tests showed significant differences in terms of undrained shear

behaviour. The isotropic consolidated triaxial test displayed a notably higher value of s_u from its associate anisotropically consolidated triaxial test. Moreover, the resulting undrained shear strength in triaxial compression and extension was different due the strength anisotropy of the soil (refer to subchapter 2.2). It is interesting to notice that the influence of the K_0 value in the case of the triaxial extension test is even higher than the triaxial compression test. Finally, the difference between the resulting normalised undrained shear strength obtained from $C_{K0}UC$ and CIUC triaxial tests was additionally highlighted from Kulhawy and Mayne (1990) . After the examination of a data base of 48 different clays (Figure 68) it was resulted that the normalised undrained shear strength under anisotropic consolidation can be estimated through the equation 33.

$$\left(\frac{s_u}{\sigma'_{vc}}\right)_{CAUC} = 0.15 + 0.49 \left(\frac{s_u}{\sigma'_{vc}}\right)_{CIUC} \tag{33}$$
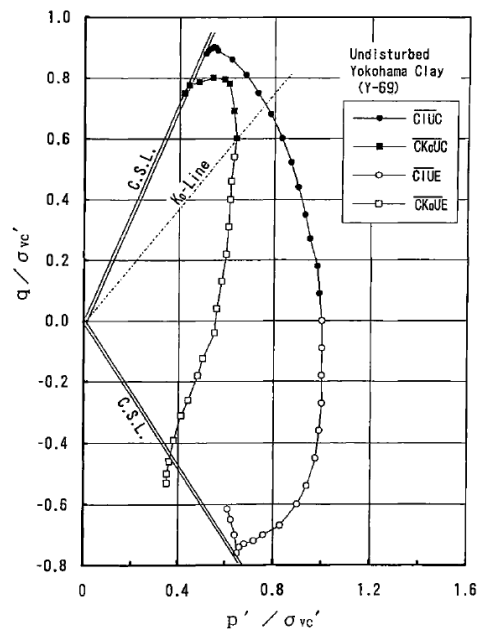
Figure 67: Comparison of the effective stress path obtained from four types of triaxial test. (Kamei, 1996)
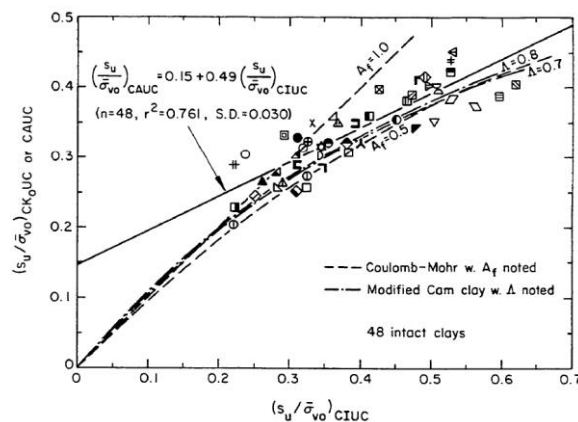
Figure 68: Comparison of undrained shear strength ratio for NC clays after anisotropic and isotropic consolidation (Kulhawy and Mayne, 1990).

3.4 Soil Test Facility

In this subchapter the responses of the considered constitutive models are examined in a single stress element level in the SoilTestFacility offered from Plaxis 2D.2018. The aim of this investigation is to verify and optimise the estimated input stiffness parameters for the considered models. Thereby, in the following sections the best possible fit responses between the simulated and experimental data is presented for both peat and clays.

A distinction was made between samples obtained from the crest and the toe area of the dike and the calibration conducted with experimental data obtained from soil samples consolidated with in situ stresses which represent the stiffness characteristics that the materials exhibit in the field. Moreover, as shown in subchapter 3.3 the induced NC state samples in some cases, produced unrealistically high values of stiffness for both clays and peats. For the SHANSEP NGI-ADP model the calibration established by the means of the shear strength vs the shear strain (τ vs γ) for peat and deviatoric stress vs the axial strain (q vs ε_1) for clays. For the HS and SS models the assessment was further realised with the examination of the stress path (τ vs σ_{yy}) for peats and the excess pore pressures vs strain (P_w vs ε_1) and the stress path (s' vs t) for clays, since the development of pore pressures with strain and the stress path are essential for the correct estimation of the available s_u (refer to subchapter 3.1.4). For the calibration of the SHANSEP NGI-ADP model the maximum measured s_u was used whereas for the undrained A models the measured peak friction angle φ_{peak}. No distinction was made between the response of the models in the critical state and the small strain levels since there are adequately determined in subchapters 3.2.1 to 3.2.3 with the use of the NC state samples. Finally, it has to be noted that input stiffness parameters such as E_{oed} (HS) and λ^*(SS) can be further optimized with the simulations of one-dimensional compression tests. The available input data required for the simulation (i.e. time steps) are not available and thus the examination in one dimensional compression could not established.

3.4.1 Peat.

Figure 69 display the best-fit stress strain response of the examined constitutive models along with the measured in the laboratory. The SS model response is entirely elastic for the DSS test applied in the toe leading to a much stiffer response than the measured as opposed to the sample obtained from the crest where the response appears to be better. This is possibly explained from the fact that in the DSS test applied in the toe the difference between the confining pressure and the preconsolidation pressure is higher leading to an explicit generation of elastic strains. The HS model, seems to display sufficiently the elastoplastic behaviour of the peat, capturing properly the nonlinearity of the material for both tests. It is noted that both models reproduced accurately the experimental measured response in the service conditions strain levels. Considering the SHANSEP NGI-ADP performance it is observed that the best fit curve is almost identical with the measured for both tests. It is obvious that the combination of the τ_0/s_u^A the G_{ur}/s_u^A and the γ_f^{DSS} is very beneficial for capturing properly the strain hardening of the material. In addition, the best fit G_{ur}/s_u^A fits well the estimated G_{50}/s_u^A. The default value of τ_0/s_u^A seems suitable for the material. It is noted that the γ_f^{DSS} value applied in the model matches completely the experimental measured value.

For the SS model the λ^* parameter is identical with the measured while with the k* parameter had to be slightly increased to 0.05 for the DSS applied in the crest. The default value

of 0.9 for the RF parameter remained unchanged. With regards to the unloading reloading poison ratio the best fit curves achieved with a value of 0.2.

As it concerns the stress path the response of both models is governed with an elastic response until failure in the case of the DSS shear test applied in the toe. In the crest the elastic response is up to a point. After exceeding that point most probably the yield surface is activated thus, resulting in the accumulation of plastic strains. Table 22 contains the best fit parameters of the examined models along with the necessary parameters that need to be implemented in the Soil TestFacility to obtain the curves.

Table 22: Best fit values obtained from the crest and the toe area of the dike for the peat.

Model	Parameter	Best fit crest	Best fit toe	Units
SHANSEP NGI-ADP	G_{ur}/s_u^A	25	35	[-]
	γ_f^C	18	28	%
	γ_f^{DSS}	25	40	%
	γ_f^E	37	55	%
	τ_0/s_u^A	0.7	0.7	[-]
	ν	0.2	0.2	[-]
	ν_u	0.495	0.495	[-]
HS	E_{50}^{ref}	3000	2850	(kPa)
	E_{oed}^{ref}	1400	1300	(kPa)
	E_{ur}^{ref}	6250	5800	(kPa)
	m	1	1	[-]
	K_0^{NC}	0.3	0.34	[-]
	p_{ref}	100	100	(kPa)
	RF	0.9	0.9	[-]
	ν_{ur}	0.2	0.15	[-]
SS	λ^*	0.3	0.2	[-]
	κ^*	0.05	0.03	[-]
	K_0^{NC}	0.35	0.3	[-]
	ν_{ur}	0.15	0.2	[-]
φ_{peak}		46	51.25	(degrees)
s_{upeak}		69.5	20	(kPa)
OCR		1.6	2.5	
σ_{yy}		100	24	(kPa)
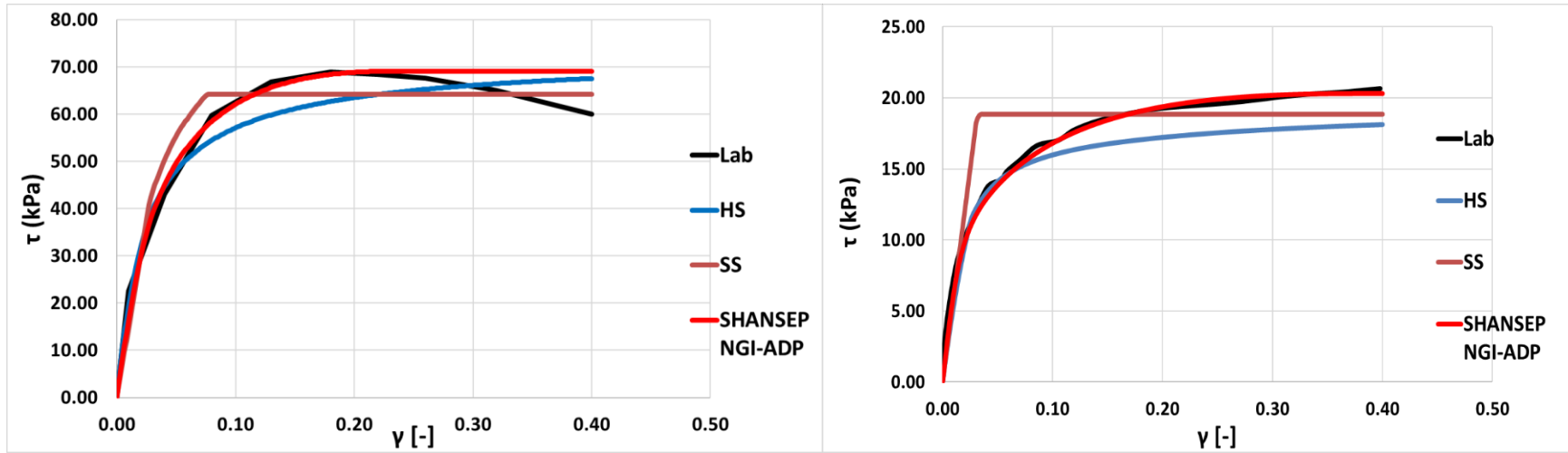
Figure 69: Stress strain response for peat obtained from the crest (left) and the toe (right)
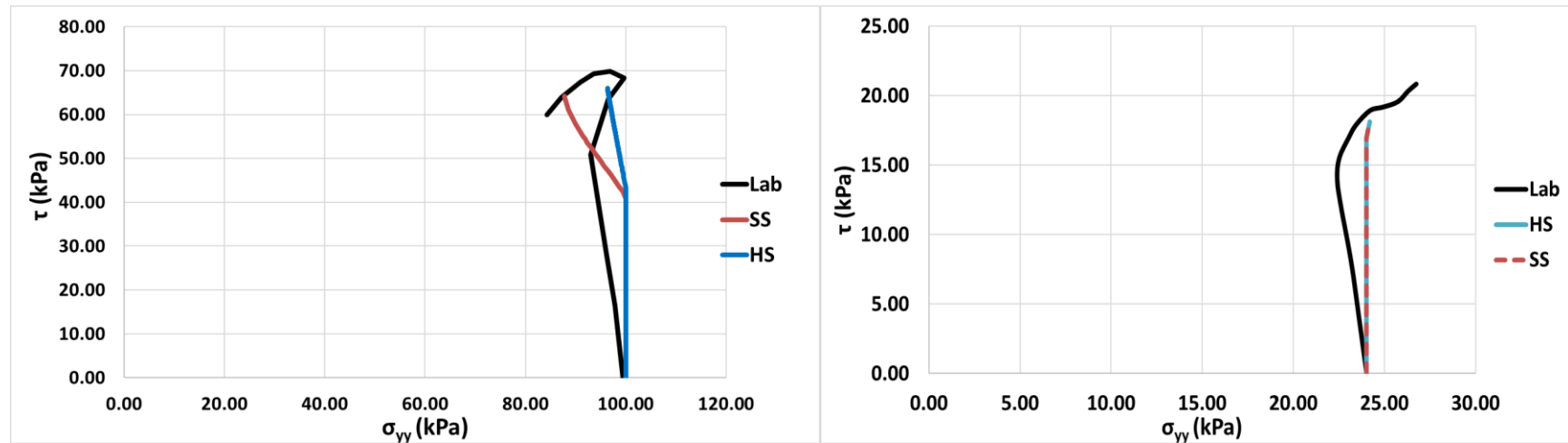
Figure 70: Stress path for peat obtained from the crest (left) and the toe (right).

3.4.2 Clays

Similarly, with peats the best fit response is achieved through the SHANSEP NGI-ADP model. Once again, the default value of for τ_0/s_u^A seem suitable for describing the strain hardening of the materials. Moreover, the γ_f^c deviated minimally from the estimated. In the case of the G_{ur}/s_u^A the identified best fit value lied above the estimated G_{50}/s_u^A. Thus, for the optimal estimation of the G_{ur}/s_u^A it is recommended to either carefully calibrate the parameter as illustrated in this subchapter or by applying an unloading reloading step in the executed triaxial tests. The SS is again dominated with an elastic response but in the case of clays the difference is less obvious due the stiffer pre-failure response that describes the materials. The κ^*, λ^* deviated minimally from the measured. Once more the HS seems to capture more properly the elastoplastic response of the materials experienced after approximately 2-3% strain levels. It is noted that for the best fit responses the K_0^{NC} value had to be marginally decreased to approximately 0.3 for both the SS and the HS models. Furthermore, in the case of the HS model the m value lightly decreased to 0.8.

Concerning the prediction of the models in respect with excess pore pressures it can be argued that the response is better where only positive pore pressures are generated. In the case of the development of negative (dilative) pore pressures the prediction is becoming less acceptable. This can be visualized better for the clay dike material and the clay anthropogenic since these soil layers are located at the top of the dike thus experiencing higher values of OCR. The models are incapable of capturing the development of dilative excess pore pressure and therefore, the maximum shear strength is inevitably underestimated (q_{max}). The response of the models is becoming notably better in the deeper soil layers where the OCR reduces. In this occasion, the models are able to fit well the measured response in terms of the stress path and the development of excess pore pressures with strain. In addition, it is obvious that none of the examined models accounts for the strain softening.

Table 23: Best fit values obtained from the crest and the toe area of the dike for the organic clay 1.

Model	Parameter	Best fit crest	Best fit toe	Units
SHANSEP NGI-ADP	G_{ur}/s_u^A	70	55	[-]
	γ_f^C	7	10	%
	γ_f^{DSS}	13	19	%
	γ_f^E	20	28	%
	τ_0/s_u^A	0.7	0.7	[-]
	v	0.2	0.2	[-]
	v_u	0.495	0.495	[-]
HS	E_{50}^{ref}	12000	8800	(kPa)
	E_{oed}^{ref}	5500	3322	(kPa)
	E_{ur}^{ref}	26500	19000	(kPa)
	m	0.8	0.8	[-]
	K_0^{NC}	0.34	0.3	[-]
	p_{ref}	100	100	(kPa)
	RF	0.9	0.9	[-]
	v_{ur}	0.2	0.15	[-]
SS	λ^*	0.12	0.15	[-]
	κ^*	0.02	0.02	[-]
	K_0^{NC}	0.35	0.3	[-]
	v_{ur}	0.2	0.2	[-]
φ_{peak}		42	44	(degrees)
s_{upeak}		47.5	20.5	(kPa)
OCR		1.6	[-]	(kPa)
σ'_1		82.2	28.8	(kPa)
σ'_h		37	13	(kPa)
K_0		0.45	0.45	[-]

Table 24: *Best fit values obtained from the crest and the toe area of the dike for the organic clay 2.*

Model	Parameter	Best fit crest	Best fit toe	Units
SHANSEP NGI-ADP	G_{ur} / s_u^A	45	42	[-]
	γ_f^C	11	10.5	%
	γ_f^{DSS}	19	19	%
	γ_f^E	28	28	%
	τ_0/s_u^A	0.7	0.7	[-]
	ν	0.2	0.2	[-]
	ν_u	0.495	0.495	[-]
HS	E_{50}^{ref}	9000	9000	(kPa)
	E_{oed}^{ref}	4000	4000	(kPa)
	E_{ur}^{ref}	20000	20000	(kPa)
	m	0.8	0.8	[-]
	K_0^{NC}	0.35	0.30	[-]
	p_{ref}	100	100	(kPa)
	RF	0.9	0.9	[-]
	ν_{ur}	0.2	0.15	[-]
SS	λ^*	0.1	0.15	[-]
	κ^*	0.03	0.03	[-]
	K_0^{NC}	0.35	0.40	[-]
	ν_{ur}	0.15	0.20	[-]
φ_{peak}		47	38	(degrees)
s_{upeak}		73.5	27.9	(kPa)
OCR		1.25	1.7	[-]
σ'_1		113.3	49	(kPa)
σ'_h		51	22	(kPa)
K_0		0.45	0.44	[-]

Table 25: Best fit values obtained from the crest and the toe area of the dike for the clay dike and clay anthropogenic.

Model	Parameter	Best fit crest	Best fit toe	Units
SHANSEP NGI-ADP	G_{ur} / s_u^A	80	60	[-]
	γ_f^C	9	13	%
	γ_f^{DSS}	16	20	%
	γ_f^E	25	29	%
	τ_0/s_u^A	0.7	0.7	[-]
	v	0.3	0.25	[-]
	v_u	0.495	0.495	[-]
HS	E_{50}^{ref}	9000	10000	(kPa)
	E_{oed}^{ref}	4500	4000	(kPa)
	E_{ur}^{ref}	20000	20000	(kPa)
	m	0.5	0.8	[-]
	K_0^{NC}	0.37	0.37	[-]
	p_{ref}	100	100	(kPa)
	RF	0.9	0.9	[-]
	v_{ur}	0.2	0.15	[-]
SS	λ^*	0.08	0.09	[-]
	κ^*	0.011	0.02	[-]
	K_0^{NC}	0.37	0.3	[-]
	v_{ur}	0.15	0.15	[-]
φ_{peak}		39.5	45	(degrees)
s_{upeak}		44.5	18	(kPa)
OCR		2.42	2.65	[-]
σ'_1		64.1	17	(kPa)
σ'_h		28.85	7.65	(kPa)
K_0		0.45	0.45	[-]
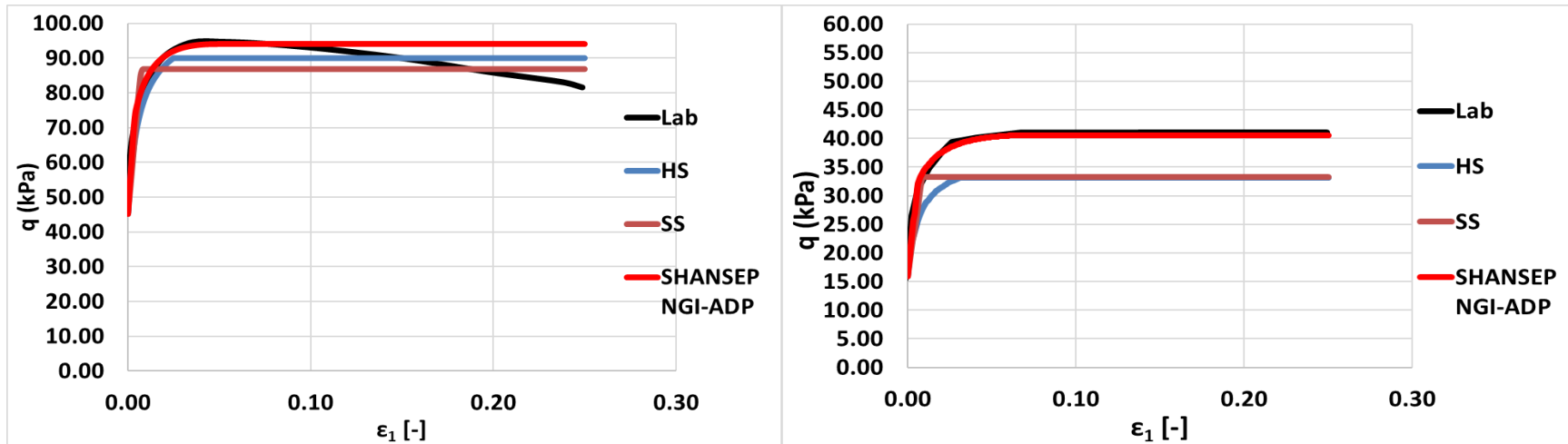
Figure 71: Stress strain response for organic clay 1 obtained from the crest (left) and the toe (right).
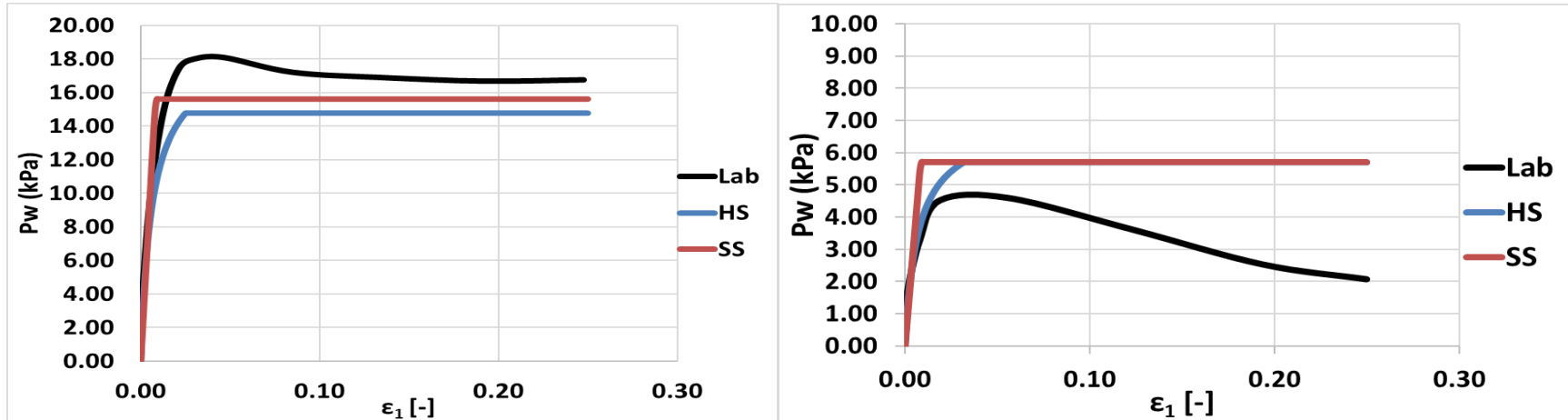
Figure 72: Excess pore pressures response for organic clay 1 obtained from the crest (left) and the toe (right).
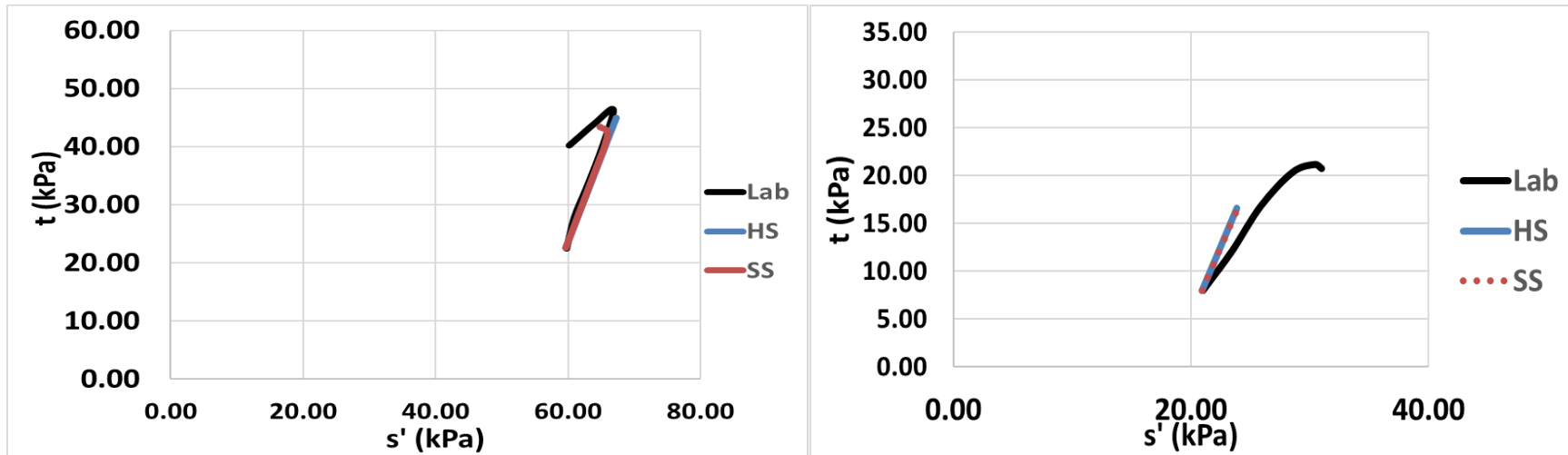
Figure 73: Stress path for organic clay 1 obtained from the crest (left) and the toe (right).
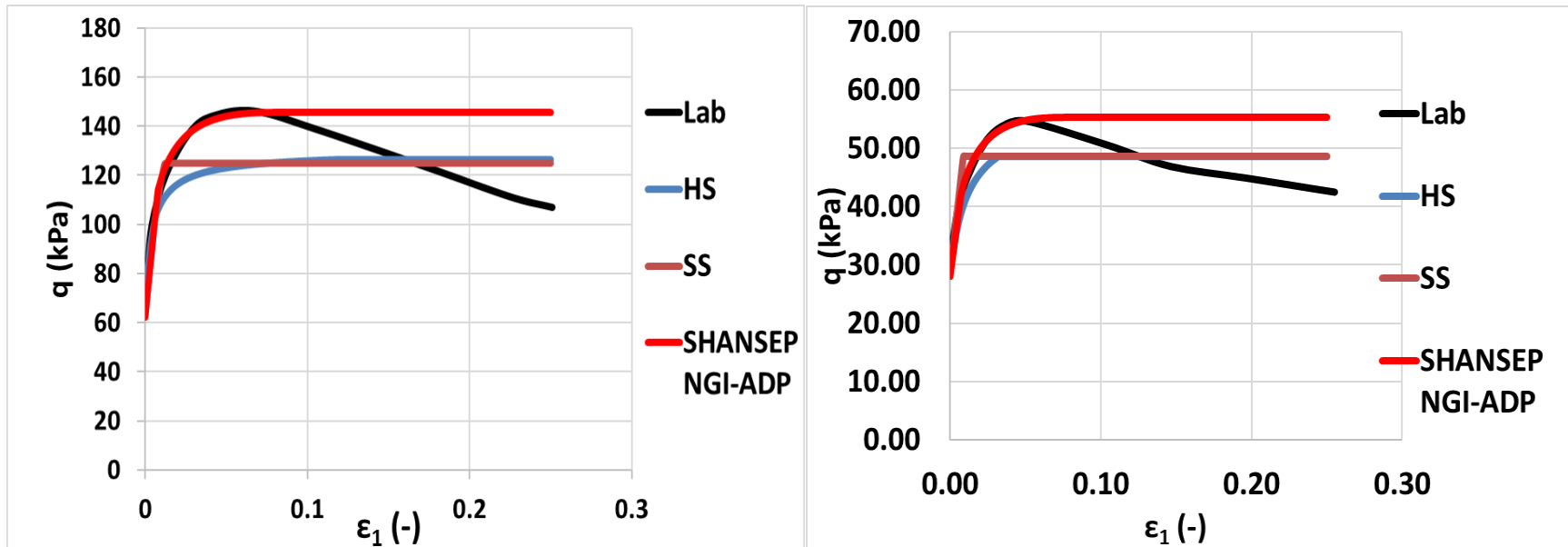
Figure 74: Stress strain response for organic clay 2 obtained from the crest (left) and the toe (right).
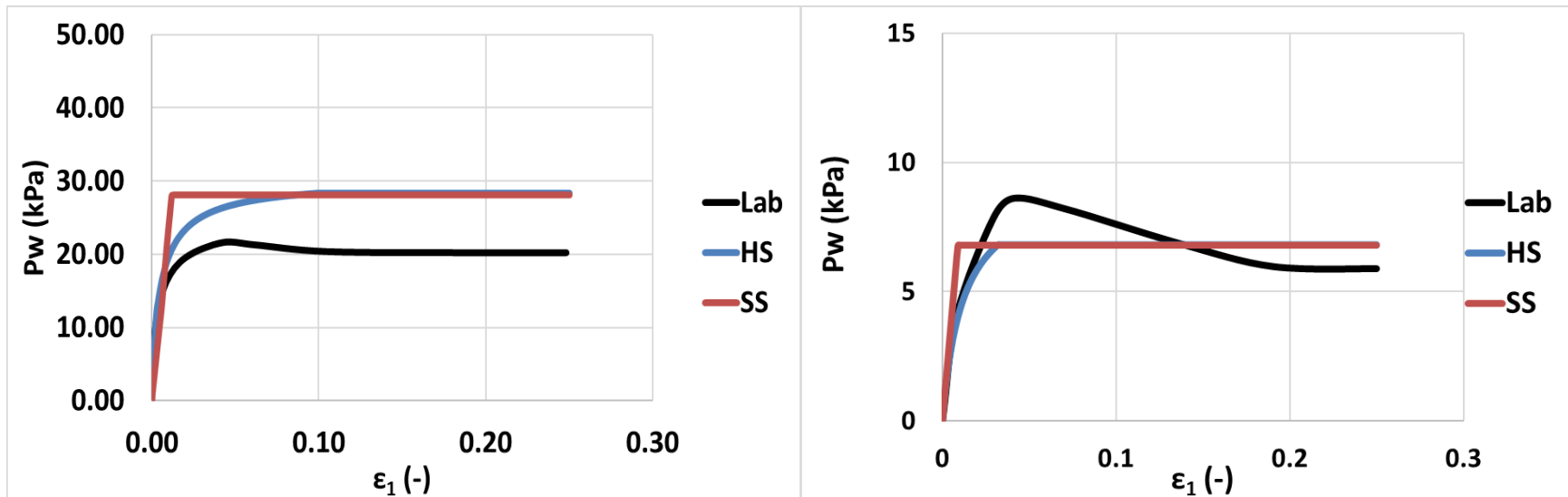
Figure 75: Excess pore pressures response for organic clay 2 obtained from the crest (left) and the toe (right).
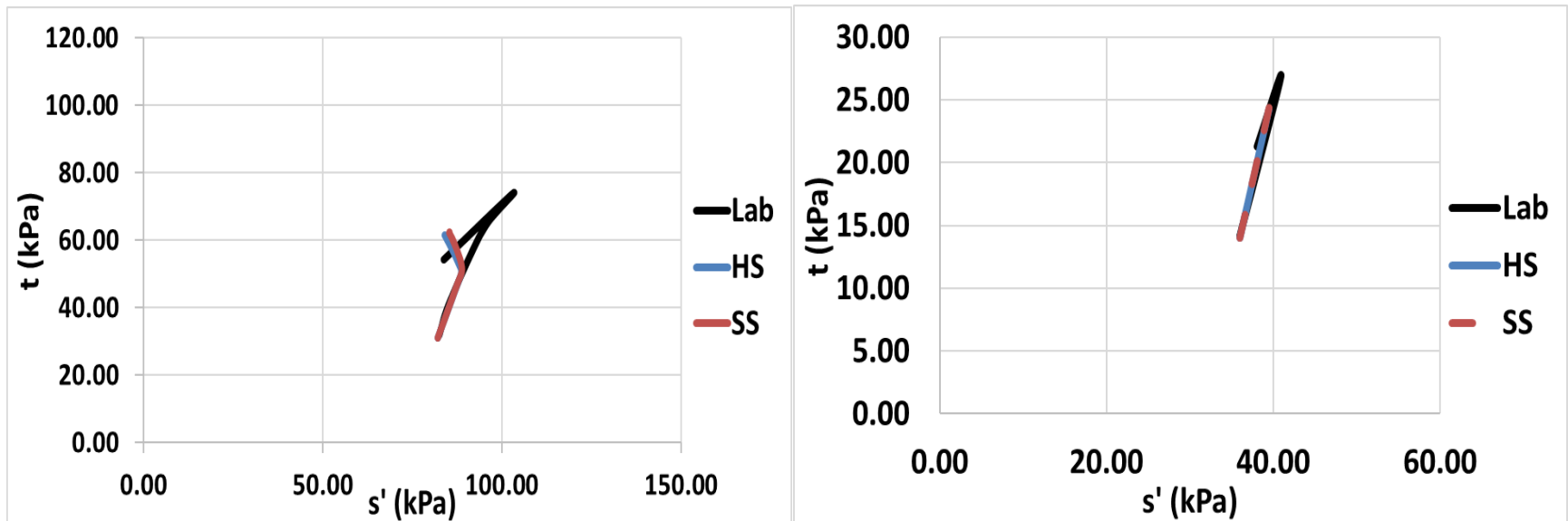
Figure 76: Stress path for organic clay 2 obtained from the crest (left) and the toe (right).
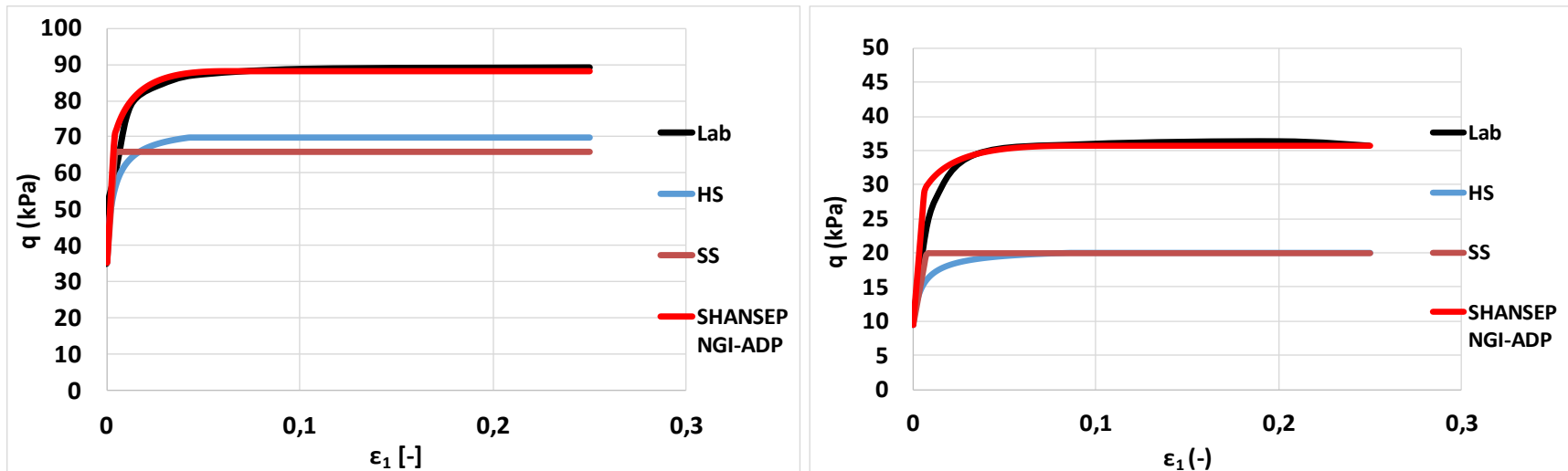
Figure 77: Stress strain response for clay dike (left) and clay anthropogenic (right)
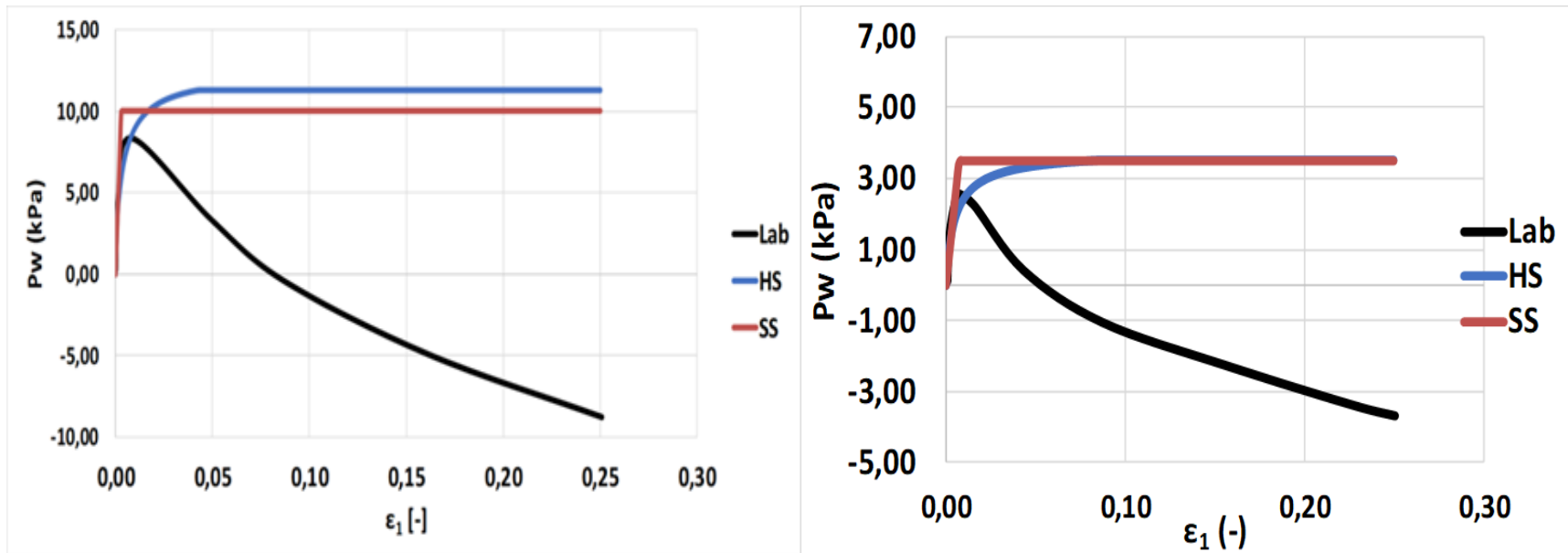
Figure 78: Excess pore pressures response for clay dike (left) and clay anthropogenic (right).
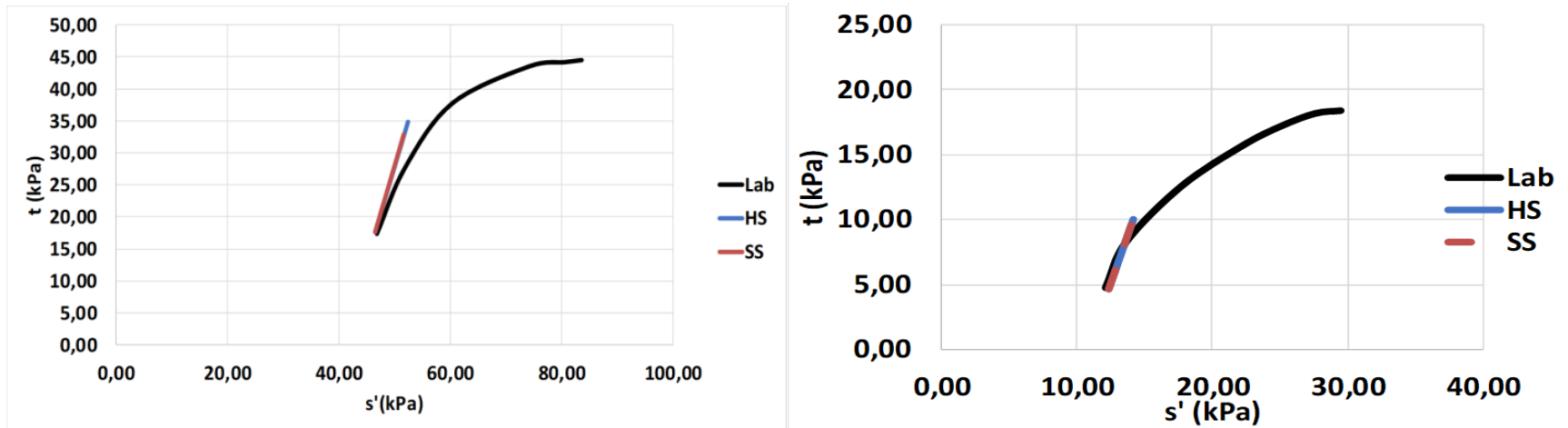
Figure 79: Stress path for the clay dike (left) and clay anthropogenic (right).

Lastly, in order to get a better feeling on how the variation of the $\gamma_f^{DSS,C}$ and the G_{ur}/s_u^A influences the resulting stress strain response given from the SHANSEP NGI-ADP model a sensitivity analysis is conducted for both a peat and a clayey sample. Figure 80 shows clearly that the G_{ur}/s_u^A influences the response of the model at the initial strains of the strain hardening process while the $\gamma_f^{DSS,C}$ determines the strain where the actual failure occurs without influencing the response of the model at the initial stages of strain hardening.
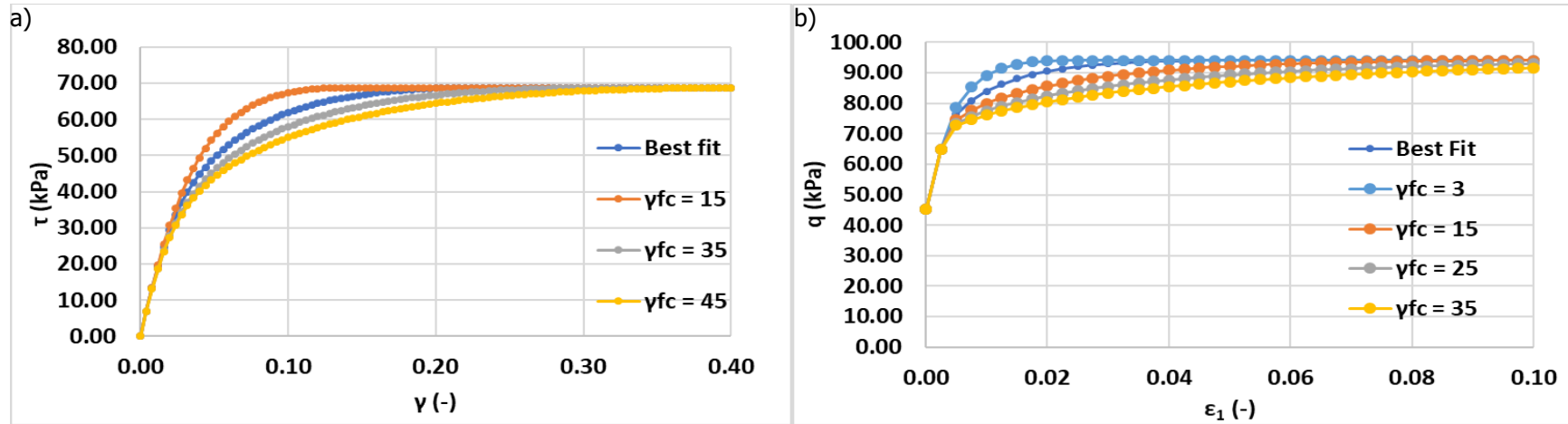
Figure 80: $\gamma_f{}^c$ variation for a) peat. b) clay.
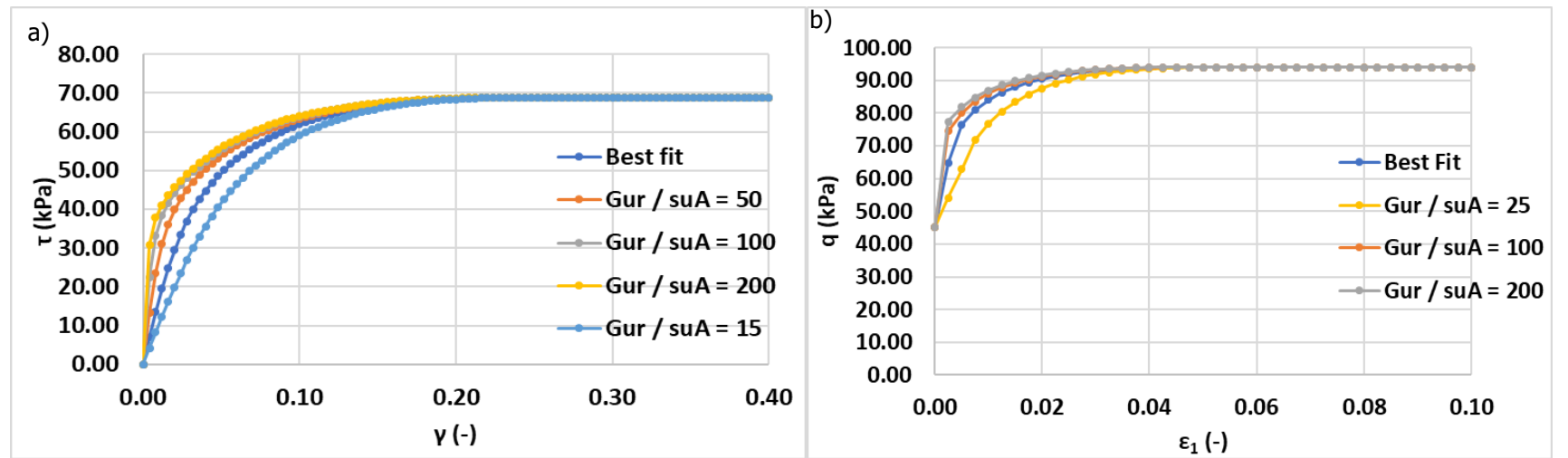
Figure 81. $G_{ur}/s_u{}^A$ variation for a) peat , b) clay.

3.5 Discussion of Chapter 3

In Chapter 3 the determination of the geotechnical parameters obtained from laboratory tests executed under the updated protocol WBI 2017 is established. These geotechnical parameters are required input parameters for the SHANSEP NGI-ADP, the HS and the SS constitutive models. These models are used in the calculation schemes proposed by POVM 2018 for assessing the dike stability with the use of finite element method. Specifically, the analysis of the data focused in the assessment of the undrained and drained shear strength parameters in service conditions and critical strain levels for clays and peats followed by the determination of their stiffness characteristics. The Chapter additionally includes the investigation conducted in the SoilTest Facility offered from PLAXIS along with the examination of the influence of the K_0 value in the resulting undrained shear strength.

Starting point is the determination of the $S_{(NC)}$ parameter where the investigation revealed that all the examined soils appear to display properly the normalized behaviour for all the considered strain levels. The value of $S_{(NC)}$ in service conditions strain levels was found to be notably higher in clays than peats. The maximum strength of the NC clayey soil was reached at approximately 2% strain level while for peats the maximum shear strength is reached at larger strains beyond the required 5% strain level. In contrary, at "critical" state strain levels the $S_{(NC)}$ value of peat is considerably higher than the clayey soils. This is explained due the softening behaviour that the clayey soil exhibits after reaching the maximum shear strength whereas for peats the maximum shear strength is mobilized at large strains. The observed behaviour of clays is in agreement with the literature in the sense that the induced NC clays under TXC reached their maximum mobilized shear strength at "small" strains followed by strain softening. Therefore, at large strains after the strain softening of the clay the available strength becomes comparable with the other modes of shearing and the stress level dependency of the s_u is becoming less significant (refer to Figure 4). However, at service conditions strain levels the clays in triaxial compression experience their peak strength and the stress path dependency of s_u is deemed to be significant. In other words, at critical state strain levels it is reasonable to assume that the $S_{(NC)25\%}$ describes well the average of the different models of shearing. In contrary at $S_{2\%}$ we are dealing with the peak strength under TXC conditions and the stress path dependency of s_u is expected to be the highest. By taking into consideration that based on the WBI 2017 the clays are thoroughly described from TXC tests; an extensive literature review of the stress path dependency of the s_u in peak state was conducted. Speaking in terms of undrained shear strength ratios s_u^P / s_u^A and s_u^{DSS} / s_u^A the investigation revealed that the s_u^P / s_u^A is typically described from values ranging from 0.4 - 0.6 (average 0.5) while the s_u^{DSS} / s_u^A is generally found in a range between 0.6 − 0.8 (average 0.7). It should be noted that for peats there is limited information regarding its strength under the different modes of shearing. However, the DSS which is applied is typically the mode of shearing which lies in the middle of the available strength offered from TXC and TXE refer to Table 1 and 2 and Figure 4.

With reference to the friction angle of the soils similar behavior with the $S_{(NC)}$ parameter was observed in the sense that at critical state strains the peat displayed a high value with the clayey soils following with lower values. On the other hand, at service conditions strain levels, the clays displayed the higher values while the peat the lowest. Additionally, at service conditions strain levels the cohesion of the soils is considered since at the critical state the cohesion is zero.

The determination of the m parameter established with two different methods as proposed from WBI 2017. The application of the two methods resulted in notably different values of m. The 2nd method (e.g. m= (b-a) / b) resulted in m values ranging dominantly from 0.88 to 0.98 for all the examined soils. On the other hand, the 1st approach (e.g. SHANSEP curve) resulted in

m values varying from 0.72-0.75 for peats and 0.74-0.86 for clays. While the 2nd method was found to be rather straight forward, it is noteworthy to address that the use 1st method is clearly advantageous in the sense that the strain level dependency of the $S_{(NC, OC)}$ parameter was considered and thus, a value of m was obtained from both service conditions and critical strain levels. Moreover, by taking into respect that the typical values of the m parameter are in the range of $m \approx 0.7 - 0.9$ with the most dominant being $m \approx 0.8$ it is concluded that the 2nd method produced values which are in the higher range of the expectancy of the m parameter while the 1st method delivered values which replicate better the typical values of the parameter. However, the obtained reliability (R^2) of the 1st method is considered rather poor, contradicting the values of reliability observed in literature. The reduced reliability is influenced from the estimated values of the $S_{(OC)}$ and the OCR. Current methodology suggests that the p_c should be determined from one dimensional compression tests with the use of empirical methods (e.g. Casagrande). Based on p_c / σ'_{vc} the OCR is determined which is later combined with its associated $S_{(OC)}$ obtained from $C_{K0}UC$ tests. This methodology incorporates errors such as overestimation or underestimation of the OCR from the empirical methods used for determining the preconsolidation pressure and errors that arise from the fact that data from two different soil samples need to be combined. The OCR was determined with the use oedometer tests while the $S_{(OC)}$ from the $C_{K0}UC$ tests. Therefore, the assumption is that the two different combined samples are fully homogenous, and that the quality of the soil samples was identical which is hardly the case for naturally deposited soils. In addition, it was observed that the stress strain response of the soil samples that were consolidated with in situ stresses deviates from the stress strain response of the soil samples consolidated beyond σ'_p (NC samples). In the case of NC samples, the 2% strain level generally describes the peak strength of the soil while for the OC samples the 2% strain level is associated with strength lower from the peak (refer to Figure 42). Possible solution for an optimized estimation of the m parameter in service conditions strain levels is by obtaining the $S_{(OC)}$ from the peak strength or the 5% strain level which is kept as close as possible to the proposed 2% strain level. Another solution is by following the stepwise procedure given from Ladd and Foott, (1974). It is suggested that the $S_{(OC)}$ should be obtained from samples that swell to known OCR levels. In this proposed way, the uncertainty in the OCR and the derived $S_{(OC)}$ will be reduced while the reliability of the derived m parameter will increase.

The induced NC samples produced a stiffer response than the soil samples consolidated with in situ stresses. Specifically, for clays the stiffness properties of the induced NC samples yielded in higher values of the stress level dependency of m, the G_{50} / s_u^A and lower values in the shear strain at failure in compression. For clays the disparity in the G_{50} / s_u^A between the NC and samples consolidated with in situ stresses was explained due the dependency of the G_{50} / s_u^A $_{NC}$ with the plasticity index. Another possible mechanism for the observed inconsistency of the G_{50} / s_u^A can be attributed to the different increasing rates between E_{u50} and s_u with increasing consolidation stress. Likewise, for peats in the case of the induced NC samples the resulting γ_f^{DSS} was found to be lower while the stress level dependency m was notably higher. Moreover, in the case of peats the G_{50} / s_u^A yielded in a more constant value between the NC and the samples consolidated with in-situ stresses.

In triaxial compression the decision of applying the same K_0 value (e.g. $K_0 = 0.45$) value for both the NC and OC samples was found to have notable influence in the obtained results in terms of the strength and the stiffness characteristics of the soils. In the case of the OC samples it appears that the maximum shear strength that the soil can mobilize along with the E_{50} were underestimated. Moreover, while the decision is rather conservative for the OC samples it was found that for the NC samples the applied value does not always fall in the conservative side. Specifically, the underestimation of s_u for the OC soil samples probably influenced the parameter

determination of the strength increase exponent m. By replicating the "correct" K_0 value for the OC soils the resulting $S_{(OC)}$ in both 2% and 25% strain levels will possibly yield in a higher value. Therefore, the SHANSEP curves established in this study would result in a different power regression line due the updated $S_{(OC)}$ and therefore an updated value of m. The underestimation of E_{50} in turn influences the resulting G_{50} / s_u^A, the stress level dependency of stiffness m and the resulting E_{50}^{ref}.

Concerning the Soil TestFacility examination useful conclusions were drawn. Regarding the stress strain examination of the models it can be argued that the SHANSEP NGI-ADP performance was exemplary. The produced strain hardening of the model was almost identical with the experimental. Evidently, the combination of the τ_0/s_u^A the G_{ur}/s_u^A and the γ_f^C, γ_f^{DSS} for both peats and clays is very beneficial for capturing properly the stress strain behaviour of the materials. The HS model performed reasonably well describing satisfactory the elastoplastic behaviour of both peats and clays while the SS displayed the poorest results. The best fit curves obtained from the SS were dominated with an elastic response which caused the predicted response to behave stiffer than the experimental.

Regarding the development of excess pore pressures with strain and the stress paths both the HS and the SS models displayed similar results. It was noticed that in the case of the examination of laboratory data obtained from soil samples which experienced the highest values of OCR in the field (e.g. clay dike) the response of the models was rather poor. However, with decreasing over consolidation, the produced responses were drastically improved being able to capture properly the strain development with excess pore pressures along with the measured stress path.

The examination revealed that the estimated values of G_{50}/s_u^A (obtained from the samples with in situ stresses for clays and peats) described sufficiently the peats but in the case of clays the estimated G_{50}/s_u^A lied below the identified best fit. Moreover, the default value of τ_0 / s_u^A seems proper for both peats and clays. The estimated λ^* and κ^* fitted very well the estimated with minor adjustments and the default value of v_{ur} remained unchanged almost in all the cases. The E_{50}^{ref} deviated from the estimated for both peats and clays. The estimated γ_f^{DSS} matched entirely the γ_f^{DSS} which produced the best fit curves for peats while for clays the γ_f^C estimated from the equation (31) seems to describe satisfactorily the values of γ_f^C which produced the best fit response. It has to be noted that the estimated shear strains at failure (γ_f^c and γ_f^{DSS}) concerned the value derived from the specific laboratory test used for the comparison purposes and not the average value like the rest of the parameters. The shear strains at failure displayed a high variability and thus, the description of an examined soil layer with the average value of the shear strain might lead to inaccurate results. Therefore, for the shear strains at failure it is recommended to use data which are as close as possible to the area of interest. Furthermore, the calibration of the E_{50}^{ref} through the Soil Test Facility is highly recommended due the fact that the translation of the drained E_{50} from the E_{u50} is accomplished with the use of empirical formulas (refer to equation 26). Thus, the resulting value of E_{50} is an approximate value which probably deviates from the reality. For the optimal estimation of the G_{ur}/s_u^A it is recommended to either carefully calibrate the parameter as illustrated in 3.4 subchapter or by applying an unloading reloading step in the executed triaxial tests.

Speaking in terms of versatility for calculating the input parameters of the constitutive models it was noted that for the SS the procedure was rather straight forward. In addition, the stiffness parameter of the model (λ^* and κ^*) displayed low variability. For the HS model the level of difficulty increases due the larger number of required input parameters along with the attention that has to be paid in the input values of the different stiffnesses for the different stress paths. In addition, due to some model restriction e.g. E_{50} / E_{oed} > 2 the stiffnesses might need to

compromise to the internal recommendations given from the model. The determination of the parameters of the SHANSEP NGI-ADP model is arguably a challenging process, especially due the fact that the input parameters of the model require experimental data from three different shear laboratory tests.

Finally, the general conclusions of Chapter 2 and 3 can serve as an indication for the modelling analysis which will take place in the following chapters. Regarding the Green dike examination, it is safe to assume that the $S_{25\%,40\%}$ and $m_{25, 40\%}$ possibly describe reasonably the average value of the three different modes of shearing. The examined clays under triaxial compression at large strains experienced strain softening which resulted in a residual strength lower than the peak. Thus, the residual strength of the clayey materials is possibly comparable with the shear strength in triaxial extension and direct simple shear (refer to Figure 4). The direct simple shear which is used for peats is reported to be the mode of shearing which typically describes the average strength between the triaxial compression and extension. However, in the case of the Blue dikes the derived S describes the peak strength of the clayey materials. Therefore, the difference between the different modes of shearing is expected to be the highest and the ADP framework should be applied. For peats it is questionable if the 5% strain level would yield in different values under the different modes of shearing. An answer to this question can only be accomplished by the application of laboratory investigation. For the purposes of this research a sensitivity analysis will be applied along with a sensitivity analysis of the shear strains at failure which incorporated the highest uncertainty after the careful parameter determination.

The Chapter 3 concludes with the Table 26 which depicts the relevant analysis that will be conducted for the Green and Blue type of dikes along with the Tables 27 to 30 where the input parameters of the constitutive models are summarized.

Table 26: Analysis for Green and Blue type of dikes.

Type of dike	Model	Strength parameters	s_u^{DSS} / s_u^A	s_u^P / s_u^A
Green dike	SHANSEP NGI-ADP	$S_{25, 40\%}$ strain level	0.99	0.98
	HS	$\varphi_{cv25, 40\%}$ strain level	-	-
	SS	$\varphi_{cv25, 40\%}$ strain level	-	-
Blue dike	SHANSEP NGI-ADP	$S_{2, 5\%}$ strain level	0.99	0.98
		$S_{2, 5\%}$ strain level	0.7 (average value based on the literature)	0.5 (average value based on the literature)
		$S_{2, 5\%}$ strain level	0.5 (lower bound value based on the literature)	0.3 (lower bound value based on the literature)
	HS	$\varphi, c_{2, 5\%}$ strain level	-	-
	SS	$\varphi, c_{2,5\%}$ strain level	-	-

Table 27: Organic clay 1 parameters

Model	Parameter	Crest	Toe	Units
SHANSEP NGI-ADP	G_{ur} / s_u^A	70	55	[-]
	γ_f^C	7	10	%
	γ_f^{DSS}	13	19	%
	γ_f^E	20	28	%
	τ_0/s_u^A	0.7	0.7	[-]
	v	0.2	0.2	[-]
	v_u	0.495	0.495	[-]
HS	E_{50}^{ref}	13000	8800	(kPa)
	E_{oed}^{ref}	5500	3322	(kPa)
	E_{ur}^{ref}	26500	19000	(kPa)
	m	0.8	0.8	[-]
	K_0^{NC}	0.34	0.3	[-]
	p_{ref}	100	100	(kPa)
	RF	0.9	0.9	[-]
	v_{ur}	0.2	0.15	[-]
SS	λ^*	0.12	0.15	[-]
	κ^*	0.02	0.02	[-]
	K_0^{NC}	0.35	0.3	[-]
	v_{ur}	0.2	0.2	[-]
	OCR kar	1.6	1.8	[-]

Table 28: Organic clay 2

Model	Parameter	Crest	Toe	Units
SHANSEP NGI-ADP	G_{ur} / s_u^A	42	45	[-]
	γ_f^C	10.5	11	%
	γ_f^{DSS}	19	19	%
	γ_f^E	28	28	%
	τ_0/s_u^A	0.7	0.7	[-]
	v	0.2	0.2	[-]
	v_u	0.495	0.495	[-]
HS	E_{50}^{ref}	9000	9000	(kPa)
	E_{oed}^{ref}	4000	4000	(kPa)
	E_{ur}^{ref}	20000	20000	(kPa)
	m	0.8	0.8	[-]
	K_0^{NC}	0.35	0.30	[-]
	p_{ref}	100	100	(kPa)
	RF	0.9	0.9	[-]
	v_{ur}	0.2	0.15	[-]
SS	λ^*	0.1	0.15	[-]
	κ^*	0.03	0.03	[-]
	K_0^{NC}	0.35	0.40	[-]
	v_{ur}	0.15	0.20	[-]
	OCR kar	1.25	1.4	

Table 29: Clay dike and clay anthropogenic

Model	Parameter	Crest	Toe	Units
SHANSEP NGI-ADP	G_{ur} / s_u^A	80	60	[-]
	γ_f^C	9	13	%
	γ_f^{DSS}	16	20	%
	γ_f^E	25	29	%
	τ_0/s_u^A	0.7	0.7	[-]
	ν	0.3	0.25	[-]
	ν_u	0.495	0.495	[-]
HS	E_{50}^{ref}	9000	10000	(kPa)
	E_{oed}^{ref}	4500	4000	(kPa)
	E_{ur}^{ref}	20000	20000	(kPa)
	m	0.5	0.8	[-]
	K_0^{NC}	0.37	0.37	[-]
	p_{ref}	100	100	(kPa)
	RF	0.9	0.9	[-]
	ν_{ur}	0.2	0.15	[-]
SS	λ^*	0.08	0.09	[-]
	κ^*	0.011	0.02	[-]
	K_0^{NC}	0.37	0.3	[-]
	ν_{ur}	0.15	0.15	[-]
	OCR kar	2	2.2	

Table 30. Peat

Model	Parameter	Crest	Toe	Units
SHANSEP NGI-ADP	G_{ur} / s_u^A	25	35	[-]
	γ_f^C	16	27	%
	γ_f^{DSS}	25	40	%
	γ_f^E	37	60	%
	τ_0/s_u^A	0.7	0.7	[-]
	ν	0.2	0.2	[-]
	ν_u	0.495	0.495	[-]
HS	E_{50}^{ref}	3000	2850	(kPa)
	E_{oed}^{ref}	1400	1300	(kPa)
	E_{ur}^{ref}	6250	5800	(kPa)
	m	1	1	[-]
	K_0^{NC}	0.3	0.34	[-]
	p_{ref}	100	100	(kPa)
	RF	0.9	0.9	[-]
	ν_{ur}	0.2	0.15	[-]
SS	λ^*	0.3	0.2	[-]
	κ^*	0.05	0.03	[-]
	K_0^{NC}	0.35	0.3	[-]
	ν_{ur}	0.15	0.2	[-]
	OCR kar	1.5	1.7	

Chapter 4 – Green dike analysis

The scope of this chapter is to present the outcome in terms of the estimated FoS, the developed failure mechanisms and the calculated displacements using the considered constitutive models for the case of the Green dike analysis.

The chapter is divided into three main sections. The first section describes the model set-up along with the explanation of the simulation phases proposed by POVM, 2018 for assessing the safety and the displacements. The second section focusses on the responses of the constitutive models and the results. In the last section the conclusions of the chapter are given.

4.1 Proposed guidelines and model configuration

4.1.1 Proposed guidelines

Prior to the presentation of the design guidelines established from the POVM 2018 the semi-probabilistic factors relevant for the green dikes are described.

For the "Green Dike" assessments the relevant factors are namely, the material factor (γ_n), the model factor (γ_d) and the schematization factor ($\gamma_{b; Geo}$). According to the POVM 2018 the outcome of the multiplication of these three factors results in the minimum acceptable FoS (SF min) for a specific cross-section. In addition, the multiplication of the model and the material factor may be used for reducing the characteristic ground strength (i.e. (φ, c, S) / $\gamma_n\gamma_d$) when assessing the global safety compensating the model configuration uncertainties. The value of each semi-probabilistic factor is given in Table 31 followed by a brief explanation of their purpose.

Table 31:Semi probabilistic factors for the Green Dike examination.

Model factors	Value	Apply to soil strength
Model factor (γ_d)	1.06	Yes
Schematisation factor ($\gamma_{b\ Geo}$)	1.20	No
Material factor (γ_n)	1.06	Yes
SF min = γd γb γn = 1.35		

The model factor accounts for the model uncertainty. The factor is applied in the characteristic ground strength at control of the stability and structural forces (in the case of Blue dike analysis). According to Anno 2018 $\gamma_{d.EEM}$ = $\gamma_{d.UpliftVan(WBI\ 2017)}$ = 1.06

The material factor is related to the maximum permissible failure probability at a cross section level. This maximum permissible failure probability is given through the equation:

$$\gamma n = 0.15\ \beta eis; dsn; Geo + 0.41 \tag{34}$$

Where:
- *βeis;dsn;Geo is the required reliability index at a cross section level.*

The schematization factor accounts the uncertainties about the subsoil strength and the hydraulic loads. More specifically the uncertainties considered in the schematization factor are as follows:

- *The location of the phreatic line in the crest of the dyke*
- *The height of the residual profile*

- *Uncertainties regarding the thickness of the houmous clay layer and the peat.*
- *Uncertainties in the thickness of the soil layers in a plane strain model since the soil stratigraphy is based on point measurements e.g. CPT.*

The flowchart given below (Figure 82a) depicts the proposed consecutive phases which are implemented in the stage construction mode in PLAXIS. As an example, the phases implemented in the stage construction mode in Plaxis are shown (Figure 82b). The drained steps and the switch to the Undrained A analysis was followed twice in order to examine the response of both the HS and SS models.
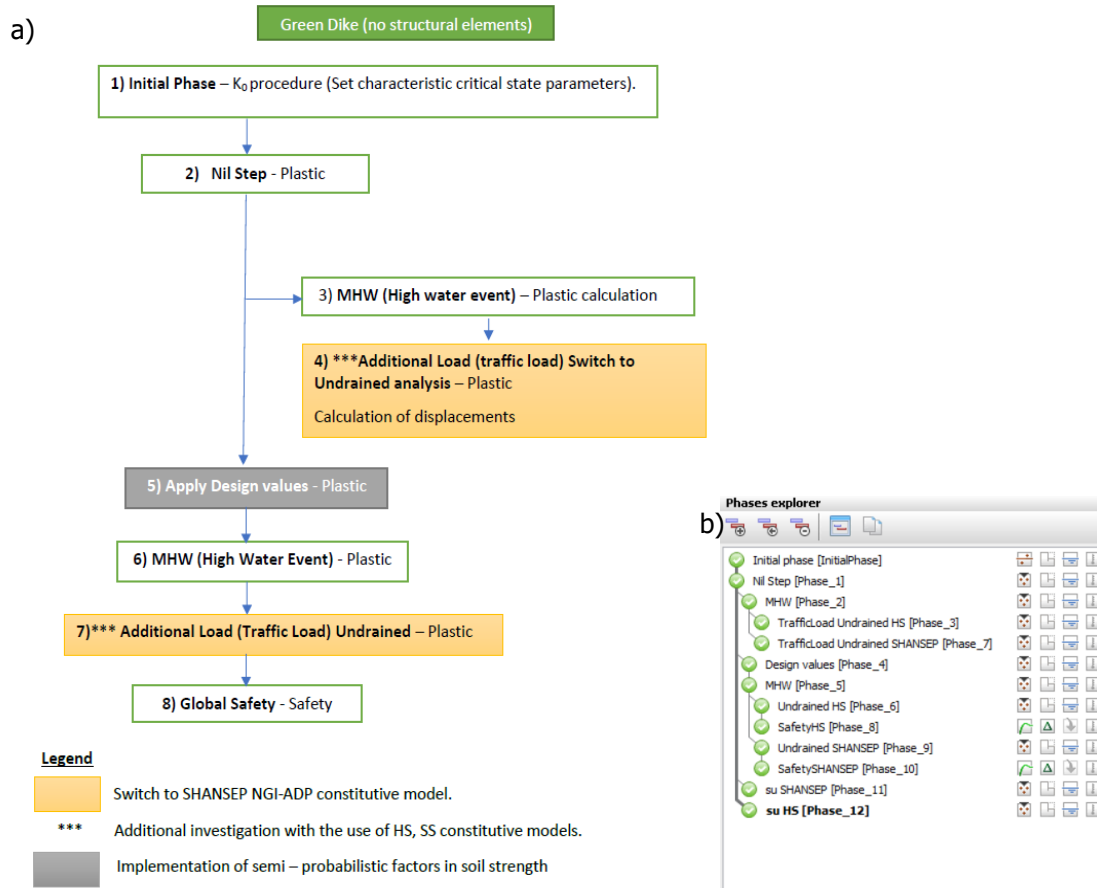
Figure 82: a) Flowchart followed for the analysis of the Green dike, b) steps in stage construction mode in Plaxis.

The highlighted boxes with the orange colour indicate the switch to the undrained behaviour of the soils. For the analysis two main paths need to be followed. The one path is intended for the calculation of displacements while the second path purpose is for assessing the global safety of the dike through the shear strength reduction technique (refer to Figure 30). Specifically, in the first path the characteristic strength values obtained from the critical state are used along with reduced values of stiffness. The reduced values of stiffness are obtained by the application of the material factor γ_d which equals to 1.5. For the Hardening Soil and the SHANSEP NGI-ADP model the E_{50}^{ref} and the G_{ur}/s_u^A are divided from γ_d. For the Soft Soil model, the k^* and λ^* are multiplied with γ_d. However, for the purposes of this research the carefully derived (calibrated) stiffness parameter of the soils will remained unchanged without applying any reductions. For the

second path the semi – probabilistic material factors are applied in the soil strength and the global safety of the dike is assessed.

The overview of each modelling step and its purpose is given below:

- *In the initial phase the existing dike situation is generated through K_0 procedure. The K_0 calculation defines the stresses of the model (both vertical and horizontal). In addition, with the use of advance constitutive models the stress history of the soil can be taken into account by specifying a value of OCR or POP (as explained in Subchapter 3.1.1).*
- *The K_0 procedure is followed by a zero-load step (plastic nil step). This step is used to restore equilibrium and solve large out of balance forces. Such situation is likely to occur if the initial stress field is generated through K_0 procedure for non-horizontal layering surface. In addition, with the use of the zero-load step the stress distribution and the rotation of the principal effective stresses takes place. The stress distribution also affects the initial overconsolidation.*
- *After the NIL step the high-water level is appointed along with the associate increase in the piezometric head of the aquifer. This step and the preceding steps are executed with drained conditions with the use of the Hardening Soil or the Soft Soil models.*
- *The next step includes the switch to the undrained analysis along with the activation of a uniform traffic load. This traffic load is equal to 13.3 kN/m² and has a width of 2.5 m. This load is located in the middle of the crest following the design recommendations of POVM 2018 and it is in accordance with the Constructive Guidelines Designs (TAW, 1994).*
- *After the switch to the undrained analysis the global safety of the dike is assessed and the arc-length control[2] is enabled.*

It must be noted that after the NIL step the POVM guideline recommends the implementation of an additional step including the optional dike reinforcement with a berm or with ground injection. In this study the Green dike is assessed with the in-situ dike conditions. This subchapter concludes with Table 32 where the characteristic and design strength parameters obtained from 25% and 40% strain levels for clay and peat respectively.

Table 32: Characteristic and design values of the strength parameters for the examined soils.

Soil	$S_{25,40\% \text{ kar}}$	$S_{25,40 \text{ design}}$	$m_{25,40\%}$	$\varphi_{cv\ 25,\ 40\% \text{ kar}}$ (degrees)	$\varphi_{cv25,40\% \text{ design}}$ (degrees)
Clay dike	0.33	0.29	0.75	29.1	26
Organic clay 1	0.31	0.28	0.77	31.6	28.2
Organic clay 2	0.27	0.24	0.87	32.7	29.2
Peat	0.36	0.32	0.74	35.7	31.9

4.1.2 Model configuration

The model is set to plane strain and the finite element mesh is comprised of 3611, 15-noded triangular elements. The propriety of the mesh was verified by conducting a sensitivity analysis in the generated quality mesh. The mesh which created the highest value of minimum quality was used in the analysis and it is shown in Figure 83. Refinements were implemented in the upper dike soil layers with an average element size equal to 0.25m² and the fine custom mesh

---

[2] Information regarding the Arc length control option is given in the APENDIX

option was used. The resulting mesh and the soil stratigraphy and the model dimensions are demonstrated in Figure 84.

Concerning the mechanical boundary conditions, the lateral boundaries were set fixed in the horizontal direction but free in vertical direction. The upper boundary was set to free for both vertical and horizontal directions while in the lower boundary full fixities were imposed.

The calculation model contains two pairs of water levels. The first pair corresponds to the daily river water level along with the associated piezometric head of the sand under daily conditions. The second pair corresponds the high-water level along with the elevated piezometric head due to the river head increase. The water levels are shown in Figure 85. The soil clusters highlighted with an orange colour are set to the interpolate pore pressures option to enable the vertical interpolation of the pore pressure distribution of the cohesive layers located below the piezometric head of the sand.
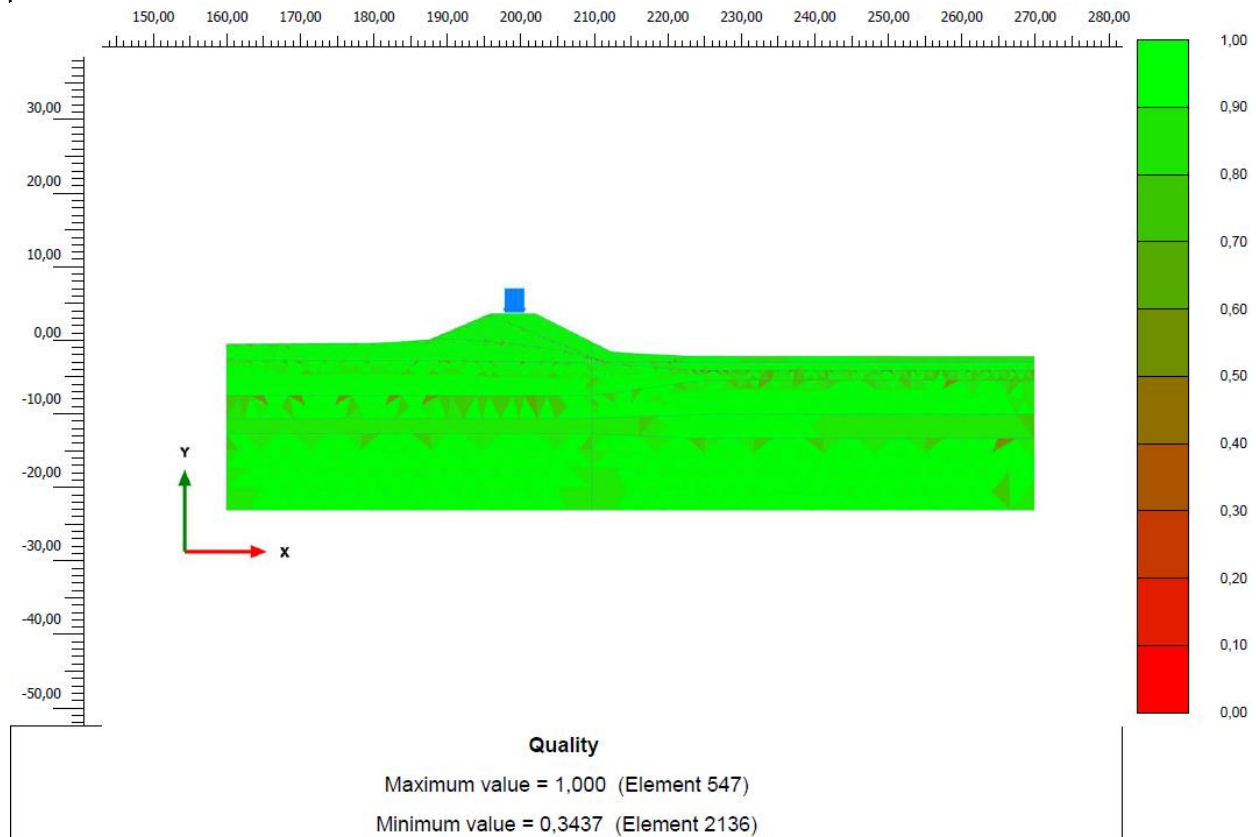
Figure 83: Quality of mesh.
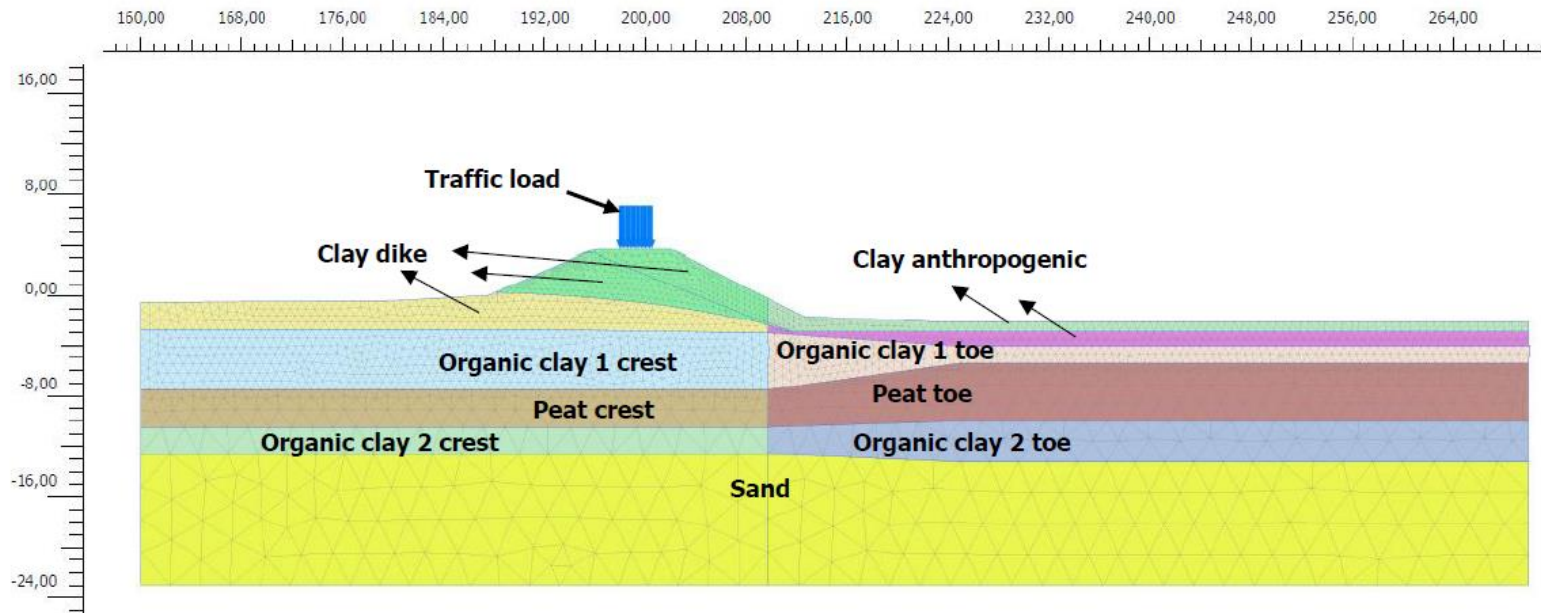
Figure 84: Soil stratigraphy and mesh discretisation.
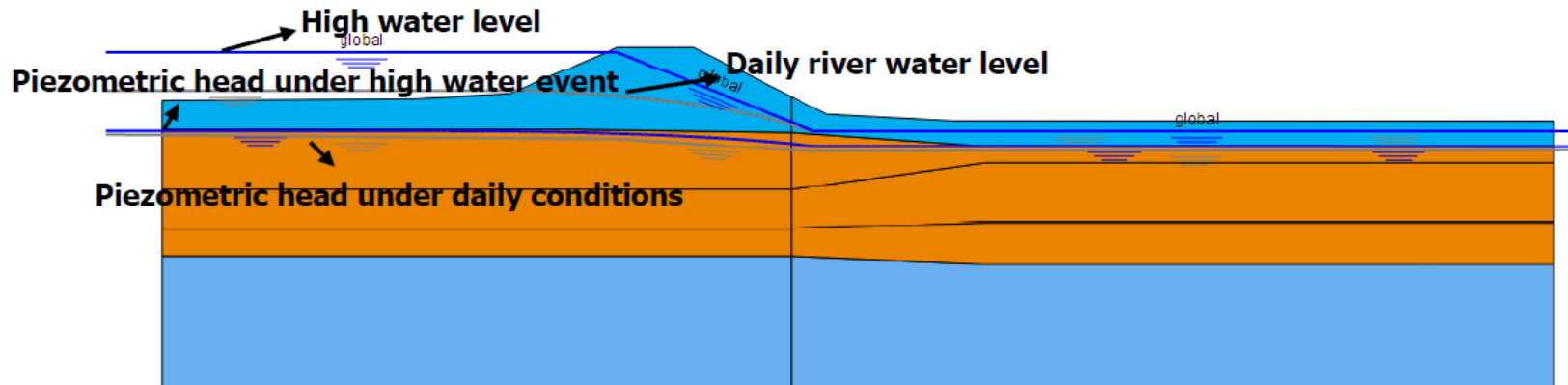
Figure 85: Water levels.

4.2 Results of the analysis

4.2.2 Estimated safety factor and developed failure mechanisms

Before examining the response of the models in terms of safety factor and the developed failure mechanisms, the available strength given from the models is inspected and compared with a cautious characteristic undrained shear strength (in critical state strains) given from the available laboratory tests from samples consolidated with in situ stresses. In the case of the organic clay 1, 2 and the peat the measurements were obtained from the middle point of the soil layers at coordinates x=200 (middle of the crest) and x=225 (measurements in the hinterland). The selected coordinates reflect the locations where the soil samples were retrieved. For the clay dike material, the available strength was obtained from points below the phreatic surface. The depths of the measurements, the available shear strength given from the models and the characteristic undrained shear strength describing the soil layers are given in the Table 34. In addition, the Table contains the undrained shear strength predicted from the models at the critical event (phase 4) with the use of characteristic soil strength. The s_u given from the models at initial conditions was obtained by adding two additional phases after the nil step as shown in Figure 82b. Lastly, the available $s_{u25,40\%}$ of the samples consolidated with in situ stress against the depth of the measurement is given in Figure 87a for all the examined soil layers.

The undrained shear strength profile with depth was examined with the use of the CPTu and compared with the undrained shear strength profile with depth given from the SHANSEP NGI-ADP and HS, SS models.

The calculation of the undrained shear strength based on CPTu data is achieved through the following equations (POVM 2017).

$$s_u = \frac{q_{net}}{N_{kt}} \tag{35}$$

$$q_{net} = q_t - \sigma_{v0} \tag{36}$$

$$q_t = q_c + (1 - \alpha)\, u_2 \tag{37}$$

Where:

N_{kt} = empirical correlation factor
σ_{v0} = the total vertical stress
q_t = the corrected tip resistance
q_c = the CPT tip resistance
u_2 = the pore pressure measured behind the cone shoulder (u_2) position
α = the cone's alpha factor (equal to 0.25).

For all the examined soil layers a N_{kt} value is derived as shown in Figure 86. The N_{kt} values were computed via linear regression by fitting the data with the least square's method. The objective is to derive the values of N_{kt} for which the sum of squares of the residues exhibits the lowest value (F_{kt} min). Distinction has been made between the s_u value in the peak strength, the small and critical state strain levels and thus, a representative N_{kt} value associated for these strain levels is available in Table 33.

$$Fkt = \sum_{i} \left(s_{u,i} \frac{N_{kt}}{q_{net,i}} - 1 \right)^2 \qquad (38)$$

Where:

$s_{u,i}$:the undrained shear strength from laboratory tests consolidated with in situ stresses at the depth i

$q_{net,i}$: the net cone resistance which corresponds to $s_{u,i}$

The uncertainty in the above correlations can be expressed via the coefficient of variation as follows which is additionally given in Table.

$$VC_{N_{kt}} = \sqrt{\frac{\sum_{j=i}^{n} \left(\dfrac{s_{u,i} - \dfrac{q_{net,i}}{Nkt}}{\dfrac{q_{net,i}}{Nkt}} \right)^2}{n-1}} \qquad (39)$$

Where:

VC_{Nkt}: the coefficient of variation of the difference $s_u - q_{net}/N_{kt}$

n = the number of $q_{net,i} - s_{u,i}$ combinations.

It should be noted that the CPT tests were performed close to the location of the sampling boreholes within a horizontal distance in X and Y direction that does not exceed 1 meter.
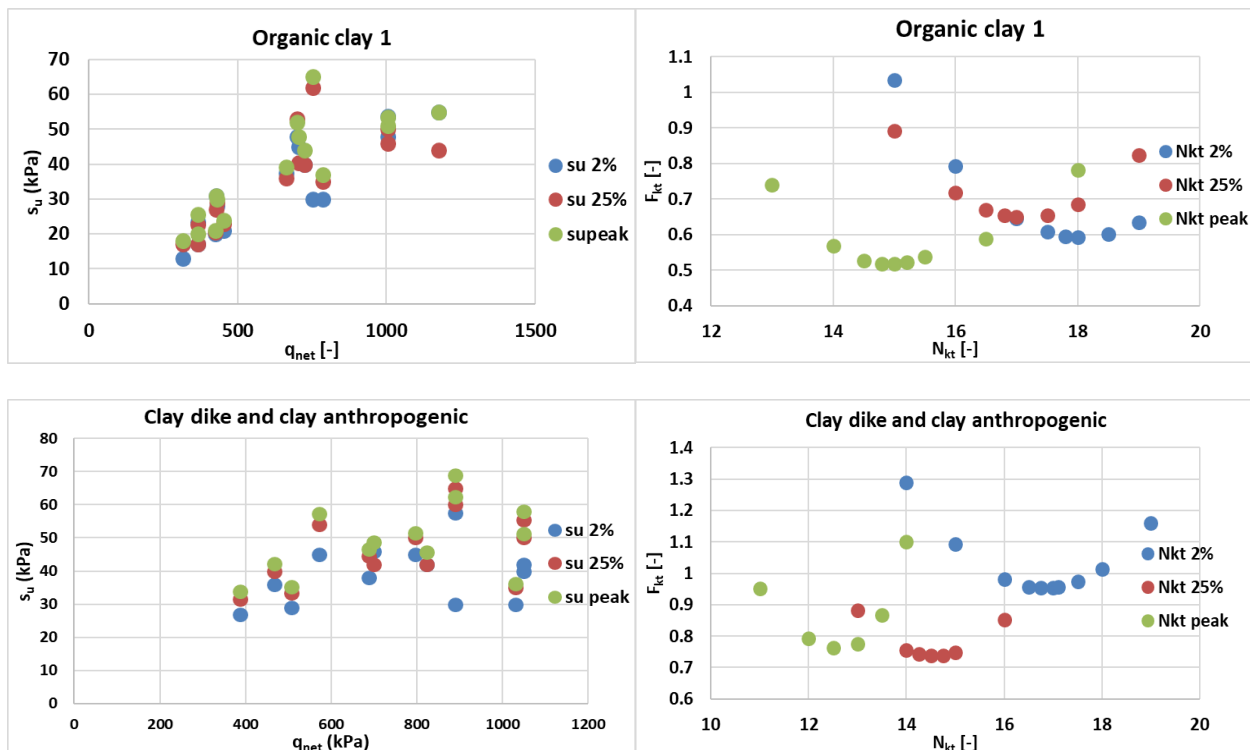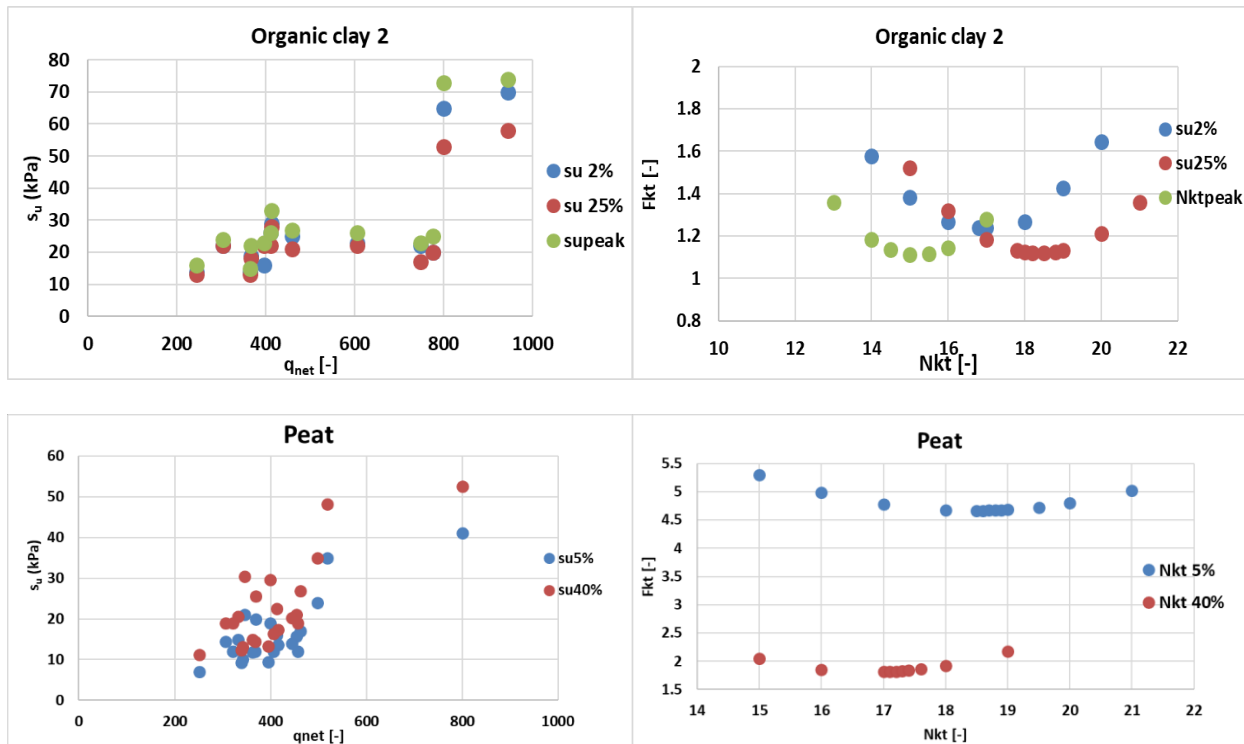
Figure 86: In the left graphs the s_u values against q_{net} is given. The right graphs illustrates the N_{kt} value which produced the lower F_{kt} min.

The undrained shear strength profile with depth at locations x = 200 and x = 225 between the CPT, the SHANSEP NGI - ADP and HS, SS are visualized in Figure 87b and c.

Table 33: Estimated N_{kt} values and coefficient of variation (VC) for the examined soil layers at small and critical state strain levels.

Material	$N_{kt\ 2,\ 5\%}$	$N_{kt\ 25,\ 40\%}$	$N_{kt\ peak}$	$VC_{\ 2,\ 5\%}$	$VC_{\ 25,\ 40\%}$
Clay dike / clay anthropogenic	16.75	14.50	13.20	0.95	0.73
Organic clay 1	16.80	18.50	15.10	1.24	1.10
Organic clay 2	17.00	18.00	15.00	0.59	0.70
Peat	18.50	17.00	17.00	2.65	1.80
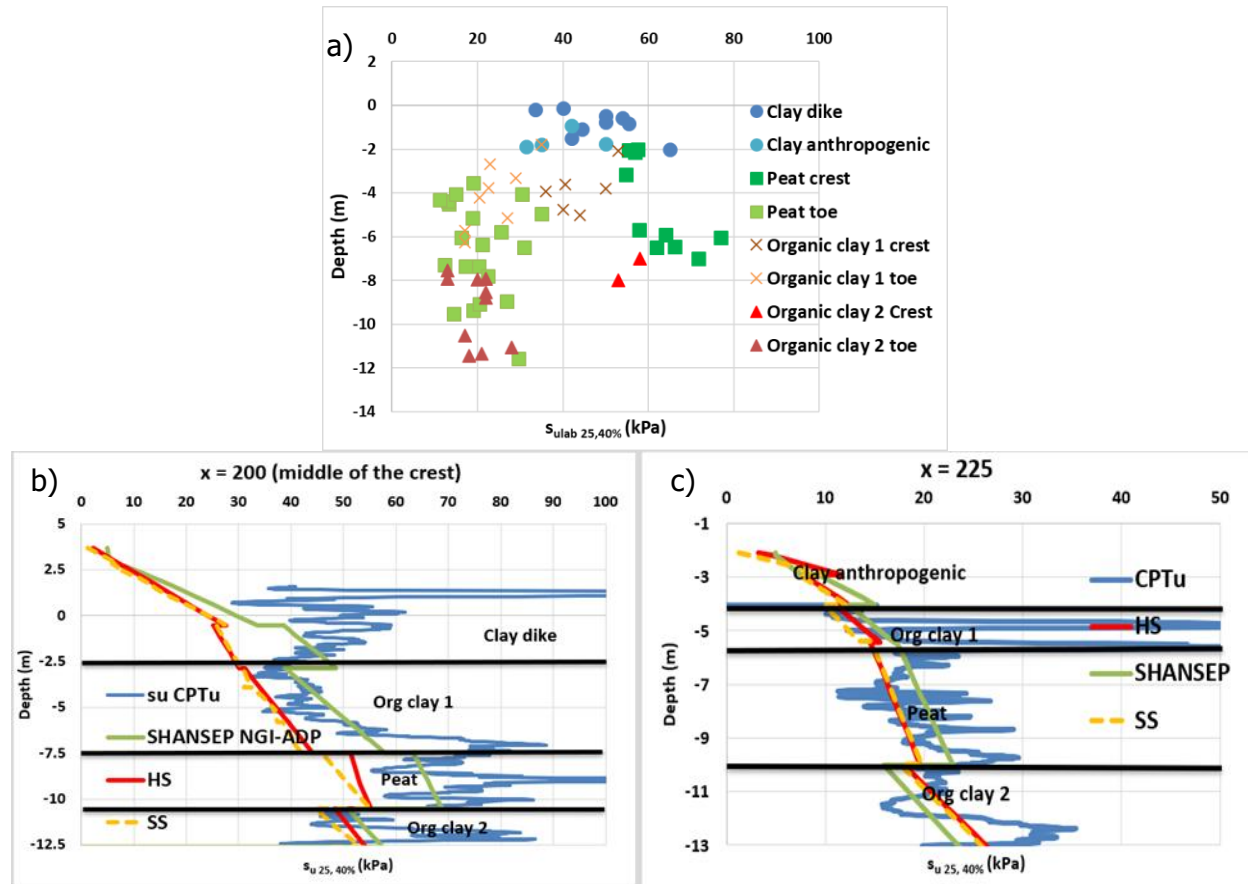
Figure 87: a) $s_{u\ 25,40\%}$ with depth obtained from lab, b) comparison of the $s_{u\ 25,\ 40\%}$ with the $s_{u\ 25,\ 40\%}$ estimated based on CPTu for the crest area of the dike, c) comparison of the $s_{u\ 25,\ 40\%}$ with the $s_{u\ 25,\ 40\%}$ estimated based on CPTu for the hinterland.

Table 34: depths of the measurements, the available shear strength given from the models and the characteristic undrained shear strength describing the soil layers.

Nil Step (Initial State)										
Soil layer	Depth (m)	X=200 τ_{max} (kPa) HS	X=200 τ_{max} (kPa) SS	X=200 s_u^A (kPa)	Depth (m)	X=225 τ_{max} (kPa) HS	X=225 τ_{max} (kPa) SS	X=225 s_u^A (kPa)	$s_{u40\%}$ kar lab crest (kPa)	$s_{u40\%}$ kar lab toe (kPa)
Clay dike / anthropogenic	-1.5	27.3	26.6	44.5	-3.50	10.20	9.93	12.2	44.0	38.0
Organic clay 1	-5.25	37.55	36.98	50.0	-5.25	15.10	14.0	16.4	43.0	20.0
Peat	-9.2	52.82	51.62	67.3	-9.20	18.40	18.6	21.8	65.0	23.0
Organic clay 2	-12	51.9	51.15	55.5	-12	23.50	23.1	20.9	53.0	19.0
Phase 4 (Final State)										
Soil layer	Depth (m)	X=200 τ_{max} (kPa) HS	X=200 τ_{max} (kPa) SS	X=200 s_u^A (kPa)	Depth (m)	X=225 τ_{max} (kPa) HS	X=225 τ_{max} (kPa) SS	X=225 suA (kPa)	$s_{u40\%}$ kar lab (kPa)	$s_{u40\%}$ kar lab toe (kPa)
Clay dike / anthropogenic	-1.5	22.3	21.46	42.65	-3.5	12.27	11.64	12.83	[-]	[-]
Organic clay 1	-5.25	32.55	31.72	48.40	-5.25	17.95	16.3	17.2	[-]	[-]
Peat	-9.2	49	47.63	66.2	-9.2	18.5	18.6	21.8	[-]	[-]
Organic clay 2	-12	50.7	48.42	55.5	-12	23.3	23	20.9	[-]	[-]

It is evident that the SHANSEP NGI-ADP model matches properly the available shear strength given from the laboratory and CPTu data for each soil layer for both the crest and the

hinterland areas of the dike. It is apparent that when the soils experience appropriately the normalised undrained shear strength the SHANSEP formulation proves to be very beneficial since the s_u distribution below the dike can be achieved in a sufficiently good manner.

Furthermore, the available strength given from the SS and the HS is almost identical and lies below the available shear strength given from the SHANSEP NGI-ADP model especially, for the clay dike material and the organic clay 1 in the crest area of the dike (x=200). The deviation is further intensified when the critical event is occurring. The intensification is attributed in the significance of the OCR in the SHANSEP formulation. Considering the immediate increase of the hydraulic load and the associate decrease of the effective vertical stress a rapid increase in OCR is experienced by the soils. Therefore, the increase of OCR is compensating the decrease of effective vertical stress for the SHANSEP NGI-ADP model (refer to equation 1) while for the HS and SS models the decrease in the effective stress (refer to equation 5) leads to a notable decrease in the resulting undrained shear strength. The OCR development between the daily river conditions and the critical event is shown in Figure 88 along with the difference experienced in the s_u^A and the τ_{max} given from the SHANSEP NGI-ADP and the HS model. The OCR development is obtained from a vertical cross section at coordinates x=200 (middle of the crest).An example of the horizontal cross sections are shown in Figure 89. It has to be noted that for clarity the following Figures contain only the τ_{max} obtained from the HS model, since both the HS and SS models displayed almost identical values in terms of strength.
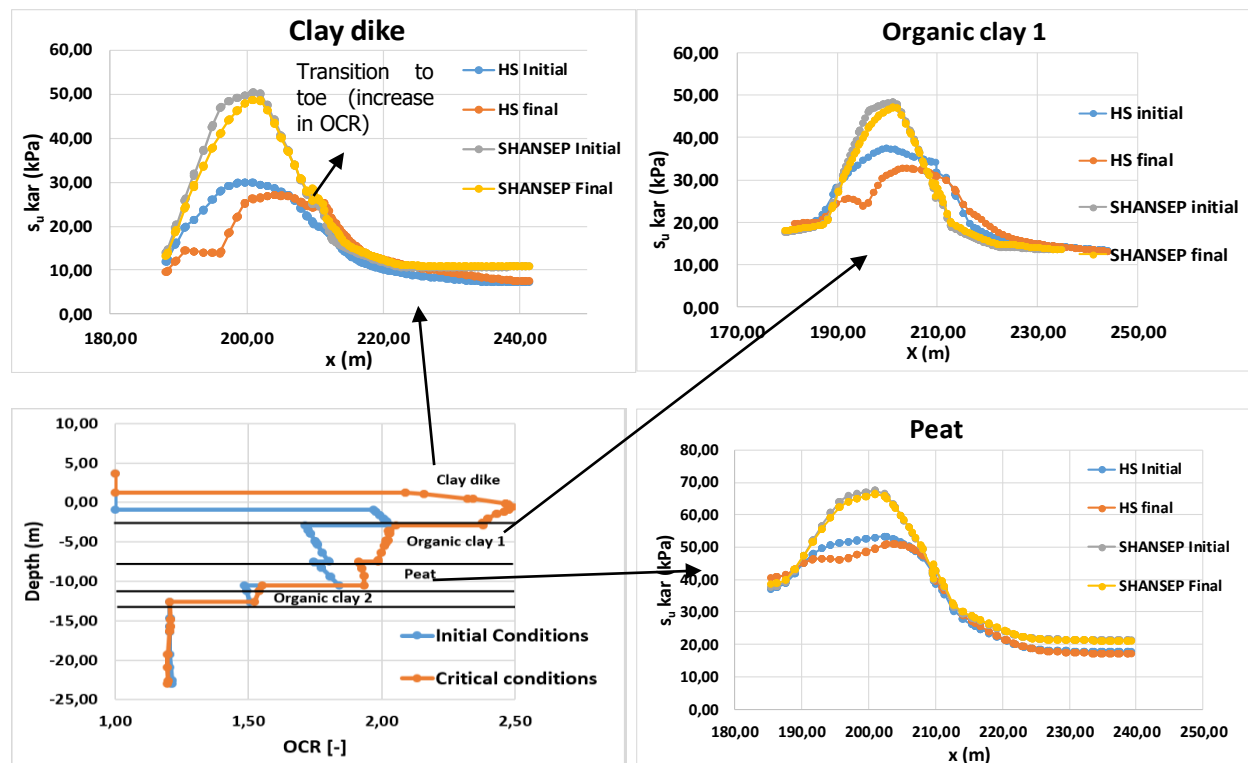
Figure 88: OCR and strength distribution between the initial (daily water level) and the final state (critical loading).
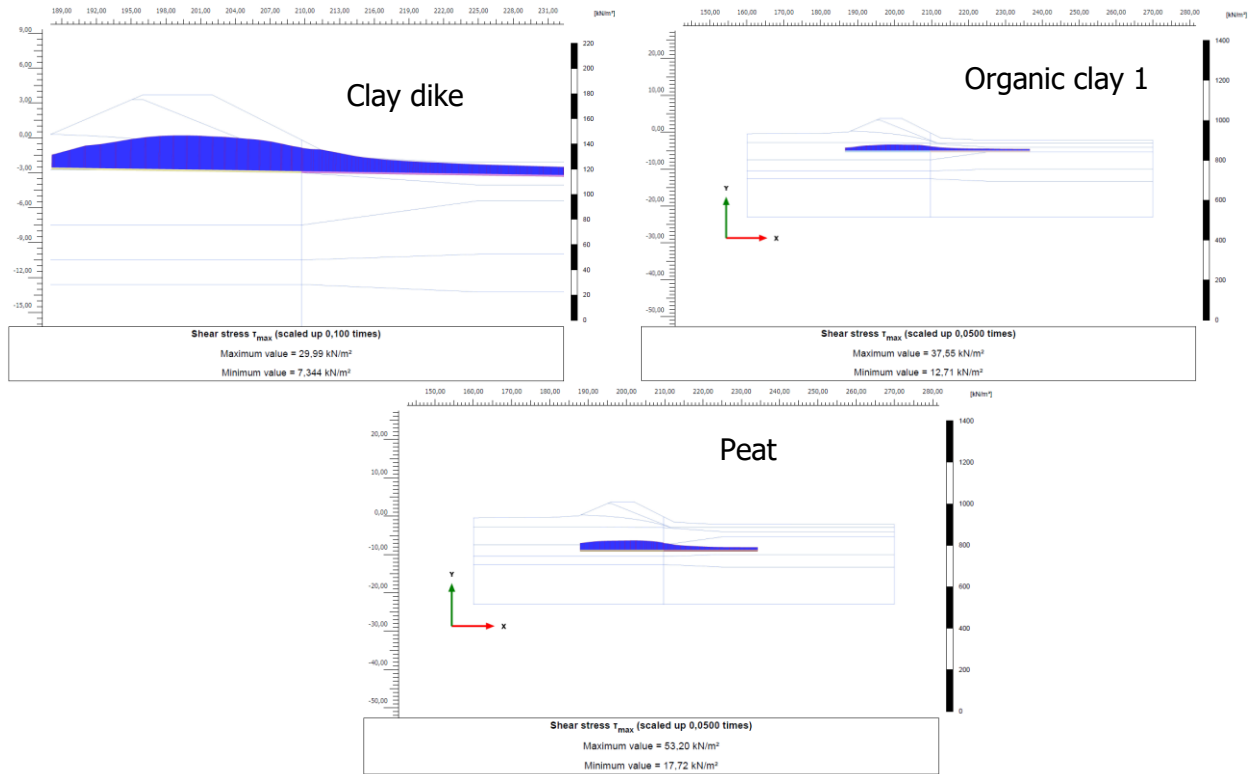
Figure 89: Horizontal cross sections.

Another interesting observation is that in the coordinates x = 225 the models exhibit comparable values in terms of strength. This is due to the rotation of the principal stresses below the dike body as visualised in Figure 90.

The blue colour denotes the passive area of the dike. In that area the dominant stress is the horizontal which influences the resulting τ_{max} given from the HS and SS models while the rotation of σ'_1 in turn affects and the s_u^A given from the SHANSEP NGI-ADP model. In addition, at these coordinates the τ_{max} increases during critical loading for both the HS and the SS and the passive zones slightly expanses as shown in Figure 90.
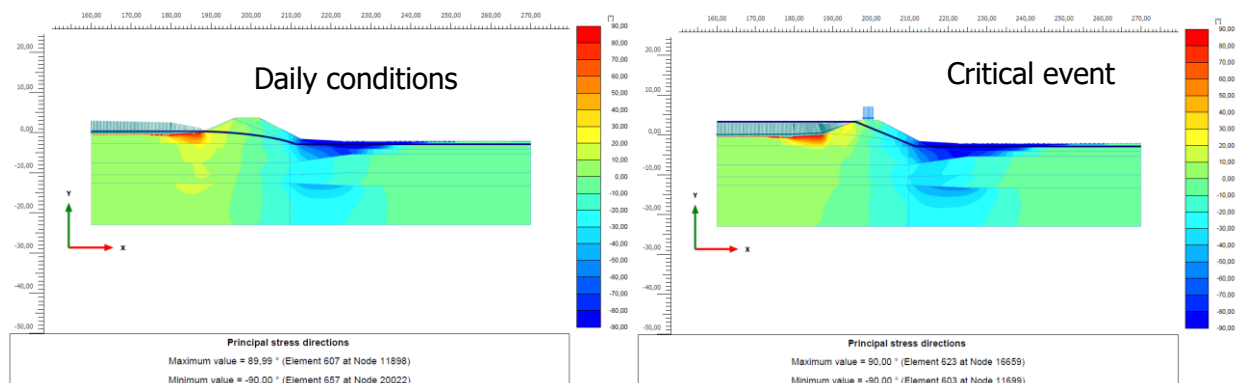
Figure 90: Rotation of principal stresses at daily conditions and critical event.

Lastly, the Figure 91 display the s_u^A and the τ_{max} obtained from the SHANSEP NGI-ADP and HS models in the daily and critical event conditions.
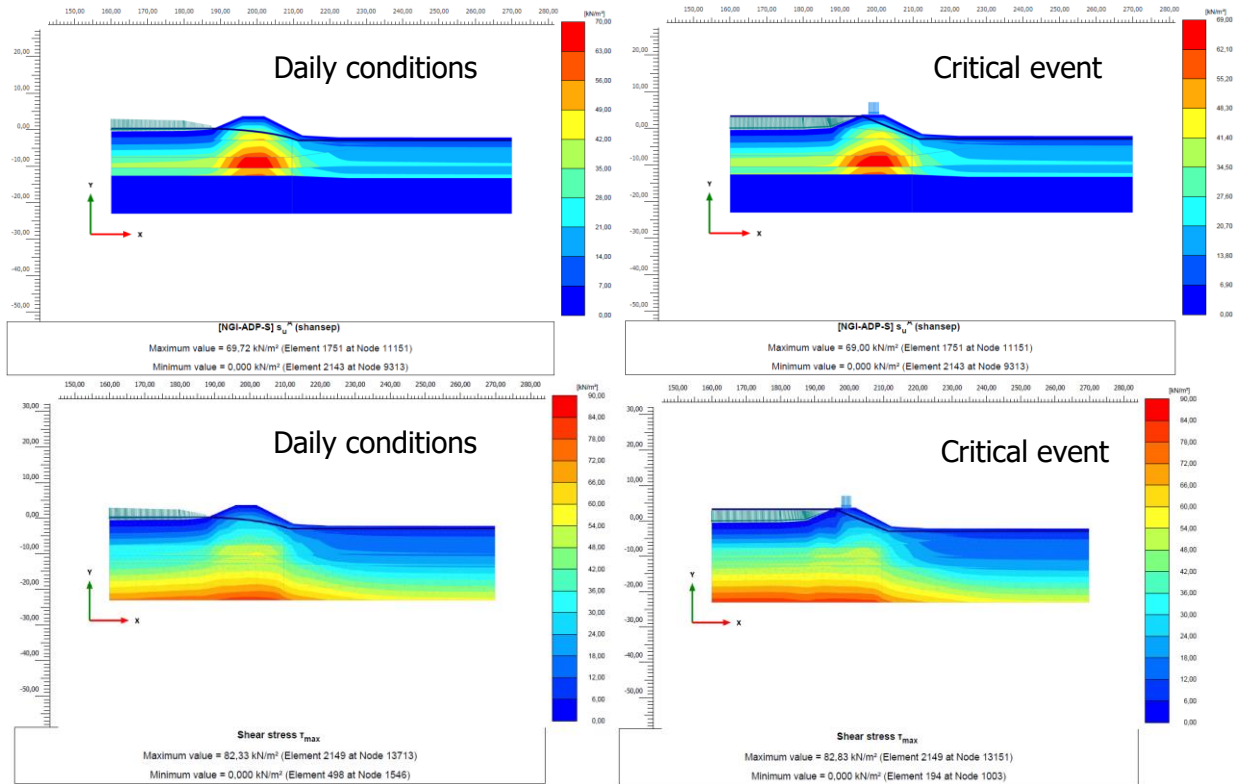
Figure 91: Available shear strength.

The estimated factor of safety obtained from the considered models is shown in Figure 92. The SHANSEP NGI-ADP model gives the higher FoS equal to 1.59 followed by the SS and HS with the values which are comparable, i.e. equal to 1.31 and 1.33 respectively. The estimated FoS from the SHANSEP NGI-ADP is shown twice. The SHANSEP NGI-ADP (HS) denotes that the calculation model used in the drained steps was the HS while the SHANSEP NGI-ADP (SS) denotes that the model used was the SS.
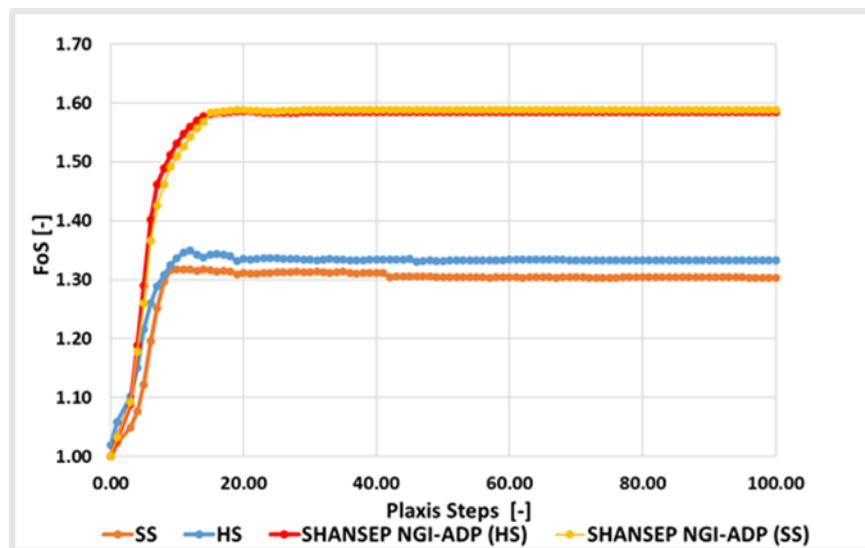
Figure 92: Obtained safety factor from the considered constitutive models

The higher FoS obtained from the SHANSEP NGI-ADP model was an expected outcome since the SHANSEP NGI-ADP model displayed higher values in terms of strength than the HS and SS models. Moreover, the estimated FoS obtained from the SHANSEP NGI-ADP is not affected by the use of either the SS or the HS in the preceding drained steps. This implies that both models transfer equally well the stress history of the soils.

An interesting observation is the different developed failure planes between the SHANSEP NGI-ADP model and the HS and SS models. The use of the SHANSEP NGI-ADP model may lead to a critical failure plane which is relatively deep and large. In contrary, the developed failure mechanisms obtained from the HS and the SS models are identical with a shallower and narrower slip plane. As described in the previous subchapters the strength of the materials in the case of the Green dike examination is obtained from the critical state of the soil. Thus, the strength of the soil is described thoroughly from the critical state friction angle, since the cohesion of the material in the critical state is zero. Additionally, for both the HS and the SS models the maximum shear strength is obtained based on the MC failure criterion (refer to subchapter 3.1.1 and 3.1.2). The cohesion of the materials is particularly essential in the soil layers which are located at the top of the dike where the effective vertical stress is almost zero. There, the positive influence of the cohesion in the shear strength of the soil is becoming more relevant. By setting a cohesion equal to zero for the upper layers (e.g. clay dike) and apply the phi-c reduction technique the MC failure criterion is "forced" to be reached relatively fast. This eventually causes the failure plane to develop in a relatively shallow shape.

Another possible reason behind the dissimilarities in terms of the estimated strength, the resulting factor of safety and the developed failure planes was already a point of interest in the soil TestFacility examination. The soils which are located at the top of the dike exhibit higher values of OCR and thus, based on the Undrained A option a possible underestimation in the undrained shear strength is expected. Finally, the developed failure mechanisms from the considered models are illustrated in Figure 93. The Figure 94 illustrates the developed failure mechanism of the SHANSEP NGI-ADP in terms of the deviatoric strain development. A closer look into the Figure demonstrates that the SHANSEP NGI-ADP reached an equilibrium in the shallow clayey layers leading to a deeper and enlarged failure mechanism.
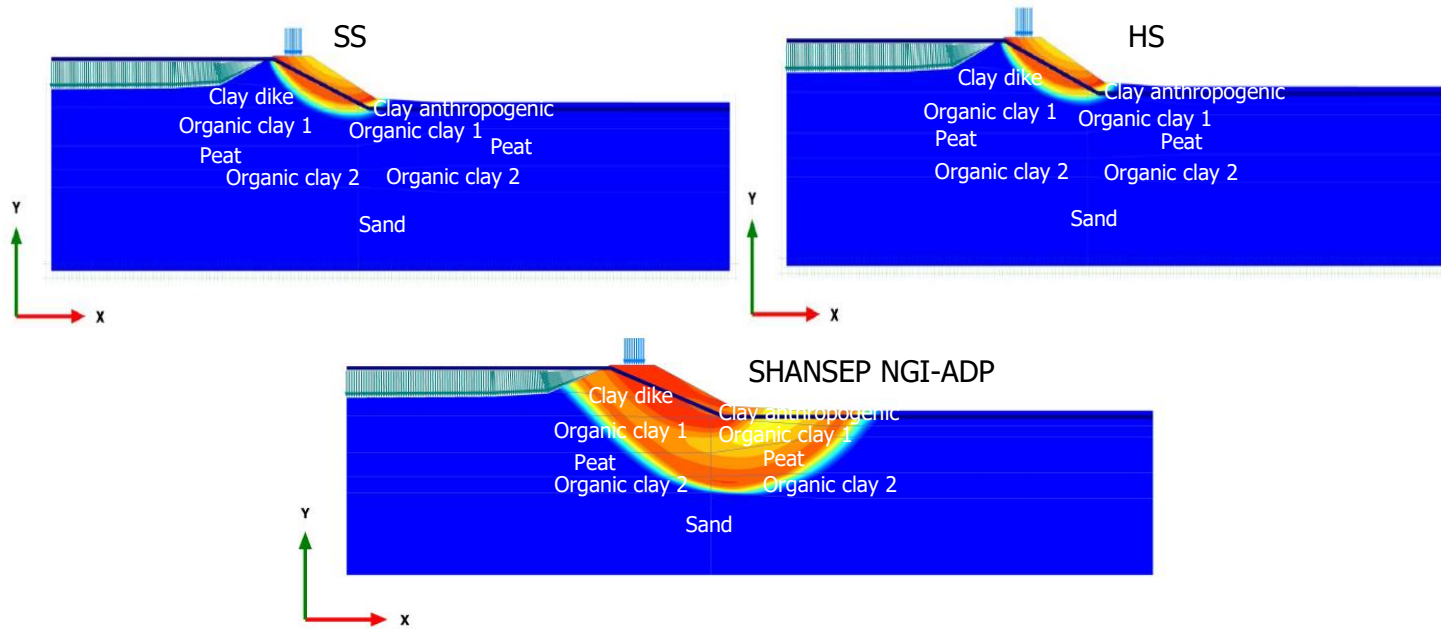
Figure 93: Developed failure mechanisms from the considered constitutive models.
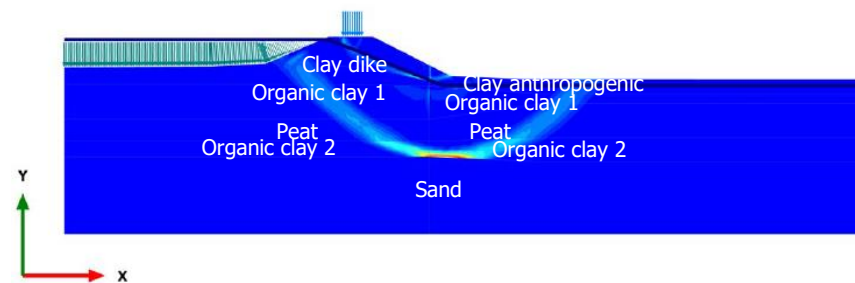
Figure 94: Shear strains development at the safety analysis for the SHANSEP NGI-ADP model.

4.2.3 Displacements

The generated lateral displacements during the undrained analysis step for the considered constitutive models in three different locations namely edge of the inner crest, middle of the slope and edge of the slope are demonstrated in Figure 95. In this way the development of the lateral displacements below the dike body moving towards the hinterland is examined. The predicted displacements obtained from the SHANSEP NGI-ADP are shown twice. The SHANSEP (HS) denotes the displacements given from the model when the calculation scheme in the drained steps incorporated the use of the HS. Similarly, the SHANSEP (SS) implies that the calculation model in the drained steps incorporated the SS model.

The predicted displacements between the constitutive models share comparable values. Specifically, the largest amount of displacements is found in the edge of the crest with the constitutive models predicting displacements varying from 0.052 to 0.065 m. The SS seems to generate the lowest amount displacements while the HS the largest. The predicted displacements of the SHANSEP NGI-ADP lie in the middle of the two extremes.

Regarding the SS it can be argued that the "stiffer" response was an expected outcome since the model in a single element level behaves stiffer than the other considered models (refer to subchapter 3.4). In addition, the over consolidated state imposed on the model resulted in the dominant accumulation of elastic strains. In contrary, as it concerns the HS model the larger amount of lateral displacements can be attributed to the activation of the deviatoric yield surface which caused a stiffness degradation and accumulation of plastic strains.

It has to be noted that it is rather hard to indicate which of the constitutive models produced the most accurate response in terms of displacements since there are no field measurements for comparison. At this point, it is noteworthy to address that the updated guidelines suggest that the calculation of the displacements and the structural forces (in the case of the Blue dike) is done explicitly with the use of the SHANSEP NGI-ADP model. Thus, it is important to note that the constitutive model which is used for the calculation of the drained steps may have an influence on the resulting response of the SHANSEP NGI-ADP in terms of displacements.
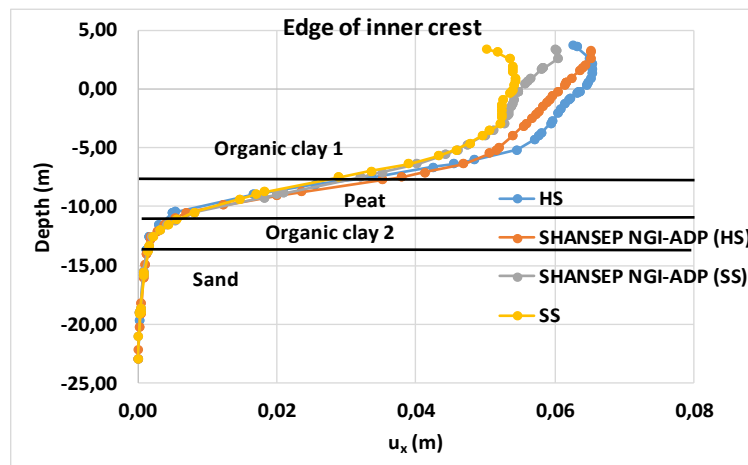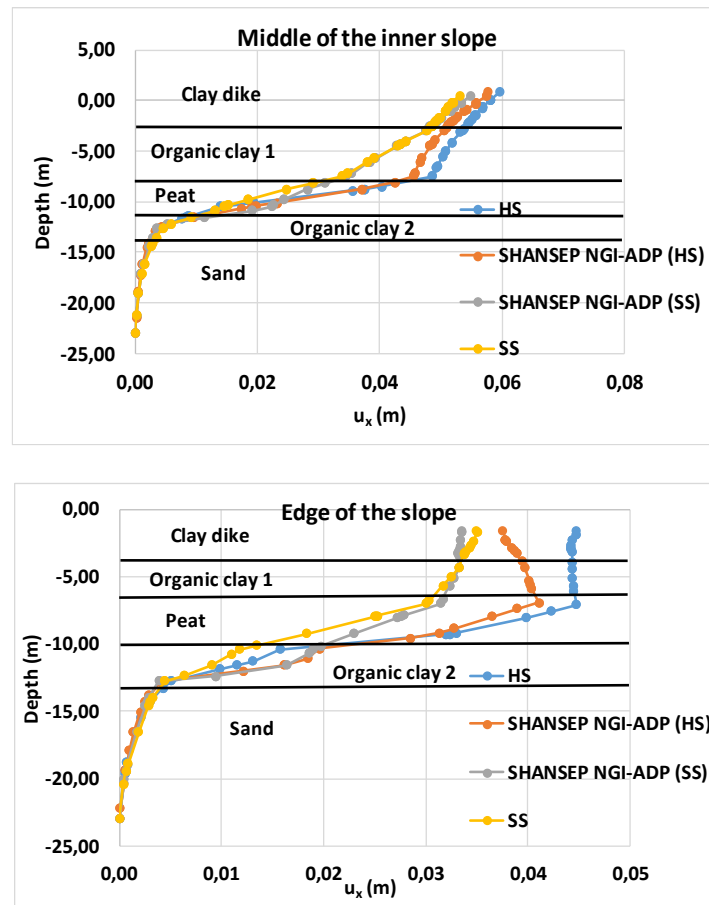
Figure 95: Generated displacements from the considered constitutive models.

4.3 Influence of the strain level dependency of the strength parameters on the Green dike analysis

In this subchapter, the influence of the strain level dependency of the strength parameters for the Green dike analysis is investigated and discussed. Thus, the strength parameters determined from the service conditions strain levels are additionally used in the analysis. In this way, the comparison in terms of the predicted FoS, the developed failure mechanism and the generated deviatoric strain can be established. It should be noted that the comparison is realised with the use of the HS and the SHANSEP NGI-ADP model. This is considered a reasonable decision since, both the HS and the SS displayed almost identical response in terms of the estimated FoS and the developed failure mechanism as well qualitatively and quantitively comparable values in terms of the displacements. Lastly, the purpose of this subchapter is no longer the comparison of the responses of the constitutive models but rather the examination of the response of the HS and the SHANSEP NGI-ADP upon variation of their strength parameters based on the considered strain levels. The reader may refer to subchapter 4.2 for more information regarding the comparison of the results of the examined constitutive models.

Starting point is the illustration of the s_u distribution below the dike body. With the use of the strength parameters obtained from the critical state strain levels the peat exhibits the higher values of the s_u among the soil stratigraphy. Contrarily, the use of the service conditions strain levels drastically reduces the s_u that the peat exhibits (refer to 3.2.1 and 3.2.3 subchapters for more information). Moreover, it is obvious that in the crest area of the dike where the effective

stress is considerably higher than the toe and the hinterland areas of the dike the s_u exhibits the highest values. Therefore, for every soil layer it's s_u peak is given exactly below the crest body. The s_u distribution shown in the Figures is obtained from Phase 7 which is prior the safety analysis (refer to Figure 82a). It should be noted that the τ_{max} of the sand layer is excluded from the Figure 97 in order to emphasize in the available s_u that the soft soil layers exhibit based with the use of the HS model.
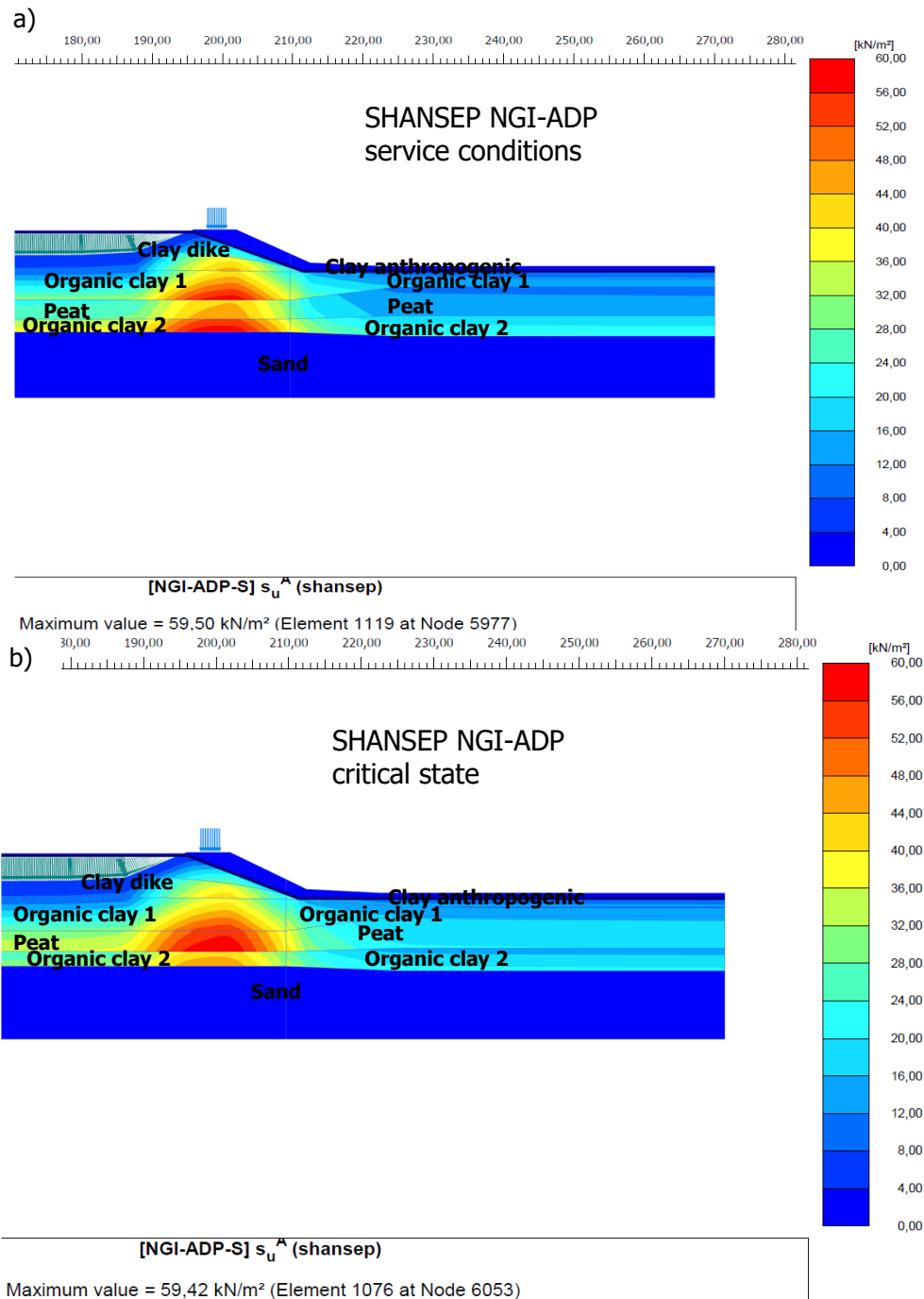
Figure 96: Predicted s_u given from the SHANSEP NGI-ADP model from strength parameter determined from (a) service conditions strain levels, (b) critical state strain levels.
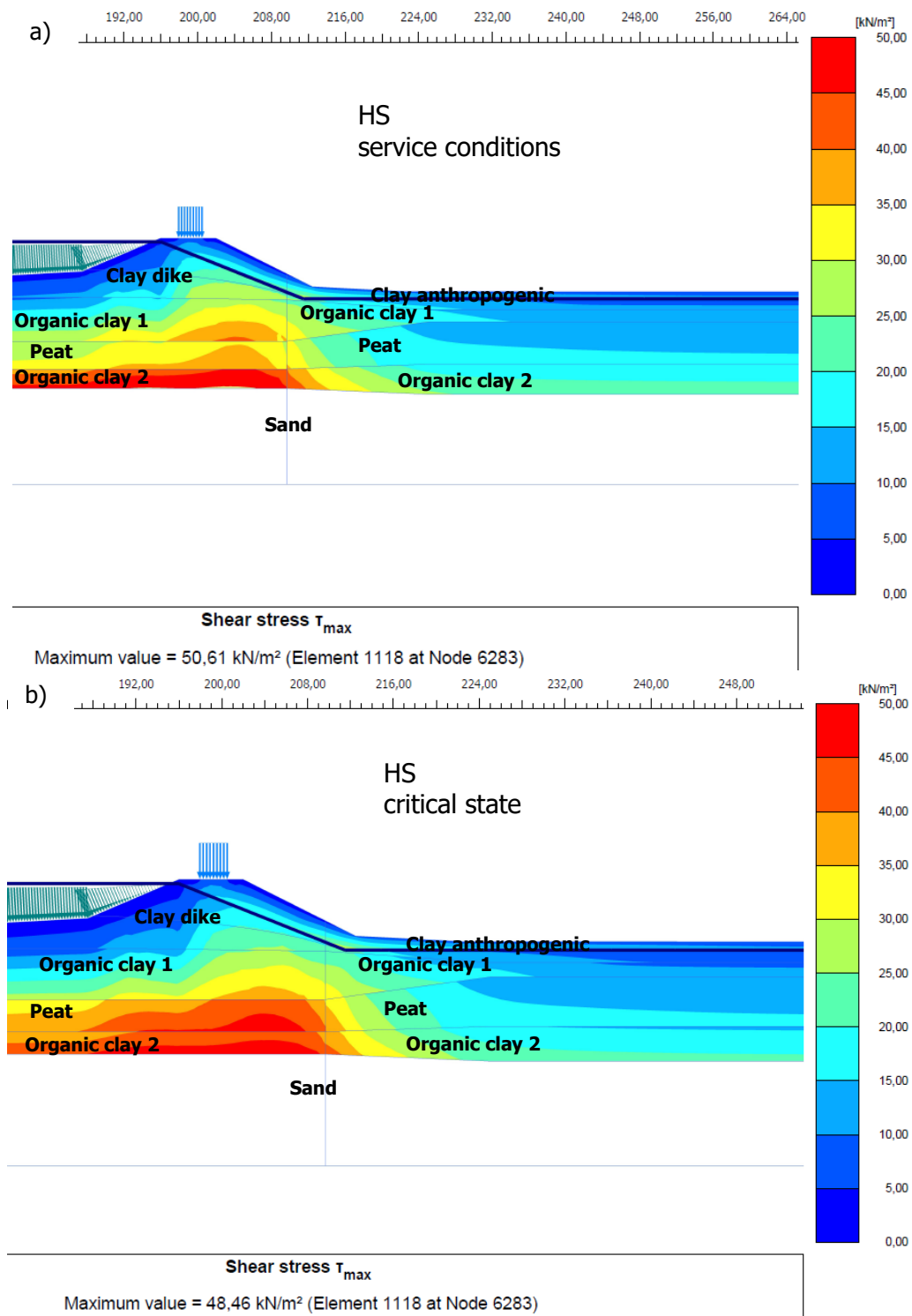
Figure 97: Predicted s_u given from the HS model from strength parameter determined from (a) service conditions strain levels, (b) critical state strain levels.

Figure 98 and Figure 99 illustrate the development of the deviatoric strain in phase 4 (refer to Figure 82a) which demonstrate an overview of the pre-failure response of the dike. With the usage of the serviceability strength parameters the deviatoric strain is largely mobilized in the

interface between the peat and the organic clay 2. With the use of the critical state strength parameters the deviatoric strains seem to penetrate deeper and mobilized in the interface between the Organic clay 2 and the sand. This is more obvious in Figure 99b. It should be noted that since we are dealing with the pre failure behavior of the dike the stiffness characteristic of the soil dominate the response in terms of the amount and the development of the deviatoric strain. Thus, this explains why there is a large amount of deviatoric strain development into the peat layer irrespective of the applied value of the strength parameters. As shown in the parameter determination (subchapter 3.2.4) the peat exhibits notably lower values of stiffness characteristics (i.e. E_{50}^{ref}, G_{ur} / s_u^A) than the clayey soils.
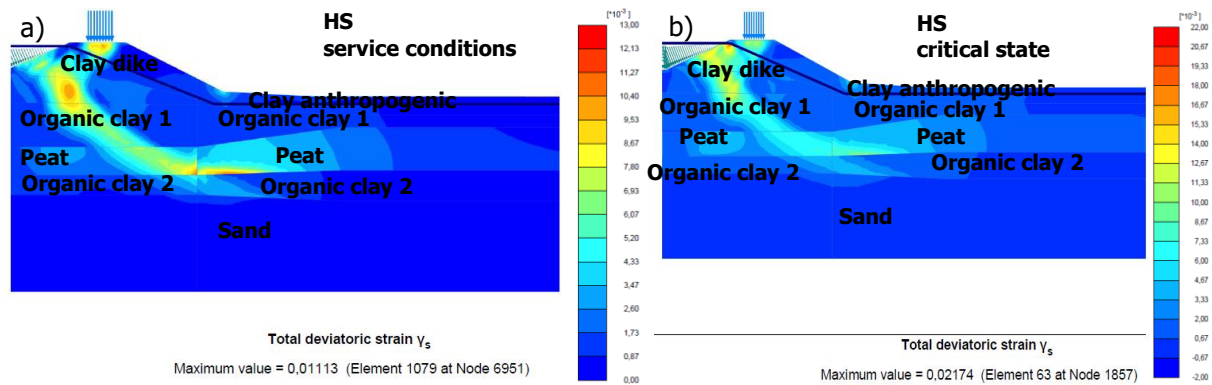
Figure 98: Deviatoric strain development of the HS model with the use of strength parameters determined from, (a)service conditions strain levels, (b) critical state strain levels.
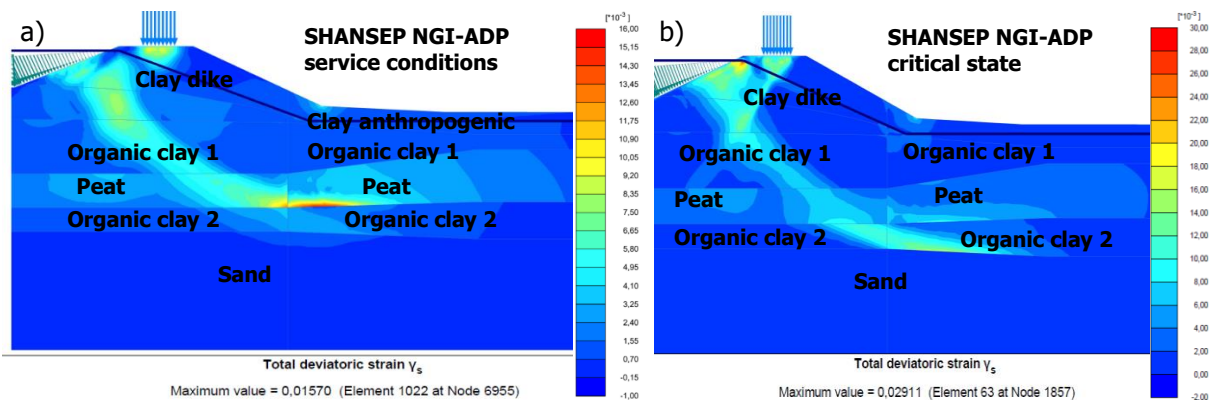
Figure 99: Deviatoric strain development of the SHANSEP NGI-ADP model with the use of strength parameters determined from, (a)service conditions strain levels, (b) critical state strain levels

Last part of this investigation is the comparison of the developed failure mechanism and the estimated FoS of the constitutive models (Figure 100 and Figure 101) upon variation of the strength parameters based on the considered strain levels. In the case of the strength parameters obtained from the service conditions strain levels both models predict a failure mechanism which occurs in the interface between the peat and the organic clay 2 which is merely tied with the low values of the s_u that peat exhibits. Conversely, the use of the critical state strength parameters for the case of the SHANSEP NGI-ADP results in a deeper failure mechanism since the peat is no longer the weakest soil layer. Thus, the failure occurs in the interface between the organic clay 2 and the Sand. The HS model on the other hand fails at shallow depths. The dissimilarity between the different failure mechanisms between the HS and the SHANSEP NGI-ADP is given in subchapter 4.2. Lastly, it is obvious that the estimated FoS is influenced from both the use of the

constitutive models and the strain level dependency of the strength parameters especially for the case where the parameters are determined from the critical state strain levels. Lastly, it is illustrated that when the HS model is described with the critical state strength parameters the deviatoric strain development prior the safety analysis is not in accordance with the developed failure mechanism (refer to Figure 98b).
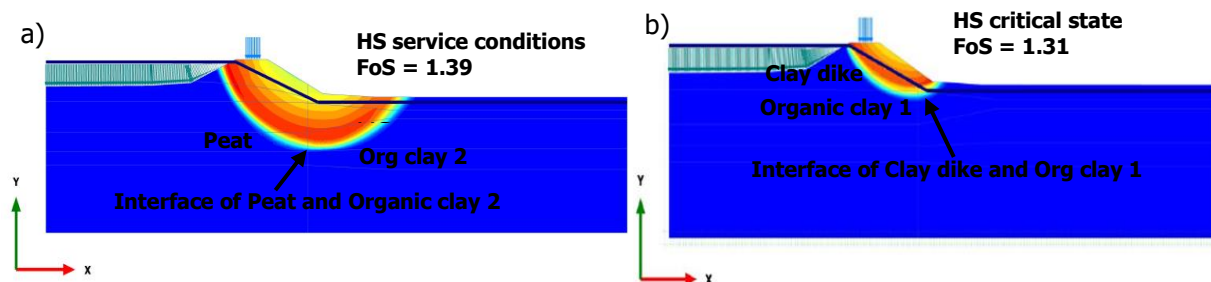
Figure 100: Developed failure mechanism and FoS of the HS model with the use of strength parameters determined from, (a)service conditions strain levels, (b) critical state strain levels.
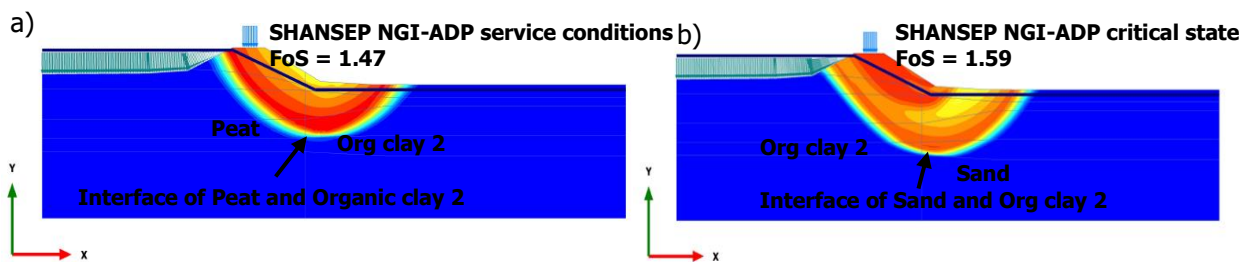
Figure 101: Developed failure mechanism and FoS of the HS model with the use of strength parameters determined from, (a)service conditions strain levels, (b) critical state strain levels.

4.4 Discussion on the Green dike analysis

Regarding the obtained FoS it was noted that the SHANSEP NGI-ADP model produced the higher value than those by the Soft Soil and Hardening Soil models. In addition, the developed failure plane from the SS and HS models was identical while the failure mechanism obtained with the use of SHANSEP NGI-ADP was deeper and larger. The observed dissimilarities in terms of the estimated FoS and the developed failure planes can be attributed to the following reasons:

1. *The SHANSEP NGI-ADP model matched appropriatelly the strength given from the laboratory data for the examined soil layers while the HS and SS lied below the available shear strength in the crest area of the dike.*
2. *Both the HS and the SS models are described based on the Mohr – Coulomb failure criterion. In the critical state the value of cohesion is zero and the strength of the materials is described thoroughly from the critical state friction angle. In the upper soil layers where the vertical effective stress exhibits minimal values the influence of the cohesion becomes significant. Upon the application of the phi-c reduction technique in the case of the HS and the SS models the MC failure criterion is "forced" to be reached relatively fast resulting in a critical failure plane which is relatively shallow and narrow.*
3. *The rise of the river head under high water conditions results in a rapid decrease of the vertical effective stress and an excessive increase in the OCR. The increase in the OCR for the SHANSEP model compensates the decrease on the effective vertical stress and the s_u*

remains almost unaffected. On the contrary, in the HS and the SS the decrease of the vertical effective stress considerably lowers the available shear strength.

4. *Given the fact that for the examined soil layers a specified value of OCR was implemented a possible underestimation of the available undrained shear strength based on the Undrained A option from the SS and the HS models was expected. The underestimation is observed in the upper soil layers which experience a higher value of OCR.*

It is noteworthy to mention that while the 2nd and the 4th reason can be considered as more universal the 3rd reason is highly dependent on the implemented design high water level which varies based on the various guidelines, the project recommendations and the engineering judgement. The lower the difference between the design high-water level and the daily river level the lower the decrease in the vertical effective stress and the less significant the increase in the OCR.

In terms of displacements the constitutive models predicted comparable values. Specifically, it was noted that the SS model displayed the "stiffer" response while the HS the "softer" response. The prediction of the SHANSEP NGI-ADP model lies in the middle of these two responses.

Furthermore, it was shown that either the use of the HS or the SS in the drained steps have no influence as it concerns the estimated FoS given from the SHANSEP NGI-ADP model. On the contrary, in terms of displacements the use of the HS or SS on the preceding drained steps may lead to a different response of the SHANSEP NGI-ADP model.

Lastly, it was found that the application of the strength parameters determined from the service conditions strain levels influenced the results in terms of the predicted developed failure mechanism, the estimated FoS as well and the development of the deviatoric strains. In particular, with the use of the strength parameters from the service conditions strain levels the developed failure plane reached until the interface of the peat with the below lying Organic clay 2 soil layer since, the peat exhibits the lower values of the s_u. The similarity in the predicted failure mechanism between the constitutive models led to a more comparable value of the FoS in contrary with the use of the critical state strength parameters where the SHANSEP NGI-ADP predicted a considerably higher value than the HS model.

Chapter 5 - Blue dike analysis

The purpose of this chapter is to present the outcome in terms of the estimated FoS, the developed failure mechanisms, the calculated displacements and the structural forces acting on the sheet pile wall using the considered constitutive models for the case of the Blue dike analysis.

The chapter is divided in three main sections. The first section deals with the model set-up along with the elaboration of the simulation phases proposed by POVM 2018 for assessing the dike safety and the displacements. Moreover, this section highlights the design requirements for the Blue dike analysis emphasizing in the use of the unanchored sheet pile wall. In the second section the outcome of the analysis is presented and discussed. Lastly, in the third section the overall conclusions of the Blue dike analysis are given.

5.1 Calculation phases, design requirements and set up of the model

The flowchart (Figure 102) illustrates the required calculation steps established from POVM 2018 for the analysis of the Blue dike followed by the elaboration of each step and the explanation of the required semi probabilistic factors.
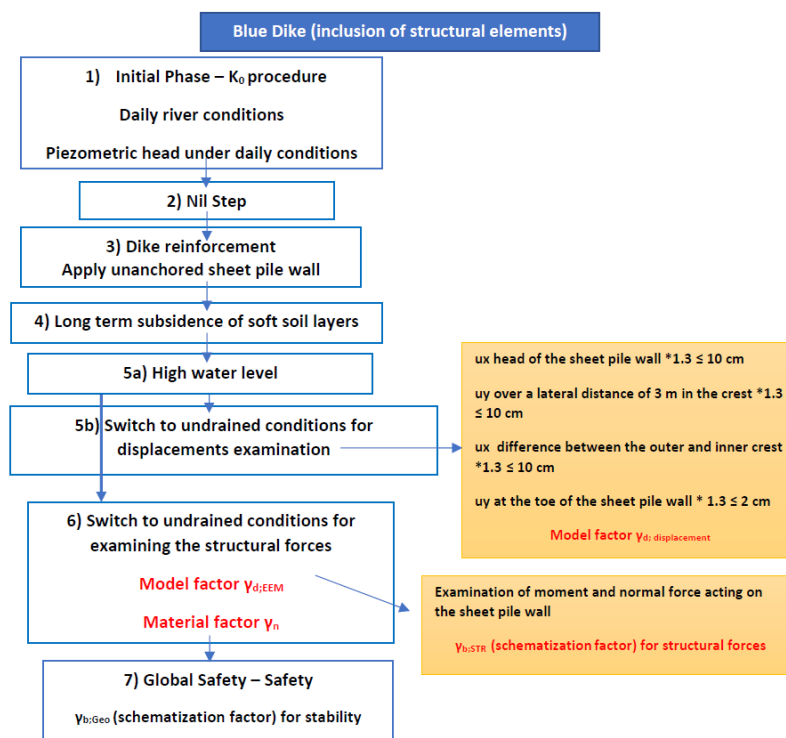
Figure 102: Calculation steps proposed by POVM 2018 for the analysis of the Blue dike for FEM analysis.

The detailed elaboration in the calculation steps is given below following the numbering denoted in the Figure 102.

1) Existing situation in daily circumstances under drained conditions. The initialization of the stresses is accomplished with the K_0 conditions followed by the Nil Step. For more information regarding the K_0 conditions and the NIL step refer to subchapter 4.1. The considered stress history of the soil is given in Table 41.

2) Addition of the unanchored sheet pile wall under drained conditions.

3) Consider the long-term subsidence of the soft layers after the installation of the structural element in drained conditions. In this way, the effect of the settlement of the soft layers in the resulting structural forces is accounted. The long-term subsidence can be simulated by two options. The first option is accomplished with the usage of the SSC model through the advanced μ* parameter (creep index). This method is necessary for horizontally placed structural elements (e.g. geotextiles). The second method can be accomplished by setting a vertical contraction through the volumetric ε_{yy} option of a soil layer in the selection explorer in PLAXIS. According to POVM the use of this method results in different displacements and therefore resulting structural forces.

4) Application of the high-water event along with the piezometric head elevation under drained conditions

5a) Apply the traffic load and calculate the associated displacements under undrained conditions. The resulting displacements need to be multiplied by the model factor equal to 1.3. This step additionally requires the reduced values of stiffness but similarly with the green dike analysis as it concerns the calculation of the displacements the carefully calibrated stiffness parameters remained unchanged. This traffic load is equal to 13.3 kN/m^2 and has a width of 2.5 m. This load is located in the middle of the crest following the design recommendations of POVM 2018 and it is in accordance with the Constructive Guidelines Designs (TAW, 1994).

5b) Calculation of moments and forces at high water and traffic load incorporating reductions in strength and the stiffness parameters of the soil under undrained conditions.

6) Control of the global safety during high water and traffic load.

The Table 35 depicts the semi probabilistic factors which are required for the Blue dike analysis. Distinction has been made between the factors that are used for reducing the ground strength and the factors which are applied in the obtained displacements or structural forces from the PLAXIS output. It should be noted that more information regarding the the material factor (γ_n), the model factor (γ_d) and the schematization factor ($\gamma_{b; Geo}$) are given in subchapter 4.1.1.

Table 35: Partial factors for the Blue dike analysis.

Partial Factor	Value and Description	Reduce ground strength
γ_n (material factor)	1.06 Refer to subchapter 4.1.1	Yes
$\gamma_{d.EEM}$ (model factor)	1.06 Refer to subchapter 4.1.1	Yes
$\gamma_{b;Geo}$ (schematization factor) for stability	1.05 (Larsen et al., 2013)	No
$\gamma_{b;STR}$ (schematization factor) for structural forces	1.08 (Larsen et al., 2013) The obtained forces acting on the steel sheet pile wall (i.e. moments and normal forces are multiplied with $\gamma_{b;STR}$. More information regarding the schematization factor is given in subchapter 4.1.1.	No
$\gamma_{d;displacements}$ (model factor for displacements)	1.3 (Visschedijk, 2018) The obtained displacements at critical loading conditions are multiplied with $\gamma_{d;displacements}$.	No

For the analysis a relatively stiff cantilever sheet pile wall is selected. The decision is considered reasonable since the sheet pile wall does not include an anchorage for further strengthening. In the practice of steel sheet piles the 100-year design life must be considered. Thus, a corrosion contribution to the cross-sectional area must be taken into account. This contribution has a maximum of 4.4mm and minimum of 2.4mm for both sides (Helpdesk Water, 2016) for the total length of the sheet pile wall. In this study an average between the two extremes is selected which equals to 3.4mm.

The flange thickness of the AZ38-700 steel sheet pile wall equals to 12.2 as shown in Figure 103. Therefore, the resulting reduced profile is given from the equation:

$$\frac{12.2-3.4}{12.2} \, 100 = 72\% \tag{40}$$
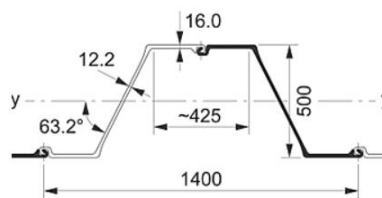
Figure 103: Sheet pile type AZ38-700 dimensions

According to POVM 2018 for the sheet pile wall design only the elastic capacity (Figure 104a) is considered. In fact, nowadays there is an extensive investigation revealing the benefits for accounting the plastic yielding of the sheet pile wall in the design, since it is believed there is a considerable gain in costs savings. Nevertheless, this falls outside the scope of the research and only the elastic capacity is considered. The Table 36 indicates the sheet pile wall properties before and after the corrosion. The total length of the sheet pile wall and the length of the embedment in the sand are given in Table 37. Specifically, the embedment of the unanchored steel sheet pile wall in the sand should be large enough in order to achieve a stable resistance at the bottom of the sheet pile. The selection of 4 meters follows the recommendation of the latest POVM example where the analysis of a cantilever sheet pile wall in dike stability is established.
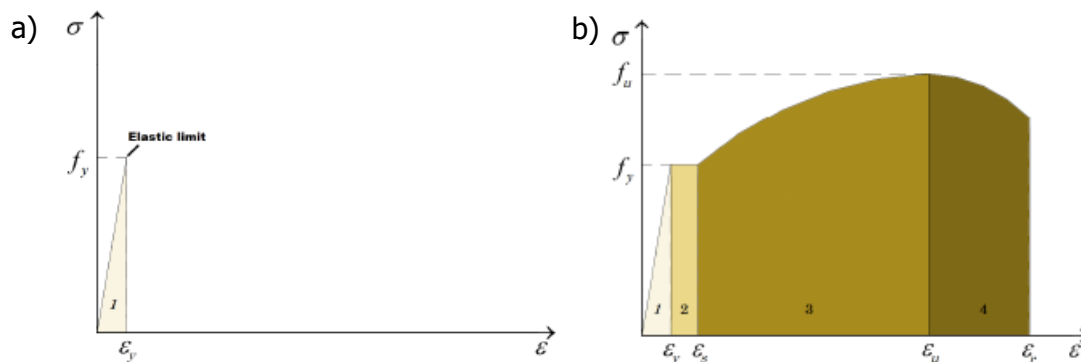
Figure 104: (a) illustration of an elastic sheet pile wall capacity, (b) illustration of the stress strain curve of steel when plastic yielding is accounted.

Table 36: Sheet pile wall properties.

Parameter	Initial	After corrosion	Units
A (sectional area)	230	166	cm^2
Wel (elastic section modulus)	3795	2732	cm^3
I (moment of inertia)	94840	68285	cm^4
EI (bending stiffness)	199164	143398	kN/m^2/m^1
EA (axial stiffness)	48300000	34860000	kN/m^1

Table 37: Additional information on the sheet pile wall

Property	Value	Units
Length of the sheet pile wall	18.275	m
Embedment of the sheet pile wall in the sand	4	m

According to POVM 2018 the structural strength of the unanchored sheet pile wall is described through the following requirement examinations.

The calculation values of the bending moment and the normal forces at critical loading (phase 6 – refer to Figure 102) are given from:

$$M_{s;d} = f_{open}\gamma_{corr;dw}\gamma_{b;str}M_{s;max;EEM} \tag{41}$$

$$N_{s;d} = f_{open}\gamma_{corr;dw}\gamma_{b;str}N_{s;max;EEM} \tag{42}$$

Where:

- $M_{s;d}$: *value of bending moment (kNm/m)*
- $N_{s;d}$: *value of Normal force (kN/m)*
- F_{open} : *factor opening percentage*
- $\gamma_{corr;dw}$: *correction factor of the bending moment (-)*
- $\gamma_{b;str}$: *schematization factor for structural elements (-) (refer to Table 35)*
- $M_{s;max;EEM}$: *maximum bending moment in the wall obtained from the PLAXIS (kNm/m)*
- $N_{s;max;EEM}$: *maximum normal force in the wall obtained from the PLAXIS (kN/m)*

According to the POVM 2018 the tension of the steel is examined through the following equation:

$$\sigma_{s;dw;d} = \frac{M_{s;d}}{W_{el;corr;open}} + \frac{N_{s;d}}{A_{corr}} \leq f_{y;dw;d} \tag{43}$$

Where:

$M_{s;d}$: calculated value of bending moment (kNm/m)
$W_{el;corr;open}$: elastic resistance after corrosion (m^3/m)
$N_{s;d}$: calculated value of normal force (kN/m)
A_{corr}: sectional area after corrosion (m^2/m)
$F_{y;dw;d}$: calculation value of the yield stress according to Eurocode 3 (kN/m^2)

The transverse force is checked in accordance with NEN EN1993-5 (NEN, 2008), with the use of the following equation.

$$V_{s;dw;d} \leq V_{r;dw;d} \tag{44}$$

With:

$$V_{r;dw;d} = \frac{A_{v;corr}\, f_{y;dw;d}}{\sqrt{3}} \tag{45}$$

$$V_{s;dw;d} = f_{open}\, \gamma_{b;str}\, V_{s;max;EEM} \tag{46}$$

Where:
$V_{s;dw;d}$: Calculation value of the transverse force in the sheet pile wall (kN/m)
$V_{r;dw;d}$: Calculation value of the shear force capacity of the sheet pile wall (kN/m)
$A_{v;corr}$: Shear surface after corrosion (m³)
$F_{y;dw;d}$: calculation value of the yield stress according to Eurocode 3 (kN/m²)
F_{open}: opening percentage of the sheet pile wall (-)
$\gamma_{b;str}$: (schematization factor) for structural forces (-)

As it concerns displacements according to POVM 2018 the following requirements should be examined (phase 5b – refer to Figure 102):

➢ *Less than 10cm horizontal displacement at the head of the sheet pile wall.*
➢ *Less than 10cm vertical displacement over a width of 3m in the crest of the dike. The cross section should be obtained in shallow depths.*
➢ *Less that 10cm lateral displacement difference between the outer and inner slope.*
➢ *Less than 2cm vertical displacement at the toe of the sheet pile wall.*

The additional reduction factor R_{inter} in the interface between the sheet pile wall and the soil is set equal to φ′ = 2/3 for all types of soils. This selection is based on CUR-166 (Visschedijk, 2018). For the SHANSEP NGI-ADP model the interface strength is given from the material properties as shown in Figure 105.

Interface material properties	
E_{oed}^{ref}	kN/m²
c_{ref}	kN/m²
φ (phi)	°
ψ (psi)	°
UD-Power	
UD-P ^{ref}	kN/m²

Figure 105: Interface material properties for the steel sheet pile wall.

The E_{oed}^{ref}, c_{ref} and φ_{inter} were set equal to 2/3 of the design value used for each soil layer. The ψ was set equal to 0 and the UD – power and the UD-P^{ref} remained equal to their default value which is 0 and 100 respectively.
Coming back to the subsidence of the soft soil layers for this study the vertical compaction option was used. This is considered a reasonable decision mainly for two reasons a) with the

usage of the SSC model special attention needs to be given in the increasing OCR as a result of the creep. The increasing OCR in turn influences the s_u based on the SHANSEP concept and eventually the estimated FoS may be affected, b) the option of vertical contraction is allowable for a cantilever sheet pile wall design since no horizontally placed structural elements are included which allow only for the subsidence through the SSC model.

The area surrounding the Hollandsche IJssel, and thus the dikes of the Hollandsche IJssel, are prone to subsidence. Based on historical measurements, it was found that the subsidence is approximately equal to 45 cm per 50 years or 0.9 cm/year (Van der Kraan, 2012). The subsidence map for the examined area along with the water defences is demonstrated in Figure 106. The overall subsidence from 2015 to 2050 will be approximately 31.5 cm and in 2100 approximately 76.5 cm.
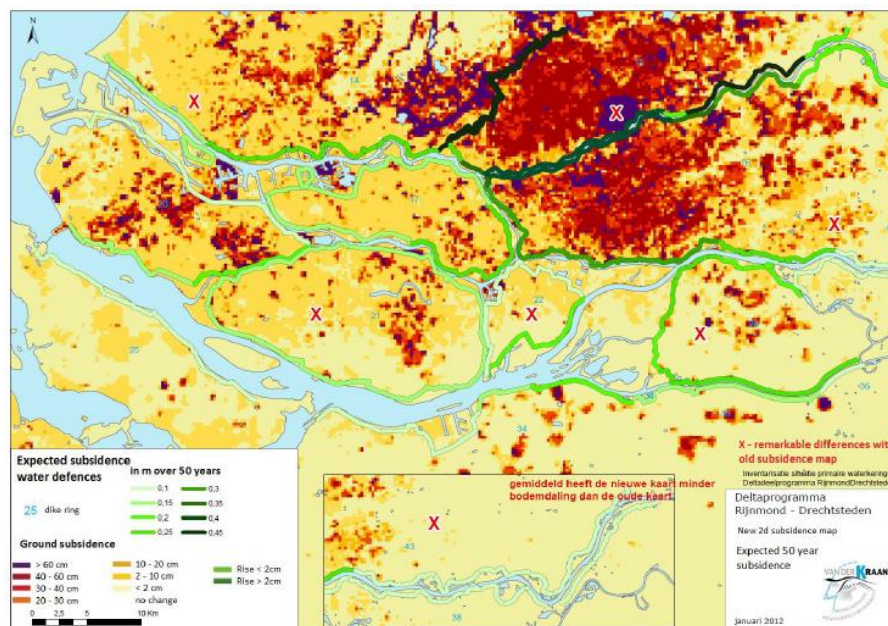
Figure 106: Subsidence map of the area surrounding the Hollandsche Ijssel (Van der Kraan, 2012).

This comes in accordance with an extensive research made from the Environmental Assessment agency (PBL, 2016) where it is suggested that in the Schieland and Krimpenerwaard areas the expected subsidence until 2056 is 33cm for a stratigraphy which is described from a clay layer which lies over a deep peat layer (Table 38). In addition, it is addressed that the peat layer is responsible for approximately the 50 to 70% of the total subsidence. Therefore, for this study the average value of 60% is used. By taking everything into consideration the vertical compaction for all the soil layers is given in the Table 39. The thickest part of each soil layer was subtracted with the expected subsidence and a vertical contraction was derived in percentage. The derived value is assigned in the ε_{yy} value in the phases explorer menu in the PLAXIS structures mode for each soil layer. It is noteworthy to mentioned that calculating accurately the subsidence of the soft soil layers is an extremely difficult task. Despite the fact that detailed investigation was performed for finding the most representative values of the subsidence expectancy of the examined soil layers the implemented value of the vertical contraction of the soft soil layers incorporates a certain amount of engineering judgement and it can be considered as a rough approximation.

Table 38: Subsidence in cm from years 2016 – 2056 (PBL, 2016)

Areas	Deep peat	Shallow peat	Clay on deep peat	Clay on shallow peat	Sand on deep peat	Sand on shallow peat	Subsidence in 40 years (average)	Subsidence in mm per year (average)
Amstel, Gooi and Vecht	36	47	32	20	39	21	36	9
Friesland	50	52	37	29	49	23	44	11
The Stichtse Rijnlanden	29	37	22	13	29	20	22	6
Hollands Noorderkwartier	26	42	29	16	28	24	27	7
Schieland and Krimpenerwaard	45	44	33	19	30	26	41	12
Rhineland	36	37	36	18	34	26	33	8
Riverland	28	44	22	18	22	07	22	6
The entire study	37	50	30	20	36	23	34	9

Table 39: Expected value of subsidence in a reference year of 2075.

Soil layer	Existing thickness (cm)	Thickness in year 2075 (cm)	ε_{yy} (vertical contraction) (%)
Existing clay dike material	613	608.5	1
Organic clay 1	500	488.5	2.3
Peat	460	433	6
Organic clay 2	300	288.5	3

Lastly, it should be noted that in contrast with the Green dike examination for the Blue dike analysis the strength parameters are derived from service conditions strain levels which are 2% axial strain level for clays under triaxial compression and 5% shear strain for peats under direct simple shearing. The characteristic values of strength along with the design values and the K_0 value with the OCR are given in the Table 40 and 41 respectively.

Table 40: Strength parameter used in the Blue dike analysis.

Soil layer	φ_{kar} (degrees)	φ_{design} (degrees)	c_{kar} (kPa)	c_{design} (kPa)	S_{kar}	S_{design}	m
Clay dike and clay anthropogenic	30.85	27.55	3.2	2.86	0.34	0.30	0.80
Org clay 1	32.14	28.70	2.1	1.88	0.35	0.31	0.77
Peat	26.65	23.80	2.8	2.50	0.25	0.23	0.74
Org clay 2	33.92	30.28	2.8	2.50	0.35	0.31	0.87

Table 41: K_0^{OC} and OCR used in the Blue dike analysis.

Soil layer	K_0^{OC} crest	K_0^{OC} toe	OCR crest	OCR toe
Clay dike and clay anthropogenic	0.83	0.88	2	2.2
Org clay 1	0.71	0.78	1.65	1.9
Peat	0.47	0.49	1.6	1.8
Org clay 2	0.48	0.5	1.25	1.35

This section concludes with the updated geometry used for the Blue dike analysis as demonstrated in Figure 107. For more information regarding the updated slopes for the KIJK dike design requirement refer to subchapter 2.6. Concerning the mesh quality, the water levels (Figure 108) and the mechanical boundaries similar format maintained with the Green dike analysis (refer to subchapter 4.1.1). In the case of the Blue dike analysis however, a further refinement was applied in the sand layer in order to obtain reliable displacements in the toe of the pile as shown in Figure 107.
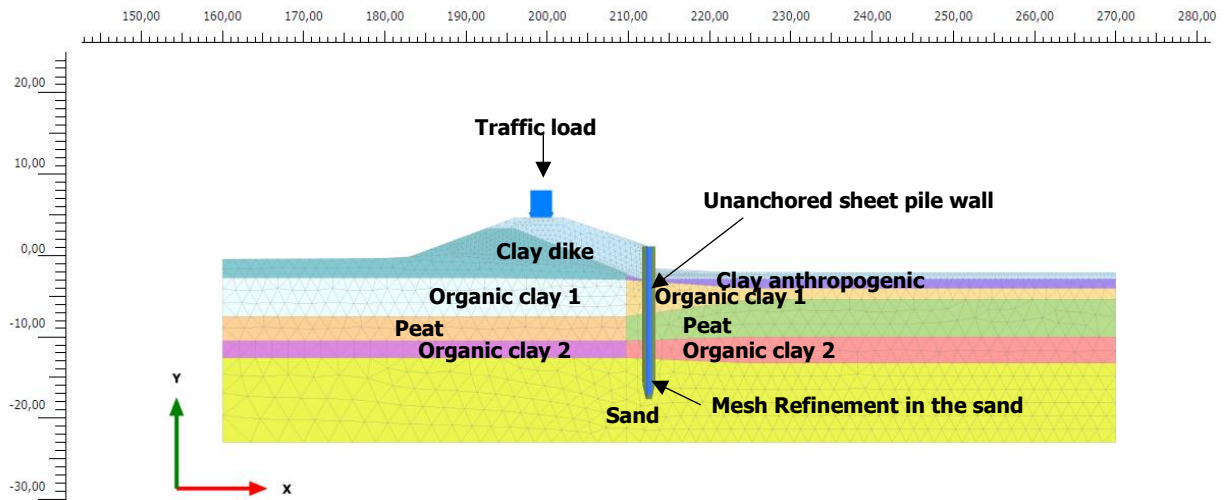
Figure 107: Updated geometry for the Blue dike analysis.
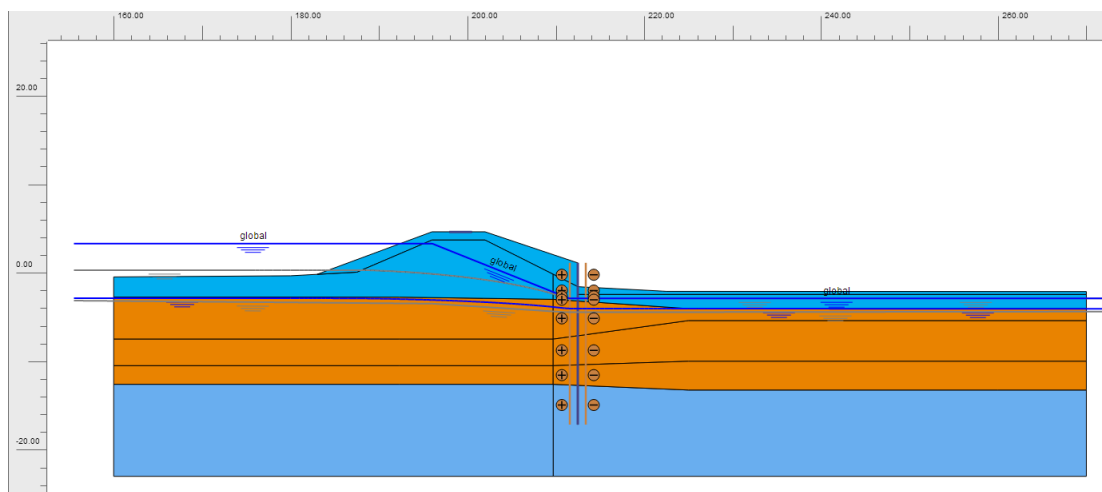
Figure 108: Water levels for the Blue dike analysis.

5.2 Results of the analysis

The results subchapter is divided in four main sections. In the first section the comparison of the available strength offered from the CPT and the considered models is shown. The second section deals with the response of the models in terms of the estimated FoS and developed failure mechanisms. The third section demonstrates the generated displacements following the design criteria given from POVM along with the structural forces. The last section summarizes the overall results.

5.2.1 Predicted s_u from the considered constitutive models

As explained in Chapter 4 the first and essential step prior to the initiation of the required steps for assessing the global safety of the dike is the validation of the undrained shear strength with the use of the s_u profile with depth obtained from a CPTu or with the comparison of the available undrained shear strength given from your models at the middle point of each soil layer with a cautious characteristic value obtained from the laboratory tests (refer to subchapter 4.2.2 for further information).

The Figure 109 and Figure 110 illustrate the predicted undrained shear strength profile with depth from the considered constitutive models in comparison with the undrained shear strength profile with depth given from the cone penetration test. It should be noted that for clays the $s_{u(OC)peak}$ is used for the derivation of the N_{kt} parameter since, as illustrated in Chapter 3 the $S_{(NC)}$ at 2% strain level is typically found at the maximum shear strength that the soil can mobilize. Thus, in order to have a valid comparison both the $s_{u(NC)}$ and $s_{u(OC)}$ should be obtained from the peak strength. Similarly, with the Green dike analysis the SHANSEP NGI-ADP matches properly the available s_u whereas the HS and the SS underestimate the s_u below the dike body. Additionally, it is likewise found that at the hinterland area of the dike the models predicted comparable values. This similarity is attributed to the influence of the distribution of the principal effective stresses below and next to the dike body. The reader may refer to Figure 90 and subchapter 4.2.2 for additional information.
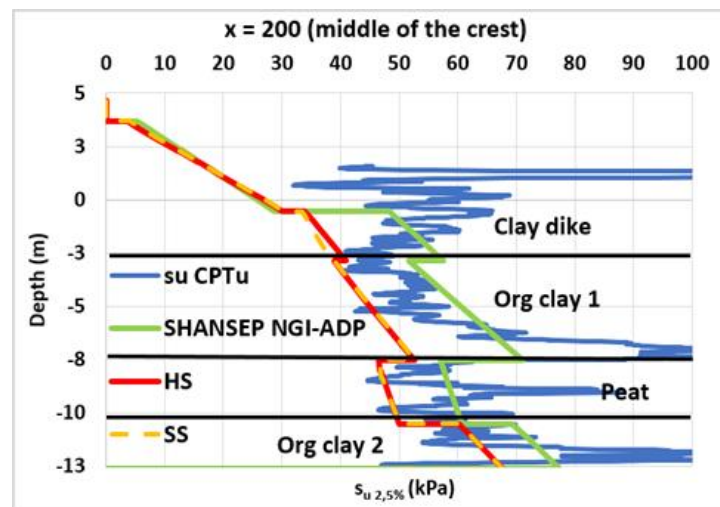
Figure 109: Comparison of undrained shear strength profiles at the middle of the crest.
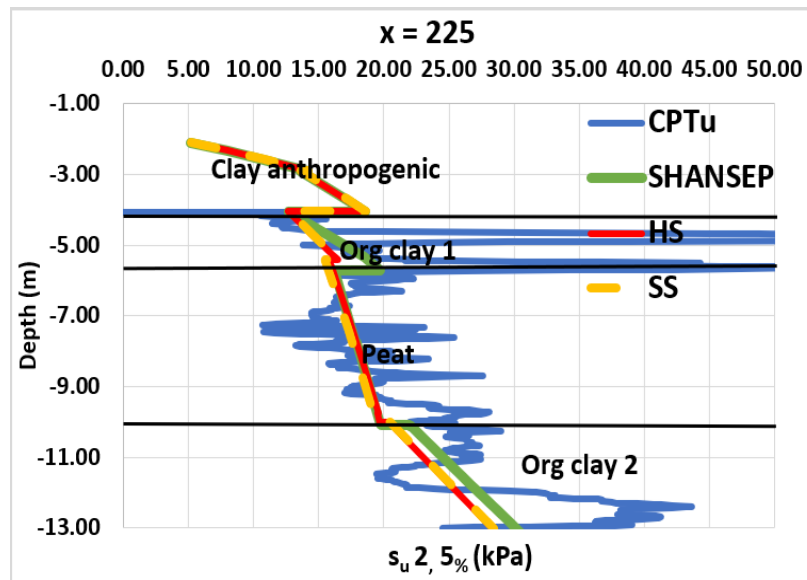
Figure 110: Comparison of the undrained shear strength profiles at the hinterland.
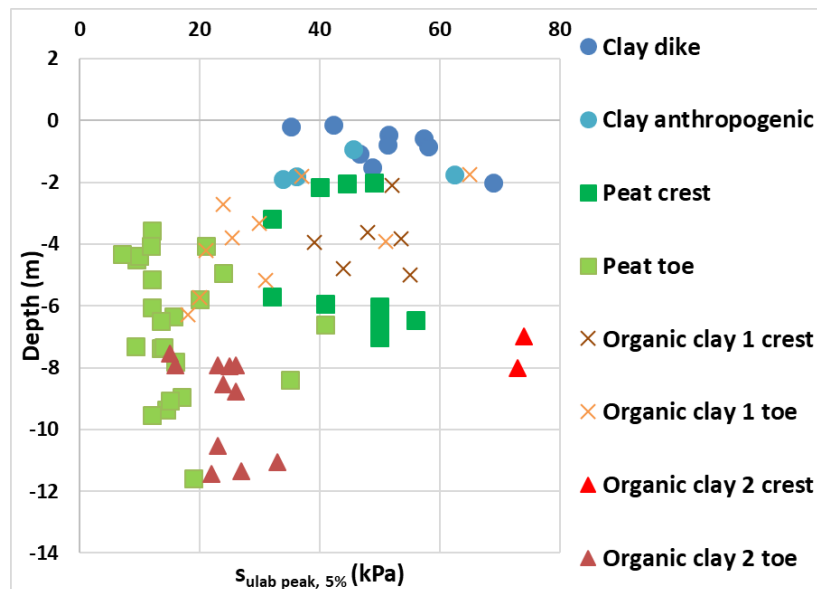
Figure 111: Available undrained shear strength given from the laboratory at service conditions strain levels.

5.2.2 Estimated FoS and developed failure mechanism

The predicted FoS given from the considered constitutive models is shown in Figure 112. The predicted FoS from the SHANSEP NGI-ADP is shown twice. The SHANSEP NGI-ADP (HS) denotes that the calculation model used in the drained steps was the HS while the SHANSEP NGI-ADP (SS) denotes that the model used was the SS. This distinction showed that both models transferred equal stress history of the soil and the resulting FoS given from the SHANSEP model results in an identical value.

In the case of the Blue dike analysis the estimated FoS given from the SHANSEP NGI-ADP model is marginally higher (1.35) than the HS and SS which share similar values at 1.30 and 1.29 respectively.

The comparable values in terms of the predicted FoS among the considered models is mainly explained due the similar developed failure mechanism between the models (Figure 113 and Figure 114). Moreover, other factors that may cause the similarity in the obtained FoS is the influence of the cantilever sheet pile wall in the design as well and the incorporation of the cohesion of the materials at shallow depths for the HS and SS models which is particularly essential for the shear strength of the materials at shallow depths. The influence of the sheet pile wall in the design will be more obvious in subchapter 5.3. Moreover, in subchapter 5.3 the resulting developed failure mechanism is also shown by means of the deviatoric strain (γ_s).
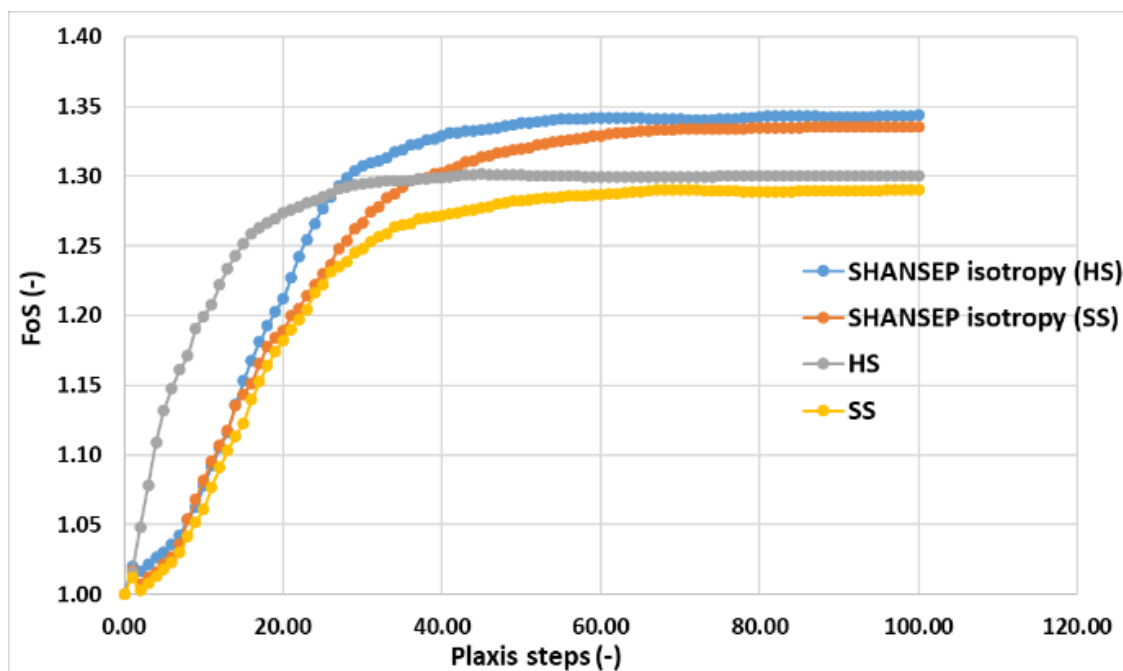
Figure 112: Estimated FoS from the constitutive models.
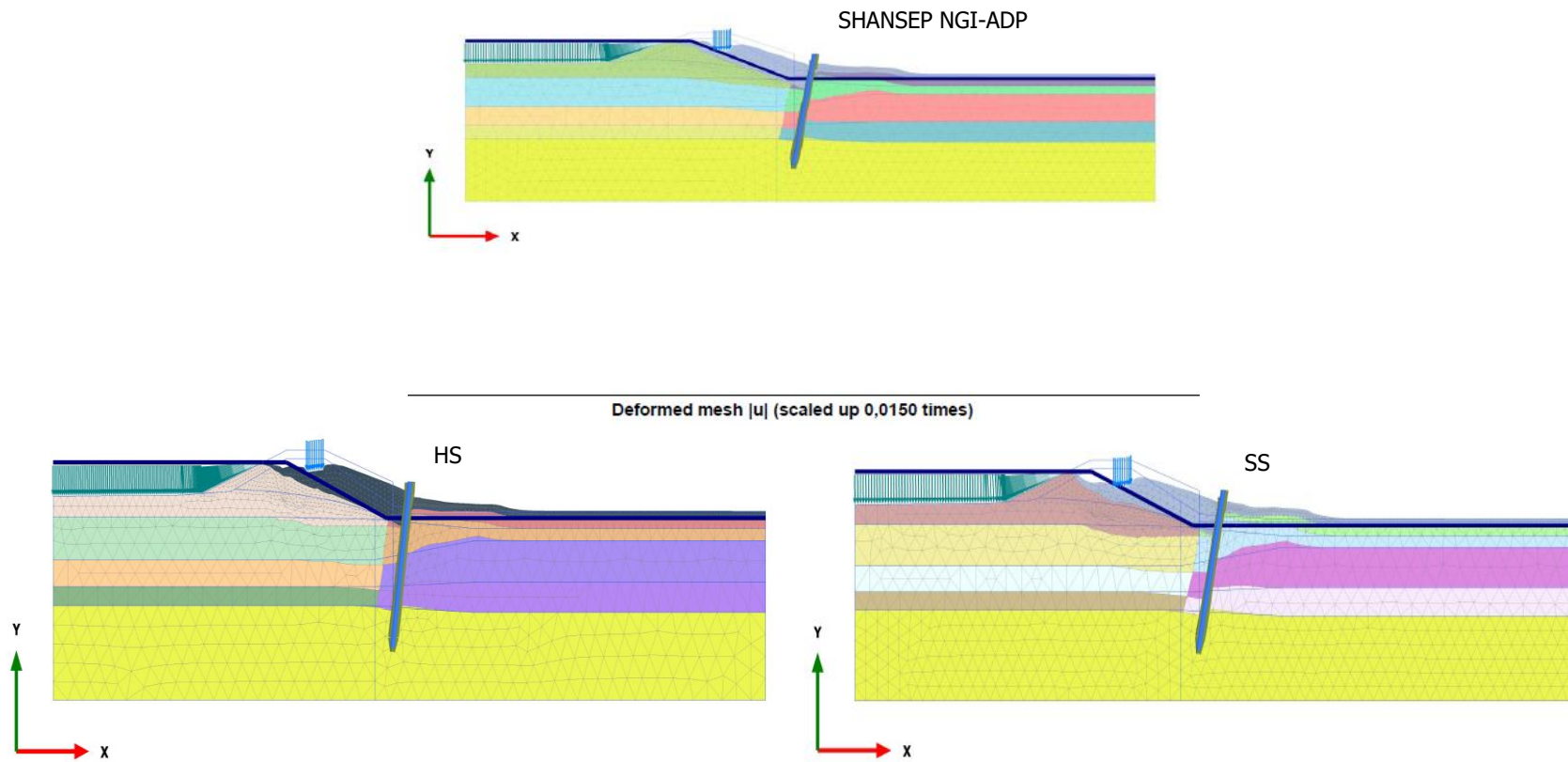
Figure 113: Deformed mesh obtained from the safety analysis. The scale is given in the middle area of the Figure (0.0150 times).
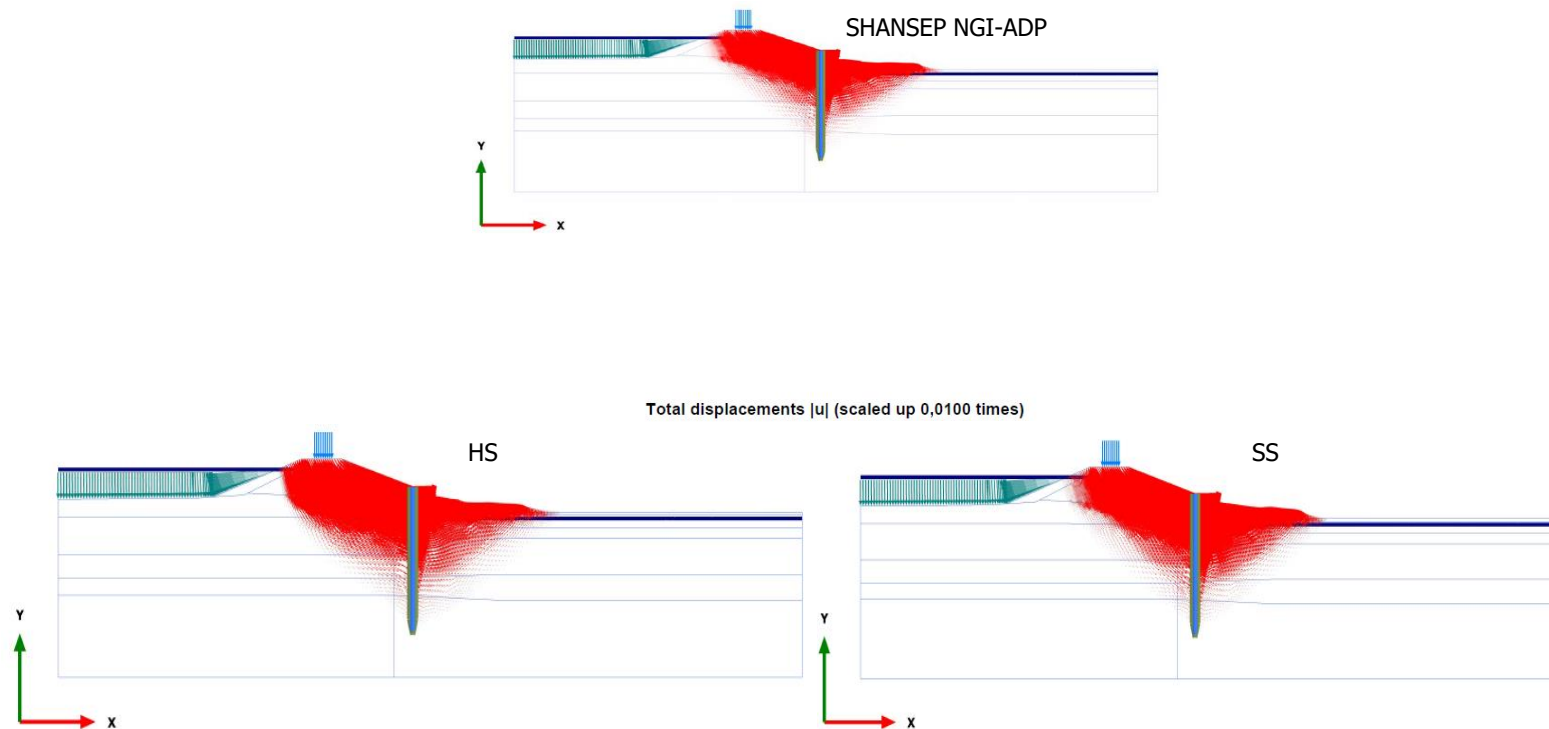
Figure 114: Developed failure mechanisms with the arrow option for illustrating the displacements.

As explained in previous chapters the strength parameters of the clays are obtained from anisotropically consolidated undrained triaxial tests whereas for peats from direct simple shearing. Based on this, two main conclusions were drawn. The first conclusion is that at the service conditions strain levels the $S_{(NC)2\%}$ for clays generally describes the peak strength, or it deviates minimally from the peak for all the examined clayey soil layers. The second conclusion is that there is a common agreement from previous studies (refer to Table 1) that at the peak strength of a triaxial compression test the stress path dependency of the s_u is expected to be significant and thus, along with the derived $S_{(NC)2\%}$ obtained from the considered clays the advanced feature of the NGI-ADP to account for the stress path dependency of the s_u through the s_u^{DSS} / s_u^A and s_u^P / s_u^A ratios needs to be utilized.

The Figure 115 a and b illustrates the response of the SHANSEP NGI-ADP when the reduction of the s_u ratios is deducted. Speaking in terms of percentages it can be seen that the overall safety when the average values based on the literature review are used (s_u^{DSS} / s_u^A = 0.7, s_u^P/s_u^A = 0.5) the reduction is 12.5% whereas with the lower bound (s_u^{DSS} / s_u^A = 0.5, s_u^P/s_u^A = 0.3) values the reduction is 17%.

It is particularly interesting to examine the response in terms of the FoS when no stress path dependency of the s_u is considered for the peat. This examination is considered reasonable for two reasons. The first reason is that the DSS applied in Peats is considered to be the mode of shearing which generally averages the available strength given from TXC and TXE tests. The second reason lies on the fact that it is rather unknown if the 5% strain of peats would yield in a different value under different stress paths since the 5% is lying considerably below the maximum shear strength that the soil can mobilize. The Figure 115b illustrates that when the stress path dependency of peats at 5% strain level is not considered there are notable gains in terms of the FoS. In this case the reduction is 8% and 12.5% with the use of the average and lower bound s_u ratios respectively. Lastly, it was found that with decreasing s_u ratios the response in terms of the developed failure mechanism remained identical as shown in Figure 116 where the lower bound values of the s_u ratios were used.
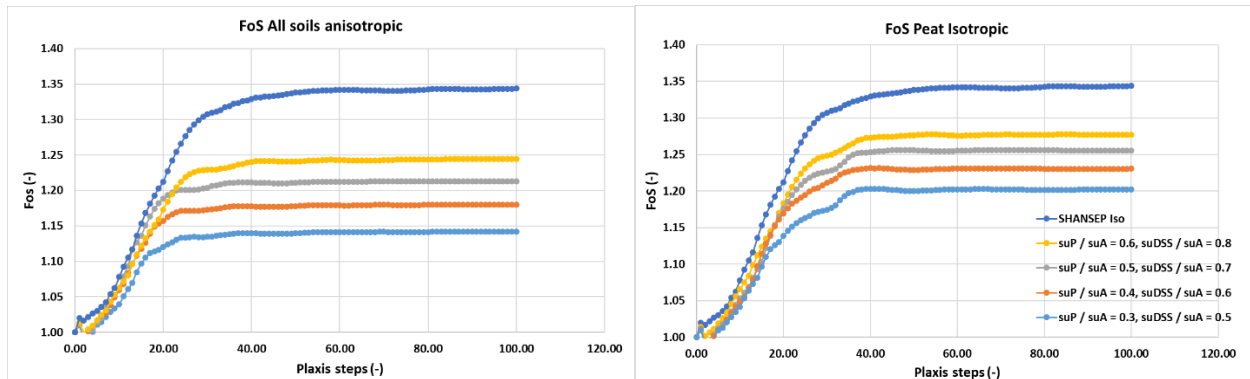
Figure 115: Sensitivity analysis in the estimated FoS.

SHANSEP NGI-ADP
s_u^{DSS} / s_u^A = 0.5, s_u^P/s_u^A = 0.3
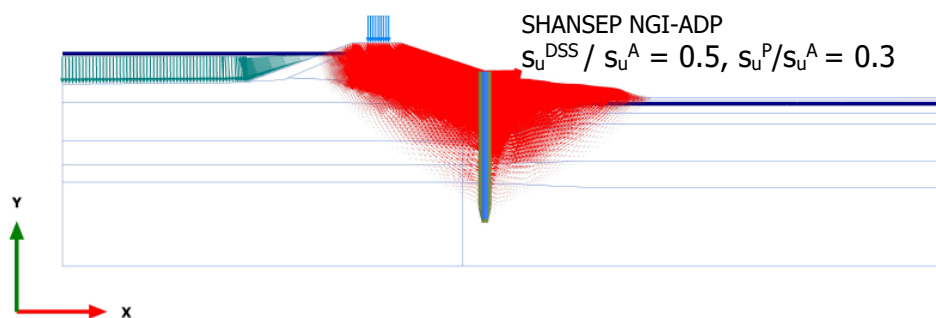
Total displacements |u| (scaled up 0,0150 times)

Figure 116: Developed failure mechanism with the implementation of the lower bound value s_u ratios.

5.2.3 Generated displacements

In this subsection the results in terms of displacements with reference the various requirements for the pre-failure examination of the dike are presented. Distinction has been made between the predicted displacements of the SHANSEP NGI-ADP model when the preceding model in the drained step was either the HS or the SS. These requirements were taken from phase 5b (refer to Figure 102).

5.2.3.1 Generated u_x on the sheet pile wall, stretching criterion, u_y at the upper dike body and u_y in the toe of the sheet pile wall.

The Figure 117, 118, 119 and 120 demonstrate the generated displacements of the various requirements given from the POVM. The investigation shows that the considered constitutive models displayed comparable values among all the requirements. In the case of the u_y at the teen of the sheet pile wall only the results of the HS models are given since the sand is explicitly described with the HS model. It is particularly interesting to notice that in the case of the Blue dike analysis the displacements predicted from the SS model yielded in a slightly higher value than the displacements given from the HS model. As explained in the subchapter 2.6 the KIJK dike requires an increase in the crest height and the slopes of the dike. In drained conditions, the soil body below the dike crest faces a primary compression load and a decrease in the OCR due the increase in the vertical effective stress. The decrease in the OCR along with the fact that for the drained material there is no OCR incorporated led to the activation of the cap yield surface and thus, the generation of plastic points as illustrated in Figure 121. Furthermore, it is obvious that the use of either the HS or the SS influence the quantitative response of the SHANSEP NGI-ADP model. Lastly, the values of the various requirements are synopsized in Table 42.

HS

SHANSEP NGI-ADP (HS)

Total displacements u_x (scaled up 100 times)

Maximum value = 0,05815 m (Element 11 at Node 8021)

Total displacements u_x (scaled up 100 times)

Maximum value = 0,06325 m (Element 11 at Node 8021)

SS

SHANSEP NGI-ADP (SS)

Total displacements u_x (scaled up 100 times)

Maximum value = 0,06433 m (Element 11 at Node 8021)

Total displacements u_x (scaled up 100 times)

Maximum value = 0,06589 m (Element 11 at Node 8021)

Figure 117: Generated horizontal displacements on the sheet pile wall.

HS
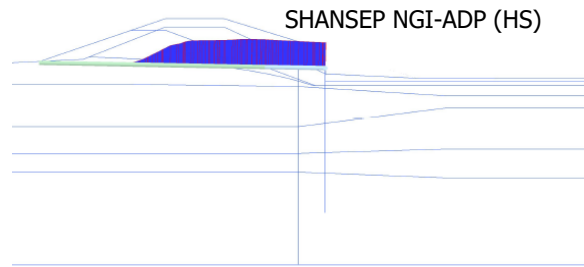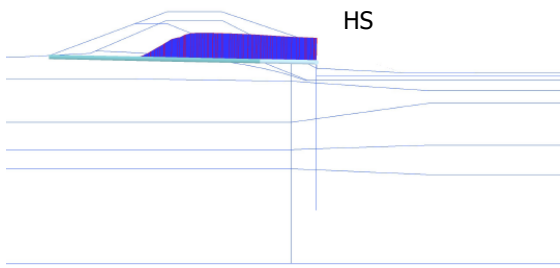
Total displacements u$_x$ (scaled up 50,0 times)

Maximum value = 0,05953 m

Minimum value = -4,283*10^{-3} m

SHANSEP NGI-ADP (HS)

Total displacements u$_x$ (scaled up 50,0 times)

Maximum value = 0,06176 m

Minimum value = -3,104*10^{-3} m

SS
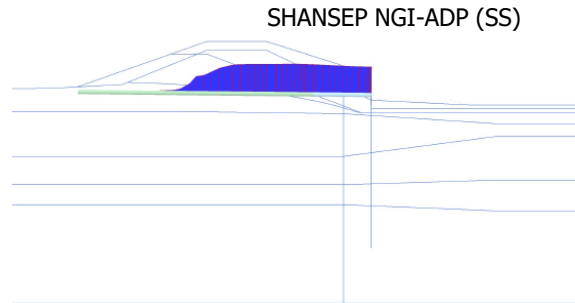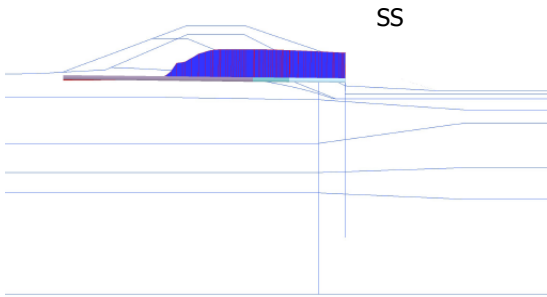
Total displacements u$_x$ (scaled up 50,0 times)

Maximum value = 0,06199 m

Minimum value = -6,314*10^{-3} m

SHANSEP NGI-ADP (SS)

Total displacements u$_x$ (scaled up 50,0 times)

Maximum value = 0,06374 m

Minimum value = -1,631*10^{-3} m

Figure 118: Horizontal displacement difference under the inner and outer slope of the dike.
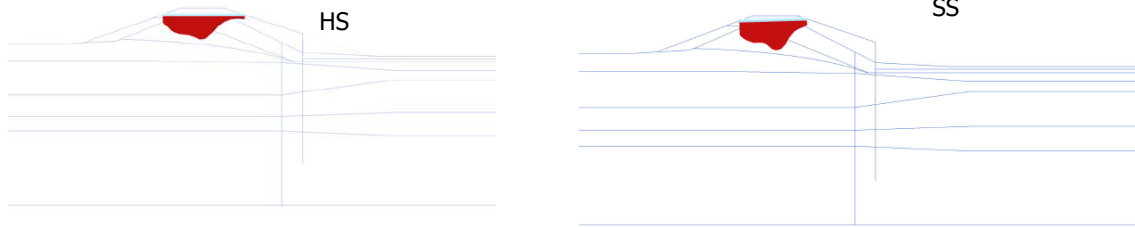
Total displacements u$_y$ (scaled up 100 times)

Maximum value = -5,409*10^{-3} m

Minimum value = -0,03449 m

Total displacements u$_y$ (scaled up 100 times)

Maximum value = -8,511*10^{-3} m

Minimum value = -0,04014 m

Figure 119: Vertical displacements over a distance of 3m in the upper crest body.
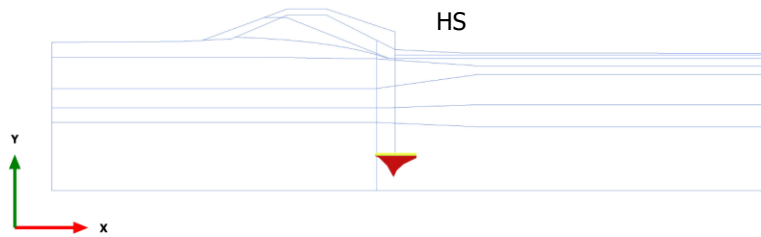
Total displacements u$_y$ (scaled up 2,00*10^3 times)

Maximum value = -0,1282*10^{-3} m

Minimum value = -1,726*10^{-3} m

Figure 120: Vertical displacement at the toe of the sheet pile wall.
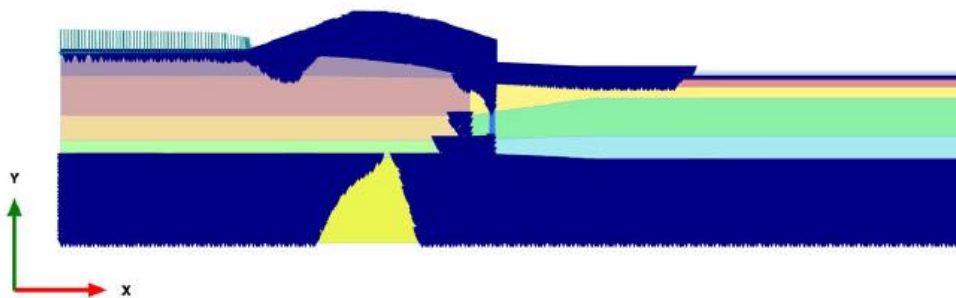
Figure 121: Generated cap points for the SS model obtained from phase 4 (refer to Figure 102).

5.2.4 Structural forces

The Figure 122 and 123 demonstrate the forces acting on the sheet pile wall. These results were obtained from phase 6 (refer to Figure 102). The considered constitutive models predicted similar qualitative and quantitively response of the structural forces acting on the sheet pile wall. It is also interesting to note the decrease of the moments in the peat interface due the lower strength that describes the material at a 5% strain level. In addition, as shown in Figure 124 at the peat location (right side of the sheet pile wall) the rotation of the principal stress does not signify a passive mode like the overlaying clay materials which in turn influences the moment distribution.
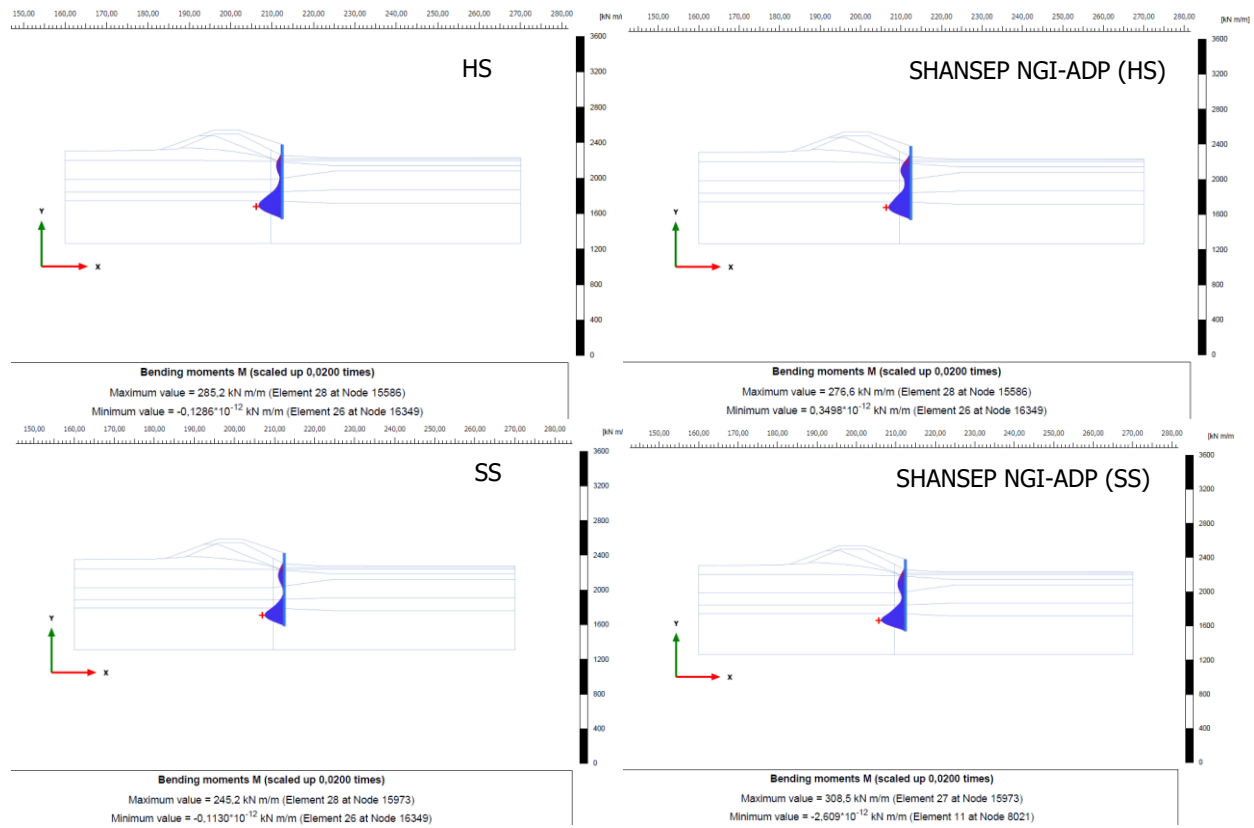
Figure 122: Moment distribution given from the considered constitutive models.

HS

Axial forces N (scaled up 0,0500 times)
Maximum value = 5,051 kN/m (Element 26 at Node 16349)
Minimum value = -193,2 kN/m (Element 25 at Node 15433)

SS

Axial forces N (scaled up 0,0500 times)
Maximum value = 5,519 kN/m (Element 26 at Node 16349)
Minimum value = -191,2 kN/m (Element 28 at Node 15584)

SHANSEP NGI-ADP (HS)

Axial forces N (scaled up 0,0500 times)
Maximum value = 2,700 kN/m (Element 26 at Node 16349)
Minimum value = -139,7 kN/m (Element 25 at Node 15433)

SHANSEP NGI-ADP (SS)

Axial forces N (scaled up 0,0500 times)
Maximum value = 1,105 kN/m (Element 26 at Node 16349)
Minimum value = -110,8 kN/m (Element 25 at Node 15433)

Figure 123: Normal Forces given from the considered constitutive models.

Clay dike

Org clay 1

Peat
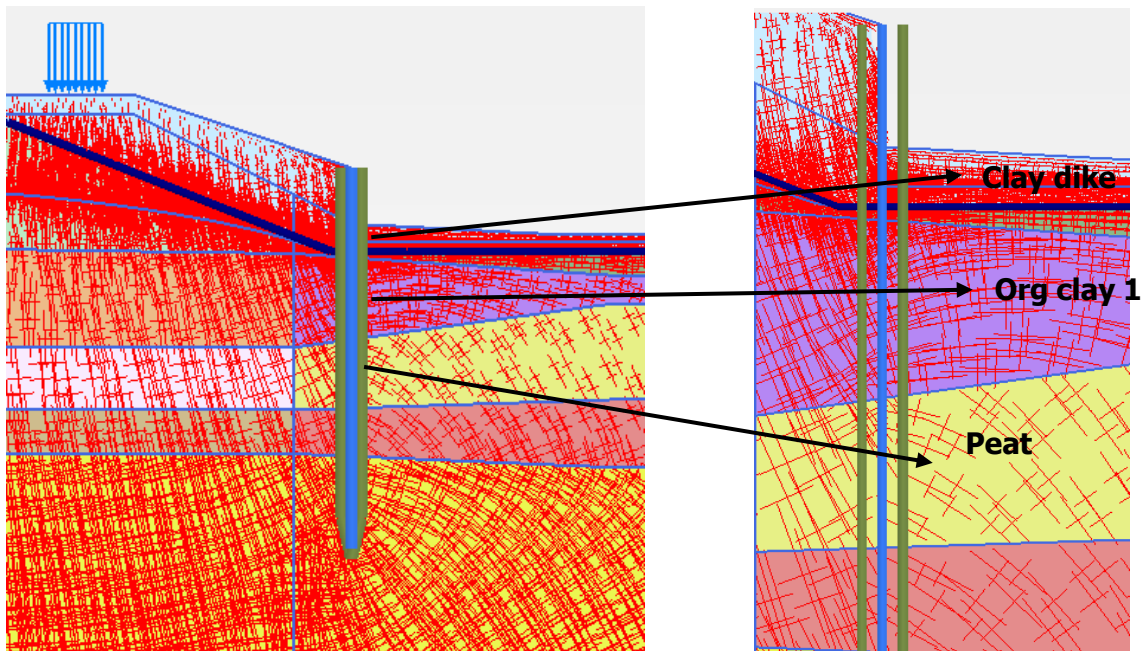
Figure 124: Rotation of the principal stresses adjacent the sheet pile wall.

5.2.5 Overall Results

The Table 42 summarizes all the design requirements necessary for the Blue dike examination. Table 43 and Table 44 summarizes the development of the structural forces per calculation phase as illustrated in the Figure 102. Distinction has been made between the development of structural forces when the HS or the SS was used in the drained steps. The analysis shows that in the phase where the long-term subsidence of the soft soil layers in the reference year of design is accounted the moments distribution drastically increases which is in agreement with the latest findings of POVM 2018.

Table 42: Overall Results for all the required examination for the Blue dike analysis.

Examination		Phase	Model	Value	Units
Geotechnical	Global safety	7	HS	1.3	[-]
			SS	1.29	[-]
			SHANSEP NGI – ADP (HS,SS)	1.35	[-]
Displacements	ux head sheet pile	5b	HS	0.058	[m]
			SS	0.063	[m]
			SHANSEP NGI ADP HS SHANSEP NGI ADP SS	0.063 0.066	[m]
	ux outer inner slope		HS	0.064	[m]
			SS	0.068	[m]
			SHANSEP NGI ADP HS SHANSEP NGI ADP SS	0.065 0.065	[m]
	uy		HS	0.034	[m]
			SS	0.040	[m]
	uy toe sheet pile		HS (sand layer)	0.002	[m]
Structural Forces	Bending Moments	6	HS	285	[KNm/m]
			SS	245	
			SHANSEP NGI ADP HS SHANSEP NGI ADP SS	277 308	
	Normal Force		HS	193	[kN/m]
			SS	191	
			SHANSEP NGI ADP HS SHANSEP NGI ADP SS	139 110	
	Shear Force		HS	127	[kN/m]
			SS	132	
			SHANSEP NGI ADP HS SHANSEP NGI ADP SS	134 162	

Table 43: Development of the structural forces with the use of the HS in the drained steps.

HS (development of structural forces)			
Step	Moments [KNm/m]	Normal Force [kN/m]	Shear Force [kN/m]
Installation	2.5		
Long term subsidence	165		
High water level	209		
Traffic Load – Undrained A	220		
Traffic Load - SHANSEP	224		
Structural forces HS – Undrained A	285	193	127
Structural forces – SHANSEP	277	140	134

Table 44: Development of the structural forces with the use of the SS in the drained steps.

SS (development of structural forces)			
Step	Moments [KNm/m]	Normal Force [kN/m]	Shear Force [kN/m]
Installation	3		
Long term subsidence	177		
High water level	226		
Traffic Load – Undrained A	231		
Traffic Load - SHANSEP	232		
Structural forces SS – Undrained A	265	191	132.5
Structural forces – SHANSEP	308	111	162

5.3 Influence of the strain level dependency of the strength parameters on the Blue dike analysis

In this subchapter, the influence of the strain level dependency of the strength parameters for the Blue dike analysis is investigated and discussed. Thus, the strength parameters determined from the critical state strain levels are additionally used in the analysis. In this way, the comparison in terms of the predicted FoS, the developed failure mechanism the generated deviatoric strain the displacements and the moments acting on the sheet pile wall can be established. It should be noted that the comparison is realised with the use of the HS and the SHANSEP NGI-ADP model. This is considered a reasonable decision since, both the HS and the SS displayed almost identical response in terms of the estimated FoS and the developed failure mechanism as well and qualitatively and quantitively comparable values in terms of the displacements. Lastly, it should be noted that the purpose of this subchapter is no longer the comparison of the responses of the constitutive models but rather the examination of the response of the constitutive models upon variation of their strength parameters based on the considered strain levels. Nevertheless, in some cases the illustration of the results as well and the relevant discussion serves as an additional comparison between the constitutive models. The reader may refer for more information to subchapter 5.2.

Starting point is the demonstration of the s_u distribution below the dike body. With the use of the strength parameters obtained from the critical state strain levels the peat exhibits the higher values of the s_u among the soil stratigraphy. Contrarily, the use of the service conditions strain levels drastically reduces the s_u that the peat exhibits (refer to subchapter 3.2.1 and 3.2.3 for more information). Moreover, it is obvious that in the crest area of the dike where the effective stress is considerably higher than the toe and the hinterland areas of the dike the s_u exhibits the highest values. Therefore, for every soil layer it's s_u peak is given exactly below the crest body. The s_u distribution shown in the Figures 125 and 126 is obtained from Phase 6 (refer to Figure 102). The τ_{max} of the sand layer is excluded from the design in order to emphasize in the available s_u that the soft soil layers exhibit.

The examination of the available strength before the safety analysis is highly recommended since you acquire an important information regarding the following:

a) *The resulting s_u after the incorporation of the semi – probabilistic factors on the strength.*
b) *The resulting s_u after the modification of the geometry for the Blue dike analysis based on the available guidelines and the project recommendations.*
c) *The resulting s_u prior the safety analysis after following all the required phases given from POVM.*
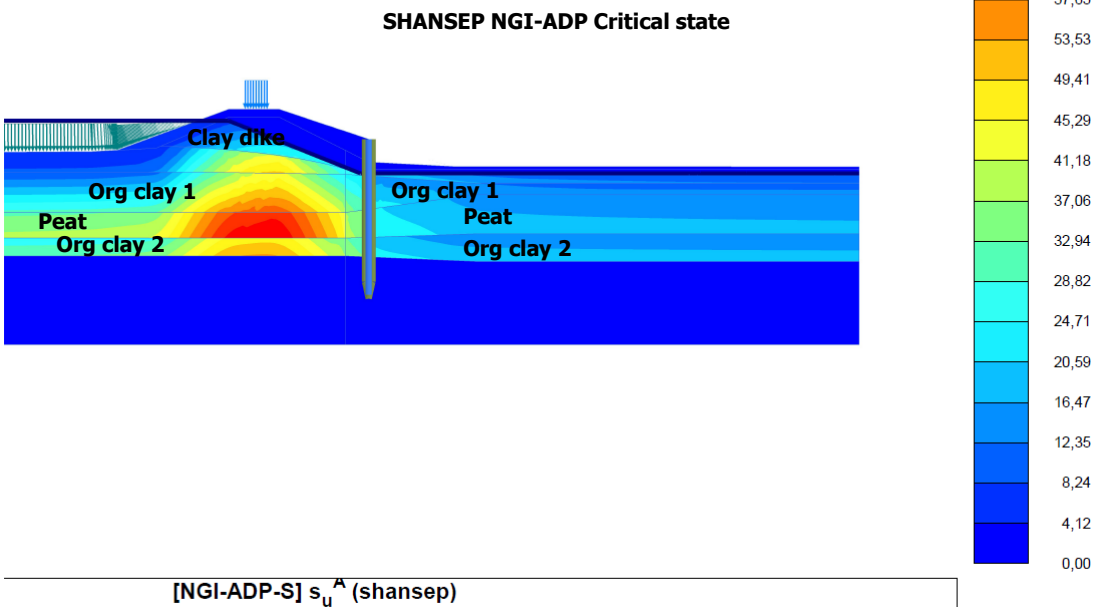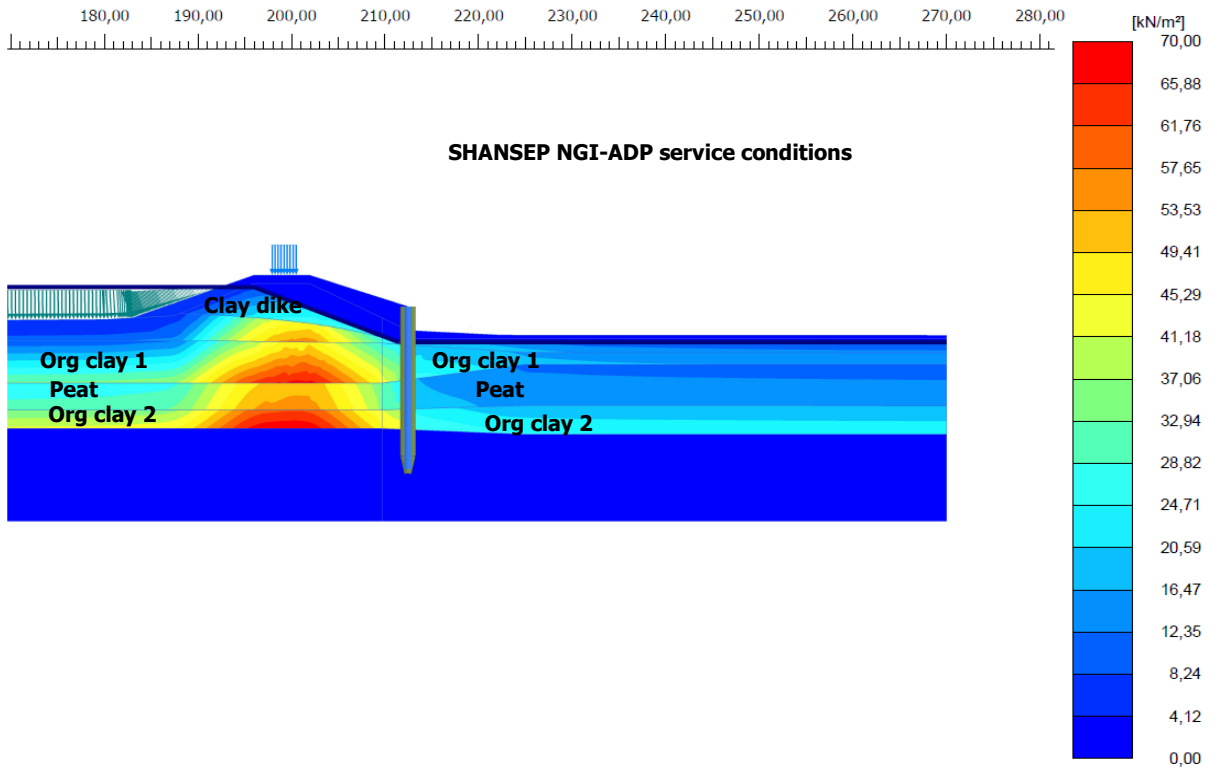
Figure 125: Predicted s_u prior the safety analysis from the SHANSEP NGI-ADP model.

Figure 126: Predicted s_u prion the safety analysis from the SHANSEP NGI-ADP model.
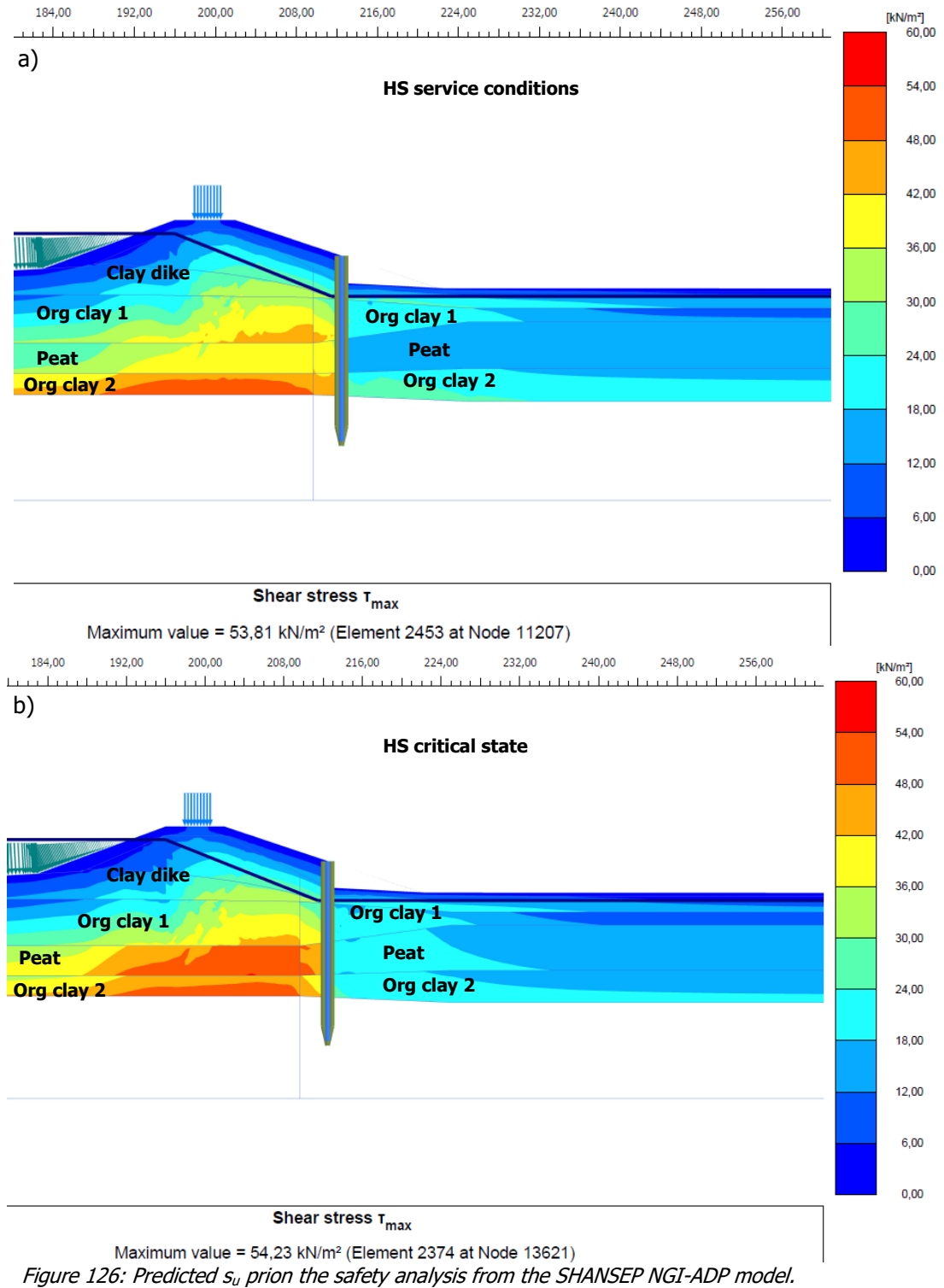
The Figure 127 and Figure 128 display the difference in the deviatoric strain development into the dike at critical loading conditions with the use of the service condition and the critical state strain levels obtained from phase 5b (refer to Figure 102). The investigation suggests that the deviation of the strength parameters based on the considered strain levels has no drastic

influence on the predicted amount of the deviatoric strain. Although the use of the serviceability strength parameters leads to lower values of the maximum γ_s the difference is neglectable. Moreover, it is similarly obvious like the Green dike analysis that the shear strain development is influenced by the stiffness characteristics of the materials. Thus, the peat layer which exhibits the lowest stiffness characteristics, experiences large development of deviatoric strain. However, for the case of the Blue dike, irrespective the applied strength parameters, the resulting developed failure mechanism is in agreement with the illustrated deviatoric strain development.
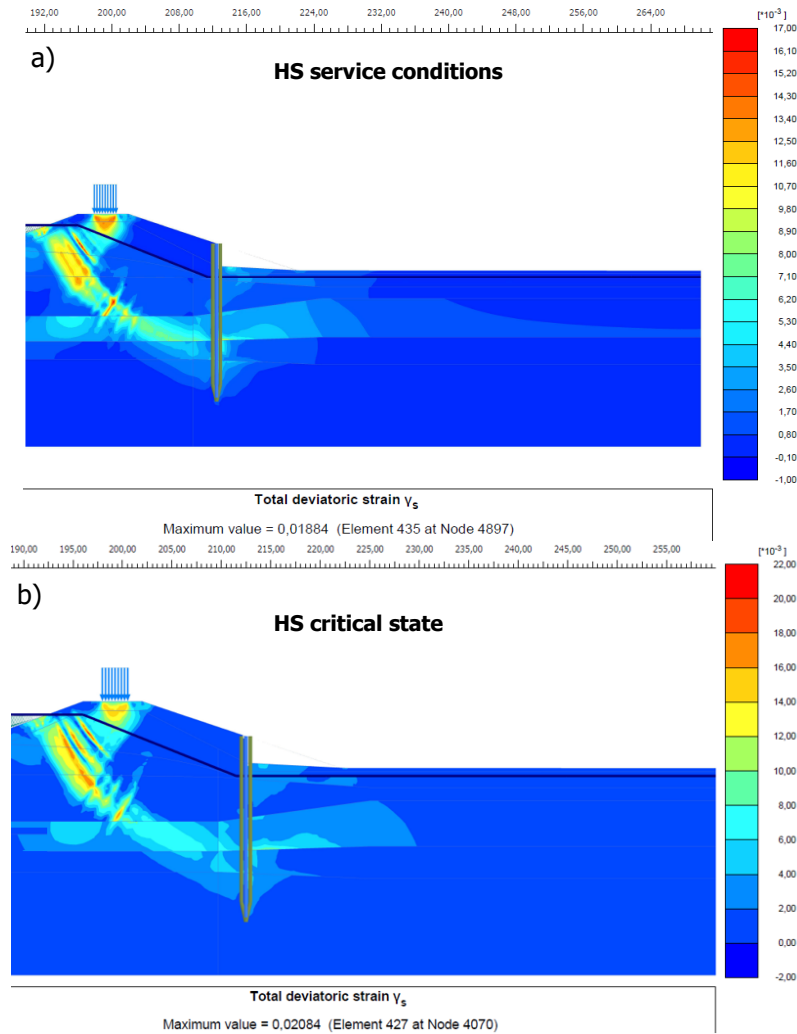
Figure 127: Deviatoric strain development of the HS with, a) serviceability strength parameters and b) critical state strength parameters.
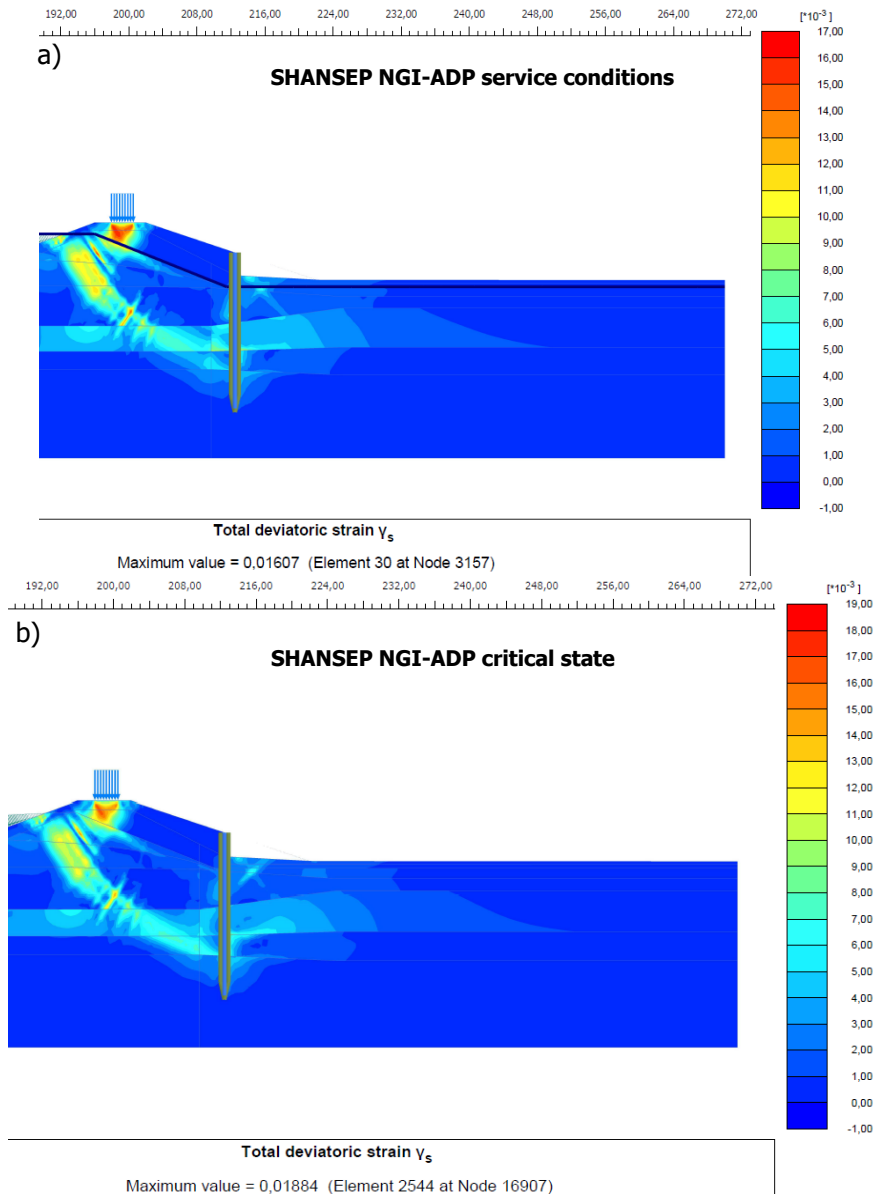
Figure 128: Deviatoric strain development with the use of the SHANSEP NGI-ADP model.

The Figure 129 displays the generated u_x of the sheet pile wall while the Figure 130 illustrates the development of the moments distribution upon the variation of the strength parameters based on the considered strain levels. Concerning the u_x it is illustrated that the use of the critical state strain levels results in larger values of u_x in the sheet pile wall. Regarding the moments distribution the response is found to be both qualitatively and quantitively different. With the use of the critical state strength parameters the moments in the peat layer display notably higher values than the case of the serviceability strength parameters. This is explained by the higher value of strength that the soil posses with use of the critical state strength parameters.

SHANSEP NGI-ADP critical state   **SHANSEP NGI-ADP service conditions**

Bending moments M (scaled up 0,0200 times)   Bending moments M (scaled up 0,0200 times)
Maximum value = 367,9 kN m/m (Element 28 at Node 15586)   Maximum value = 276,6 kN m/m (Element 28 at Node 15586)

HS critical state   **HS service conditions**

Bending moments M (scaled up 0,0200 times)   Bending moments M (scaled up 0,0200 times)
Maximum value = 324,6 kN m/m (Element 28 at Node 15585)   Maximum value = 285,2 kN m/m (Element 28 at Node 15586)

Figure 129: Comparison of moments distribution acting on the sheet pile wall.

SHANSEP NGI-ADP critical state   **SHANSEP NGI-ADP service conditions**

Total displacements u_x (scaled up 100 times)   Total displacements u_x (scaled up 100 times)
Maximum value = 0,07058 m (Element 11 at Node 8021)   Maximum value = 0,06325 m (Element 11 at Node 8021)

HS critical state   **HS service conditions**

Total displacements u_x (scaled up 100 times)   Total displacements u_x (scaled up 100 times)
Maximum value = 0,06390 m (Element 11 at Node 8021)   Maximum value = 0,05815 m (Element 11 at Node 8021)

Figure 130: Comparison of the generated u_x on the sheet pile wall.

Last part of this investigation is the comparison of the developed failure mechanism and the estimated FoS of the constitutive models upon variation of the strength parameters based on the considered strain levels. Concerning the critical state strength parameters, the HS predicted a slightly lower FoS while the SHANSEP NGI-ADP a marginally higher value than that of using serviceability strength parameters. Although the difference is not as significant as the case of the

Green dike upon a closer observation of the deviatoric strain development some useful conclusions are drawn. Similarly with the Green dike, the HS seems to be more subjectable in failure at the shallow layers since at Figure 131d it is illustrated that at these depth the deviatoric strains are intensified (black arrow). On the other hand, the SHANSEP NGI-ADP reaches an equilibrium at shallow depths due the enhanced s_u profile which considers properly the OCR and the deviatoric strains are mobilised up until the interface of the organic clay 2 and the sand (red arrow) showing less intensification at the shallow depths. Moreover, the usage of the serviceability strength parameters results in a more similar failure pattern as shown in Figures 133c and 134c. However, as an overall conclusion it seems that in the case of the Blue dike the difference in the developed failure plane and in turn the FoS is less obvious signifying the influence of the cantilever sheet pile wall in the dike behaviour at critical loading conditions.
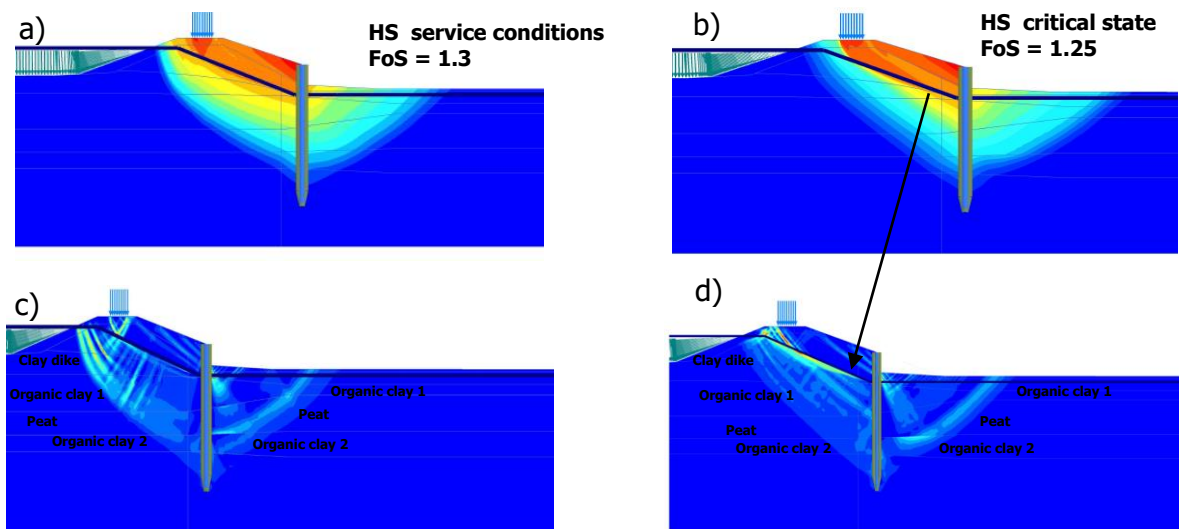
Figure 131: Developed failure mechanism in shades (a, b) plots and deviatoric strain (c,d) for the HS model.
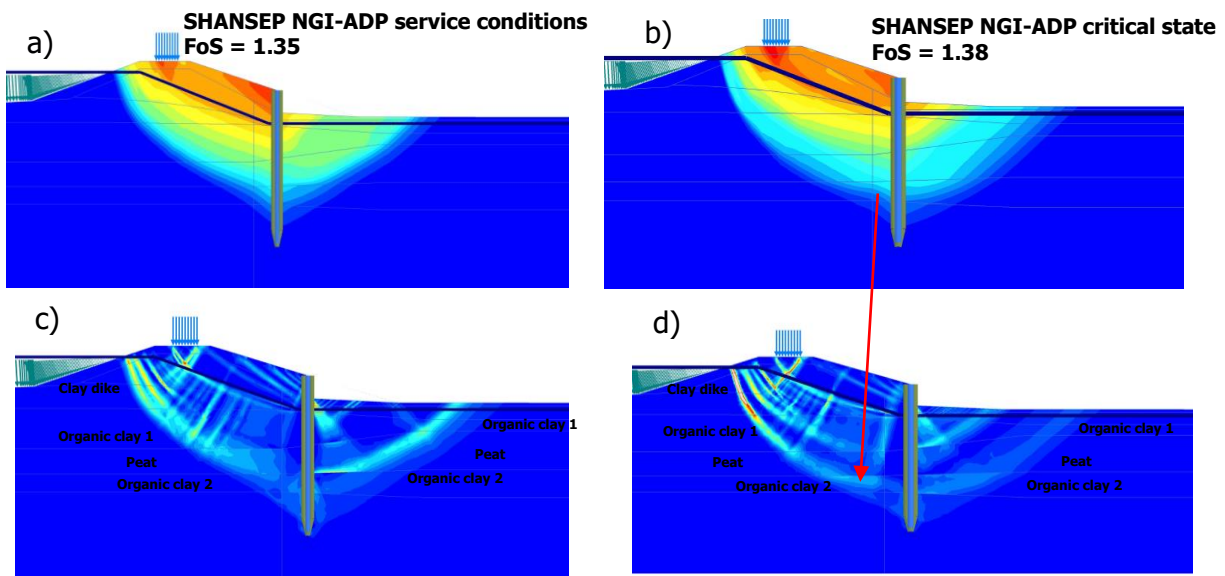
Figure 132: Developed failure mechanism in shades (a, b) plots and deviatoric strain (c,d) for the SHANSEP NGI-ADP model.

6 Conclusion and Recommendations

6.1 Recap of Objectives

In this study the research objectives are divided into two main categories.

> *The first category deals with the determination of the input parameters (strength and stiffness) of the considered constitutive models and emphasizes important aspects governing their behaviour (i.e. strain level dependency). Moreover, solutions and recommendations are given for an optimized determination of the necessary parameters for both clays and peats always referring to the WBI 2017 laboratory protocol.*
> *The second category deals with the actual analysis and the comparison of the role of the considered constitutive models on the estimated FoS, the developed failure mechanisms and the generated displacements for both the Green and the Blue dike cases. In this way, the recently developed SHANSEP NGI-ADP model which is the recommended model to be used in the assessment of dike stability is compared with other fundamental isotropic constitutive models (HS, SS) which are greatly used in the engineering practice. Thus, within these objectives a direct elaboration of the recently introduced design guidelines (POVM 2018) is accomplished concerning the KIJK dike project. Lastly, the influence of the strain level dependency of the strength parameters on the design is highlighted.*

6.2 Conclusions regarding the parameter determination

The answer of the formulated sub-research questions concerning the first category is given below followed by the main conclusion. Due to the interdependency of the first and second objective the given answer elaborates for both.

> *Determine the strength parameters from the service conditions strain levels and the "critical" state strain levels. How does the strain level influence the strength of the examined clays and peats and how should this be translated in the design?*
> *After the application of the two proposed methods given by the WBI 2017, what are the differences in the resulting value of the strength increase exponent m and which method is recommended for use in the design?*

Firstly, it was found that all the examined soils (clay dike material, organic clays and peats) displayed the expected normalised behavior at all the considered strain levels.

The value of $S_{(NC)}$ at the service condition strain levels, was found to be notably higher for clays than peats. This can be explained from the fact that the maximum strength of the clayey soil was reached at approximately 2% strain level while for peats, the maximum shear strength is reached at larger strains beyond the required 5% strain level. Conversely, at "critical state" strain levels, the clays experienced strain softening and the value of $S_{(NC)\ 25\%}$ typically lies below the maximum shear strength. For peats the $S_{(NC)\ 40\%}$ generally describes the peak or shows a similar values to the peak strength since no strain softening observed.

Concerning the actual analysis, upon consideration of the aforementioned observations and the extensive literature review the following recommendations are given:

With the use of the $S_{(NC)25\%}$ for clays it is reasonable to assume that the strain softening experienced from the clays under TXC reached a state which is comparable with the strength

mobilized from the other modes of shearing. Thus, the s_u stress path dependency at that strain level is not significant.

However, with the use of the $S_{(NC)2\%}$ or in other words the use of the $S_{(NC)peak}$ for clays which is obtained from a triaxial compression test, it is recommended to utilize the advanced feature of the NGI-ADP model which accounts for the stress path dependency of the s_u through the input values of the s_u ratios. There is a common agreement that the use of TXC test for clays at low strain levels results in a higher value of the s_u in comparison with the s_u mobilized at DSS and TXE tests at the associated low strain levels. In this way, it is ensured that the maximum strength among the various modes of shearing is no longer applied. By taking into consideration that based on the WBI 2017 the clays are thoroughly described from TXC tests; a literature review of the stress path dependency of the s_u in peak state was conducted. Speaking in terms of undrained shear strength ratios s_u^P / s_u^A and s_u^{DSS} / s_u^A the investigation revealed that the s_u^P / s_u^A is typically described from values ranging from 0.4 to 0.6 (average 0.5) while the s_u^{DSS} / s_u^A is generally found in a range between 0.6 and 0.8 (average 0.7).

Concerning the peats, the DSS test which is applied in the soil is considered to be the mode of shearing which typically lies in the middle of the TXC and TXE tests. This comes in accordance with a recent study made by Zwanenburg and Jardine (2015). The experimental investigation conducted on Dutch peat specimens revealed that the $S_{(NC)}$ determined from a direct simple shear test yielded in marginally lower values than the $S_{(NC)}$ determined from a CIUC test.

With reference to the friction angle of the soils, similar behavior with the $S_{(NC)}$ parameter was observed in the sense that at "critical" state strains, the peat displayed the highest value while the clayey soils followed with lower values. On the other hand, at service conditions strain levels, the clays displayed the higher values whereas the peat the lowest. Additionally, with the use of the service conditions strain levels the apparent cohesion of the soils is considered whereas at the critical state strain levels the intercept cohesion of the soils is zero.

The determination of the m parameter was established with two different methods as it is proposed by the WBI 2017. The application of the two methods resulted in notably different values of m. The second method (e.g. m= (b-a) / b) resulted in m values ranging dominantly from 0.88 to 0.98 for all the examined soils. On the other hand, the use of the first approach (e.g. SHANSEP curve) resulted in m values varying from 0.72 to 0.75 for peats and 0.74 to 0.86 for clays. While the second method was found to be rather straight forward, it is noteworthy to mention that the use of the first method is advantageous in the sense that the strain level dependency of the $S_{(NC, OC)}$ parameter was taken into consideration and thus, a value of m was obtained from both the service conditions strain levels and the critical state strain levels.

> *Which soil input parameters of the constitutive models incorporate the highest uncertainties and difficulties for their determination considering the WBI 2017 protocol?*

By taking into consideration that the current laboratory protocol suggests that the clays and peats are thoroughly described from $C_{K0}UC$ and DSS respectively, the determination of the stiffness parameters of the SHANSEP NGI-ADP model is arguably the most challenging process, since the model requires the shear strains at failure from three different shear tests (γ_f^C, γ_f^{DSS}, γ_f^E). Moreover, the model requires the determination of an unloading reloading shear modulus concerning the advanced input parameter G_{ur} / s_u^A. Lastly, the initial mobilisation τ_0 / s_u^A can only be determined and optimized from a calibration point of view using the STF offered by PLAXIS.

In this study, it was found that the G_{ur} / s_u^A can be effectively correlated with the use of the G_{50} / s_u^A through the following equations for each soil layer:
Clay dike: $G_{ur} / s_u^A \approx 1.85 \ G_{50} / s_u^A$

Organic clay 1 $G_{ur} / s_u^A \approx 1.55 \ G_{50} / s_u^A$
Organic clay 2 $G_{ur} / s_u^A \approx 1.65 \ G_{50} / s_u^A$
Peat $G_{ur} / s_u^A \approx G_{50} / s_u^A$

Regarding the shear strains at failure at compression for clays it is essential to examine if the empirical equation $\gamma_f^C = (3/2) \ \varepsilon_{1f}^C$ reflects properly the reality. After a careful calibration of the SHANSEP NGI-ADP model with the use of several experimental data through the STF for each soil type it was verified that the determined γ_f^C fitted well the γ_f^C which produced the best fit curves. In addition, it was found that the γ_f^{DSS} which is directly determined from the experimental stress strain curves of peats matched properly the best fit γ_f^{DSS}.

Moreover, based on the extensive literature review and by taking into consideration the valid combinations accepted internally from the SHANSEP NGI-ADP model the γ_f^{DSS} can be described with $\gamma_f^{DSS} = (1.5 \ to \ 2) \ \gamma_f^C$ (average 1.75) while the γ_f^E through $\gamma_f^E = (2.5 \ to \ 4) \ \gamma_f^C$ (average 3.25).

Regarding the τ_0/s_u^A the default value of 0.7 may be used for both peats and clays.

> *What is the influence of applying the same K_0 value on the resulting undrained shear strength and the stiffness, in both the normally consolidated (NC) and over consolidated (OC) soil samples? How does this affect the results?*

In triaxial compression the decision of applying the same K_0 value (e.g. $K_0 = 0.45$) value for both the NC and OC samples was found to have notable influence in the obtained results in terms of the strength and the stiffness characteristics of the soils. In the case of the OC samples it appears that the maximum shear strength that the soil can mobilize along with the E_{50} were underestimated. Specifically, the underestimation of s_u for the OC soil samples influenced the parameter determination of the strength increase exponent m. By replicating the "correct" $K_{0consolidation}$ for the OC soils the resulting $S_{(OC)}$ in both 2% and 25% strain levels will yield in a different value. Therefore, the SHANSEP curves established in this study will result in a different power regression line due to the updated $S_{(OC)}$ and therefore an updated value of the strength increase exponent (m). The underestimation of the E_{50} in turn influences the resulting G_{50} / s_u^A, the stress level dependency of stiffness m and the resulting E_{50}^{ref}. Speaking in terms of percentages based on the simulation tests it was found that in the case of the OCR equal to 1.5 (lightly over consolidated state) the s_u and the $S_{(OC)}$ were underestimated by a factor of 15% and 16% respectively while for the case where the OCR equal to 2.5 (over consolidated state) the s_u and the $S_{(OC)}$ were underestimated by a factor of 36% and 28% respectively. Lastly, in the case of the NC samples it seems that the applied K_0 value is not always in the conservative side since the organic clays in some cases displayed a K_0^{NC} lower than the applied 0.45.

6.3 Conclusions regarding the FE analysis

> *What are the response of the considered constitutive models regarding the safety factor, the developed failure mechanisms, the resulting displacements as well the forces acting on the sheet pile wall (in the case of Blue Dike)?*

The first and important step is the verification of the s_u derived from the considered constitutive models along with the s_u profile with depth determined from the available cone penetration tests which are located within the generated cross section in PLAXIS at the initial conditions.

In order to correctly derive the s_u based on the CPT for both the Green and Blue dike analysis it is recommended to account for the strain level dependency of the N_{kt} value. In other words,

the derived value of the N_{kt} differs if the $s_{u\ (OC)}$ is determined from the service conditions strain levels the peak or the critical state. Thus, the resulting s_u profile with depth is strongly associated with the determined value of the N_{kt} since the s_u determined from a CPT test is given through $s_u = q_{net} / N_{kt}$.

This study showed that the undrained shear strength predicted from the SHANSEP NGI-ADP model are in a good agreement with the undrained shear strength profile for both the service conditions strain levels as well as critical state strain levels in the crest and the hinterland areas of the dike. Therefore, the determined $S_{(NC)}$ along with the incorporation of the OCR in the design with combination with the strength increase exponent m are capable of estimating properly the s_u that the soil exhibits in the field.

The HS and SS displayed almost identical prediction in terms of the s_u since both models describe the shear strength likewise. Under the crest area of the dike the response of the HS, SS models was rather poor and underestimates the available s_u for both the critical state strains and the service conditions strain levels. The calculation of the s_u based on the effective strength parameters in combination with the incapability of the models to reproduce properly the behavior of an OC soil results in an undrained shear strength profile which deviates from the s_u that the soils exhibits in the field. This is particularly relevant for the shallow depths where the soils experience the higher values of the OCR.

At the toe and the hinterland areas of the dike the HS, SS models predicted comparable values with the SHANSEP NGI-ADP model highlighting the influence of the principal stresses in the resulting value of the s_u (refer to equations 5 and 17).

Concerning the estimated FoS it was found that for both the critical (Green dike) and the service conditions (Blue dike) strain levels the SHANSEP NGI-ADP resulted in the highest FoS. The HS and SS models resulted in comparable values and were lower than that of the SHANSEP NGI-ADP. Moreover, it was noted that both the HS and SS models transferred equally the stress history of the soil and thus, at critical loading conditions the resulting FoS estimated from the SHANSEP NGI-ADP yielded in identical values irrespective the selection of either the HS or the SS models in the preceding drained steps.

The difference between the SHANSEP NGI-ADP and either the HS and SS in terms of the predicted FoS was particularly obvious in the Green dike analysis. The latter is explained based on the different developed failure mechanisms generated from the constitutive models. The developed failure mechanisms obtained from the HS and SS models resulted in a shallow and narrow size. The reached depth was the interface between the clay dike material with the Organic clay 1. On the contrary, with the use of the SHANSEP NGI-ADP model the developed failure plane reached until the interface between the Organic clay 2 material and the sand resulting in a considerably deeper and enlarged failure mechanism. As explained previously for the Green dike analysis the strength parameters were described from the "critical" state of the soil ($S_{25\%,\ 40\%}$ and $\varphi_{25\%,\ 40\%}$) and for the HS there was no cohesion considered in the soils. The cohesion is particularly essential at shallow depths where the effective stress exhibits low values and the contribution of the cohesion in the shear strength of the material becomes significant. Therefore, as it concerns the HS and SS models upon a φ, c reduction technique and in combination with the fact that the s_u is unavoidably underestimated (refer to subchapter 3.4) the failure plane was deemed to be reached relatively fast resulting in a shallow and narrow size. However, the SHANSEP NGI-ADP model predicts an enhanced s_u profile which considers the OCR properly. In this case, the resulting failure surface is not located at the shallow layers but rather in the interface of the deeper soft soil layer (organic clay 2) with the sand. This explains and the notably higher FoS obtained from the SHANSEP NGI-ADP model.

In the Blue dike analysis, the strength parameters were determined from the service conditions strain levels ($S_{(NC)2\%, 5\%}$ and $\varphi_{(NC)2\%, 5\%}$). In other words, for clays the $S_{(NC)peak}$ and $\varphi_{(NC)peak}$ along with cohesion is considered while the peat is described from a state which lies considerably below the maximum shear strength that the soil can mobilize.

Therefore, the HS and SS models were described with an enhanced s_u profile in the shallows clay layers and the resulting failure mechanism is in substantial agreement with the failure surface predicted by the SHANSEP NGI-ADP model. Although, it is rather difficult to distinguish a clear failure pattern in the case of the Blue dike a closer examination of the deviatoric strain development in the safety analysis shows that the majority of the displacements is occurring at the interface of the peat with the underlying organic clay 2 soil layer.

In addition, as explained in the 6.1.1 with the use of the $S_{(NC)2\%}$ or in other words $S_{(NC)peak}$ under triaxial compression the advanced feature of the NGI-ADP to account for the stress path dependency of the s_u through the s_u^{DSS} / s_u^A and s_u^P / s_u^A ratios needs to be utilized. In the absence of specific data, a sensitivity analysis was performed to evaluate the consequence of this uncertainty. With the use of the most typical values of s_u ratios ($s_u^{DSS} / s_u^A = 0.7$, $s_u^P / s_u^A = 0.5$) the reduction in the FoS is around 12.5% compared to the no reduction case. With the use of the lower bound values ($s_u^{DSS} / s_u^A = 0.5$, $s_u^P / s_u^A = 0.3$) the reduction is 17%. Lastly, the reduction influences the average strength but not the failure mechanism which remained identical upon the variation of the s_u ratios.

> *What is the influense of the strain level dependency of the strength parameters in the desing analysis of the "Green" and the "Blue" dike?*

In the Green dike analysis, the use of the strength parameters determined from the service conditions strain levels resulted in a slip plane reaching until the boundary between the peat and the underlying organic clay 2 for both the SHANSEP NGI-ADP and the HS models. The similarity in the developed failure mechanism resulted in more comparable values of the predicted FoS than the use of the critical state strength parameters. With the use of the serviceability state strength parameters the SHANSEP NGI-ADP model predicted a lower FoS whereas the HS model a higher value of FoS in comparison with the estimated based on the strength parameters determined from the critical state strain levels.

In case of the Blue dike analysis the results showed that the response in terms of the FoS and the developed failure mechanism seems to be less sensitive upon the selection of the strain level where the strength parameters are determined as well and the selected constitutive model. However, the variation of the strength parameters based on the considered strain levels led to a deviation in the generated displacements u_x on the sheet pile wall as well and a qualitative and quantitative deviation in the bending moments distribution. This implies the dominance of the cantilever sheet pile wall in the dike behavior at critical loading conditions. To be exact though, with the use of the critical state strength parameters the HS model estimated a slightly lower FoS as well and mobilization of the deviatoric strains at shallow depths. On the other hand, the SHANSEP NGI-ADP predicted a slightly higher FoS with the deviatoric strains reaching up until the interface of the Organic clay 2 and the sand.

6.4 Final Conclusion

Based on the evaluation of the models in both the STF and the response in the design analysis it is concluded that the SHANSEP NGI-ADP behaves better the HS and SS models. At the single element level, the model was able to reproduce accurately the strain hardening of both the clays and the peat. The combination of the shear strains at failure, the G_{ur} / s_u^A along with the τ_0 / s_u^A seems very beneficial for capturing properly the elastoplastic behavior of both peats and clays. Moreover, the model was able to match properly the s_u determined from a CPT. In addition, the model incorporates the stress path dependency of the s_u which is an important factor to consider when dealing with the $S_{(NC)}$ determined from the peak state or a state nearby the peak of a TXC test.

In addition, the findings of this study point out that the use of the service conditions strain levels led to a better agreement of the responses of the constitutive models in terms of the developed failure mechanism and the estimated FoS. At the service conditions strain levels, the use of the cohesion enabled an enhanced s_u profile for both the HS and SS models. The use of the critical state strain levels increases the probability of the generation of shallow slip planes since the shallow layers (i.e. clay dike, organic clay 1) are described with a $S_{(NC)25\%}$ which lies notably below the peak strength for the SHANSEP NGI-ADP model. For HS, SS model the generation of shallow planes is a consequence of not considering the apparent cohesion of the soils. Moreover, the low values of the developed deviatoric strain found in this study may indicate that the strength parameters determined from the service conditions strain levels are more representative, especially for peat, since the strength obtained from a mobilized shear strain of 40% might deviate considerably from the mobilized strength that the peat exhibits upon the critical loading conditions.

Lastly, in the drained steps the use of the HS model is preferred than the SS model. Even though the determination of the stiffness parameters of the SS model is a rather straightforward process the HS model advance feature to account three stiffnesses in different paths is certainly advantageous. Moreover, the HS model behaved notably better in the STF examination being able to capture reasonably well the stress strain response of both the clays and peats.

6.5 Recommendations

In the next points recommendations for further study are given. Distinction has been made between the recommendations regarding the modelling and the laboratory tests.

6.5.1 Recommendations regarding the FEM modelling

➢ *Widen the analysis of the influence of the s_u ratios and apply a sensitivity analysis in important design factors i.e. location of the sheet pile wall, location and thickness of the soft soil layers, water level height in daily and high-water situations and evaluate the following:*
a) Are there any combinations for which the s_u ratios influences significantly the FoS?
b) Are there any combinations for which the s_u ratios led to a significant differentiation of the developed failure mechanism?

➢ *Apply the aforementioned analysis but in this case consider aspects which govern the sheet pile wall design i.e. stiffness properties, penetration depth within the sand layer.*

> ➢ *Consider a time dependent analysis especially in the step where the high-water level is adopted in the design. In this way, the analysis of the dike considers essential aspects such as the consolidation of the soils which in turn couples the permeability of the soils and the duration of the high-water event. For this examination a hydrograph of the Hollandse Ijssel river is needed where the increase in head with time for the high-water level event can be illustrated.*

> ➢ *Perform the analysis using a three-dimensional (3D) model and compare the responses in terms of the estimated FoS and the generated displacements with the two-dimensional (2D) analysis conducted in this study. Hence, the strength of the subsoil in the direction perpendicular of the dike will be investigated along with the influence of the constraining effects given from the "shoulders" of the dike for both the prefailure and the failure behavior of the KIJK dike. In addition, the evaluation of the results (i.e. difference in the predicted FoS) will give an important feedback on whether a 3D analysis which is more time consuming and expensive is necessary.*

6.5.2 Recommendations regarding the laboratory tests

> ➢ *Apply CK_OUE and constant volume DSS tests in clayey soils which typically describe the soil stratigraphy in the Netherlands with the aim to identify the stress path dependency of the s_u at the considered strain levels. Furthermore, along with the shear tests execution it is recommended to additionally determine the Atterberg limits and examine if the material dependency (i.e. PI) of the s_u^{DSS} and s_u^P additionally applies for the Dutch soils. As a starting point in this study it was verified that the $S_{(NC)}$ obtained from TXC is independent from the PI of the material which agrees with the findings of previous researches. As it concerns peats it is recommended to apply TXC and TXE tests with the aim to examine the response of the material in service conditions strain and critical strain levels (5, 40% strain level) and identify if the values under different stress paths yield in notable deviations.*

> ➢ *Current practice in the Netherlands suggests that for clays the value of the $S_{(NC)}$ and the friction angle should be obtained from 25% axial strain level in TXC which represents the "critical state" of the soil. In this study it was shown that the stress strain response of the induced NC clays is in agreement with the findings of the previous researches in the sense that the clays experienced strain softening after reaching their peak. However, the strain softening experienced from the various type of clays was different. This observed uncertainty may lead to an underestimation or overestimation of the average s_u under different stress paths for a specific type of clay at the given $S_{25\%}$ strain level. In addition, the interpretation of the mechanisms causing the strain softening is a challenging topic which is still missing in the literature. Thus, a study that will explicitly deal with the phenomenon of strain softening is of importance and useful for the Dutch practice with the final aim of providing a common guideline at which strain level the actual critical state for each soil sample is reached.*

> ➢ *Application of the exact step wise procedure given from Ladd and Foott, (1974) for the determination of the strength parameters $S_{(OC, NC)}$ and the strength increase exponent m. The analysis will expose on how the values of the parameters determined with the step-wise procedure given from Ladd and Foott deviate from the values determined based on the WBI (2017) protocol.*

References

Abdulhadi, N.O., 2009. An experimental investigation into the stress-dependent mechanical behavior of cohesive soil with application to wellbore instability. Massachusetts Institute of Technology.

Abdulhadi, N.O., Germaine, J.T., Whittle, A.J., 2012. Stress-dependent behavior of saturated clay. Canadian Geotechnical Journal 49, 907-916.

Bay, J.A., Anderson, L.R., Colocino, T.M., Budge, A.S., 2005. Evaluation of SHANSEP Parameters for Soft Bonneville Clays, Utah Department of Transportation, Salt Lake City, Utah. 45 p.

Bjerrum, L., 1973. Problems of soil mechanics and construction on soft clays and structurally unstable soils, Proc. 8th ICSMFE, pp. 111-159.

D'Ignazio, M., 2016. Undrained shear strength of Finnish clays for stability analyses of embankments. Ph. D. thesis, Tampere University of Technology, Tampere.

Duncan, J.M., Wright, S.G., Brandon, T.L., 2014. Soil strength and slope stability. John Wiley & Sons.

Edil, T., 2001. Site characterization in peat and organic soils, Proc. Int. Conf. on in situ measurement of soil properties and case histories, Bali, Indonesia, pp. 49-59.

Grimstad, G., Andresen, L., & Jostad, H. P. (2012). NGI-ADP: Anisotropic shear strength model for clay. International journal for numerical and analytical methods in geomechanics, 36(4), 483-497.

Jaky, J., 1944. The coefficient of earth pressure at rest. J. of the Society of Hungarian Architects and Engineers, 355-358.

Jamiolkowski, M., 1985. " New developments in field and laboratory testing of soils," State of the Art Report, Proc. 11th Int. Conf. on SMFE, pp. 57-153.

Kamei, T., 1996. Undrained shear strength and interrelationships among CIUC, CKoUC, ClUE, and CKoUE tests. 15, 137-145.

Karlsrud, K., Hernandez-Martinez, F.G., 2013. Strength and deformation properties of Norwegian clays from laboratory tests on high-quality block samples. Canadian Geotechnical Journal 50, 1273-1293.

Kulhawy, F.H., Mayne, P.W., 1990. Manual on estimating soil properties for foundation design. Electric Power Research Inst., Palo Alto, CA (USA); Cornell Univ., Ithaca, NY (USA). Geotechnical Engineering Group.

Ladd, C.C., 1991. Stability evaluation during staged construction. Journal of Geotechnical Engineering 117, 540-615.

Ladd, C.C., DeGroot, D.J., 2003. Recommended practice for soft ground site characterization: Arthur Casagrande Lecture, 12th Panamerican Conference on Soil Mechanics and Geotechnical Engineering. Verlag GmbH Essen, Germany, pp. 1-57.

Ladd, C.C., Foott, R., 1974. New design procedure for stability of soft clays. Journal of Geotechnical and Geoenvironmental Engineering 100. pp. 763-786.

Larsen, H., Lubking, P., Breedeveld, J., 2013. Ontwerp stabiliteitsschermen (typeII) in primaire waterkeringen (groene versie).

Lofroth, H., 2008. Undrained shear strength in clay slopes–Influence of stress conditions. A model and field test study, Swedish Geotechnical Institute, SE-581 93.

Obrzud, R., 2010. The hardening soil model: a practical guidebook. Zace Services.

Panagoulias, S., Brinkgreve, R., 2017. SHANSEP NGI-ADP. PLAXIS bv, Delft, the Netherlands.

Plaxis. (2018). *Plaxis 2d 2018 - Material models manual* (R. B. J. Brinkgreve, S. Kumarswamy, & W. Swolfs, Eds.). PLAXIS bv, Delft, .the Netherlands.

Plaxis. (2018a). *Plaxis 2d 2018 - Reference manual* (R. B. J. Brinkgreve, S. Kumarswamy,& W. Swolfs, Eds.). PLAXIS bv, Delft, the Netherlands.

POV Macrostabiliteit. (2017). POVM Rekentechnieken - Basisrapport Eindigeelementenmethode, versie 1.0.

POV Macrostabiliteit. (2017). Verbetering berekeningswijze restprofiel.

POV Macrostabiliteit. (2017). SHANSEP NGI-ADP - Validatie cases.

POV Macrostabiliteit. (2018). Parameterbepaling EEM, Deltares rapportnummer 11201294-002-GEO-0001.

Raissakis, I., 2012. Comparison of limit finite element analysis and strength reduction techniques. na. MSc Thesis. Graz University of Technology. Graz

Rijkswaterstaat, 2013. Parameterbepaling EEM.

Rippi, A., 2015. Structural Reliability Analysis of a dike with a sheet pile wall: Coupling Reliability methods with Finite Elements. MSc thesis. Delft University of Technology.

Schofield, A., Wroth, P., 1968. Critical state soil mechanics. McGraw-Hill London.

Seah, T., Lai, K., 2003. Strength and deformation behavior of soft Bangkok clay. Geotechnical Testing Journal 26, 421-431.

Tan, T.S., Phoon, K.-K., Hight, D., Leroueil, S., 2006. Characterisation and Engineering Properties of Natural Soils, Two Volume Set: Proceedings of the Second International Workshop on Characterisation and Engineering Properties of Natural Soils, Singapore, 29 November-1 December 2006. CRC Press. 1252 p.

Ukritchon, B., Boonyatee, T., 2015. Soil parameter optimization of the NGI-ADP constitutive model for Bangkok soft clay. Geotech. Eng 46, 28-36.

van Duinen, T., 2014. Handreiking voor het bepalen van schuifsterkte parameters, wti2017 toetsregels stabiliteit. Technical Report 1209434-003, Deltares.

Vergouwe, R., 2016. The national flood risk analysis for the netherlands. Rijkswaterstaat VNK Project Office.

Vermeer, P., Vergeer, C., Termaat, R., 1985. Failure by large plastic deformations, Proc. XIth Int. Conf. On Soil Mech. And Found Eng., San Francisco, 12-16 Aug. pp. 2045-2048

Visschedijk, M., 2018. Basisrapport Eindige-elementenmethode (onderdeel 6.2.6A). 151.

Yamaguchi, H., Ohira, Y., Kogure, K., MORI, S., 1985. Undrained shear characteristics of normally consolidated peat under triaxial compression and extension conditions. Soils and Foundations 25, 1-18.

Zdravković, L., Jardine, R., 2001. The effect on anisotropy of rotating the principal stress axes during consolidation. Geotechnique 51, 69-83.

Zwanenburg, C., Van Duinen, A., & Rozing, A. (2013). Technisch rapport macrostabiliteit. Deltares rapport 1204203-007-GEO-0003-gbh voor RWS-WD.

Zwanenburg, C., Jardine, R., 2015. Laboratory, in situ and full-scale load tests to assess flood embankment stability on peat. *Geotechnique*, 65(4), 309-326.